THE EFFECTS OF ALLOYING ELEMENTS ON THE PROPERTIES OF PIPE LINE STEELS

By

CORNELIUS OCHEKOR IKWUAGWU EMENIKE

A THESIS SUBMITTED FOR THE DEGREE OF

DOCTOR OF PHILOSOPHY

THE UNIVERSITY OF ASTON IN BIRMINGHAM

February, 1987

TITLE: The Effects of Alloying Elements on the Properties of Pipeline Steels.

NAME: Cornelius Ochekor Ikwuagwu Emenike

YEAR: 1987

SUMMARY

Strong, tough and HIC resistant pipeline type of steels have been produced by a combination of compositional and thermomechanical designs. The essential variables are comparable varying levels of Ti and V for fixed Nb content and isothermal rolling temperatures in the range 1250°C to 900°C, following a soaking treatment at 1250°C.

The good toughness exhibited by these steels is attributed mainly to ferrite grain refinement, cleanness and N-removal by microalloying elements while the high strength is rationalised mainly on the basis of the interaction amongst grain size, composition and microalloying precipitates. The HIC resistance is interpreted in terms of fine microalloying precipitates, together with the factors that enhance toughness of these steels.

Precipitate analysis by STEM-EDAX-TEM indicates that the precipitates in a multiple microalloyed steel are of mixed composition (composites) and of various morphologies. The former is explained in terms of isomorphology and non-stoichiometry exhibited by most of the precipitates while the latter is, to a large extent, composition dependent. These composite precipitates persist up to the soaking temperature of 1250°C.

Temperature-composition diagrams have been drawn to highlight the phenomenon of co-precipitation associated with multiple microalloyed steels.

Key Words: Multiple Microalloyed Steels, Pipeline, Rolling, HIC.

Dedication

TO EMENIKE'S FAMILY

TO WORLD PEACE

ACKNOWLEDGEMENTS

My profound thanks to the Nigerian Government for providing the financial support and the erstwhile Metallurgy Department (now absorbed into Mech/Prod.Eng.Dept.) for providing the facilities for the project.

I am highly indebted to my main supervisor, Dr.J.C.Billington, for his fatherly and indefatigable guidance throughout the course of the investigation. Also administrative assistance by my associate supervisor, Mr.L.Crane, is appreciated.

I am grateful to Dr.S.Murphy for his help in electron diffraction analysis and to Profs. Loretto and Smallman of Birmingham University for providing the supplementary facilities for inclusion and microalloying precipitate analyses, and Dr.F.B.Pickering of Sheffield City Polytechnic for useful discussions.

Support by my research colleagues deserves a mention and co-operation/assistance from technicians, Ted Watson, Dave Farmer, John Foden, Roger Howell and Carl Johnson is acknowledged.

Ecumenical satisfaction derived from the UAB Christian group, especially Fr.Teddy O'Brien, Rev.John Austen, emeritus Prof.T.Mulvey, Anne Friel and Christine Fritsch is highly appreciated. The importance of ecumenism in the present religious and moral climate cannot be overemphasised.

Finally, my thanks go to Mrs.Ann Howell for typing the manuscript from my almost indecipherable writing.

Words of mouth cannot express my appreciation.

CONTENTS

LIST OF TABLES

List of Figures

1. INTRODUCTION

The increased demand for energy in the world has been the major impetus for the continuous increase in the production of line pipe type of steel which is used in mass production of oil and gas. Consequently, safety and economy of operation dictate that such pressurised pipe should be of high quality and minimum weight.

The design of pipeline for oil and gas transportation has tended towards increased sizes working under high operational pressures for maximum throughput. Accordingly the API* specification has progressed through a series of modifications since its inception in 1948(55). For instance, the original (5LX) X-42 grade with sizes under 30 inches (762 mm) has been upgraded to X-70 with diameters up to 64 inches (1626 mm). In addition, the specification for ultra high-test heat treated line pipe (5LS) for grades U-80 and U-100 was established in 1972, and the latest specification for spiral-weld line pipe (5LS) includes sizes up to 80 inches (2032 mm) diameter. The recent interest in enhanced recovery process at oil wells with extremely high pressure water or gas places a high premium on heavy-wall high strength pipe. A typical application of water injections under high pressure in the United Arab Emirates uses pipe of 24 inches outside diameter with 1.125 - 1.250 inches wall thickness (610 by 29 to 32 mm) and pipe 18 inches outside diameter by 0.875 to 1.00 inches wall thickness (457 mm by 22 to 25 mm).

* API = American Petrol Institute

The development of gas and oil fields in the Arctic Circle including Alaska, North Sea and U.S.S.R. stimulated the need for stronger and tougher line pipes at low temperatures. The production of large diameter line pipe for Trans-Alaska pipe line system which started in 1969 was epoch-making with respect to the high toughness requirement. However, the low temperature toughness in these environments, especially for gas transmission, is becoming more stringent. High energy absorbed as well as low transition temperature is mandatory in such situations.

The construction of large scale submarine transmission systems has been very active since 1970, and in such cases heavy-wall high strength pipe must be used to prevent the collapse and/or buckling at the time of pipeline installation in deep water. Several submarine projects in the North Sea (150 m deep) used the 32 O.D.* X 0.750 inches WT* (813 mm X 19 mm) X-65 pipe, while in the Trans-Mediterranean pipe line at the Sicilian Channel in water depths of about 500 m, the pipes used were 20 inches OD X 0.75 to 0.812 WT (508 mm X 19 to 21 mm) of grade X-65.

Another recent response to energy demand is the exploration of lean oil/gas wells with the concomitant exposure of line pipes to sour gas environments. The discovery of oil and gas with H_2S content accelerated the demand of anti corrosion line pipe steel with high resistance to Hydrogen Induced Cracking (HIC)

* O.D = Outside diameter

WT = Wall thickness

and Sulphide Stress Corrosion Cracking (SSCC) under wet H_2S environments. Corrosive gas containing wet carbon dioxide (CO_2) assigns another important task to line pipe steel as CO_2 attacks the steel in a wet environment. Other applications requiring specially anti-erosion and extremely low temperature toughness include slurry and LNG pipelines respectively.

These improvements in line pipe properties have been made possible by the evolutionary trend of high strength low alloy (HSLA) steel development, the basis of line pipe steels.

The original HSLA steels dating from the early 1900's were mainly used for structural and constructional purposes, and were designed mainly on the tensile strength with little attention to toughness, formability and weldability, in what were essentially rivetted artefacts[28]. Inexpensive carbon at 0.3% was the main alloying element used with, in some cases, up to 1.5% Mn. The introduction of welding fabrication and the need to improve toughness both contributed to the necessity to lower the %C and at the same time it was appreciated that yield stress was the more important design criterion than tensile strength.

By the 1950's the beneficial effects of ferrite grain refinement on both yield stress and toughness were fully accepted, together with the realisation of the significance of Mn in depressing the transformation temperature. The understanding of structure-property relationships also greatly accelerated developments to produce the Al grain-refined 0.15%C - 1.5% Mn steels with increased yield strength and reduced Impact

Transition Temperature (ITT) or low Fracture Appearance Transition Temperature (FATT).

Subsequent developments used microalloying additions such as Nb, V and Ti, which under appropriate processing conditions could both grain refine and precipitation strengthen by virtue of their carbides/nitrides. However, the impact toughness was not good because the as rolled-grain size was coarse, consequent upon a high finish-rolling temperature resulting in coarse austenite grain size. To overcome this, the development of controlled rolling was promoted to permit much lower finish-rolling temperature and consequently, producing fine ferrite grain size. Yield stress of 450 - 500 MPa with FATT value as low as $-80^{o}C$ were produced. This technique of controlled rolling is now applicable to all microalloyed steels albeit under different processing conditions in conformity with the solubilities of the various microalloy carbo-nitrides. Yield stress in the range (550 - 600) MPa can be achieved with FATT values in the range $-50^{o}C$ to $-70^{o}C$.

Equally developments in HSLA Bainitic steels of yield stress between 400 and 900 MPa occurred almost contemporaneously with those of ferrite-pearlite steels. Initially, these bainitic steels suffered from inferior toughness. Subsequent improvement in toughness has been achieved by the production of low carbon acicular ferrite with proof (yield) stress values of 500 - 750 MPa. Yet another approach has been to use HSLA steels in the quenched and tempered condition, and due to the low hardenability, various non-martensitic structures are produced, especially in thicker section sizes with maximum yield (proof)

stress value of 800 MPa and FATT values as low as -80°C. The economic advantage of using water or accelerated cooling instead of expensive, scarce and strategically sensitive alloying elements was thus established.

Formability requirements also dictated low carbon levels, hence some of the acicular ferrite or bainitic steels have carbon contents as low as 0.03%. The use of relatively low finish rolling temperature in controlled rolling, whilst producing an ideal matrix structure for strength and toughness, unfortunately causes any inclusions to be distributed in elongated stringers thus paving the way for recrystallisation rolling as a possible alternative. For example, the relative plasticity of MnS increases with decreasing finish rolling temperature so that highly detrimental co-planar ribbons of MnS are formed, particularly in killed steels, in which Type II MnS predominates in the original as-cast condition. The outcome of this is low through-thickness toughness and ductility in plates and flat rolled products. These result in lamellar tearing during welding; and longitudinal cracking during bending. Considerable use is being made of inclusion shape controllers such as Zr, Ti, Ce or Ca to overcome these problems resulting in improved through-thickness toughness and ductility. Another benefit is increased resistance to hydrogen assisted cracking usually encountered in sour oil and gas wells.

During the last decade, there has been a revolution in HSLA technology in which combinations of the conventional micro-alloying elements are used, together with a new generation of

such elements[25-28]. The understanding of the interactions between these multiple microalloying additions and Al and nitrogen is far from complete, especially in terms of their dependence on processing variables.

Coincidentally, the development of these steels and customer requirements have proceeded at a time when world steel over-capacity and tight economic conditions have demanded such steels at minimum cost. Hence, emphasis has been placed on control of composition, maximising yield and minimising energy consumption throughout the steel making process route, and the majority of these grades are produced via continuous casting, a further change in technology during the last twenty years which has introduced its own processing and engineering demands such as the design of the various shroudings during casting for enhancing cleanliness of the steels.

1.1 THE AIMS OF THE PRESENT INVESTIGATION

These are mainly:-

(i) Production of clean HSLA steels.

(ii) Production of clean HSLA steels containing Nb with three different levels of V.

(iii) Production of clean HSLA steels containing Nb and three different comparable levels of Ti.

(iv) Assessment of the effect of thermomechanical treatments on the mechanical properties of the steels.

(v) Measurement of the cleaness of the steels through the quantification of non-netallic inclusion parameters.

(vi) Appraisal of the HIC resistance of rolled steels.

(vii) An attempt to understand the precipitation behaviour of the carbides, nitrides and carbonitrides.

(viii) Finally a study of the overall effects of these microalloying elements on the optimisation of the properties in the finished steels.

2. REVIEW OF LITERATURE

In this section the emphasis will be mainly on the post foundry fabrication of pipeline steels especially on the role of microalloying additions. Subsequently, environmental degradation of pipelines will be appraised.

2.1 HIGH STRENGTH LOW ALLOY (HSLA) STEELS

The sixties witnessed a new class of steels - the HSLA steels. These steels find major applications in pipelines, automobiles, ship plates and off-shore structures. In fact, the versatility of such steels can be judged by the number of conferences held within the past few years to discuss their production, properties and applications. In effect, these conferences (1-24) examined the evolutionary trend of the development of these steels.

In subsequent sections the properties of these steels pertinent to linepipe applications will be examined.

2.2 MICROALLOYING ELEMENTS

These include elements like niobium, titanium and vanadium, whose concentrations are usually small (less than 0.10%)[32]. The most important effect is to increase the strength of ferritic or ferrite-pearlite steels, both by precipitation hardening and solid solution hardening. Fig.1 summarises the potential of certain metals to form oxides, sulphides, carbides and nitrides, and their precipitation-strengthening potential (arranged similar to the periodic table).

Grain refining additives include aluminium, niobium, titanium and vanadium. Al and V produce nitrides of limited solubilities, niobium can form carbo-nitrides Nb(C,N) or carbide, NbC, and titanium forms nitrides and carbides together with vanadium. These carbides are more stable than iron carbide, with lower solubilities in austenite, consequently, during hot working, fine precipitation of these carbides/nitrides takes place both on austenite grain boundaries and on dislocation arrays within the grains.

2.2.1 THE EFFECT OF ALUMINIUM

Aluminium is not one of the usual microalloying additions but it plays an important role when its nitride precipitates during thermomechanical treatment. It is well known that the residual Al in low alloy and carbon steels produces a fine austenite grain size during heating to normal austenitising temperatures for heat treatment. A typical steel contains 0.01%N and 0.03%Al and the AlN formed takes part in a grain

refining action. The thermodynamics and kinetics of aluminium nitride precipitation have been extensively documented[31-36], only the salient points are highlighted here. The kinetics of aluminium nitride precipitation in austenite are generally slow and dependent upon thermal history.

Aluminium nitride can occur as a precipitation phase in Al-killed nitrogen containing steels. In steels, the precipitate is a simple nitride with an equiatomic stoichiometry. In contrast, the nitrides of Ti, V and Nb are essentially non-stoichiometric.

Hot deformation of austenite has been found to significantly accelerate the kinetics of AlN precipitation[33,41-42]. The maximum in precipitation kinetics occurred between 800°C and 900°C. Michel and Jonas[35] determined the start and finish times for the dynamic precipitation of AlN during the deformation. The investigators found that AlN precipitation was most rapid for Al-rich, off-stoichiometric composition, and rationalised this on the basis of a reaction controlled by Al-diffusion. They also concluded that the interaction of dynamic AlN precipitation with dynamic recrystallisation is dependent upon the magnitude of strain rate. At higher strain rates ($\dot{\varepsilon} > 10^{-2}\ s^{-1}$) dynamic precipitation had no effect upon dynamic recrystallisation consistent with previous work[33]. At lowest strain rates, rapid coarsening of AlN was inferred and this is harmful to toughness.

Recent evidence[33] suggests that the precipitation of AlN is enhanced in the presence of silicon and the higher levels of

AlN attainable could be correlated with greater post deformation microstructural stability.[33] The effect of silicon may be due to an increase in the activity of nitrogen in the austenite, thus decreasing the solubility of AlN and/or raising the Ar_3 temperature to produce more ferrite in which AlN can form readily.

The situation becomes somewhat more complex when the steel is micro-alloyed with other strong nitride-formers, such as V and Ti. An interaction between V and Al in competition for nitrogen, had been proposed for Al-killed V-microalloyed steels[33] with sufficient annealing time at elevated temperature. The interaction has been recently confirmed at 788°C by the thermomechanical work of Brown et al[33].

Aluminium nitride precipitation has been observed to retard recovery and recrystallisation of cold worked ferrite matrix when precipitation occurred just prior to, or simultaneously with, recrystallisation of the ferrite[33,41]. The AlN particles that inhibit recovery and recrystallisation of ferrite were found to be extremely fine[31,33]. A portion of the extremely fine AlN precipitates possessed a cubic NaCl-type (B1) crystal structure with a lattice parameter of approximately 4.00[33]. A dendritic appearing cubic AlN had been found to precipitate at grain boundaries and deformation bands in cold worked specimens and to transform in-situ, to the hexagonal form of AlN. It is unclear from the available literature whether cubic AlN precipitate exclusively in ferrite. The morphologies of coarsened AlN precipitates are thin plates and needles with crystallographic orientation

relationship with ferrite[36]. The orientation relationship of these morphologies with the austenite is[33]

$$(001)_{AlN} \;//\; (111)$$
$$\langle 100\rangle_{AlN} \;//\; \langle 1\bar{1}0\rangle$$

These fine AlN particles restrict the austenite grain size and hence preserve a refined austenite grain size, with the usual metallurgical benefits.

An interesting feature is that the austenite grain size is most refined at an Al content of between 0.02/0.03% because:
(a) this corresponds to the stoichiometric ratio[58] with 0.010/0.015%N at which there is the greatest temperature dependence of the solubility of AlN, and therefore the greatest number of fine precipitates i.e. largest volume fraction.
(b) Al contents much above 0.04% lead to much larger amounts of undissolved AlN on which the AlN precipitates on reheating to 900°C, thereby giving fewer fine AlN particles and larger grains.

It is interesting to note that the grain coarsening temperature is at a maximum when the Al content is 0.02/0.03, a phenomenon associated with the growth or coarsening of AlN particles rather than their solution.

2.2.2 VANADIUM, NIOBIUM AND TITANIUM

These three elements are the traditional microalloying additions in HSLA steels and consequently have stimulated much research interest[26-43]. Therefore, it is only intended here to discuss those principles pertinent to the present study.

These metal carbides and nitrides are very hard, with hardnesses between 2500 to 3000 DPH[37] which possibly makes them non-deformable. The general properties are summarised in Table 1, and for completeness, AlN is included. Their presence in a matrix implies shearing by migrating dislocations only when the precipitates are extremely small. The maximum precipitation hardening which results from the competing shear and Orowan mechanisms is therefore reached in the ferrite and microalloy-precipitate systems as soon as very small precipitates occur. The strengthening exerted by carbonitrides in steel exceeds that of precipitation strengthening caused by other phases such as pearlite, see equations 6 & 10 shown later.

Another characteristic of V, Nb, Ti carbides and nitrides (MeX) is the partial coherence between ferrite matrix and precipitate as shown by the orientation relationships[44-46]

$$\{100\}_{MeX} \;//\; \{100\}_{\alpha\text{-Fe}}$$
$$\langle 010\rangle_{MeX} \;//\; \langle 011\rangle_{\alpha\text{-Fe}}$$

These three elements form carbides having the NaCl type of F.C.C. structure with approximately equal numbers of metal

atoms and carbon atoms per unit cell. The crystal structure can be represented by two interpenetrating F.C.C. lattices with metal atoms in one lattice and C-atoms on the other. In the absence of any vacancies the compounds can be given the chemical formulae VC, NbC and TiC. They may, however, have vacant sites and it is only if the number of vacancies in each of the two lattices is equal, that stoichiometric composition would occur. Generally, there are more vacancies on the lattice containing C atoms, so that the formula for the compounds is often given as MX where M may be V, Nb or Ti and X is $\leqslant$ 1.0. The value of X for the carbides found in the HSLA steels is rather indeterminate but available evidence[30,52] seems to indicate that X ranges between 0.85 and 1.0 for NbC but it is usually close to 1 for TiC. Vanadium carbide shows the biggest deviation from stoichiometry[30,52] with X going down to 0.75, in fact the carbide is often given the formula V_4C_3.

The three elements also form nitrides which also have the NaCl type of crystal structure, but with slightly different lattice parameters. The nitrides also can show deviation from stoichiometry as a result of imbalance of vacancies on the two lattices but these deviations seem to be rather less than those observed for the carbides.

Since the crystal structure of these components are similar and the lattice parameters insignificantly different, these carbides and nitrides are isomorphous and completely soluble in each other[30,37,52]. In fact the same workers have confirmed that carbonitrides whose composition is dictated by N/C ratio in steel are formed in steels containing Nb or V.

The higher N/C ratio gives more nitrogen in the carbonitride. Since microalloy nitrides are usually much more stable and less soluble than the corresponding carbides, a high formation temperature favours more nitrogen in the compound. An extreme case is found in Ti steels where TiN is virtually insoluble at temperatures high enough for TiC to be totally soluble. Consequently, TiN forms, often in liquid, and uses as much nitrogen as is dictated by Ti/N ratio; thus TiC formed at lower temperature is virtually free from nitrogen.

It would seem reasonable to suppose that the metal atoms could also share the same lattice,giving rise to the mixed metal carbides, nitrides or carbonitrides. However, there is little evidence that this occurs to a marked degree although some intersolubility is likely with multiple microalloying additions.

Meyer and Heister-Kamp,[37] using an Arrhenius plot, determined the activation energy of these alloying systems. They found that activation energy was of the same magnitude, suggesting that the diffusion of microalloy metal atoms in ferrite controls the precipitation rate. A corollary is that the difference in kinetics and extent and efficiency of precipitation of Nb and Ti, compared to V, are due to greater solubility of VN/V_4C_3. Thus, the faster particle growth rate is caused by higher diffusion rates. The diffusion of vacancies associated with the non-stoichiometric nature of these nitrides/carbides cannot also be overlooked.

2.3 OTHER ELEMENTS OF IMPORTANCE TO PIPELINE STEELS

Manganese, carbon, copper, nickel, chromium and molybdenum are some of the elements whose importance to pipeline steels will be examined, albeit briefly. In addition, the impurity elements such as oxygen, sulphur and phosphorus will be mentioned.

2.3.1 MANGANESE AND CARBON

The addition of manganese to pipeline steels has a number of important effects. Addition in the range 1.0 to 1.5 %Mn lowers the temperature at which austenite transforms to polygonal ferrite by $50^{o}C$[47]. This results in a significant ferrite grain size refinement, and consequent increase in strength and toughness. But this may cause the austenite to transform to acicular ferrite rather than polygonal ferrite. Higher manganese levels promote the transformation of the austenite to microstructures comprising mixed phases such as M-A*, bainite, etc. The segregation of manganese levels in excess of 1.0 %, has been identified as one of the causes of hydrogen induced cracking[48]. Manganese contents in excess of 1.0 % may cause the steel to be dirty by reacting with the silica component of the refractory lining, but this problem is usually obviated by handling the steel in high alumina or basic lined refractory vessels.[49-50]

The restriction of the carbon content to the range of

* M-A = Martensite-Austenite

0.05 – 0.15 % for ferrite-pearlite steels is dictated by the need for weldability and high shelf energies. In fact, the recent acicular ferrite bainitic steels contain carbon as low as 0.03 %. The effect of higher carbon contents on increasing the amount of weld underbead cracking is well documented[31] and the coefficient of carbon in the carbon equivalent equation indicates this danger. Bendability and other toughness requirements dictate relatively low carbon contents[31]. The small decrease in yield strength caused by this lowering of the carbon content can easily be compensated for by the use of other strengthening mechanisms.

2.3.2 MOLYBDENUM

Molybdenum kinetically suppresses ferrite transformation and, therefore slightly lowers transformation temperature. This can cause a slight reduction in grain size and hence moderate increase in strength.

More significantly, molybdenum suppresses the formation of pearlite. As a result, in the steels that contain high percentage Mo, the austenite remaining after polygonal ferrite formation will transform to lower temperature products such as acicular ferrite, bainite and a martensite-austenite (M-A) constituent. In addition, the local segregation of alloying elements could encourage bainite or martensite formation in the segregated area by virtue of enhanced hardenability.

2.3.3 COPPER, NICKEL AND CHROMIUM

Copper and nickel are expected to have effects on the transformation behaviour similar to that of manganese, in that they lower the transformation temperature. These two elements may thus refine the grain size slightly and lead to less precipitation of carbo-nitrides in the ferrite. They may also contribute to a small solid solution hardening effect[47]. The effects of copper and nickel on transition temperature in these steels is not well documented, although nickel in larger amounts has a beneficial effect in lowering the transition temperature because of its effect on cross-slip. Andrews[53] evolved an equation showing the effect of various alloying elements on the austenite to ferrite transformation temperature. The regression coefficient of nickel in the equation is more negative than that of manganese, thus suggesting that the former has a more depressing influence than the latter.

It has been reported[48,54] that Cu in the range (0.20-0.30%) reduces corrosion rate in hydrogen sulphide environment within the pH range 4.8 to 5.6 or greater than 5.0[48], and hence minimises the incident of hydrogen induced cracking.

Chromium has been studied least of all the alloying additions, but it is expected that its major effect in conjunction with molybdenum is to alter the transformation characteristics of the steel and promote the formation of the M-A constituent.

2.3.4 SULPHUR, OXYGEN AND PHOSPHORUS

A downward trend is advocated for these elements. The first two lead to the formation of non-metallic inclusions whose deleterious influence on toughness, for example, is well documented[57,59-64]. The last element is known to segregate enormously[48], thus promoting hydrogen induced cracking, possibly through the formation of hard low transformation products. Baker et al[56] summarised in Fig.2 the trend of sulphur levels in pipeline steels.

The influence of some of these alloying elements is summarised in Fig.16 and Tables 3 and 4.

2.4 TYPES OF LINE PIPE STEELS

In general, the microstructural features of HSLA steels are too complex to be described in a manner which is sufficiently quantitative to enable a definite comparison to be made between the microstructure and the resultant mechanical properties. However, a general classification can be made based on their major microstructural constituent and deformation behaviour. These are conventional ferrite-pearlite steels, which have discontinuous yielding behaviour, and bainite/acicular ferrite steels and multiple phase steels, which both have continuous yielding behaviour.

2.4.1 FERRITE-PEARLITE STEELS

The majority of conventional HSLA steels, which are used in pipelines, drilling rigs and general off-shore applications comprise mainly ferrite-pearlite structures. The major disadvantage of this family of steels is the depression of tensile/yield stress during the forming of pipe from plate by the U-O-E process, this is known as the Bauschinger effect, but recent evidence[65] has shown that this effect can be eliminated by carrying out the U-O-E process under warm conditions.

2.4.2 ACICULAR FERRITE STEELS

There is still controversy regarding the distinction between acicular ferrite and bainite, but the crucial difference is the very low carbon content (0.03-0.06 %)[28,66-68] of the

acicular ferrite steel, which by removing interlath carbides, produces much improved toughness. In addition, carbides precipitate between the ferrite laths in upper bainite, while in lower bainite, the carbides are finely distributed in the matrix, both having specific orientation relationship between the ferrite lath and carbide[25].

Acicular ferrite has many morphological similarities to low carbon bainite, comprising lath like ferrite grains containing high dislocation density. This ferrite forms by a diffusion controlled shear transformation, in packets in which the Kurdjumov-Sachs orientation variant are severely restricted[66,63]. Several such packets occur within a given austenite grain.

It is often quoted that acicular ferrite contains martensite islands making it in effect a dual phase structure, and that it forms at slightly higher temperature than upper bainite. As acicular ferrite is almost always produced from either fine recrystallised or thin uncrystallised controlled rolled austenite, the acceleration of transformation to bainite would inevitably lead to a higher transformation temperature.

The structure-property relationships are not so well understood as those of polygonal ferrite structures[70], largely due to complexity of structure and difficulty of obtaining qualitative measurements of many of the structural parameters. Because of the transformation mechanism the planar arrays of interphase precipitates do not occur, and precipitation strengthening is due to precipitation in the ferrite, most probably on the many dislocations present. This general

precipitation has been referred to as strain induced[66,71] but such a description should be reserved for conditions in which the rolling is carried out below Ar_3, when the ferrite may be genuinely deformed and yet not recrystallised due to the low temperature.

There is some controversy with respect to toughness of this structure, some workers[72] suggesting that 100 % acicular ferrite has a high DBTT* and the best results are attained when a small amount of very fine polygonal ferrite is mixed with acicular ferrite. However, this can slightly lower the proof stress. Other workers[73] suggest that a fully acicular ferrite of low carbon content (0.035 %) is required for good toughness. It is possible that some of these discrepancies may simply reflect the very important effect of carbon on the toughness of upper bainites. Little or no attention seems to have been given to the structure-property relationships of mixed low carbon acicular-polygonal ferrite structures. In fact, it is known that if polygonal ferrite is coarse grained the toughness deteriorates as also does the strength[72].

As might be expected, the principle of controlled rolling can be applied to the acicular ferrite steels. Generally, the greater the deformation and the lower the finish rolling temperature, the more polygonal ferrite is introduced in the structure, this ferrite will be fine as it is formed from fine recrystallised austenite, or very elongated unrecrystallised austenite. In acicular ferrite structures and bainites the DBTT

* DBTT = Ductile Brittle Transition Temperature (^{o}C)

is related to the fracture facet[74-76] size, which in turn, depends on the ferrite lath packet[77] or to prior austenite grain size[74,76,78]. It is sometimes difficult with very fine elongated austenite grains to establish the precise relationship between the austenite grain size and morphology, and the packet size, respectively, to relate them to the fracture facet size. Suffice it to say, however, that the finest or thinnest austenite grains are essential.

The composition of the acicular ferrite steels is also important as they depend on the hardenability effect depressing the transformation of the austenite into the acicular ferrite region. Consequently, the early steels contained 0.035%C, 1.4-2.0%Mn, 0.25-0.35%Mo with niobium[66-68]. Other details are documented elsewhere[25,66].

2.4.3 MULTIPHASE STEELS

Multiphase steels consist of a polygonal ferrite matrix with dispersions of second-phase particles. The second phase can be acicular ferrite, bainite, martensite or combinations of these, depending on alloy compositions and processing variables[25]. Multiphase steels are essentially similar in metallurgical principles to the dual phase steels developed for sheet applications, although the former are produced by controlled rolling, while the latter are produced mainly by intercritical annealing. The strength of multiphase steel is generally determined by the volume fraction and the type of the second phase. The transformation of the austenite to strong second phase introduces a high density of mobile dislocations

in the surrounding polygonal ferrite matrix, which allows the steel to be deformed at low stresses with continuous yielding. In addition, the multiphase steels generally have higher initial work hardening rates than the ferrite-pearlite and bainite/acicular ferrite steels. This causes the multiphase steel to have a high yield strength, approaching ultimate tensile strength, after pipe-forming.

Multiphase steels have a wide range of alloy compositions as shown in Table 2. In these steels sufficient alloying additions and/or the application of accelerated cooling after rolling is necessary to influence a strong second phase in place of pearlite in the ferrite matrix. Correlation of mechanical properties with microstructure is difficult because of the complexity of structural features (volume fraction, type and distribution of second phase). However, some general conclusions can be made. It has been shown that the amount of second phase should be above 4% to ensure a continuous stress-strain curve[25], although the type of second phase is also important. Martensite gives a stronger effect than bainite[25].

The size and distribution phase depends upon the severity of controlled rolling in the second stage (austenite non-recrystallisation region) when the reduction is not enough to produce homogeneous deformation, ferrite forms first at the earliest nucleation sites where deformation is highest. The second phase nucleates at sites where nucleation is less easy and hence tends to be coarse[25]. In plain carbon steel, where partial recrystallisation of austenite occurs in the lower temperature range of controlled rolling, coarse second phase

also forms. The results of Shiga et al[79] indicated that the presence of coarse second phase adversely affects the toughness, although Kim[25] reported conflicting results. The difference might be attributed to differences in the shape and distribution of the second phase. An increase in the volume fraction of second phase raises the strength without affecting DBTT, but with a deterioration of Charpy impact energy. Changing the type of second phase from the softer to the harder (e.g. from bainite to martensite) gives similar results.

The subsequent sections will concentrate on the ferrite-pearlite (conventional HSLA) steels in conformity with the present project.

2.5 REQUIREMENTS OF LINEPIPE STEELS

Some of the major requirements for this type of steel are listed below without necessarily ranking:

a) Ease of weldability

b) High yield strength

c) Low impact transition temperature

d) Good formability

e) Minimum cost

f) Corrosion resistance especially in sour environments.

Comprehensive requirements are summarised in Figures 3 and 4.

2.5.1 WELDABILITY

The advent of welding rather than rivetting as a method of joining necessitated weldability as a design criterion. Because of both longitudinal welding in pipe-mill (e.g. during the U.O.E. process) and circumferential welding on site, the plates for pipe must have very good weldability, which is typical of low carbon steels.

The criteria for maintaining a high level of weldability are the M_s temperature and the hardness of the martensite. Too low an M_s temperature and too high a hardness of the martensite leads to HAZ and weld cracking. An empirical carbon equivalent $(CE)^{(31,80-81)}$ is frequently used, above which welding has a high risk factor. One such carbon equivalent is given by:

$$CE = \%C + \frac{\%Mn}{6} + \frac{\%Si}{24} + \frac{(\%Ni + \%Cu)}{15} + \frac{(\%Cr + \%Mo)}{10} \qquad ...(1)$$

This is basically a statement of the observed effects of these elements on the depression of M_S temperature. Typical C.E. values are in the range 0.35 % to 0.43 %.

Another index of weldability is the cold cracking susceptibility of steel plate (Pcm), originally developed by Ito and Bessyo, quoted by Jones[82].

$$Pcm = \%C + \frac{\%Si}{30} + \frac{\%Mn + \%Cu + \%Cr}{20} + \frac{\%Ni}{60} + \frac{\%Mo}{15} + \frac{\%V}{10} + 5B \quad ..(2)$$

A low value is advocated, consistent with strength requirements. The details of welding are documented in API 5L, British Gas Supplementary Specification (BGC Specification Ps/LX1) and Canadian Specification Z245.1. Elaboration of other requirements is done in subsequent sections.

2.6 CRITICAL REVIEW OF STRENGTHENING MECHANISMS IN FERRITE-PEARLITE STEELS

This section appraises the strengthening mechanisms with emphasis on the merits and demerits of each in association with the requirements.

2.6.1 GRAIN SIZE

Refinement of the polygonal grain size increases the yield stress and yet decreases the impact transition temperature. In this respect the grain size is unique, and consequently, is the most desirable strengthening mechanism. This accounts for the extensive use of steels which are grain refined, for example by aluminium-nitrogen or niobium additions.

2.6.2 PEARLITE CONTENT

Pearlite has virtually no effect on the yield stress and, whilst causing an increase in tensile strength, it has a particularly detrimental effect on the impact transition temperatures. As will be shown later, pearlite also increases the work hardening rate. Consequently, increasing the pearlite content, i.e. the carbon content, is the most undesirable method of increasing the strength.

One feature devoid of full quantification is the effect of Fe_3C particle size at the ferrite grain boundaries. These carbides can become larger during the slow cooling of thick plates or during tempering for stress relief. It is known that

the DBTT is increased as these carbides become larger[83], but recent work also shows that they influence the yield and tensile strengths[66]. The reason for this latter effect is as yet uncertain, as also are the compositional and the heat treatment conditions which can eliminate such large carbides, but increasing manganese is certainly an advantage[47,66].

2.6.3 SOLID SOLUTION STRENGTHENING

Solute elements increase both the yield and tensile strengths, the effect largely depending on the difference in atomic size difference between the element and iron[31]. Both substitutional and interstitial solutes obey a linear relationship between strength and the square root of their concentration, but over the limited ranges encountered, this may be conveniently simplified to a linear relationship.

The effects of substitution solutes on strength are generally small, and it would be expensive and uneconomical to try to use them deliberately. On the other hand interstitials are more potent strengtheners, but their solubility is limited and so they cannot be used widely.

Both substitutional and interstitial solutes are,with the exception of nickel, harmful to the impact properties, especially the interstitial solutes. Solutes may have other effects such as altering the ferrite-pearlite ratio, refining the grain size by decreasing the transformation temperature (e.g. the addition of 1.0% to 1.5%Mn lowers the transformation temperature by 50°C) producing precipitation

effects (e.g. aluminium, titanium, niobium). This latter effect is very beneficial to impact properties as shown in Figure 5. Thus good impact properties are obtained in aluminium treated steels.

2.6.4 DISLOCATION STRENGTHENING

The flow stress, σ_f, i.e. yield stress is related to the dislocation density, (ρ) by[31]

$$\sigma_f = K\sqrt{\rho} \qquad \text{.....(3)}$$

where K is a constant.

In general, decreasing the transformation temperature by either alloying or increasing the cooling rate, both refines grain size and increases the dislocation density. This increased dislocation density increases the yield stress by about 50 MPa. Also dislocation-interaction with interstitial solutes[31,86] can cause added strengthening if the interstitial content is increased by faster cooling rates. All these effects lead to a decrease in impact toughness. It is also reported[25,47,31] that a low finish rolling temperature (temperature $\approx$ 730°C) increases dislocation density and impact transition temperature by the phenomenon of splitting or separation, probably associated with crystallographic textures.

2.6.5 PRECIPITATION STRENGTHENING

Precipitation effects markedly increase the strength but lower the impact resistance. Recent developments have combined

precipitation hardening with grain refinement by the use of niobium, vanadium or titanium. The effectiveness of these elements depends on their solubility in austenite, which controls the amount that can be dissolved and is thus available for precipitation. Several such data are available in literature[87-89] with the general form:

$$\text{Log } [B][C]^n = -\frac{X}{T} + Y \qquad \ldots\ldots(4)$$

where [ ] is the concentration of element in wt %

X and Y are constants, T is temperature in K

One such relationship is given for Nb(C,N)

$$\text{Log}\left[(Nb)\left(C + \frac{12}{14}N\right)\right] = \frac{-6770}{T} + 2.26 \qquad \ldots\ldots\ldots(5)$$

The incremental yield stress associated with precipitation hardening is reflected in the well known Ashby - Orowan model shown below[90]:

$$\sigma\sim\ (\text{MPa}) = \frac{5.9\sqrt{f}}{\bar{x}} \cdot \ln \frac{\bar{x}}{2.5 \times 10^{-4}} \qquad \ldots\ldots\ldots(6)$$

where $\sigma\sim$ = incremental yield stress (MPa)

f = volume fraction of precipitates

$\bar{x}$ = Mean Precipitate Size (μm)

Since $\frac{1}{\bar{x}}$ is the predominant function in the equation, the stress increment due to fine non-deformable precipitates increases with the reduction in precipitate size and increases in fine precipitate fraction as shown in Figure 6.

This incremental yield stress is accompanied by a detrimental effect on impact properties.

2.7 CONTROLLED PROCESSING OF CONVENTIONAL HSLA STEELS

An important factor in the evolution of polygonal ferrite structure is the thermomechanical processing of the steel. The essence of controlled rolling and controlled cooling is that the structure of the austenite is conditioned to allow it to transform to ferrite with the finest possible grain size and thus produce the greatest strength and optimum toughness. What is required therefore, is a high ferrite nucleation rate and a low growth rate, and indeed the nucleation and growth of the microalloy carbides/nitrides are also of utmost importance. In fact, nucleation and growth phenomena are important in thermomechanical processing, as they are also used to control recrystallisation during hot working[91-93].

The requirements to produce the necessary fine ferrite grain size are fine austenite grain size, or pancaked unrecrystallised grains, as these provide the greatest area of austenite grain boundary for ferrite nucleation. Nucleation can also occur on deformation bands in unrecrystallised austenite, on recovered substructural boundaries particularly if these contain precipitates, and on undissolved carbides/nitride particles[94]. Consequently, the two conditions to be aimed for are, either the finest possible recrystallised austenite, or heavily deformed but unrecrystallised austenite. It has long been established that the rate of recrystallisation and the grain size of the recrystallised austenite during hot rolling follows the classical laws of recrystallisation behaviour. Consequently, a small starting grain size would be beneficial, Fig.7, and one of the effects of microalloying additions is to achieve

this by particles of carbide/nitrides restricting austenite grain growth at the reheating temperature. The stability and solubility in austenite of various microalloy carbides and nitrides are, however, different (Figure 8). Nitrides are more stable than carbides, and the stability increases or solubility decreases, in the order V, Nb, Ti. Consequently, whereas the earlier generation of HSLA steels usually contained only a single microalloying addition, current steels tend to employ combinations e.g. Nb-V. The NbC or VN (using enhanced nitrogen) tend to restrict grain growth, whilst the more soluble VN is used to precipitation strengthen ferrite. More recently attention has been focussed on the potential use of Ti in combination with V in order to take advantage of the stability of TiN and its slower growth rate, which provides it with the capability to act as a grain growth inhibitor at high reheating temperatures prior to hot working. The amount of Ti needed is usually small, 0.01-0.015%, and whilst the control of such additions is difficult, it is by no means impossible with the currently available ladle injection techniques. Too large a Ti addition must be avoided otherwise large TiN particles are formed which do not restrict austenite grain growth. The extent of inhibition of grain growth is critically dependent on the dispersion of TiN, and, indeed, of any other grain growth inhibiting precipitates, variations in the size distribution and volume fraction being able to change the grain coarsening temperature up to 300°C[66] for the same steel composition. Consequently, attention should be paid to the effects of casting conditions on the precipitate distribution in continuously cast products, and to the effects of hot working prior to the slab stage in conventional ingot products.

Microalloying additions also have another important effect during controlled rolling, in that they retard recrystallisation. Much work has been done to identify the nucleation sites for recrystallisation[92-94] and it is now recognised that whilst the deformed austenite grain boundaries are the preferred nuclei, recrystallisation can also nucleate at the interfaces between recrystallised and unrecrystallised grains, on deformation bands in deformed coarse grains and on large microalloy carbide/nitride particles $> 0.5\,\mu m$ in diameter. The rate of recrystallisation in C-Mn steel is very rapid, but can be markedly retarded by the microalloying additions, Figure 9, and also by Mo and Mn. There have been extensive studies of austenite recrystallisation and the precipitation effects of microalloy carbides/nitrides in deformed austenite[35,95-96]. The long standing controversy as to whether this retardation of recrystallisation is the result of solute or precipitate now seems to have been solved. There is an accumulated body of evidence to show that dissolved solute atoms can retard both recovery and recrystallisation[94-97] but that a major effect is produced by precipitation in the unrecrystallised austenite[94-97]. This strain induced precipitation in austenite pins recovered sub-boundaries and inhibits recrystallisation. In order to do this, strain induced precipitation must occur prior to any substantial precipitation. Complications can be introduced by different effects of strain and strain rate on precipitation and recrystallisation kinetics and particularly by different solubilities of the various microalloy carbides and nitrides. It has been shown that the retarding effect of dissolved solute atoms on recrystallisation increases with increasing

strain caused by the solute in the austenite lattice, which influences the dislocation-solute interaction[98-99]. The effect seems to be, in ascending order of effectiveness, Mn, Al, V, Mo, Nb and Ti, on an atomic basis. The effect of microalloy carbide/nitride is less easy to predict, because it depends on the magnitude of precipitation which in turn depends on the strain applied, and the composition of the steel. Also, the overall retardation is compounded by both the solute and precipitation effects. The intensity of precipitation effect depends on the solubility of the microalloy carbides/nitrides, the greater the solubility the less the magnitude of the strain induced precipitation. Hence VC is less able to retard recrystallisation than VN at the same temperature. Whilst VN and NbC have reasonably similar solubilities, Nb seems to be much more effective in retarding recrystallisation than does V because of much greater solute effect of Nb[100]. But the severity of precipitation depends on the ratio of microalloying addition to either carbon or nitrogen with respect to the stoichiometric ratio of the appropriate carbide/nitride phase. Because the temperature dependence of the solubility is maximised at the stoichiometric ratio[58], the nearer the steel composition is to this ratio the greater will be the intensity of strain induced precipitation and greater retardation of recrystallisation will be observed. As all conventional HSLA steels are usually hypostoichiometric, a decrease in carbon content would therefore be expected to cause more strain induced precipitation, and hence greater retardation of recrystallisation. The overall alloy content of the steel is also important, carbide or nitride forming elements such as Mn and Mo decrease the activity coefficient of C or N but

increase that of Nb and V[66,96,100]. Due to this effect on the activity of the interstitial element, Mn and Mo increase the solubility of both VN and NbC[87,101] thus retarding their precipitation by lowering the supersaturation and giving rise to less strain induced precipitation.

The importance of retardation of recrystallisation during controlled rolling lies in the ability to use a low finishing temperature to produce elongated unrecrystallised austenite grains which can transform to very fine polygonal ferrite. This is one of the variants of controlled rolling which is derived from the classical work describing the main regimes for hot working[92-93]. However, the different microalloying elements lead to different finishing regimes to produce the heavily elongated unrecrystallised grains because of the variation in temperatures at which the different carbides/nitrides are predominantly strain induced to precipitate; for example, most rapid strain induced precipitation occurs for TiC/TiN at 1025°C[102] for NbC[96,100] and VN at 900°C[100] and for VC at 850°C[96,100].

Finishing temperatures below the Ar_3 are sometimes used and can give a pronounced increase in yield strength. The ferrite formed during rolling is deformed but does not recrystallise because of the inhibiting effects of microalloy carbide/nitride. This is only recovered ferrite,but the ferrite formed from the transformation of the unrecrystallised austenite is the normal dislocation-free polygonal ferrite. The higher strength is said to be due to the fine sub-grain structure in the deformed but unrecrystallised ferrite, and the very fine polygonal

ferrite formed during the transformation[66].

Conflicting effects on the DBTT have been reported[66]. In some cases DBTT is lowered, possibly due to textural effects producing splitting or separations and heavily polygonised sub-grain structure in which the subgrain boundaries are relatively high angle and thus behave in effect as grain boundaries[72]. On the other hand a low finishing temperature has been reported to increase DBTT, probably due to insufficient deformation resulting in less pronounced texturing and much lower angle polygonised sub-grain boundaries[57,85], or due to deformed ferrite not being recrystallised and giving high strength. It seems that this type of controlled rolling could be very difficult to operate; just as is continuum rolling[103] in which very heavy deformations at temperatures as low as 400-500°C in the ferrite region are used. These produce either a heavily textured, very fine recrystallised ferrite or a fine polygonised high angle, recovered ferrite sub-grain structure. All these effects increase the strength and decrease the DBTT.

The solubility, stability and precipitation kinetics of all the microalloy carbides and nitrides are different. The nitrides are much more stable and less soluble than the carbides[38,66]. Nitrogen, which has long been used in V steels, may therefore, become increasingly important in all micro-alloyed HSLA steels, especially if advantage is to be taken of the high stability and slow coarsening rate of TiN. The solubility of microalloy nitrides is about two orders of magnitude less than that of carbides in both austenite and

ferrite[38]. Also they are at least an order of magnitude less soluble in ferrite than in austenite[38,104], and so the supersaturation and driving force for precipitation is greatest for nitrides. Thus, nitrides occur in finer dispersions[105-106] which, if strain induced in austenite, may give more retardation of recrystallisation and inhibition of the growth of recrystallised grains. Because they occur also in larger volume fractions due to their lower solubility, they may, if formed in the ferrite, lead to greater precipitation-strengthening.

The use of multiple microalloying additions has led to the need to identify more precisely the precipitating phases. The belief that the carbides and nitrides of a given microalloying addition were completely mutually soluble to give a carbo-nitride of composition reflecting the carbon and nitrogen contents of the steel, may now be questioned. It has been shown, for example, that there are firm thermodynamic reasons[30-38] for suspecting that nitrides precipitate first, and when the nitrogen is used up, carbides precipitate. With multiple microalloying additions the situation becomes more complex, especially as under completely equilibrium conditions, many of the microalloyed carbides and nitrides are all mutually soluble to some extent[52], and indeed such mutual solubility has been observed using modern high resolution electron-optical analytical techniques[107]. Various models have been proposed in an attempt to predict precipitation sequences[34, 107] using assumptions of either complete miscibility or co-precipitation effects. These models tend to employ 'equilibrium' solubility data and do not consider the kinetic effects which

are so important. Of concern are the suggestions that the various microalloy carbide/nitride contain iron, and the iron content increases as the particle size decreases[108,109], this requires careful investigation because if it is true, it could call into question the validity of much of the work on solubility studies, as well as the relationship between the response of controlled rolling to stoichiometry. Such a study is important if it is supposed that future generations of HSLA steels will use even more complex combinations of microalloy additions, each of which has its own 'C' curve for carbide/nitride precipitation in both austenite and in ferrite. Such precipitation 'C' curves each occurring in particular temperature ranges, may then allow the optimum effects of each microalloy addition to be employed to the full in each controlled rolling regime.

2.7.1 CRITICAL ASPECTS TO BE CONSIDERED IN CONTROLLED PROCESSING OF THESE STEELS

(i) Strain induced precipitation in the austenite decreases the amount of precipitate available to form during and after transformation to ferrite, and so detracts from precipitation strengthening. However, besides preventing grain growth of the recrystallised austenite, the strain induced precipitates and microalloying elements in solution both increase the yield stress of the austenite[35,100]. When finishing temperature is low, this can materially increase the loads on the rolling mill.

(ii) Undissolved microalloy carbide/nitride precipitates at

the reheating temperature contribute nothing to strength and are generally so large as not to cause grain boundary pinning unless they are in very large volume fractions. This can be seen from the predictions of Gladman's Model[110] for grain growth inhibition, Figure 10. Consequently with the exception of TiN which is very stable and grows very slowly, there is no great benefit substantial enough to exceed the solubility at the reheating temperature. But the nearer the steel composition is to stoichiometry the more strain induced precipitate will be formed to inhibit recrystallisation and grain growth of the recrystallised grains, and also the greater will be the potential for precipitation strengthening of the ferrite. Undissolved carbides/nitrides greater than 0.5 μm in diameter are however capable of accelerated recrystallisation by particle stimulated nucleation[94].

2.7.2 CONTROLLED ROLLING METHODS

Controlled rolling of HSLA steels has been investigated by a number of workers[51,72,84-85,111]. A recent review[72] of controlled rolling has identified the methods which can be used to condition the austenite to produce the finest ferrite grain size and optimum precipitation strengthening in section sizes less than 40 mm.

2.7.2.1 METHODS FOR OPTIMUM PROPERTIES

(a) A low reheating temperature to produce a fine initial austenite grain size, but this can decrease the potential for subsequent precipitation hardening.

(b) Austenite grain refinement by recrystallisation which involves:

(i) Suitable pass schedules and reductions to obtain in the initial passes a fine, uniform recrystallised austenite.

(ii) Delay between roughing in the recrystallisation regime and finishing in the unrecrystallised regime.

(iii) Suitable reductions in the unrecrystallised regime and, in some cases, finishing below Ar_3, although this can cause difficulties.

As there are many combinations of these factors which can be successfully employed, each mill has its own preferred controlled rolling route. However, it is useful to identify two fairly typical processes applicable to different products.

2.7.3 LINE PIPE PRODUCTION

Line pipe is usually made on a plate mill, the difficulty being to give sufficient reduction per pass in the initial passes. The time between passes can produce interpass recrystallisation and uneven grain growth, so that a mixed grain structure is developed, which leads to inferior toughness. The steel is allowed to cool into the unrecrystallised regime, where large deformations are often required to produce very thin unrecrystallised grains which mitigate to some extent the problem of mixed grain size. This type of process slows production and is more difficult where size changes are frequent, but is economic on custom designed mills, and also, incongruously, on old mills which have a sufficiently low production rate not to be inconvenienced by controlled

delay[47]. As plate thickness increases it becomes increasingly difficult to produce the requisite deformation, to accept the holding delays and to withstand the increased mill loads.

2.7.3.1 PRODUCTION OF HOT ROLLED STRIP

Hot rolled strip for applications, employs a different process route because it is possible to employ accelerated cooling on the run-out table, followed by slow cooling in the coil. Roughing and finishing can employ very heavy reductions and the interpass time is very short, so that there is little time for recrystallisation and grain growth between passes. In the roughing train dynamic recrystallisation is common, whilst in the finish train the deformation is more likely to be in the unrecrystallised regime. It is possible to force recrystallisation to a very fine austenite grain size, even in the finishing train, by use of large reductions consistent with mill capacities and good terminal shapes.

Because the effective use of controlled rolling either to produce the finest recrystallised austenite or thin elongated unrecrystallised grains, prior to transformation, requires heavy reductions late in the rolling process, attention has been focussed on how very fine recrystallised grains may be produced without resort to heavy deformations at low temperatures[66]. In the past this was attempted by introducing large volume fractions of undissolved Nb(C,N) by increased niobium contents, and low reheating temperatures, with obvious loss of precipitation strengthening. Also, large

volume fractions of NbC could lead to hot tearing problems during continuous casting[66]. An alternative approach is to use a fine dispersion of a very stable precipitate, such as TiN, which is slow to coarsen and which will allow high reheating temperatures to be used to dissolve vanadium or niobium carbides/nitrides for adequate precipitation strengthening, and yet preserve a fine austenite grain size prior to rolling. By rolling, albeit with high deformations at high temperatures, such a fine initial grain size will produce fully recrystallised grains which also will be stabilised against growth by TiN or by an appropriate strain induced precipitation. This recrystallisation rolling[112-115] may enable many of the economic and production difficulties of the current controlled rolling practices to be overcome.

2.7.4 CONTROLLED COOLING

Interests in accelerated cooling subsequent to controlled rolling of plates have been motivated principally to increase throughput of rolling mills by the elimination of bottlenecks in cooling-bank areas[114,116-118].

The principal benefits as regards microstructure/properties in HSLA steel plate which are derived from the applications of accelerated cooling techniques are:-[112-114]

(i) Grain refinement of polygonal ferrite for a given austenite grain size by the virtue of reduced Ar_3-temperature and/or inhibition of austenite grain growth before transformation.

(ii) Augmented precipitation strengthening from microalloy additions, the lower the ferrite transformation temperature range resulting in fine precipitates.

(iii) Promotion of strong, tough low-carbon bainite if the steel chemistry is appropriate.

(iv) Possibility of reducing the carbon equivalent of the steel, which is advantageous from the point of view of weldability, formability and toughness, without detriment to strength; and

(v) Elimination of pearlite banding.

Controlled cooling can also be used to improve the properties in thick sections by lowering transformation temperature to promote further ferrite-grain refinement. This can be achieved by blast or water spray, but martensite or bainite formation at the surface must be avoided.

Process optimisation calls for careful control of Finish Rolling Temperature (FRT), cooling rate and water-end temperature. Systematic investigations[113,117-118] have established FRT of above 800°C for the effectiveness of accelerated cooling. Such a high FRT, greater than Ar_3, appears to be reminiscent of on-line accelerated cooling (OLAC) process. These workers suggested a cooling rate in the range (5-10)°C per second as the optimum. The water-end-temperature at which normal air cooling is resumed should be controlled. Temperatures of 500°C and 600°C have been recommended[117] for various API grades in conformity with structure-property relationship.

Another important consideration is the austenite grain size existing immediately preceding the start of accelerated cooling. To prevent bainite formation, hardenability must not be high and rolled austenite grain size should be fine.

A major drawback of accelerated cooling is the maintenance of acceptable shape and flatness, the distortion arising as a result of the transformation of austenite at different points in time through the thickness, furthermore, the natural temperature difference between the edges and the centre is accentuated. In commercial systems for accelerated cooling of plate, such as that developed at Nippon-Kokan in Japan[112], the cooling arrangement incorporates levellers and straighteners together with on-line control of flatness as well as the cooling condition.

Another variant of controlled cooling is the interpass cooling stimulated by throughput maximisation via reduction in processing time. Hence, some investigation of the application of accelerated cooling between individual roughing and finishing passes has been carried out[112]. The process runs into the possible danger of generating mixed structure/grain size because prolonged exposure to water during the hold period may promote differential cooling rate between surface layers and the core, but limited work has claimed that the conventional rolled steel exhibited equivalent properties with one subjected to interpass cooling[112]. Further work is suggested.

2.7.5 THE EVOLUTION OF THE AUSTENITE MICROSTRUCTURE

During controlled rolling the paramount requirement is the production of the conditioned austenite to produce the finest possible ferrite grain size. Attempts are therefore being made to predict and calculate the evolved austenite grain size and morphology during the controlled rolling process[84,112,115,119-122], and also the ferrite grain size developed from the austenite during transformation[66,121]. These studies use the temperature and stress dependence of the strain rate, and the strain during a pass on the recrystallisation rate and recrystallised grain size, the effect of initial grain size on recrystallisation kinetics and recrystallised grain size, and the kinetics of grain growth during the interpass interval, to calculate the grain size developed during each pass of a rolling sequence. Equations are produced describing the dependence of the recrystallised grain size on the initial grain size, the strain or strain rate, and the temperature. Some of these equations are produced by empirical analysis of data, whilst others are developed from basic principles. These equations can then be fed into a computer program for calculating the recrystallised grain size after each pass, and hence the evolution of the austenite structure.

A further refinement is to allow for the elongation of the unrecrystallised grains in terms of an 'effective' grain size which incorporates the effective austenite grain boundary area. Consideration of rolling in the non-recrystallisation regime is possible[93,123]. The evolved austenite grain size can then be used to predict the ferrite grain size.

In order to apply these sophisticated calculations to an actual rolling mill requires that strain, strain rate and temperature in each pass are not only known, but are also constant. Simply to obtain data on these parameters for a commercial mill is not easy, and it has also been shown recently that major variations in the parameters can occur transiently during any particular rolling pass[66]. Clearly much more work requires to be done in this important field of study. It is not beyond the bounds of possibility that by making measurements on a mill during actual rolling it may be possible, by a computerised feed-back technique, to continually adjust the rolling parameters, not only to simply control the physical dimensions and shape of the rolled product, but also to continually monitor the evolution of the microstructure[66].

2.7.6 TRANSFORMATION OF AUSTENITE

The requirement for finest ferrite grain size necessitates a high ferrite nucleation rate during the transformation. As ferrite nucleates predominantly at austenite grain boundaries, the need for a fine austenite grain size is apparent. The parameter which has often been used to indicate the nucleation frequency for ferrite is the austenite grain boundary area per unit volume, S_V[93,114], which increases with a refinement of the recrystallised austenite grain size and with increasing elongation of the unrecrystallised grains, Figure 11. It has been suggested that because the driving force for ferrite formation is small, a few hundred $J\,mol^{-1}$ even at large undercooling, only the most potent nucleation sites will be

effective[124-125]. As it was shown that for a given Sv, the ferrite grain size was finer when produced from unrecrystallised austenite[94,123], Figure 12, then it seemed that ferrite nucleated more potently at the deformed austenite grain boundaries. This was attributed to serrations or bulges at such boundaries[124] acting as particularly potent nucleation sites, and so it was concluded that elongated austenite grains were highly desirable. This is in fact so, particularly if they are so thin that the ferrite grains from opposite boundaries can impinge with minimum growth. However, more recent work[121,123] has shown that at very high Sv values i.e. small austenite grain sizes, the ferrite grain size depends only on Sv irrespective of austenite grain shape. Thus, for the most effective austenite grain refinement, deformation below the austenite recrystallisation temperature may not be necessary: all that is required is a very fine austenite grain size. Hence the potential for recrystallisation rolling. The various nucleation sites for ferrite have been well documented[123]. They are not only austenite grain boundaries, but also include second phase particles (particularly undissolved microalloy carbides/nitrides), recovered sub-grain boundaries, especially if decorated by precipitates, and even non-coherent ledges on twin boundaries. A mechanism is now also available to explain multiple or cascade ferrite nucleation[123] which has long been known to be associated with deformed austenite boundaries. Because many of these sites occur particularly in unrecrystallised austenite, the finest ferrite grain size will be produced from the finest austenite rolled to a maximum extent below the recrystallisation temperature[93], Figure 13. An important question,

however, is how fine must the austenite be, which depends on the ratio of the austenite grain size to ferrite grain size. As shown in Figure 13, the ferrite grain size can almost equal the austenite grain size if the latter is very fine, but for large austenite grain sizes the ferrite grain size may be less than one tenth of that of the austenite[123].

A useful method of refining the ferrite size for a given austenite grain size is to decrease the transformation temperature. This increases the ferrite nucleation rate and the effect may be achieved by alloying (the reason for high Mn content in HSLA steels), or by increasing the cooling rate. Care must be taken not to depress the transformation temperature too far, otherwise bainite may form and lower the yield stress, as well as impairing toughness. However the introduction of bainite into the structure eliminates discontinuous yield and minimises the Bauschinger effect which has advantages in line pipe production[35,47]. Bainite is more readily produced in steels which contain small molybdenum additions which suppress pearlite formation and result in structures giving polygonal ferrite with bainite or acicular ferrite[47].

An interesting feature is the increase in the transformation temperature which occurs when unrecrystallised austenite is transformed at a given cooling rate[66]. This can be explained by the acceleration of the transformation by strain inducement. It might be expected that this increase in transformation temperature would produce coarser ferrite, but this is not the case, presumably due to the overall ferrite nucleation rate in unrecrystallised austenite. Studies of the rate of nucleation

and growth in austenite deformed and recovered to various extents would be useful.

In plate rolling, the cooling rate is largely controlled by the plate thickness. Due to practical difficulties in controlled rolling the thicker plates, these are often normalised. In order to optimise the strength and toughness, some form of accelerated cooling is not infrequently used to increase the cooling, decrease the transformation temperature and refine the ferrite grain size. The transformation temperature also controls the size and distribution of precipitates in ferrite. Recently an equation has been obtained which defines the ferrite grain size in terms of the recrystallised austenite grain size and rate of cooling[112] as shown below:-

$$D^{\alpha} = 3.8 + 0.18D^{\gamma} + 1.4\left(\frac{dT}{dt}\right)^{-\frac{1}{2}} \qquad \ldots\ldots\ldots(7)$$

where, D^{α} and D^{γ} refer to the recrystallised ferrite and austenite grains.

$\frac{dT}{dt}$ refers to the cooling rate.

In general it would be expected that the constants in the equation would vary with steel composition and possibly also with varying austenite morphology.

2.7.7 CARBIDE/NITRIDE PRECIPITATION IN AUSTENITE

Precipitation is sluggish in undeformed austenite, although more rapid when strain induced in unrecrystallised or recovered austenite. The intensity of such precipitation is controlled by the amount of retained strain, which determines

the dislocation density and distribution, and by the degree of supersaturation as determined by the solubility-temperature relationships. The crystallographic match of the precipitate to the matrix austenite is also important, and whilst the orientation is the same cube-on-cube relationship for all microalloy carbides/nitrides, the misfit between the lattice depends mainly on the carbide/nitride lattice parameters. AlN is the exception, being of hexagonal structure, and it is not surprising that it precipitates more slowly than the normal microalloy carbides/nitrides. It is clear that the progress of recrystallisation during controlled rolling is determined by the rate of coarsening of strain induced precipitates[66]. Much work is required to study the kinetics of coarsening, as the finest and most stable distribution of precipitates is required. Under dynamic condition, it has been indicated[126] that this coarsening for Nb(C,N) obeys the kinetic laws indicating dislocation precipitation. Similar work on V-Nb steels in which the precipitating phase was (V.Nb)(C,N) did not find a similar effect[66]. It is apparent that further work is required, although some information on the growth rate of various alloy carbides, including VC and NbC in deformed austenite is available[127]. Besides inhibiting recrystallisation, the precipitates formed in the austenite also inhibit grain growth of recrystallised austenite. In general it has been shown that the Gladman-Pickering[94,128] model seems to be obeyed, in which the temperature dependence of grain coarsening is controlled by both the growth and solution of the precipitates, but some complex effects have been observed in Al-V steels[94]. These are interpreted as due to the interactions between AlN and VN, and due to the supersaturation

dependence of the rate of growth of these precipitates. It might be anticipated that even more complex effects would result from multiple Al-V-Nb-Ti microalloying additions, particularly in the presence of nitrogen.

2.7.7.1 CARBIDE/NITRIDE PRECIPITATION IN FERRITE DURING AND AFTER TRANSFORMATION

The precipitates formed in austenite do not contribute to the precipitation strengthening in the ferrite, and in fact detract from it. However, only a portion of the available precipitate is formed in the austenite, that remaining in solution in the austenite then precipitating either:

(i) as interphase precipitates at the austenite-ferrite interface during the transformation, the precipitates occurring as planar arrays.

Basically, these interphase precipitations occur both statically and dynamically[32]. While the former is portrayed by the Al-Cu system, the latter is exhibited by microalloyed steels. Two mechanisms have been found to occur[32,129], these are shown in Figures 14a and 14b. In the case of ledge mechanism, step migration occurs along planar interfaces and in the other the interface bows around the precipitate. However, this alternative mechanism does not predominate in microalloyed steels, it has been observed in steels containing copper (e.g. Fe-2Cu-2Ni) which can precipitate during the γ/α transformation[32,130].

(ii) in the ferrite after transformation has occurred in

which case the precipitates form on dislocations, or generally in the matrix if the dislocation density is low. The precise nature of the precipitate morphology and distribution depends on the supersaturation as indicated by the solubility of the phase, the rate of cooling which is deterministic with regard to the kinetics of precipitation, and the dislocation density as determined by the transformation temperature which, in turn, depends on cooling rate and the general alloy content of the steel. These complex effects are yet imperfectly understood, particularly with respect to what may happen on subsequent tempering[66].

These precipitates all cause strengthening of the ferrite which can be quantified by an Ashby-Orowan model[90]. They also increase the DBTT by about 0.3°C per MPa increase in yield stress[66].

When precipitation occurs during transformation of austenite, largely as interphase precipitation, the intensity of precipitation strengthening is a maximum when the steel has the stoichiometric composition for the precipitating phase[104] Figure 15. On the other hand precipitation strengthening, which occurs in the ferrite after transformation, is maximised when the stoichiometric ratio in the ferrite is achieved, and this does not occur at the stoichiometric composition for the alloy as a whole because much of the carbon is in the form of Fe_3C in the pearlite[104].

Whether there are major differences in the way interphase, dislocation nucleated or grain boundary precipitates affect

the DBTT is uncertain although some evidence indicates that all have similar effects[66].

The over-ageing characteristics of the carbides/nitrides precipitated in the ferrite are important as they control the ability to maintain strength and resist ferrite grain coarsening during slow cooling, and also influence the properties of the heat affected zone during welding operations. The rate of over-ageing, as depicted by the carbide/nitride particle growth characteristics is very different for the various microalloy species. The initial particle size before growth occurs is also different, and depends to a large extent on solubility which controls the degree of supersaturation. The greater the supersaturation, the finer the initial particle size, as shown by the fact that VN tends to produce a finer dispersion than VC[105]. It also appears that the stability of the carbide/nitride affects the growth rate, and it has been observed that VN grows less rapidly than VC[106]. The growth of the carbide/nitride precipitates occurs by Ostwald ripening, and from the well known equation it can be predicted that growth would be retarded by a decrease in diffusion rate (or an increase in its activation energy), a decreased molar volume of precipitates, a decrease in the solubility and a decrease in precipitate/matrix interfacial energy. These predictions tend to support the observation that VN grows more slowly than VC, but the operative diffusion rate is not always simply the diffusion rate for the appropriate elemental species because diffusion of vacancies is often the rate controlling feature. The effect of microalloying elements, especially in combination, and their interaction energy with

vacancies would seem to be important. Moreover, it has been shown that the early stages of growth for vanadium carbides/nitrides occurs by interface controlled particle growth[66,106] whereas later in the growth process pipe diffusion along dislocations was the controlling process. Presumably dislocations are pinned by the particles, but the important feature is that the diffusion conditions may alter during the growth process. Clearly more information is required on the effect of both single and multiple microalloy additions on the coarsening characteristics of the various carbides and nitrides. It can however be predicted that TiN would coarsen most slowly, although its use as a precipitation strengthening agent could be limited by its low solubility. It may well be that the slower growing precipitates give the least potential precipitation strengthening.

2.8 STRUCTURE-PROPERTY RELATIONSHIPS

The structure-property relationships in these steels are well established[57,74,90] as summarised in Figure 16. Perhaps the most important development was the appreciation that the ferrite grain size played a most important role in controlling the properties of ferrite in terms of both the yield stress[31] and the ductile-brittle transition temperature.[25,27,31,90]

There are two relationships on which the structure-property relationships are based:-

(i) Hall-Petch equation

$$\sigma_y = \sigma_i + K_y d^{-\frac{1}{2}} \qquad .....(8)$$

(ii) Petch equation

$$BT_c = \ln B - \ln C - \ln d^{-\frac{1}{2}} \qquad .....(9)$$

where

B and C are constants

σ_y is the yield stress

σ_i is friction stress

K_y is the grain size coefficient, related to the stress concentration required to activate slip-dislocation sources.

d is the grain size of polygonal ferrite and

T_c is the impact transition temperature.

2.8.1 YIELD STRESS

The equation relevant to plain C-Mn steel is:

$$\text{Yield stress } (MN/M^2) = 15.4\left[3.5+2.1(Mn)+5.4(Si)+23(N_f)+1.13d^{-\frac{1}{2}}\right] \quad \ldots\ldots\ldots(10)$$

where ( ) is the weight % of alloying element and

N_f is the free nitrogen.

It should be observed that:

a) Pearlite (i.e. carbon) has little or no effect on the yield stress of low carbon steels.

b) Free nitrogen (N_f) has a pronounced effect but its solubility is limited. Also it has a detrimental effect on impact properties, as will be shown later.

c) There is a pronounced strengthening effect of grain refinement.

2.8.2 TENSILE STRENGTH

The tensile strength of low carbon steels comprising ferrite-pearlite structures can be described by[31]

$$\text{Tensile strength } (MN/M^2) = 15.4\left[19.1+1.8(Mn)+5.4(Si)+0.25(\text{Pearlite})+0.5d^{-\frac{1}{2}}\right] \quad \ldots\ldots(11)$$

where (Pearlite) is the % pearlite in the structure. It should be noted that both pearlite and grain refinement contribute to tensile strength.

2.8.3 IMPACT TRANSITION TEMPERATURE

The impact transition temperature can be described by[31,86]

$$\text{Impact Transition Temperature } (^{o}C) = -19 + 44(Si) + 700(N_f) + 2.2(\text{Pearlite}) - 11.5d^{-\frac{1}{2}} \quad .....(12)$$

The main features of this equation are:

(a) Pearlite is detrimental

(b) Free nitrogen is very detrimental

(c) Substitutional solutes are detrimental

(d) There is no apparent effect of manganese because its effect is incorporated in that of grain size.

(e) Grain refinement is very beneficial.

2.9 BASIC DESIGN PHILOSOPHY

The design criteria used are:-

(a) A high yield stress and a low impact transition temperature. Therefore, alloying elements and microstructural parameters which give the least increase in impact transition temperature per unit increase in yield stress are required.

(b) Good weldability which is achieved by low carbon equivalent, low value of Pcm and low contents of liquatable solutes. Also, a minimum non-metallic inclusion content is required to prevent lamellar tearing.

(c) Good formability in flat rolled thin sections which require forming into pipes.

(d) Minimum cost.

Data showing the change in yield stress and impact transition temperature per weight % of the varying alloying elements are given in Table 3. The effect of varying microstructural and compositional parameters on the change in impact transitional temperature per 15 MN/M^2 increase in yield stress are shown in Table 4.

In conclusion, the basic design criterion is for the impact transition temperature per unit increase in yield strength to have the largest negative value, and the effect of the different compositional and microstructural parameters on this ratio has already been shown in Figure 16. It can be seen that a low carbon, Al grain refined high Mn steel is to be preferred, Al

being particularly beneficial as it removes much of the nitrogen as AlN. High energy absorbed as a measure of low temperature toughness is also mandatory in Arctic environments.

2.10 HYDROGEN SULPHIDE CRACKING IN LINE PIPE STEELS

Several recent reviews of hydrogen embrittlement have been made[134,164], hence this section will focus on line pipe degradation in sour environments. There is strong evidence[133,147] that sour gas is associated with lean oil/gas wells at depths of 4500 m (15000 ft) or more.

Hydrogen induced cracking(HIC) and sulphide stress corrosion cracking (SSCC) are two major forms of hydrogen embrittlement associated with oil industry equipment operating in sour gas environments. Examples of these forms of cracking are shown in Figures 17 and 18. HIC[131-132,139,144] otherwise called hydrogen pressure cracking (HPC), hydrogen induced blister cracking (HIBC), stepwise cracking (SWC), manifest themselves in steels of any strength level in the form of surface blisters and/or internal cracks in the absence of an applied stress, while SSCC occurs in high strength steels under an applied stress and in oil/gas line pipes in the region of high hardness around the weldment[48]. Both types of cracking have resulted in service failures[131-132,144]. Subsequent sections will concentrate on HIC which has been studied in the present project.

2.10.1 MECHANISMS OF HYDROGEN SULPHIDE CRACKING

The earliest theory proposed to account for the adverse effect of hydrogen on mechanical properties of the steel was the planar pressure theory [166]. According to this, hydrogen can precipitate in material internal cavities with

the resultant development of high internal pressures being sufficient to cause cracking and premature failure. To obtain such pressures, the external hydrogen activity (fugacity) should be high, which is the case of H_2S in sour environments.

Since the demonstration of embrittlement in a high strength steel exposed to 10^5 Pa (1 bar) hydrogen, the pressure theory has been found to be inadequate[163,167]. Embrittlement may be attributed to reduction of the interatomic cohesive forces by interstitial or trapped hydrogen[137-138], to a decrease in surface energy due to absorbed hydrogen[167]. Thus, the two mechanisms (pressure build-up and embrittlement) can operate simultaneously especially when the steel is exposed to an environment of high hydrogen activity/fugacity.

These mechanisms may be schematically synthesized as shown in Figure 19. Whatever the mechanism(s) operating, a crack will be initiated whenever $\sigma_T^H \geqslant \sigma_C^H$, which corresponds to a critical value C_K of the amount of hydrogen C_H trapped on the pre-existing defect.

Both C_H and C_K depend on a variety of parameters described in detail elsewhere[48,136-137,138,160], the summary of which follows.

2.10.1.1 SHAPE / MORPHOLOGY

This influences the final hydrogen pressure developing at the interface, the stress system around the defect/inclusion and the diffusion of hydrogen toward the defect/inclusion. All

available data points toward a detrimental effect of elongated inclusions i.e. C_K decreases as the shape becomes elongated.

2.10.1.2 SIZE

Large sizes are detrimental ie: C_K is lower and C_H larger because they increase the probability that the inclusion will be located in a zone of low cohesion (e.g. grain boundaries), while encouraging the entrapment of more hydrogen.

2.10.1.3 DISTRIBUTION AND DENSITY

A large density of homogeneously distributed inclusions may be beneficial because C_H on each particle increases slowly. However, this is a temporary solution as C_K may eventually be reached. A nil density of inclusion is obviously beneficial. On the other hand, heterogeneous distribution of inclusions (e.g. Stringers) will be deleterious because they will trap hydrogen and its effects (decohesion, stresses) will facilitate crack propagation.

2.10.1.4 NEIGHBOURING STRUCTURE

A hydrogen embrittlement sensitive structure will obviously facilitate crack initiation at an inclusion tip. Current data on the sensitivity of microstructures to hydrogen in ferritic materials give bainite and martensite as the most sensitive, followed by normalised, then tempered and normalised, quenched and tempered, and spheroidized structures. Of importance too is the fact that MnS stringers may be located in segregated

zones (that may be bainitic, have high hardness, and contain noxious elements such as phosphorus...) i.e. in low C_K regions.

2.10.1.5 GRAIN REFINEMENT

The beneficial effect of ferrite grain refinement is that hydrogen is more evenly distributed and consequently, has a less chance of attaining a critical concentration. This is attributed to the fact that a coarse grain structure has high angle grain boundaries that occlude large amounts of hydrogen.

2.10.2 FACTORS INFLUENCING HYDROGEN INDUCED CRACKING

The factors affecting hydrogen assisted cracking have been cited in literature[48,131-132,135-163]. Here only a brief discussion will be given leaving fine details to the literature cited above.

2.10.2.1 METALLURGICAL VARIABLES ASSOCIATED WITH HYDROGEN INDUCED CRACKING

The contributions of these variables to hydrogen cracking as identified by some workers are discussed in subsequent sections.

2.10.2.2. CASTING PRACTICE

The segregation of impurities and alloying elements during casting have been recognised as one of the important factors influencing hydrogen induced cracking of steels[132,143,150,154].

The first leads to concentrations of non-metallic inclusions, and the second regions of anomalous microstructure - both deleterious to the HIC resistance. Recent work by Jones et al[48] highlighted the importance of segregation. They deduced a mathematical expression to represent the susceptibility of the steel to HIC as C_s viz:

$$C_s = Mn + 0.23\theta \qquad .....(13)$$

where

Mn = the average Mn content in pearlite and segregated bands in Wt %

θ = the total projected length of inclusions in mm/mm^2, defined in Table 8A

They quoted a C_s value of 1.7 as the highest value to prevent HIC.

Many investigators have reported that the susceptibility of commercial steel plate to SWC depends on sampling location and that HIC is greatest at the most highly segregated part of the ingot[48,132,135,145,156,158,161] Moore and Warga[131] recommended that whenever possible, samples for SWC evaluation should be taken from the segregation zone (i.e. pipe section) of an ingot and other workers[132] have also followed this practice. They observed the effect of segregation on susceptibility to SWC in both ingot cast and continuously cast steels. It may be possible that centre line segregation was not eliminated in the latter steels by electromagnetic stirring.

Several investigators compared steels of different grades and

compositions including both concast and ingot cast, but reported no notable differences in SWC resistance attributable to casting mode[132]. Other investigators[143] have pointed out that continuous casting might be preferable to ingot casting in order to position the inclusions in a narrow zone away from the surfaces because they can never be completely eliminated.

It has also been reported that small laboratory ingots, or the small ingots used to make seamless tubing, minimise segregation. Thus, they have experienced difficulty in obtaining SWC in samples cut from laboratory ingots and have observed good SWC resistance in seamless tubing[132].

For a plate from large ingots, Ikeda et al through Biefer[132] have reported considerable variation in SWC susceptibility both along the length and breadth of the plate.

2.10.2.3 DEOXIDATION PRACTICE

Moore and Warga[131] have measured the susceptibility to SWC in a number of pipeline steels. They reported that: "with a single exception, all fully killed steels were more prone to cracking than the semi-killed steels", a difference attributable to the transition from ellipsoidal (lenticular) Type I MnS predominant in the latter to the elongated Type II MnS stringers dominant in the former. For the steels investigated, an analysis showed that sulphur, Mn and Si did not correlate with susceptibility to SWC, whereas Al did.

Since both deoxidation practices resulted in decreased environmental performance, this can be attributed to the large volume of inclusions present. In fact, a recent study by Charles et al[160] established 0.3% as a critical volume fraction of inclusions below which no hydrogen embrittlement occurred.

Others[132] reported that in killed and semi-killed steels, MnS inclusions were of the ellipsoidal Type I which are not easily elongated by hot rolling. Susceptibility to HIC was low in these steels and, when present, it tended to develop at manganese oxide - silicate inclusions.

2.10.2.4 NON-METALLIC INCLUSIONS (NMI)

Of all the variables associated with hydrogen assisted cracking NMI appeared to have the greatest impact.[48,131-132,135-137 141,145,150,156,161,166] Moore and Warga[131] linked the SWC service failures of sour gas transmission pipeline in 1970's with elongated Type II MnS inclusions in steel. Other workers[144] using fractography of the HIC fracture surface of a steel identified clusters of oxides (glassy silicates, alumina stringers) as well as elongated Type II MnS inclusions and massive niobium carbonitride as potential sites for HIC. A recent study[170] has indicated the presence of massive carbonitride on the path of HIC. In fact, some workers[48] have shown that HIC susceptibility (as measured by CLR, CTR or CSR) tends to increase with sulphur content, although the results have often been characterised by a wide degree of scatter. These abbreviations are defined in Figure 20. This

revelation has stimulated research into the reduction of inclusion content via sulphur and oxygen levels and inclusion shape modification. Consequently, it has been recommended that the sulphur and oxygen contents of pipeline steels should be reduced to $<$ 0.005 % (or even 0.002 % / 0.003 % for heavy sour gas/oil environments).

2.10.2.5 INCLUSION SHAPE CONTROL

Many authors[131] have shown that inclusions with sharp edges and large surfaces are the preferred sites for the initiation of SWC; geometrical shape of inclusions was considered to play a more important role than the chemical composition. Hence, other investigators[136-137] have shown that inclusion shape control by either calcium or rare earth metal (REM) additions can mitigate HIC problems provided that the optimum amount is added.[48,132,140,145-146,150,161] If the appropriate Ca/S or REM/S ratios are not achieved, cracking can occur on incompletely modified manganese sulphides or on clusters of Ca/REM rich inclusions as shown in Fig.21.

2.10.2.6 CONTROLLED ROLLING

Moore and Warga and other workers[131-132] indicated that for fully killed steels the deformability of MnS increases with decreasing temperature and thus, controlled rolling is conducive to the formation of elongated Type II MnS stringers especially at low finish-rolling temperature. Other workers[132] observed that SWC length increases with increasing inclusion length within the finish rolling temperature range 700^{o}C to

950°C. This suggests that the inclusions were deformable within this temperature range. For steel containing 0.016 % S, SWC susceptibility increased with decreasing finish rolling temperature in contrast to steel containing 0.007 % S where SWC was not observed in plates rolled at temperatures as low as 700°C.

2.10.2.6.1 COLD ROLLING

It has been suggested[132] that the effect of cold deformation upon SWC is important because there can be a certain amount of cold forming during manufacture and pipeline construction. Both cold rolling and cold tensile deformation along the rolling direction of the plates were investigated. It was found that heavy plastic reductions over 20 % can markedly increase the crack length of SWC, whereas reductions below 20 % can decrease crack length. This finding contrasted with the work of Parrini and De Vito quoted by Biefer[132] which indicated that the SWC length increased with cold strain over the range 2 to 16 %. Therefore, the effect of cold rolling is unclear and further work should be done.

2.10.2.7 MICROSTRUCTURE

There is much evidence[48,131-132,145,154] that crack propagation tends to occur along pearlite bands in ferrite-pearlite steels, or along bands of low temperature transformation products (martensite/bainite). It was also found that this anomalous structure was rich in Mn and P, thus suggesting strongly that the segregation of these elements is of concern

even though the effect of the latter should be of secondary importance because of the narrow and low concentration ranges found in modern pipeline steels. On the other hand, after SWC tests on two grades 448 (X65) line-pipe steels, Coldren and Tither (see Biefer[132]) reported that non-metallic inclusions were the only structural features consistently associated with SWC. They observed no distinct tendency for SWC to occur at pearlite bands in the Nb-V steel or at scattered islands of non-lamellar pearlite, bainite and martensite in the Mo-Nb steel.

2.10.2.8 HEAT TREATMENT

Some workers[150,154,156] have indicated that normalised or quenched and tempered steels are more resistant to HIC than controlled rolled steels, a difference attributed to both the greater uniformity of the microstructure in the heat treated steels (especially the quenched and tempered steels) and the plasticity of manganese sulphide. Of significance was the finding that the HIC susceptibility of the quenched and tempered steels was independent of Mn content, and uniform up to 1.6 %[150,161], a phenomenon that contrasted with the hot rolled steels of equivalent Mn level. Jones et al[148] confirmed the previous work but found no strict correspondence between HIC susceptibility and total projected length of NMI, possibly because of the complex nature of their steels.

2.10.2.9 WELDMENT

Moore and Warga[131] reported that sour gas pipeline failures

by SWC were always located near spiral welds but never associated them with defects. In contrast, Taira et al (see Biefer[132]) observed SWC in parent metal and in the heat affected zone but not in the weld metal. It was concluded that weld metal, with its dendritic microstructure and oxide inclusions dispersed in the form of globules, had good resistance to SWC. Other results cited elsewhere[132] have not produced any consistency. Therefore, further research is required in this area.

2.10.2.10 ALLOYING ELEMENTS

It has been shown that the addition of copper in the range 0.20 % to 0.30 % can impart resistance to SWC in mild sour conditions (typical of the BP test*) by the formation of protective films[48,132,145,150,154,159,161]. The films appear to be FeS_{1-x} enriched with Cu. Subsequently, it has been shown that copper-bearing steels will not form protective films in H_2S - containing environments with a pH less than 4.5[157] or 4.8[48] reminiscent of the immersion tests in NACE solution. Additions of Cr, Co and Ni singly or in combination can also be beneficial, details are cited elsewhere[48,132].

2.10.3 STRESS VARIABLES

Evidence[132] has been given to show that SWC occurs in steels having UTS values in the range 300 to 800 MPa (43 to 116 Ksi) and possibly above, but no correlation has been established between the steel strength and SWC susceptibility.

* This is a milder test relative to NACE for assessing HIC resistance

SWC occurs in unstressed steel by hydrogen segregation at inclusion-metal interfaces, and subsequent pressurisation of the interstice by molecular hydrogen to form blister-cracks in the rolling plane, as quoted by various workers.[136-137,140,163] The investigators postulated that the plastic regions generated at the blister-crack tips are embrittled by hydrogen, and transverse cracks propagate through the embrittled regions to link parallel cracks.

Recent work[132] has suggested that SWC is exhibited not only in unstressed specimens, but in steel under elastic tensile stresses. At intermediate stresses, SWC shows up as arrays of stacked microcracks, which may be joined by cracks transverse to the stress direction. Limited experiments on full size pipes have not indicated that residual stresses in the vicinity of a weld promote SWC, another area for more investigations.

2.10.4 ENVIRONMENTAL VARIABLES

Elaborate investigations[132] have shown that there is a tendency towards increased SWC in solutions with decreased pH in H_2S environments over the pH range 1–6. The same work has indicated that some resistant steels would only show SWC if exposed to a pH which is sufficiently low.

A comparison of four H_2S saturated test solutions has been made using the immersion SWC test[132]. It is reported that synthetic sea water produces higher corrosion rates and hydrogen absorption than pure water. In view of the higher pH

values of the H_2S saturated synthetic sea water, this would indicate that the dissolved salts (mostly chloride) must have increased the severity of the environment. It is suggested that the chloride containing NACE solution is more aggressive than 0.5% acetic acid alone, despite the similarity in pH of the two solutions.

Other workers[132] have confirmed the above trends, showing that synthetic sea water solutions with a pH of 3.5 to 4.3 promoted corrosion rates, hydrogen absorption and SWC compared with pure water solutions of similar conductivity.

It is evident[132,171] that typical corrosive ingredients in natural gas are CO_2 and H_2S. These gases, P_{CO_2} at ≥ 0.5 atm, and P_{H_2S} at ≥ 0.1 atm, respectively[171] become corrosive in the presence of moisture. The corrosion severity of natural gas is therefore, determined almost solely, by the values of P_{CO_2} and P_{H_2S}.

Although gas pipelines are not used in a corrosive environment in usual applications, a temperature drop in the gas flowing in a pipeline to its dew point, due to the temporary shutdown of the pipeline or an increase in the moisture due to failure of the dehydration, makes the fluid corrosive, leading to damage of the pipeline.

The effects of other environmental variables such as immersion solution test temperature and H_2S concentrations are detailed elsewhere[132].

It is clear from this appraisal that hydrogen assisted cracking is strongly affected by the level, nature and morphology of non-metallic inclusions, which may justify the mammoth investments in steel deoxidation, desulphurisation, dephosphorisation and inclusion shape control. Anomalous microstructures may be ranked second, even though this latter effect cannot be completely divorced from the segregation of impurities such as phosphorus.

3. EXPERIMENTAL PROCEDURES

3.1 GENERAL MELTING TECHNIQUE

A series of 18 kg pipeline steel scrap melts were made in a 25 kg capacity induction furnace of nominal power 60 kW and 3 kHz under an argon atmosphere to minimise oxidation. The charge was contained in an alumina rammed-in crucible of approximate dimensions 31 cm deep, 15 cm in diameter and 1 cm thick. At clear melt out the temperature was measured and at approximately 1600°C, deoxidation by aluminium was carried out, followed by alloying additions. These additions were made by plunging into the steel bath. After all were melted, the temperature was measured again in readiness for casting at a temperature of 1600°C ± 10°C.

A tapered cast iron mould of internal dimension 80mm X 80mm X 340 mm was used for casting the ingots. The molten steel was teemed into a previously heated refractory coated mould under argon shroud and subsequently covered with a proprietary hot topping compound. The slag left in the crucible was immediately decanted and the crucible cleaned out in readiness for subsequent melts.

The furnace assembly is shown in Figure 22.

3.2 STEEL ANALYSES

In each case, samples were taken from different sections of the ingot, i.e. top, bottom, middle and analysed for the

required elements and to ascertain the extent of segregation of these elements. Subsequently, the analysis was used to calculate the Carbon Equivalent (CE) and the cold cracking propensity, Pcm. Further predictions based on structure-property relationships were also made. A summary of the analyses is shown in Table 5. Sampling locations are shown in Figure 23.

3.3 HOMOGENEITY OF INGOTS

Prior to rolling, the homogeneity of the ingots was tested by the traditional sulphur-print technique to minimise the effect of sample location on properties such as HIC and the Charpy energy absorbed during impact testing.

Based on the understanding that segregation is a function of increasing sulphur and phosphorus levels, the ingot with the highest levels of these metalloids (S = 0.006%, P = 0.015%) was sectioned longitudinally, ground and finally subjected to the sulphur-print test. The result is shown in Figure 24 and indicates the insignificant amount of segregation. In addition, samples taken from different parts of the ingots showed consistency of analyses.

3.4 HOT ROLLING

Prior to rolling, each of the seven cast ingots was divided into four equal parts. These samples of initial thickness 32 $\pm$ 0.5 mm consistent with roll gap constraint, were packed in a compartmental annealing box and finally heated to the

required temperature. The furnace atmosphere was controlled by a gas mixture of 90% N_2 - 10% H_2. All the samples were soaked at 1250 ± 10°C for 75 ± 5 minutes and isothermally rolled at 1250 ± 10°C, 1100 ± 10°C, 1000 ± 10°C and 900 ± 10°C. Temperatures were monitored by means of a thermocouple sited near the heated specimens. These samples were subsequently designated A, B, C, and D in descending order of temperatures.

Isothermal rolling was carried out to simulate 'recrystallisation rolling', an industrially developing technique in which finish rolling temperature is usually in the range 900°C to 1000°C (112-114).

Hot rolling was carried on a two-high mill with 508 mm diameter rolls at a peripheral speed of 1.02 ms^{-1} and inter-pass heating was employed to minimise stock temperature drop. A final thickness of 11 ± 0.2 mm was achieved in four passes giving an overall reduction of 67%. This final reduction was aimed at because of the constraint on full size Charpy specimens. A summary of rolling schedules is shown in Table 6.

3.5 SECONDARY HEAT TREATMENT (STRESS RELIEVING)

Heat treatment was carried out to assess its effect on the properties of the rolled samples. Consequently, each rolled sample was divided into two equal lengths. For comparison, one group was left in the as rolled condition while the other was stress-relieved at 650 ± 10°C for 60 ± 5 minutes to simulate post weld heat treatment mandatory in many instances.

3.6 MECHANICAL TESTS

Charpy and tensile tests were conducted on samples to assess the effect of rolling schedules and subsequent heat treatments on these properties.

3.6.1 CHARPY V-NOTCH TEST

Charpy tests were carried out on full size standard specimens using an impact machine with a striker energy of 300 joules and linear striking velocity of 5 m/second.

The tests were conducted on specimens in the two orientations shown in Table 7 at a temperature of $-20 \pm 1^{o}C$ consistent with specification[117]. This temperature was achieved by a solution of solid carbon dioxide in acetone. To compensate for heat loss to the environment during transfer to the impact machine specimens were held in the solution at a temperature of the order of $5^{o}C$ below the actual test temperature. The final results tabulated are the average of two specimens.

3.6.2 TENSILE TESTS

These tests were conducted on all the fifty-six specimens using a 50 Tonne screw driven Instron machine.

Rectangular specimens of gauge length 3.40 ± 0.05 cm and cross-sectional area 40.32 mm^2 were used for the tests. The cross-head speed was fixed at 1 mm/sec.

The change in width and thickness of the specimens for the calculations of the fracture strain and percentage reduction in area was carried out on a shadow graph at X20 for the average of three measurements.

Calculations made were :-

a) Yield Stress (MPa) = $\frac{\text{Load at Yield (N)}}{\text{Original Cross Sectional Area}(m^2)}$

.....(14)

b) Ultimate Tensile Stress (MPa) = $\frac{\text{Maximum Load (N)}}{\text{Original Cross Section Area}\ (m^2)}$

.....(15)

c) Percentage Elongation = $\frac{\text{Change in Length (m)}}{\text{Original Length (m)}} \times 100$ ....(16)

d) Percentage Reduction in Area = $\frac{\text{Change in Area}(m^2)}{\text{Original Cross Sectional Area}(m^2)} \times 100$

.....(17)

e) Fracture Strain = $\text{Ln}\ \frac{Ao}{Af}$ .....(18)

where Ao and Af are the original and final cross sectional areas, respectively.

The results of mechanical tests reflecting a mean of two specimens with a maximum scatter in the range (10 - 30) MPa are shown in Table 7.

3.7 METALLOGRAPHY AND MICROANALYSIS

Metallographic examination involved mostly optical and

electron microscopy.

3.7.1 OPTICAL MICROSCOPY

Conventional specimen preparation was achieved using ¼μm diamond polishing prior to examination.

3.7.1.1 INCLUSION ASSESSMENT

The appraisal of non-metallic inclusion parameters was done on AMS SYSTEM III IMAGE ANALYSER at X40 (Courtesy of Professor Smallman, Met & Mats. Dept., Birmingham University.)

Samples were carefully metallographically prepared making sure that neither scratches nor etch pits were left on them after ¼μm finish, because the image analyser could not discriminate between these mechanical defects and non-metallic inclusions.

Subsequently, a hundred fields of each unetched sample were assessed from which the mean area fraction, mean length and the average projected length were obtained through the linked computer printout.

The results are tabulated (see Table 8).

3.7.1.2 FERRITE GRAIN SIZE MEASUREMENT

The assessment of grain size was done on all the samples in the rolling direction using the traditional mean linear

intercept (m.l.i.), sometimes referred to as Heyn intercept.

These samples were polished and etched in 2% nital and a total of fifty different fields were measured in each case using a Reichert inverted microscope.

Quantitatively, the mean grain size, $\bar{d}$, is given by:

$$\bar{d} = \frac{L}{x}/N \qquad \text{.....(19)}$$

where

L = Length of linear traverse (in this case 10 cm)

x = Magnification of microscope

N = Number of grains per linear traverse.

The values of m.l.i.($\bar{d}$) were subjected to statistical analysis as summarised in Table 9. Subsequently, the values of the mean polygonal ferrite grain size were fed into the relevant models of structure-property relationships to predict some of the theoretical properties.

3.7.1.3 OPTICAL MICROGRAPHS

Micrographs were taken in both unetched and etched conditions, the former to portray inclusion morphology and distribution and the latter to reveal the structure of the steels. These micrographs are shown in Figures 25,26,27.

3.7.2 ELECTRON MICROSCOPY

The electron microscopy investigation used Scanning Electron

Microscope (SEM), Transmission Electron Microscope (TEM) and Scanning Transmission Electron Microscope (STEM).

3.7.2.1 SEM INVESTIGATION

The nature of fracture surfaces of some Charpy specimens was investigated to ascertain the mode of fracture i.e. brittle or ductile or a mixture of both. SEM model S 150 was used. In addition, the same SEM in conjunction with the Link System was employed for the analysis of some inclusions including their concentration profiles. Typical micrographs were taken as shown in Figures 28 and 29.

3.7.2.2 STEM AND MICROANALYSIS

Conventional carbon extraction replicas were prepared from the selected samples identified in Table 10. Etching in 2% nital prior to carbon coating, scoring and eventual stripping by 5% nital produced a precipitate distribution suitable for microanalysis.

Individual precipitates were quantitatively analysed using STEM / EDAX of Philips Model EM 400 (at Birmingham University) for 200 live seconds. The intensities of the elements were subsequently fed into a computer from which the precipitate analyses in both Wt% and atom% were produced. The analysis shown in Table 10 is the mean of three readings. Qualitatively the precipitates were classed into coarse, intermediate and fine, as a time saving alternative to quantitative size range(s) bearing in mind that the objective of the transmiss-

ion work was to ascertain the precipitate morphology and chemistry and to relate these two parameters to the steel's composition. Subsequently, the analyses were used in modelling the sequence of precipitation. Eventually, micrographs showing precipitate morphologies, diffraction pattern and other features were taken on a Philips TEM and Jeol Model 100 B as shown in Figure 30.

3.8 EXAMINATION OF HIGH TEMPERATURE PRECIPITATION

This investigation was carried out to elucidate the STEM/EDAX analyses i.e. an attempt to ascertain the evolution of precipitate anayses, size and morphology. It involved hot rolling and quenching experiments.

3.8.1 HEAT TREATMENT

Two samples each of cast numbers 0,1,4, of Table 5 with initial thickness of 20 ± 1 mm were heated at $1250 \pm 10^{o}C$ for 48 ± 2 minutes. The furnace atmosphere was controlled by a gas mixture of $90\% N_2 - 10\% H_2$. Subsequently, one sample from each cast was quenched in a tank of water with agitation to disperse the vapour blanket. This quenching was done to differentiate between soluble and insoluble precipitates at $1250 \pm 10^{0}C$.

3.8.2 HOT ROLLING

The other three samples were hot rolled in the laboratory mill. Hot rolling was carried out on a two-high mill with

204 mm diameter rolls at a peripheral roll speed of 0.42 ms^{-1} for only one pass, achieving the same reduction of about 17 % as in the previous rolling.

Stock-temperature drop on emerging from the rolls was monitored by means of a thermocouple inserted into the sample. The samples were immediately quenched from the rolls.

Specimens were taken for optical and electron microscopy and the left over reheated under the same conditions, given a second pass and the reduction this time was 23 %. Samples were equally quenched immediately from the rolls and specimens for electron microscopy taken. A summary is presented in Table 12.

Finally, TEM, STEM/EDAX were employed as described previously.

3.9 HYDROGEN INDUCED CRACKING TEST

The test was carried out to ascertain the effects of composition and thermomechanical processing on the resistance of these steels to hydrogen assisted cracking, common phenomena encountered in sour oil and gas wells.

Steel coupons measuring 60 mm by 20 mm by 10 mm (all dimensions to the nearest 0.5 mm) were ground and subsequently degreased in acetone.

A typical NACE solution[131-132,172] consisting of 0.5 % acetic acid and 5 % sodium chloride solution was used and the pH noted.

The samples were loaded in a perspex box without the coupons making contact with each other. Subsequently, the NACE solution was poured gently onto the samples for complete immersion and the box made as airtight as possible. 10% sodium hydroxide solution was used as a trap on the exit side of the hydrogen sulphide flow as shown in Figure 3 1

De-aeration of the solution was commenced immediately with nitrogen purging at an optimum pressure 3 psi (20.7 MPa) for at least one hour consistent with specification[132].

Saturation was achieved by bubbling H_2S through the de-aerated solution at the rate of 45 cc/min/litre for the first hour and 17 cc/min/litre for 96 hours.

At the end of 96 hours, the test was stopped and the pH noted. A summary of experimental conditions are shown in Table 13

Finally coupons were sectioned into three pieces and examined metallographically for cracks both in unetched and very lightly etched conditions. The latter condition hopefully would reveal any crack covered by polishing debris. Cracks were examined both in face transverse to the rolling directions and rolling face.

4. RESULTS

4.1 COMPOSITION CONTROL

The good composition control achieved in this project is reflected in the results in Table 5. Of interest are the low values of oxygen, sulphur and phosphorus, the modern trend in pipeline steel development. The deleterious effects of these impurities and the basis for their downward trend is emphasised elsewhere.[48,57,59-64]

It can be seen from the same table that carbon is low and constant, typical of the Northern Borders pipe network specification of 0.10% mean carbon content and the North West Alaskan project of 0.12% maximum carbon content[82], a restriction intimately associated with weldability.

The Mn level of 1.31% maximum, Table 5, (in the range 1.13 - 1.31%) is much lower than those shown in Table 2, and is a compromise between its conflicting role in grain refinements by the depression of the austenite-ferrite transformation temperature[47] and its HIC inducement via segregation[48]. In addition, there is a cost benefit in achieving the lower bracket of the alloying element specification. This aim is portrayed in both the Mn and Si levels shown in Table 5.

4.2 MECHANICAL PROPERTIES

Generally, these are measured by strength values, ductility and toughness values as summarised in Tables 7, 14-16.

4.2.1 STRENGTHS

The trend for increasing strength, larger diameter and heavier wall thickness for pipeline is stimulated by the need for increased operating pressure[56,82]. Consequently, both yield and tensile strengths have become a design requirement.

4.2.1.1 YIELD STRESS (YS) OF THE AS ROLLED SAMPLES

The values are shown in the first column of Table 7. The letters A,B,C,D refer to the rolling temperatures of 1250°C, 1100°C, 1000°C and 900°C respectively, and the subscripts designate the serial numbers from Table 5. For simplicity and clarity, the steels are categorised into three, and this classification will be adopted throughout this and subsequent sections unless otherwise stated.

a) The base steels (i.e. steels with subscript 0)

It is evident from Table 7 that as the isothermal rolling temperature decreases, the yield stress diminishes in the order 354MPa, 346, (368MPa) and 314MPa ignoring the result for 1000°C rolling.

b) Nb-Ti-Al with varying V content (i.e. steels with subscripts 1,2,3)

The same pattern of decreasing yield stress with lower rolling temperature is repeated. In addition, the yield stress increases as the V content is raised, although there is only a marginal difference between the 0.030 V steel and the base steel, a difference attributable to the effect of the volume fraction of the precipitates.

c) Nb-V-Al with varying Ti content (i.e. steels with subscripts 4,5,6)

The rolling temperature - yield stress or composition - yield stress relationship appears to be erratic but falls within the range of values of the two previous classes. It can be said that there is no significant change in yield stress due to Ti additions at the levels 0.074, 0.037 and 0.027 (Wt %), thus raising a question mark about their economic and technological benefit for the thermomechanical regimes employed in this work.

4.2.1.2 U.T.S. OF THE AS-ROLLED SAMPLES

a) The base steels

These values of 480, 474, 466 and 432 MPa in descending order of the rolling temperature is analogous to those of the corresponding yield stress.

b) Nb-Ti-Al with varying V content

The U.T.S. values are of the same pattern as their corresponding yield stress values i.e. decreasing U.T.S. with diminishing rolling-temperature and the sum of the traditional microalloying contents.

c) Nb-V-Al with varying Ti content

Similar variable results to those of the corresponding yield stress values are shown. In addition, these values are intermediate to those of the base steel and the vanadium variants.

4.2.1.3 THE YIELD STRESS/U.T.S. RATIO

These values confirm the yield stress and U.T.S. values. It should be noted that since all the specimens displayed discontinuous yielding behaviour typical of ferrite-pearlite steels, the upper yield value was taken in each case.

All the ratios obtained fall within the range 0.70 to 0.82 in conformity with specification.[82]

4.2.2 DUCTILITY

Traditionally, this property is measured by the percentage elongation and percentage reduction in area. Another measure of ductility is the fracture strain or the total ductility to fracture. Generally, this is not usually quoted in pipeline specification but its importance is reflected in the formability equations shown later.

4.2.2.1 PERCENTAGE ELONGATION

a) The base steel

The values, in the range 36 to 30% in descending order of the rolling temperature, maintain a similar trend as the yield stress levels. Since the range is approximately 6% it can be said, therefore, that the percentage elongation has not changed very much with the rolling temperatures.

b) Nb-Ti-Al with varying V content

These steels exhibit similar values and patterns to the base steel. In fact no significant difference can be deduced, but there is a tendency for relatively higher values at both low V content and rolling temperature.

c) The Nb-V-Al with varying Ti content

The results are similar to those of the vanadium variants but tend to show slight improvement with decreasing rolling temperature. The relationship with the Ti level is not linear.

4.2.2.2 PERCENTAGE REDUCTION IN AREA

All the values fall within the range 70-81% indicating that these steels combine high strength with good ductility.

a) The base steel

The values exhibit no significant difference.

b) Nb-Ti-Al with varying V content

There is a definite improvement as both the V level and rolling temperature decrease, indicating the beneficial effect of low volume fraction of strengthening precipitates and ferrite grain refinement at 1000°C and 900°C.

c) Tne Nb-V-Al with varying Ti content

There is a general improvement at temperatures $\leq$1100°C. The values are virtually insensitive to the Ti levels employed in this work probably because the Ti rich precipitates were insoluble at the soaking temperature of 1250°C.

4.2.2.3 FRACTURE STRAIN

The values fall with the range 1.22 to 1.64.

a) The base steels

The sensitivity of the values to the rolling temperatures is very low. In addition, no definite pattern emerged within the constraints imposed by the number of rolling temperatures.

b) The Nb-Ti-Al with varying V content

Overall, the values are shown to improve with both decreasing V content and rolling temperatures, thus confirming the results of the percentage reduction in area. In fact, the best result is achieved at the lowest rolling temperature.

c) The Nb-V-Al with varying Ti content

Again, the results show improvement at temperatures of $\leq 1100^{o}C$. In addition, the values are enhanced in ascending order of Ti level but show slight deviation at $900^{o}C$. Overall, these values are slightly higher than the corresponding V levels.

4.2.3 TOUGHNESS

One of the methods of establishing toughness is the energy absorbed during the impact testing of Charpy type specimens. The values are usually quoted at $-20^{o}C$[117] and are shown in Table 7. These values are so high that most of the specimens did not break completely, thus acting as 'hammer-stoppers', hence the 'greater than sign' assigned to them.

a) The base steels

In the longitudinal orientation, the specimens displayed extremely high values of > 300 Joules. Similar results were portrayed by the transverse samples with a slight decrease at the rolling temperature of 1250°C.

b) The Nb-Ti-Al with varying V content

In the rolling direction, the highest V steels suffered a diminution of the order of 20 J in the temperature range 1250°C to 1000°C which contrasted with that of 900°C rolling. The corresponding transverse specimens showed slightly poorer values. Also, as the V level decreased, the energy absorbed improved marginally, reaching a peak at the lowest V content. This may be attributed to decreasing volume fraction of precipitates as the V content drops.

c) The Nb-V-Al with varying Ti content

Toughness appears to be insensitive to both rolling temperature and Ti content, ignoring the two low values of 245 J and 274 J for samples B4 (longitudinal direction) and B6 (transverse direction) respectively. Overall, these results tend to confirm the trend shown in both percentage reduction in area and the fracture strain.

Summarising, it appears that the future of recrystallisation hot rolling (typical of the last two rolling temperatures) for producing relatively higher strength lies in improving the contribution of grain size to strength. This can be achieved (as indicated in Section 2.7.4) by controlled cooling[114,116-118]

which achieves, inter alia, further ferrite grain refinement and reduced precipitate size, albeit with some sacrifice of toughness. The process optimisation involved in the use of accelerated cooling has already been indicated in Section 2.7.4.

4.3 LINEAR REGRESSION ANALYSES

Regression analyses are aimed at establishing a linear relationship between two variables in the form $Y = A \pm mx$, using standard notation. The relationships below are valid for each of the rolling temperatures.

4.3.1 1250°C ROLLING TEMPERATURE i.e. A - SERIES

YS (MPa) $\pm$ 41.3 = 471.3 - 2.9 % EL ; r = -0.4 ....19(a)

UTS(MPa) $\pm$ 51.2 = 680.8 - 5.7 % EL ; r = -0.6 .... (b)

YS (MPa) $\pm$ 41.3 = 1179.3 - 10.8 % RA ; r = -0.4 .... (c)

UTS(MPa) $\pm$ 51.2 = 1214.0 - 9.8 % RA ; r = -0.3 .... (d)

YS (MPa) $\pm$ 41.3 = 974.0 - 435.2 ε_T ; r = -0.7 .... (e)

UTS(MPa) $\pm$ 51.2 = 1228.6 - 540.0 ε_T ; r = -0.7 .... (f)

UTS(MPa) $\pm$ 51.2 = 81.6 + 1.1 YS ; r = 0.9 ..... (g)

4.3.2 1100°C ROLLING TEMPERATURE i.e. B-SERIES

YS (MPa) $\pm$ 52.8 = 868.3 - 14.9 % EL ; r = -0.5 ....20(a)

UTS(MPa) $\pm$ 62.6 = 1116.9 - 18.5 % EL ; r = -0.6 .... (b)

YS (MPa) $\pm$ 52.8 = 898.6 - 7.3 % RA ; r = -0.8 .... (c)

UTS(MPa) $\pm$ 62.6 = 1150.4 - 9.1 % RA ; r = -0.9 .... (d)

YS (MPa) $\pm$ 52.8 = 601.4 - 180.9 ε_T ; r = -0.8 .... (e)

UTS(MPa) $\pm$ 62.6 = 784.1 - 224.2 ε_T ; r = -0.9 .... (f)

UTS(MPa) $\pm$ 62.6 = 66.4 + 1.2 YS ; r = 0.98 .... (g)

4.3.3 1000°C ROLLING TEMPERATURE i.e. C-SERIES

YS (MPa) ± 23.7 = 338.7 + 0.7%EL ; r = 0.2 ....21(a)

UTS(MPa) ± 6.8 = 452.4 + 0.4%EL ; r = 0.4 .... (b)

YS (MPa) ± 23.7 = 328.8 + 0.5%RA ; r = 0.1 .... (c)

UTS(MPa) ± 6.8 = 420.6 + 0.6%RA ; r = 0.6 .... (d)

YS (MPa) ± 23.7 = 345.9 + 12.2 ε_T ; r = 0.1 .... (e)

UTS(MPa) ± 6.8 = 444.5 + 16.4 ε_T ; r = 0.6 .... (f)

UTS(MPa) ± 6.8 = 417.2 + 0.1 YS ; r = 0.5 .... (g)

4.3.4 900°C ROLLING TEMPERATURE i.e. D-SERIES

YS (MPa) ± 28.0 = 316.2 + 0.4%EL ; r = 0.1 ....22(a)

UTS(MPa) ± 22.1 = 409.7 + 1.1%EL ; r = 0.3 .... (b)

YS (MPa) ± 28.0 = 253.0 + 1.0%RA ; r = 0.2 .... (c)

UTS(MPa) ± 22.1 = 320.3 + 1.7%RA ; r = 0.3 .... (d)

YS (MPa) ± 28.0 = 303.4 + 18.5 ε_T ; r = 0.1 .... (e)

UTS(MPa) ± 22.1 = 395.5 + 36.2 ε_T ; r = 0.3 .... (f)

UTS(MPa) ± 22.1 = 238.6 + 0.6 YS ; r = 0.8 .... (g)

In all cases:

YS = yield stress

UTS = ultimate tensile stress

%EL = percentage elongation

%RA = percentage reduction in area

ε_T = fracture strain

r = regression coefficient

It is apparent from equations that rolling at temperatures $\geqslant$1100°C results in the usual increasing strength - decreasing

ductility relationship. This differs from the results of rolling at 1000°C and 900°C. This evidence is clearly born out in the sign of the slopes and regression coefficients. It can be deduced that the degree of scatter (measured by the modulus of the regression coefficients) is more for the 1000°C and 900°C rolled specimens than the A and B - Series.

In all but the C-Series, the UTS - YS relationship appears to give the best fit. i.e. consistently high values of regression coefficients almost approaching its maximum value of unity after 1100°C rolling.

4.4 EFFECT OF STRESS RELIEVING TREATMENT AT 650°C

These regression analyses have been repeated to establish the effect or otherwise of such thermal treatment on the relationships discussed previously. The definitions of symbols remain unchanged

4.4.1 A-SERIES

YS (MPa) $\pm$ 46.5 = 481.3 - 2.9 %EL ; r = -0.9 ....23(a)

UTS(MPa) $\pm$ 66.1 = 568.0 - 2.3 %EL ; r = -0.2 .... (b)

YS (MPa) $\pm$ 46.5 = 1664.3 - 16.7 %RA ; r = -0.8 .... (c)

UTS(MPa) $\pm$ 66.1 = 1837.1 - 17.6 %RA ; r = -0.6 .... (d)

YS (MPa) $\pm$ 46.5 = 961.9 - 398.6 ε_T ; r = -0.9 .... (e)

UTS(MPa) $\pm$ 66.1 = 1159.0 - 461.3 ε_T ; r = -0.7 .... (f)

UTS(MPa) $\pm$ 66.1 = -18.3 + 1.3 YS ; r = 0.9 .... (g)

4.4.2 B - SERIES

YS (MPa) $\pm$ 51.1 = 693.8 - 10.4 %EL ; r = -0.9 ....24(a)

UTS(MPa) $\pm$ 48.4 = 777.8 - 9.4 %EL ; r = -0.8 .... (b)

YS (MPa) $\pm$ 51.1 = 1054.0 - 9.3 %RA ; r = -0.7 .... (c)

UTS(MPa) $\pm$ 48.4 = 983.4 - 6.9 %RA ; r = -0.5 .... (d)

YS (MPa) $\pm$ 51.1 = 662.1 - 221.1 ε_T ; r = -0.7 .... (e)

UTS(MPa) $\pm$ 51.1 = 693.4 - 163.4 ε_T ; r = -0.5 .... (f)

4.4.3 C - SERIES

YS (MPa) $\pm$ 45.8 = 122.4 + 6.8 % EL ; r = 0.5 ....25(a)

UTS(MPa) $\pm$ 22.0 = 430.8 + 0.7 % EL ; r = 0.1 .... (b)

YS (MPa) $\pm$ 45.8 = 57.3 + 4.1 % RA ; r = 0.7 .... (c)

UTS(MPa) $\pm$ 22.0 = 369.1 + 1.1 % RA ; r = 0.4 .... (d)

YS (MPa) $\pm$ 45.8 = 225.4 + 97.1 ε_T ; r = 0.7 .... (e)

UTS(MPa) $\pm$ 22.0 = 419.0 + 25.0 ε_T ; r = 0.4 .... (f)

UTS(MPa) $\pm$ 22.0 = 429.5 + 0.1 YS ; r = 0.8 .... (g)

4.4.4 D - SERIES

YS (MPa) $\pm$ 34.8 = 320.6 + 0.8 % EL ; r = -0.1 ....26(a)

UTS(MPa) $\pm$ 18.1 = 551.8 + 2.9 % EL ; r = -0.6 .... (b)

YS (MPa) $\pm$ 34.8 = 422.3 - 1.0 % RA ; r = -0.9 .... (c)

UTS(MPa) $\pm$ 18.1 = 381.6 + 0.9 % RA ; r = 0.2 .... (d)

YS (MPa) $\pm$ 34.8 = 377.4 - 19.8 ε_T ; r = -0.1 .... (e)

UTS(MPa) $\pm$ 18.1 = 418.8 + 20.0 ε_T ; r = 0.2 .... (f)

UTS(MPa) $\pm$ 18.1 = 485.1 - 0.1 YS ; r = -0.2 .... (g)

The heat treatment appears not to alter the as-rolled regression relationships, except for the cases shown in equations 26c, 26e and 26g. A bit worrying is the UTS - YS relationship shown in equation 26g i.e. increasing UTS - decreasing YS association, but the magnitudes of the slope and regression coefficient (range 10 to 20%) reduces the concern. These regression lines are plotted in Figures 32-39 .

4.5 FORMABILITY

The theoretical values of the formability parameters calculated from equation 30-34 (Section 5.3) are summarised in the last four columns of Tables 16A and 16B.

4.5.1 FLOW STRESS AT FIXED STRAIN

a) Base steels

The flow stress increases slightly as the rolling temperature decreases, reaching a steady value at the last two rolling temperatures. The effect of stress relief treatment is marginal.

b) Nb-Ti-Al with varying V content

It can be deduced that its values increased as the V content decreased. This behaviour persists at all rolling temperatures. For a fixed V level, these values increase as the rolling temperature decreases. There is no significant difference in flow stress after rolling at 1000°C / 900°C. On the average, the effect of stress relief is not significant.

c) Nb-V-Al with varying Ti content

For the highest Ti level, the flow stress decreases marginally as the rolling temperature decreases. Its relationship with other two Ti contents is variable, reaching a maximum of 1062 MPa for the 0.027% Ti, after 1100°C rolling. The effect of stress relief is slightly variable but not significantly different from the as-cast steels.

4.5.2 WORK HARDENING RATE AT FIXED STRAIN

a) Base steels

Like the flow stress, this increased slightly as the rolling temperature decreased. Equally, there was a very slight gain due to stress relief.

b) Nb-Ti-Al with varying V content

On the average, the values increased as the V level dropped. This is true for all rolling temperatures. Also this parameter increased as the rolling temperature decreased provided that the V content was fixed. On the average the effect of stress relief is not significant.

c) Nb-V-Al with varying Ti content

The highest Ti level displayed the same behaviour as the flow stress. There is no definite relationship with the other Ti levels and/or rolling temperatures. The effect of stress relief is not pronounced.

4.5.3 MAXIMUM UNIFORM STRAIN / FRACTURE STRAIN

All the values of the maximum uniform strain are in the range 0.07-0.11. The proximity of these values may be due to the similarities in input variables in equation 33.

A similar explanation can be offered for the range of values (1.55-1.62) of the fracture strain. In addition, the grain size coefficient in equation 34 is so low (0.015) that its impact for the $\bar{d}^{\frac{1}{2}}$ values on the total fracture strain shown

in Tables 9A and 9B would not be much.

For both formability parameters, the effect of stress relief appears to be negligible, consistent with subsequent minimal changes in grain sizes and compositions.

4.6 INCLUSION ASSESSMENT

Table 8A shows the variation of non-metallic inclusion parameters with specimen orientation and rolling temperatures, for sample A4. Sample A4 has the highest S level (0.003 Wt %) and its sum of O,S,P is not significantly different from the others (see Table 8B). Consequently, its result could be deemed as representative of the whole series of steels.

It can be deduced from Table 8A that on the whole the inclusion parameters are low, typical of the values of Spitzig.[64]

The isotropy exhibited in Table 8A is confirmed by the minimal variation of these properties with orientation.

The values of area fraction suggests that the matrix is greater than 99.9% pure.

It can be said that thermomechanical treatments in the range 900°C to 1250°C appear to have no major effects on these inclusions. This view is supported by the non-metallic inclusion distribution shown in Fig.25. The same micrograph portrays an inclusion morphology which is predominantly

spherical, thus suggesting that the inclusions were resistant to deformation at these rolling temperatures. This non-deformability may be due to a low area fraction;[64] small sizes of the inclusions;[183] the composite nature of the inclusions;[176] as shown in Figure 29, and the high rolling temperatures, some of which are typical of recrystallisation hot rolling.[112-114]

Interests in other aspects of non-metallic inclusions, such as inclusion size distribution, inter inclusion spacing, etc., considered elsewhere;[64] will not be considered here since their discussion would not be pertinent to the main thrust of this work.

4.7 GRAIN SIZE DISTRIBUTION

The polygonal ferrite grain size distribution shown in Tables 9A and 9B has been utilised at several stages in the project, thus justifying both man-hours invested in deriving it and equipment utilisation. It is worthy of note that the low values of standard deviation consistently associated with the grain size analysis places a high premium on the reproducibility involved. On the whole the grain size falls within the range ASTM No.8-10 corresponding with absolute values of 20 μm - 10 μm.

4.7.1 THE BASE STEELS

These steels show a significant decrease in grain size as the rolling temperature decreases from 1250 / 1100°C to 1000 / 900°C.

The 650°C stress relief results only in a marginal change in grain size.

4.7.2 Nb-Ti-Al WITH VARYING V CONTENT

On the average, maximum grain refinement occurred after rolling at 1000 / 900°C. Apparently, better grain refinement took place in the temperature range 1100 to 900°C, for the lowest V content which may be attributed to less participation of V in the high temperature composite precipitation by virtue of the lower V concentration. The effect of stress relief is marginally variable.

4.7.3 Nb-V-Al WITH VARYING Ti CONTENT

For the highest Ti level, best grain refinement occurred at the high rolling temperatures i.e. 1250 / 1100°C. No such relationship was observed for other Ti contents. After 1250°C rolling, grain refinement was in descending order of Ti levels. The effect of stress relief was variable but no major changes were observed.

Overall, it can be said that these multiple microalloyed steels have good grain coarsening resistance after one hour stress relief at 650°C.

4.8 MICROSTRUCTURES OF THE AS-ROLLED STEELS

These steels portray a microstructure comprising essentially of ferrite with small amounts of pearlite, as shown in micrographs (Figure 27). There is evidence of non-uniform distribution of pearlite. Obviously, the microstructure is devoid of pearlite banding.

4.8.1 THE BASE STEELS

Sample Ao (Figure 27A) contrasts with Sample Do (Figure 27B) in terms of polygonal ferrite grain size and pearlite distribution i.e. the 1250°C rolling produced coarse ferrite grain size, more uniform distribution of the pearlite and bigger pearlite colonies relative to the 900°C rolling.

4.8.2 Nb-Ti-Al WITH VARYING V CONTENT

The micrographs of the highest V level has been shown as an example. Like the base steels, there is evidence of slight ferrite grain coarsening, more uniform distribution and coarser pearlite colonies after 1250°C rolling compared with the 900°C rolling (Figure 27C and Figure 27D).

4.8.3 Nb-V-Al WITH VARYING Ti CONTENT

Compared with the previous two steels, the highest temperature rolling (A_4 Figure 27E) portrays a microstructure consisting of finer ferrite grain size, finer pearlite colonies and more

pearlite segregation than the low temperature rolled sample (D_4 Figure 27F). In fact, A_4 has the finest grain size and apparently the least amount of pearlite. The latter observation is supported by the calculation summarised in Table 29.

On the whole, the non-uniform distribution of pearlite observed in some of the microstructures may be associated with the internal stress distribution. This possible internal stress gradient may act as one of the pearlite nucleation sites, thus resulting into non-uniformly distributed pearlite.

4.9 ELECTRON DIFFRACTION PATTERN

Figure 30D shows the electron diffraction spots of Sample A_4 whose analysis is shown in Table 10.

Figure 30E portrays the solution to the diffraction, usually obtained by indexing, using angular measurements and vector addition. It can be deduced that there is a major pattern (shown by open circles) typical of a f.c.c. structure. In addition, there is a minor superimposed pattern (shown by the dark circles) which cannot be easily identified. This latter pattern might have been caused by lattice rotation, or the presence of another phase with a different crystal structure.

By applying the zone law (stated subsequently) the direction $[UVW]$ parallel to the electron beam was found and eventually a stereographic projection was drawn, with the zone axis indicated in Figure 30F. No zone near to the $\langle 110 \rangle$ could be

found which gave the minor pattern of diffraction spots.

It can be concluded, therefore, that the composite precipitates resulted into an f.c.c. electron diffraction pattern with $[1\bar{1}0]$ zone axis. Bearing in mind that this is the same pattern as TiN, TiC, NbC, VN, VC;[88] consequently, this diffraction pattern cannot be used to confirm the stoichiometry of the precipitate analysis. Such a reservation has been made elsewhere.[172]

4.9.1 APPLICATION OF ZONE LAW

This is basically a law for finding the direction parallel to the electron beam $[UVW]$.[181]

For any two sets of planes $(h_1k_1l_1)$ and $(h_2k_2l_2)$ which satisfy vector addition for the diffraction spots, the mathematical statement for the zone axis is given by:

$$U = k_1l_2 - k_2l_1 \qquad \text{.....27}$$

$$V = l_1h_2 - l_2h_1 \qquad \text{.....28}$$

$$W = h_1k_2 - k_1h_2 \qquad \text{.....29}$$

Upon substitution for indices of the planes

$$U = 2.1 - 0.1 = 2$$

$$V = 1.2 - 0.1 = 2$$

$$W = 1.0 - 0.1 = 0$$

i.e $[UVW] = [220] = [1\bar{1}0]$

4.10 MICRO ALLOY PRECIPITATES

4.10.1 PRECIPITATE MORPHOLOGIES

This analysis was made on the As-Cast and Rolled Samples in the first part of the project.

a) Base Steel

The precipitate morphology is predominantly spherical as evident in Tables 10A and 10B.

b) Nb-Ti-Al with varying V content

The morphologies are various as reflected in Table 10 i.e. cuboids, hexagons, spheres and needles.

c) Nb-V-Al with varying Ti content

The morphologies are similar to those of the preceding group / class (b).

All these similar morphologies are cited in literature (40-42,112,121)

Some of these shapes / forms are portrayed in the micrographs in Figure 30.

4.10.2 PRECIPITATE ANALYSES

It is evident in Table 10 that the precipitates of multiple microalloyed steels are of mixed compositions or composites. Similar analyses[107,115,172] have been documented for steels involving a combination of microalloys.

4.10.3 SOLUTE DISTRIBUTION

The solute content of the precipitates tends to show size dependence consistent with documentation elsewhere.[107,172] Apparently, Nb and V show a great affinity for fine, spherical precipitates which contrasted with the behaviour of Ti and Al. In Sample A_4, it may be argued that Ti is partitioned approximately 50 : 50 in both fine and coarse precipitates, and a possible explanation is that the Ti / N is hyperstoichiometric in this case. Consequently, the excess Ti would form TiC whose solvus is below that of TiN but approximately the same as that of NbC / Nb(C,N)

It may be pointed out that in samples $A_4 - A_6$, the Al level in the precipitates is apparently insensitive to their sizes. This size indifference would confirm the calculations in the appendix i.e. there is either no, or insufficient, N left after TiN formation for the reaction Al → AlN.

The distribution of Nb between fine and coarse precipitates in sample A_1 to A_3 (Table 10) suggests that the Nb-containing particles formed during the early stage of precipitation i.e. the upper half of the Nb(C,N) solvus, have high probability of nucleating on TiN particles. Therefore, such early precipitates are more vulnerable to particle coarsening. In fact, the presence of Al in such high temperature precipitates e.g. TiN has been suggested[172] to accelerate the coarsening rate. The fine particles which are highly denuded in Al and probably formed at the later stages of precipitation tend to support this view. This explanation may also be advanced for the Nb behaviour in samples $A_4 - A_6$, but in

addition the Nb is apparently distributed equally between the fine and coarse precipitates. The calculations shown or summarised in the appendix throw light on this latter partitioning of Nb.

The affinity of V for small particles can be rationalised by the fact that the calculations shown in the appendix indicate the precipitation of VC in the low temperature. The same calculations show that more of its precipitation took place in the ferrite. Such late forming precipitates are likely to be fine because of the probability of the minimal influence of Ostwald ripening mechanism on them. In addition the presence of Ti and Nb in these precipitates may retard the VC growth rate.

Generally, it can be said that the first formed precipitates and / or those out of solution during soaking have a greater probability to coarsen, and this tendency to ripening is accentuated by contamination (e.g. the presence of Al in TiN). A part of this explanation is supported by the analysis carried out in the appendix, which indicates that TiN solvus in each case is greater than the soaking temperature of 1250^{o}C, reaching a maximum value in sample A_4 with a corresponding maximum of Ti and N solubility product.

4.10.4 T E M MICROGRAPH FOR SAMPLE D_4

The micrograph (Figure 42) shows copious fine precipitates in the vicinity of the prior austenite grain boundary.

This structure was probably developed during deformation and recovery at the low rolling temperature (900°C), usually a non-austenite recrystallisation temperature. Consistent with the mechanism suggested elsewhere,[123] such structural development involves the generation of sub-grain boundary network, with the associated strain gradient. Subsequently, precipitates form on this network and serve as additional ferrite nucleation sites, but this does not explain the relatively less fine ferrite grain size of this steel compared with that rolled at 1250°C, even though both steels are of the same composition (see Table 9A, A_4 compared with D_4).

4.11 DEVELOPMENT OF PRECIPITATE ANALYSES AND SIZES

Table 11 shows composite precipitates of samples quenched from a high temperature (1250°C) as described in Section 3.8.

Sample A_o quenched from 1250°C portrays fine, dense, spherical Ti rich precipitates ($\approx$ 70 AT % Ti and 30 AT % Nb). This analysis contrasts with those of the as-cast or the as-rolled steels shown in Table 10. Note the Nb and Ti values are reversed.

After 20% deformation and quenching from the rolls, a new set of fine spherical and less dense precipitates emerged. These resulted in a microstructure comprising of a mixture of Ti rich precipitates and the new ones. These latter were Nb-rich ($\approx$ 70 AT % Nb, 30 AT % Ti) and their analyses were closer to those of A_o and the as-cast steel No.0 given in Table 10.

This stoichiometry could not be confirmed by electron diffraction analysis because the composites manifested diffraction patterns similar to those of any pure nitrides/ carbides of the traditional microalloying elements e.g. TiN, NbC, VN.

These precipitates are evident in the two micrographs, Figure 40A (1 and 2). Also present in Figure 40A(2) is the increased number of precipitates after rolling. It can, therefore, be said that rolling increased the population of the precipitates and a change in composition from the original.

Sample A_4 also quenched from 1250°C shows Ti rich dominated precipitates ($\approx$ 85 AT% Ti and 15 AT% Nb). This analysis deviates significantly from those of A_4 and as-cast steel No.4 in Table 10. These precipitates are shown in Figure 40B.

The effect of the second thermo-mechanical quenching cycle on precipitate size and distribution is shown in Figures 41A and 41B . Figure 41A(1) compared with Figure 40A(1) suggests that the intermediate heat treatment nullified the effect of the previous rolling.

Figure 41A(2) compared with Figure 40A(2) indicates that TiN or (TiNb)N grows slowly, hence there is no major difference in particle size. In contrast to Figure 40A(2), corresponding Figure 41A(2) indicates the presence of more dense spherical precipitates, suggesting that the intermediate heating did not re-dissolve completely all the prior Nb rich precipitates.

The same trend is exhibited by Figures 40B and 41 B but with a noticeable difference in particle sizes in the latter.

In all cases, the precipitate distribution appears to be even with some of the precipitates pinning the prior austenite grain boundaries / lath martensite boundaries.

Some of these micrographs portray some massive particles which may be interesting from Non Metallic Inclusion (NMI) view point but not relevant to this analysis.

5. DISCUSSION

In this work seven line pipe-type steels were produced as chill cast ingots containing four levels of titanium and vanadium contents in order to study the effect of these micro-alloying elements ($<0.1\%$) on the mechanical properties after thermomechanical processing of the ingots and also, a final stress relieving treatment at $650^{o}C$. In the second part of the project a detailed examination of some of the carbide and nitride precipitates was made to elucidate the role of the particles on the final properties achieved. Therefore, this discussion will be divided into two sections, concentrating on the mechanical properties obtained and the composition and form of the particles found in the alloys.

5.1 MECHANICAL PROPERTIES

Three major properties were determined: strength, ductility and toughness, in accordance with API recommendations, together with the resistance of the steels to HIC in a NACE type test which is obligatory for all modern pipeline steels.

5.1.1 STRENGTH

It has been stated earlier, in equations 6 (Section 2.6.5) and 10 (Section 2.8) that the strength of plain carbon steels may be estimated from their chemical compositions (mainly carbon, silicon and manganese), microstructural features including grain size and volume percentage of pearlite and

the presence of free nitrogen present. Therefore, these equations have been used to calculate the 'theoretical' strength of these steels in this work and have then been compared with the experimentally determined values.

5.1.1.1 YIELD STRESS

It was found that the calculated yield stress of the test steels were all much lower than the actual values. It is believed that this excess strength in the present alloys was due to precipitation strengthening by the carbides, nitrides and carbo-nitrides of the microalloying elements rather than the dislocation strengthening due to rolling. Since the rolling was achieved at elevated temperatures its contribution to dislocation strengthening was probably negligible.

It could be argued that the chemical composition given in Table 5 could be changed during the thermomechanical treatments applied to the ingots to produce the mechanical test specimens. However, if the aluminium contents of the latter (Table 5C) are compared with the ingots (Table 5A) it will be seen that a loss of 0.002% Al was given, and since this is the most oxygen avid element in the alloys it can be assumed that the carbon, silicon and manganese contents of the test specimens will be very similar to those recorded for the ingots in Table 5A. The free nitrogen contents of these steels can be assumed to be zero as shown in the Embury type calculation in the appendix.

The difference between the actual/measured yield stress and those calculated from equation 10 (Section 2.8) are shown in Tables14 A and B. A similar approach has been adopted elsewhere[177] incorporating incremental yield stress values in the range (60 - 130 MPa), the lower value reflecting a case of particle coarsening by batch annealing. The same work confirmed previous findings[178] that the potential for precipitation hardening is independent of precipitate analysis i.e. whether VN, VC, V(C,N), NB(C,N) TiN, etc. but only depends on volume fraction and mean precipitate size as reflected in equation 6 (Section 2.6.5). This is probably because these microalloying precipitates are very hard[37] and therefore non deformable. It is reasonable to assume that the composite nature of these precipitates should not invalidate equation 6.

The values of the yield stress may therefore be interpreted as due to the co-operation between grain refinement and effective volume fraction of precipitates and their size. It may also be pointed out that the precipitation-hardening component has an indirect eff ect on grain refinement by impairing grain growth.

The observed variation of yield stress with rolling temperature for the base steels can be attributed to any or all of the following:

1) Precipitation in the austenite during the hold period in the temperature range (1100-900°C). The temperature difference and time to achieve these rolling temperatures are the main driving force for such precipitation.

2) Strain induced precipitation in austenite, especially during the rolling at 900°C, because the austenite is unlikely to recrystallise at this temperature. Generally, precipitation in austenite detracts from precipitation-strengthening in the ferrite.[173]

3) Particle coarsening (especially during the hold period) which reduces the effective volume fraction[94] of the precipitates and increases their mean particle sizes. The above support the gradual decrease of the incremental yield stress from 1250°C to 1000°C and reducing considerably at 900°C.

4) Austenite grain growth inhibition, especially at high temperatures, by composite fine Ti-rich precipitates and the transformation of unrecrystallised austenite at the low rolling temperature. This proposition is in conformity with the grain size shown in Table 9, with maximum grain refinement after the 900°C rolling.

The Ti-Nb-Al varying V steels showed non-simple relationships of both the variation yield stress with rolling temperature and the increase of yield stress with increasing V level.

The former is analogous to that of the base steel and hence the preceding explanations could explain this behaviour. The latter could be expected when the increasing volume fraction of precipitates is obtained as the V content increased, since in all cases the VC / V(C,N) is in solution during soaking at 1250°C. It may be argued that the presence of V in the

composite precipitate shown in samples A_1 to A_3 (Table 10A) can diminish the volume fraction of V(C,N) available for precipitation strengthening in the ferrite. Such an observation has been made[173] accompanied by a decrease in grain coarsening temperature of Ti steel when combined with V or Nb. A question of great concern is by how much the participation of V in this high temperature precipitation reduces the effective volume fraction of V(C,N) to be precipitated in the ferrite? This problem is exacerbated by the maximum deficit obtained between the actual and theoretical V (see Table 10C) which suggests that the decrease in volume fraction of V(C,N) by the participation of V at the high temperature is minimal and thus precipitating mainly as pure V(C,N),and being extremely fine (maximum immunity from ripening) could not be easily detected during the EDAX-STEM analyses.

This increase of yield stress with increasing V content is clearly born out in Table 14 where the average incremental yield stress decreases as both the V level and rolling temperature are reduced, becoming constant at 1000°C / 900°C. For the lowest V content, the values are similar to those of the base steel.

Ignoring the slight deviation at 0.03 V, the same table also revealed a maximum value in incremental yield stress at the rolling temperature of 1100°C. This may be attributed to the contribution of the precipitation of Nb(C,N) / NbC to the overall volume fraction of the precipitate as indicated by the solvus-generation data shown in Tables (22-24).

In contrast to the two previous groups, these steels that contain Nb-V-Al with varying Ti displayed maximum grain refinement at the higher rolling temperatures i.e. at 1250°C and 1100°C (for the highest (0.074%) Ti level) as shown in Table 9 and Figure 27. This may be interpreted as the effect of the large amount of insoluble precipitates[39,94,123] (during soaking) which refined the austenite but coarsened during the slow cooling to the relatively lower rolling temperatures of 1000°C and 900°C.

From the present data it would be speculative that the large amount of excess (free) Al (Table 28) associated with these steels could interact in a complex manner with these precipitates at the lower rolling temperatures with the possibility of causing accelerated coarsening.

Also, it is possible that the high temperature precipitates have subsequently grown to the critical sizes of 0.5 μm[94] or ≥ 1-2 μm[94] for the enhancement of recrystallisation by providing easy nucleation sites. This may be attributed to the strain gradient development around the particle and its own interfacial energy. Such accelerated recrystallisation might off-set the 'pancaking' tendency of the austenite during the low temperature deformation.

Recent investigations[123] of the nature of prior austenite after rolling in association with large volume fraction of insoluble Nb(C,N) precipitates are in agreement with the above speculation. It may, therefore, be rewarding to examine

the nature of the prior austenite grains in these steels by the usual picral plus a wetting agent technique. This is supplemented by the fact that steels with relatively lower Ti contents did not apparently display the grain size - rolling temperature tendency mentioned previously.

Therefore, the relatively diminished value of the incremental yield stress displayed by these steels can be attributed to much of the precipitation taking place in the austenite i.e by a combination of insoluble precipitates and strain inducement. This has the usual overall effect of reducing the amount of strengthening precipitates in ferrite.

5.1.1.2 ULTIMATE TENSILE STRENGTH (UTS)

The calculated values can be obtained in terms of the parameters incorporated in equation 11 (Section 2.8) i.e. composition, grain size and pearlite content. For composition and grain size the ideas advanced for yield stress would apply here irrespective of the differences in regression-coefficients incorporated in equations 10 and 11.

It is important to emphasise that the use of the theoretical values of pearlite content (summarised in Table 29) may underestimate the actual values. In addition, the non-uniform distribution of pearlite (Figure 27) may compound the error introduced in the calculation. Such an error may throw light on the fluctuations of the differential UTS values shown in Tables 14A and 14B. This error may be compromised as an

alternative to cost and time saving strategy which does not devalue the principle of this exercise i.e. effect of micro-alloying on pearlite dilution. Therefore, it is recommended that quantitative metallography should be employed to test the calculations.

From the summary of the calculated and actual values shown in Table 14, it can be deduced that the differential UTS values are much lower than the corresponding yield stress values. This tends to give credence to the fact that the former is less structure sensitive than the latter, as evidenced by the inferior regression coefficients of the UTS (equation 11 compared with equation 10).

5.1.1.3 THE RATIO OF YIELD STRESS TO UTS

The specification of yield to tensile strength ratio calls for a maximum of 0.85 for pipe-line of a grade less than X-65(450 MPa YS) and 0.90 for higher grades[82]. Therefore, the range of 0.70 to 0.82 shown in Table 7 is in conformity with specification.

This upper boundary was imposed by pipe-line companies which hydrostatically tested the finished pipe construction to a very high stress level, often exceeding 100% of the SMYS*, in order to minimise the risk of failure during the commissioning test. It also has the effect of discouraging the practice of

* SMYS = Specified Minimum Yield Stress

achieving a desired yield strength level by excessive cold expansion of an undersize pipe, a method unknown in the past.

5.1.2 DUCTILITY

Ductility can be measured by percentage elongation, percentage reduction in area and fracture strain.

5.1.2.1 PERCENTAGE ELONGATION

The major feature of this property is its dependence on the specimen geometry, particularly the initial gauge length (l_o). Hence, results are only meaningful when the gauge length used for the test is quoted, implying that comparison of results is meaningless for different gauge lengths.

A better assessment of ductility may be obtained by measuring the uniform elongation, which is independent of gauge length but strongly composition and structure dependent, as shown by one of the formability equations in Section 5.3.

5.1.2.2 PERCENTAGE REDUCTION IN AREA

Apparently, there are no regression equations for either percentage elongation or percentage reduction in area, hence the results are difficult to interpret quantitatively, but phenomenological explanations can be advanced in terms of cleanness, grain size, microalloy precipitates and thermo-mechanical regimes employed in this project.

5.1.2.3 FRACTURE STRAIN

The results can be explained in terms of the variables associated with equation 34 (Section 5.3). From this equation, the detrimental effect of both phosphorus and sulphur is explicit, both in terms of sign and regression coefficients. Less harmful is the pearlite content and hence the benefit of pearlite dilution by microalloys cannot be over emphasised, even though this is a secondary objective of microalloying additions. Mn, Si, grain refinement and surprisingy tin improve the fracture strain. It may be worthy of mention that tin usually occurs as a tramp element in steel. Its concentration is usually low, typically those shown in Table 5.

Usually the calculated values are slightly higher than the actual values (Tables 1A and B) and a major factor which may cause this can be the non uniform distribution of pearlite. Segregation of elements is another possibility, but the sulphur print test indicated that very little segregation was present.

The correlation between the fracture strain and percentage reduction in area is apparently evident in Table 7, thus supporting the phenomenological explanation advanced previously for the behaviour of the latter. Such a correlation is evident in a previous investigation.[62]

5.1.3 TOUGHNESS

The very good energy absorbed values obtained for the samples tested in this work (Table 7) can be attributed to the very low volume / area fraction of non metallic inclusion (Table 8), fine polygonal ferrite grain size and absence of free nitrogen, N_f, as indicated by excess Al (Table 28). The harmful effect of free nitrogen, N_f, is reflected in equation 12 (Section 2.8.3). Less detrimental are silicon and pearlite due to their low regression coefficients in the same equation. Other factors for the high toughness of these steels include precipitate distribution in austenite and ferrite, and the possible avoidance of low temperature ferrite rolling. The latter has the implication of separation / splitting mode of fracture. The nearly isotropic mechanical properties exhibited by the specimens is shown by the very low orientation dependence of the inclusion parameters shown in Table 8.

These results are much better than those of Spitzig.[62] His data included steels in both modified and unmodified conditions as well as high S(0.013 % max) and relatively lower Mn(0.89 - 1.06 %). The equivalent values were for the upper shelf energy in the longitudinal direction. In addition, these values are much greater than those quoted for the operation pipeline network shown in Table 18.

To supplement the energy absorbed values, theoretical calculations of ITT were made based on a combination of equation 11 (Section 2.8.3) and Table 4,[31] the latter

reflecting the effect of precipitates on ITT, thus giving the overall equation for theoretical ITT as:

$$ITT_{eff} = ITT_{cal} + \frac{\Delta YS}{15} \times \frac{4}{1} \quad .....(30)$$

where ITT_{eff} = effective ITT (^{o}C)

ITT_{cal} = ITT calculated from equation 11 (^{o}C)

ΔYS = incremental yield stress (MPa)

The results are summarised in Table 15 from which it can be seen that the incremental yield stress due to precipitation strengthening depresses ITT, producing a relatively high value of $-29^{o}C$ for sample B_1 (Table 15B) i.e. the highest V(0.073%) rolled at $1100^{o}C$. Apparently, this is an explicit deleterious effect of fine precipitate volume fraction on toughness. Fracture surface of sample B_1 (Fig.28A) shows a transcrystalline cleavage mode of fracture irrespective of 124 J energy absorbed at $-20^{o}C$, an energy value that is much higher than most of those quoted in Table 18. This mode of fracture differs markedly with sample C_3 - ductile fracture (Fig.28B) having an ITT_{eff} value of $-54^{o}C$.

It is clear from Table 15 that the Ti-Nb-Al-V steels possess inferior ITT_{eff} especially at the high rolling temperatures of $1250^{o}C$ and $1100^{o}C$, this behaviour is contrary to the Nb-V-Al-Ti variants. This can be deduced from the explanations advanced in Section 5.1.1.1.

Based on this conflicting evidence, there remains a problem

over the use of either the Charpy energy values or ITT as a measure of toughness. This view is supported by the energy requirements quoted in association of temperatures shown in Table 18. It is, therefore, suggested that actual ITT should be obtained to provide more accurate design data for the pipe user.

5.2 THE EFFECT OF STRESS RELIEVING

5.2.1 STRENGTH

The effect of this secondary thermal treatment on yield stress appears to be variable, as shown in Table 7B. This may be attributed to the small fluctuations in the values of the polygonal ferrite grain sizes shown in Table 9A and 9B. Also, the possibility of precipitate coarsening during the heat treatment cannot be ruled out, but this latter effect cannot explain the observed increase in yield stress shown by some of the steels. Both effects are quantified in equations 10 (Section 2.8) and 6 (Section 2.6.5).

The UTS values portrayed the same pattern of changes for both the base steels and the V-variants, but the Nb-V-Al-Ti group of steels showed a definite pattern of lower tensile strengths. Since this behaviour cannot be explained absolutely in terms of grain coarsening, it is possible that pearlite distribution and growth can offer an explanation. Time did not permit quantitative metallographical investigation in this direction. Therefore, further work on the effect of such thermal treatment on the as-rolled microstructure is recommended.

5.2.2 DUCTILITY

The effect of this secondary heat treatment on the values of both percentage elongation and percentage reduction in area is insignificant as shown in Table 7B.

For the base steels, the values of the fracture strain showed a slight increase in all rolling temperatures except 1000°C.

The highest V containing steels i.e. steels with subscripts 1, showed a moderate increase in fracture strain for the rolling temperatures of 1100°C, 1000°C & 900°C, while other steels displayed moderate fluctuations. These changes may be explained in relation to the variation in the parameters incorporated in equation 34 (Section 5.3).

5.2.3 TOUGHNESS

On the average, most of the samples retained their high energy absorbed values after stress relieving, but samples A_1 and B_1 exhibited a significant depression in their values of this property in both orientations (Table 7B). Sample A_2 suffered loss in toughness in the transverse direction.

The significant loss in toughness displayed by sample A_1, B_1 and A_2 cannot be explained in terms of grain growth, because there is no evidence of this in Table 9B. Speculatively, a possible explanation is the inadvertent location of the Charpy V notch at the segregated area(s) of the pearlite. Such non-

uniform distribution of pearlite is shown in Figure 27. In addition, the growth of Fe_3C lamellae during stress relief welding treatment has been identified with loss in toughness.(66)

5.3 THE FORMABILITY OF FERRITE-PEARLITE STEELS

Flat rolled steels require to be formed into pipes, for example, by the U.O.E.* process. Significant properties include flow stress for a given strain, which governs the forming loads, work-hardening rate, maximum uniform ductility prior to plastic instability, and the total ductility at fracture. Many of these parameters can be derived from the true-stress/true-strain tensile data(31,57) but could not be accomplished within the project life span, and consequently interests were centred on such primary mechanical properties as yield stress, UTS, ductility and toughness.

Attention has been primarily concentrated on the quantitative relationships between structure, composition and plastic-deformation characteristics for ferrite-pearlite structures. For low carbon, ferrite-pearlite structures which are typical of the HSLA steels being investigated, the following relationships have been quoted in literature.(31,57)

Flow stress at strain, $\varepsilon = 0.2$

$$\sigma_{(MPa)} = 15.4\left[16+29(\%Mn)+9(\%Si)+60(\%P)+11(\%Sn)+244(\%N_f)+0.27(\%\,Pearlite)+0.97(d^{-\frac{1}{2}})\right] \quad .....(31)$$

* This pipe forming process consists basically of three stages(180)

Work-hardening rate at strain, $\varepsilon = 0.2$

$$\varepsilon_{(MPa)} = 15.4\left[25+7.2(\%Si)+30(\%P)+9.9(\%Sn)+89(\%N_f)+0.09(\%\,Pearlite)+1.0(d^{-\frac{1}{2}})\right] \quad .....(32)$$

Maximum uniform strain,

$$\varepsilon_u = 0.27-0.016(\%\,Pearlite)-0.015(\%Mn)-0.040(\%Sn)-0.040(\%Si)-1.1(\%N_f) \quad .....(33)$$

Total ductility at fracture,

$$\varepsilon_T = 1.3-0.020(\%\,Pearlite)+0.30(\%Mn)+0.20(\%Si)-3.4(\%S)-4.4(\%P)+0.29(\%Sn)+0.015(d^{-\frac{1}{2}}) \quad .....(34)$$

These equations have been applied to these steels in conformity with their microstructure and the results shown in the last four columns of Tables 16A and 16B.

5.3.1 FLOW STRESS

a) Base steels

The slight variation of flow stress with rolling temperature is mainly due to grain size because of the tight composition control achieved in this project. From the relative magnitudes of the regression coefficients of $d^{-\frac{1}{2}}$ and pearlite (equation 31) compared with the absolute values (Tables 9A and 9B, and 29), it can be said that the contribution of pearlite should be secondary to grain size for these steels.

b) Nb-Ti-Al-V steels

The apparent slight increase in flow stress with decreasing

V levels may be interpreted as more of a compositional effect than grain size and pearlite content. This is confirmed by the slight variation in Mn and Si levels shown in Table 5. For the flow stress - rolling temperature relationship, the explanation advanced for the base steels above is applicable.

c) Nb-Al-V-Ti steels

The flow stress - highest Ti level relationships is essentially a grain size effect (Tables 9A and 9B). Also the fluctuating relationship between the flow stress and the two Ti contents is significant in the grain size domain.

5.3.2 WORK HARDENING RATE

a) Base steel

The slight increase in work hardening rate with decrease in rolling temperatures may be explained in a similar way to the flow stress - rolling temperature relationship. In fact, a critical examination of the two governing equations shows that the grain size coefficients are almost equal (0.97 for equation 31 and 1.0 for equation 32).

b) Nb-Ti-Al-V steels

Because of the similarity in behaviour with the flow stress, the explanations for the flow stress should apply for the work hardening rate.

c) Nb-V-Al-Ti steels

This family of steels displayed similar behaviour for both

flow stress and work hardening rate, and therefore, one explanation should apply for both.

Since most of these formability parameters are calculated, it may be rewarding to generate the actual values from true stress - true strain tensile data for comparison.

5.4 MICROALLOY PRECIPITATES

Precipitates of interest are the carbides, nitrides and carbo-nitrides of the microalloying elements Nb, V, Ti. Also, AlN is important in this discussion.

These precipitates are usually fine and very hard.[37] They are semi-coherent with the matrix as shown by the orientation relationships.[33,44-46] Under suitable conditions, they strengthen steels as shown by the Ashby-Orowan model.[90] Some of these properties are summarised in Table 1.

5.4.1 MORPHOLOGIES

Most of the morphologies of the precipitate may be explained in terms of composition of the steels. This is supported by the fact that the base steel (A_o) with very low Ti $\approx$ 0.007%, V = 0.009%, total Al = 0.030% and Nb = 0.042% displayed spherical precipitates devoid virtually of Al. Other shapes emerged in the structure when Ti and Al levels were relatively higher (A_1 - A_6). In this project, thermomechanical treatments could not throw any further light on this because all the

steels ($A_o - A_6$) were subjected to the same thermomechanical treatment.

5.4.2 ANALYSES

The isomorphology between most of the precipitates leads to intersolubilities (where size factor and electron structure permit) and may facilitate the formation of carbonitrides. Similarities in the atomic sizes of carbon and nitrogen and in the magnitude of their diffusivities can create a conducive environment for the ease of carbon-nitrogen exchange within the non-stoichiometric lattices (except for AlN) of these complex precipitates. The existence of non-stoichiometry creates vacancies with the implication of enhanced diffusion or pipe diffusion, possibly promoted by the mutual straining of the precipitate lattices. Such changes in lattice parameters with precipitate composition have been documented.(52)

A model based on such mixed composition has been attempted elsewhere(107) but cannot be adapted to the present project because of the presence of multiple microalloying elements involved giving rise to a multitude of phases.

Alternatively, the precipitation-phenomenon is a nucleation and growth process. It is universally accepted that TiN usually forms first and it is isomorphous with other nitrides (except AlN)and carbides, therefore it would seem realistic to assume that TiN can act as nucleation sites for the subsequent precipitation of other precipitates. This leads to

possible epitaxial growth or the so-called precipitate induced precipitation. In fact, such coring phenomenon has been cited elsewhere.[115,172,173] The insignificant difference between the lattice parameters[33,88] of these nitrides/carbides may enhance this possible coring. This suggestion is strengthened by the fact that rigorous thermodynamic analyses based on the sequence of precipitation (see appendix) indicates clearly overlapping tendencies of the 'C' curves of some of the nitrides and carbides with the associated phenomenon of co-precipitation.

It may be argued that following the model of the sequence of precipitation pioneered by Embury et al[107] and modified in the appendix, that some pure phases e.g. TiN, Nb(C,N), AlN may co-exist with the composite precipitates. Such a reservation has, indeed, been made[172] but the same work confirmed by chemical analysis that most of the precipitates were of composite nature. Subsequent investigation by Embury et al was in agreement with this latter finding.

5.4.3 PARTICLE SIZE DISTRIBUTION

Qualitatively, there is evidence of various precipitate sizes in Table 10. The factors affecting precipitate size cited elsewhere[112,106,172] are processing variables. These are supported by the discovery that for the same Ti addition, relatively coarse TiN particles predominate in the structure in sand cast ingots, compared with smaller precipitates in continuously cast billets (i.e. 62 nm versus 8 nm).[112] Also

the alloy chemistry of the steel, as dictated by solubility relationships, controls the degree of supersaturation achieved and thus, the size of precipitates.

Since all the steels in Table 10 were chill cast and given the same thermomechanical treatment, the diversity of particle sizes obtained must be steel composition dependent, but it may be difficult to interpret in terms of the degree of supersaturation because of the multiple nature of the phases present.

5.4.4 THE GENERAL BEHAVIOUR OF ALUMINIUM

A close examination of sample A_o in Table 10 indicates that within the accuracy of the data, there is virtually no aluminium in the precipitates. Comparison with the work of Chen et al[185] involving the same level of total Al is made more difficult by the fact that they used Al replicas.

Samples A_1 to A_3 contrast significantly with A_o. In fact, the effective Al in the particles reached a peak value of approximately 54(Wt%) or 80(AT%) in sample A_2 corresponding to a low value of excess (free) Al as shown in Table 28.

It may be argued that kinetically, the precipitation of AlN tends to be sluggish, but improves with plastic deformation.[33,41-42] Therefore, it is probable that the association of non-stoichiometric carbides/nitrides with AlN during plastic deformation may accelerate the precipitation of the (Nb Ti V Al)

complex. Thus, the high level of Al in precipitates of samples $A_1 - A_3$ corresponds fairly well with the availability of N after TiN - finish - precipitation as summarised in the Tables (22-24). This explanation may justify the very low levels of Al in the precipitates of samples A_4 to A_6.

Calculations based on solubility relationships shown in the appendix, indicate three possible start precipitation temperatures (1096°C, 1000°C and 794°C) for AlN. For 974°C it was assumed that AlN should not form. If it should eventually form at this relatively lower temperature, then the precipitation of AlN would be subsequent to those of TiN, Nb(C,N) and NbC under the same conditions, and two possibilities arise:-

i) such relatively low temperature precipitates may be too fine to be detected in the midst of other precipitates.

ii) There may be no nitrogen left for the reaction Al ⟶ AlN.

The same explanation can be offered for the other microalloys, but Tables (22 - 27) confirm that they are not hyperstoichiometric with respect to the associated interstitials.

The apparent disagreement between the very low levels of Al in the precipitates of samples A_4, A_5, A_6 (see Table 10A) and the corresponding prediction summarised in Tables (25 - 27) that there is no excess nitrogen for AlN - formation is noteworthy. Assuming that this apparent conflict is not due to the minimal influence of background stripping on the small Al-peak, in the presence of gigantic Ti and Nb peaks, then it

is possible that diffusion and other transport processes could promote the transfer of free Al into the lattice of the other precipitates. This diffusion could be enhanced by the non-stoichiometric nature of these other nitrides / carbides.

Should this explanation be true, then the worry over the influence of the theoretical excess Al is accommodated. Otherwise, samples A_o, $A_4 - A_6$, in which most of the precipitates are virtually devoid of Al, gives concern because the calculated free/uncombined Al should be in the final steel matrix. It may, therefore, be necessary to carry out a series of melts that discriminate between AlN and Al, thereby investigating the role of Al and N in the steel making process. Until such an investigation is executed and the result established, it is advocated that caution is to be exercised in making Al additions to multiple microalloyed steels.

It is interesting to point out that calculations of the activity coefficients of Al in this multicomponent system showed no major change with steel composition for the seven steels investigated. In fact, all the values of the activity coefficients are greater than unity but fall within the range 1.08 to 1.12 (see Table 10A).

5.4.5 THE PRESENCE OF IRON IN SOME PRECIPITATES

A critical examination of Table 10 indicates that some analyses do not add up to 100%. The deficit is accounted for by the presence of iron in some of the precipitates. This

detection of iron in some of them may call into question the validity of much of the work on solubility studies. The iron probably results from nearby cementite particles[71] but conflicts with the findings that the iron content increases as the particle size decreases.[108,109]

Recent communication[174] suggests that the presence of iron in the precipitates is inexplicable. In reality, its presence is due to the contamination of the particles by iron salts produced during the etching process which adsorb onto the surface of the small particles. This explanation tends to strengthen the previous finding that the iron content increases as the particle size decreases.

It may be necessary, therefore, to identify the precipitates of the same specimen by using the two techniques of extraction replica and thin foil provided the latter is produced by ion beam technique.

5.4.6 DOMINANT EFFECT OF Nb

The mystery surrounding the dominance of Nb in most of the precipitates (even in the presence of approximately twice the level of Ti or V in these steels) may be resolved in terms of the high stoichiometric value of Nb to C and / or with the associated excess electron of a Nb atom as displayed in Table 20. The chemical affinity of Nb to C and N is equally important.

5.4.7 ACTUAL AND THEORETICAL ANALYSES

The difference between the actual and theoretical precipitate analyses shown in Table 10C may be attributed to any or all the underlisted:-

a) The insensitivity of the theoretical values to the precipitate size, hence the mean values of the actual analyses were employed.

b) The theoretical values were based on equilibrium calculations.

c) Some precipitates may not have been detected.

This may account for the consistently maximum deficit exhibited in the vanadium series, the magnitude of the deficit decreasing in ascending order of the V content of the steels. This display of maximum discrepancy by V tends to support the earlier suggestion that the participation of V in high temperature precipitation still leaves excess V for low temperature precipitation.

5.4.8 EVOLUTION OF PRECIPITATE ANALYSES AND SIZES

The analysis of the precipitates of sample A_o quenched from 1250°C reflected stoichiometry of $Ti_{0.7}\ Nb_{0.3}$ (NC). These composite high temperature precipitates are likely to be rich in nitrogen and low in carbon content, consistent with the popular view. It should also be noted that the solvus of the $Ti_{0.7}\ Nb_{0.3}$ is likely to be greater than 1250°C because these

precipitates are insoluble at 1250°C.

The precipitates that emerged during rolling or immediately after rolling but prior to quenching, i.e. those of stoichiometry $Nb_{0.7}$ $Ti_{0.3}$ (CN) must have a solvus less than 1250°C. In fact, a thermocouple measurement indicated an emergent temperature of 1100 ± 5°C, a temperature that lies between the calculated curves of Nb(C,N) and NbC (see Table 21A). The possible contamination of the thermocouple by Fe diffusion at such a high temperature may underestimate the real value, but the true temperature should be intermediate to the 'C' curves of Nb(C,N) and NbC. These latter precipitates are likely to be lean in N but rich in carbon. Only EELS* can confirm this but such an analysis is beyond the scope of this investigation.

The driving force for these Nb-rich particles is likely to be temperature gradient as opposed to strain inducement, because previous work[94,123] indicated that the prior austenite is usually recrystallised at this temperature and microalloying concentration.

A similar trend should be exhibited by sample A_4 i.e. the transition from Ti-rich precipitates to an emergent new set of precipitates.

In the evolution of the observed spectrum of precipitate sizes, it could be said that the propensity for precipitate

* EELS = Electron Energy Loss Spectroscopy

growth by the well known Ostwald ripening mechanism is in the descending order:

a) Insoluble precipitates at soaking temperature
b) Precipitates formed at high temperature e.g. TiN or (TiNb)NC
c) Low temperature precipitates e.g. VC, VN.

The presence of Nb in Ti rich particles at 1250°C suggests that a transport phenomenon is involved in the formation of composite precipitates, thus giving credence to Embury's[107] model 2. This model is based on the mechanism of mixing, but becomes highly complicated for multiple microalloyed steels because of their multicomponent nature. Model 2 will be more useful from a practical view point but requires the computer package used by Embury et al. A modification of their package may be necessary to accommodate the multiple microalloyed nature of the steels involved in this project.

The existence of insoluble Ti-rich precipitate at 1250°C for a steel of very low Ti level (0.007%) as shown in micrographs (Figure 4OA) suggests that the least soluble particles ($Ti_{0.7}Nb_{0.3}$) impede boundary motion at the highest temperature. This is a corollary of Zener's concept.[184] The usefulness of such high temperature austenite grain boundary pinning, especially during soaking or welding, has given much impetus to a low Ti addition. Recently, this addition of Ti e.g ($<0.01\%$) in some OLAC*- treated steels containing $\leq 0.003\%$ N

*OLAC = On Line Accelerated Cooling

and (>0.05%Al) has been reported;[112] while the control of such a low level of this highly reactive metal is difficult, it is not impossible by the new injection technology technique.

A quantitative approach to particle stability has been documented.[172,175] This stability as measured by the dissolution and coarsening rates at a given temperature is defined by the well known Lifshitz - Wagner equation stated below:-

$$r_t^3 - r_o^3 = \frac{K}{RT} V_m^2 \, D \gamma t \qquad .....(35)$$

where r_o and r_t are mean particle radii at zero time and time t, respectively

D = coefficient of diffusion of the solute in the matrix

γ = interfacial energy of particle matrix/ interface

V_m = Molar volume of precipitates

K = Constant

RT have their usual meaning.

It can be seen from this equation that the particle growth rate would be retarded by a decrease in diffusion rate (or an increase in its activation energy), a decrease in molar volume of the precipitates and a reduction in the precipitate/ matrix interfacial energy.

A complication is introduced in these predictions by the fact

that the observed precipitates are of a composite nature and in addition, the diffusion of vacancies for these non-stoichiometric carbides/nitrides (except AlN) cannot be ignored. Such complex effects have been observed in Al-V steels[94] and are interpreted as due to interactions between AlN and VN, and due to the supersaturation dependence of the rate of growth of these precipitates.

Therefore, overall it may be anticipated that even more complex effects would result from multiple Ti-Nb-Al-V micro-alloying, particularly in the presence of nitrogen. In quantitative terms, some of the parameters in the equation above may be modified to reflect their operative values. Such an analysis, although very useful, is beyond the scope of the present discussion

5.5 RESULT OF HYDROGEN INDUCED CRACKING (HIC) TEST

None of these steels showed any cracks in the NACE test, and therefore this very good HIC resistance may be attributed to any or all of the following:-

a) Homogeneity[48,131-132] of ingots as revealed by
   1) Sulphur prints
   2) Consistency of analyses from the different sections of the ingot
b) Smallness[132] of the ingots
c) Very low values of sulphur, oxygen and phosphorus resulting in correspondingly low volumes of inclusions typical of past investigations.[131-137] The effect of the

spherical inclusion morphology shown in Figure 25 is also important.

d) Fine microalloy carbonitrides, possibly acting as innocuous traps,[170] which are claimed to decrease the diffusion of hydrogen. The same work indicated the presence of coarse microalloy carbo - nitrides on the path of HIC, but such an effect is not observed here.

e) Fine ferrite grain size (maximum 20 μm) which is less than the upper boundary of 70 μm established recently.[160] In general, a coarse grain (> 70 μm) with its associated high angle grain boundaries which occlude large amounts of hydrogen. Such hydrogen concentration may satisfy the criterion for both the pressure and embrittlement theories of HIC. In addition, the contribution to HIC resistance of these steels by microstructure apparently devoid of pearlite bonding cannot be ignored.

It may be pointed out that the experimental conditions for the HIC test conformed to specification[132] as summarised in Table 13.

An attempt to elucidate the role of microstructure in HIC phenomenon (keeping composition constant) was done by quenching from the rolls of samples A_o and A_4.

A microstructure of lath martensite (C = 0.09%) resulted in each case (Figure 26), for example

After the HIC test, only sample A_4 showed a single, 8 mm

stepwise crack running at an angle of 45° to the short transverse and transverse plane (Figure43). This crack may be termed stress induced HIC because the observed crack is usually much longer than those observed by Keegan* under the same experimental conditions. In fact, Keegan's steels of the same impurity level (S=0.003%) in the as-rolled condition did not crack but others of higher S levels→0.019% did.

The diagnosis of the crack indicated both the presence of coarse carbo-nitrides and non metallic inclusions adjacent to the single crack, but there was no evidence of the former on the crack path. It is suggested, therefore, that the presence of these coarse carbo-nitrides apparently exacerbated the build-up of thermal stresses and subsequently facilitated by the ingress of hydrogen. This proposition is supported by the absence of cracks in sample A_o (devoid of such coarse carbo-nitrides), which was subjected to the same test.

It may be concluded from these tests that the level and morphology of non metallic inclusions have a dominant influence on HIC. Both microstructure and coarse carbo-nitrides exert minimal influence if the two non metallic inclusion parameters are favourable i.e. low value of area fraction, and with a spherical shape.

* N.Keegan, Private communication, Aston University, 1986

6. CONCLUSIONS

(A) Multiple microalloying additions resulted in composite precipitates of various morphologies. Apparently, the only condition to produce a structure dominated by spherical precipitates, within the constraint imposed by the thermo-mechanical processes employed, is to use very low Ti ($\approx$0.007%), a low value of total Al (0.030max), Nb 0.042%, N = 0.007% and C = 0.09%.

A(i) In a multiple microalloyed Ti-Nb-Al-V steel, Al has a significant influence on precipitate chemistry only when the Ti content of the steel is low (0.007%), thus leaving excess nitrogen for AlN precipitation. This observation contrasted sharply with high Ti levels (0.027 - 0.074%) when virtually all the nitrogen is used up leaving none for AlN formation. This latter case resulted in much higher theoretical excess Al in the final steel matrix whose role is unknown.

A(ii) There is a general tendency for solutes (microalloys) to show preference for their own individual precipitate sizes. Nb and V tend to show affinity for fine precipitates vis-a-vis Al and Ti.

A(iii) Nb tends to dominate the precipitate chemistry even in instances where its concentration is about half of Ti or V in the steels.

A(iv) The discrepancies between the actual and theoretical

values of the precipitate composition can be attributed to the insensitivity of the latter to precipitate sizes and / or its dependence on equilibrium conditions.The V - series showed the maximum deviation, the disparity increased in a pro rata manner with the V content.

(B) After quenching from 1250^{o}C, a multitude of Ti - rich precipitates were obtained. This behaviour is an extension of Zener's model i.e. boundary pinning at high temperature is conducive for the most stable precipitates. Rolling resulted in new precipitates (i.e. Nb rich). These must have formed by temperature differential due to the contact of the work-piece with cold rolls as confirmed by thermocouple measure-ments.

B(i) A series of heating and hot working cycles resulted in precipitate sizes not easily distinguished from their immediate predecessors. This suggests that the presence of Nb in the high temperature Ti-rich precipitates does not lower the solubility of TiN significantly, or it does not increase the TiN coarsening rate appreciably.

B(ii) Theoretical calculations indicate that the bulk of carbon in the steels is in the form of cementite (Fe_3C).

Consequently, pearlite dilution by microalloying additions is not pronounced.

(C) Tough, strong weldable steels have been produced by a combination of thermomechanical and alloy design. The factors contributing to the toughness of these steels are cleanness, fine polygonal ferrite grain size, absence of free nitrogen (N_f) and non-deformation in ferrite region.

C(i) The strength of these steels can be attributed mainly to fine polygonal ferrite grains. Precipitation in both austenite and ferrite fields is also important.

C(ii) At the same content of Ti and V in the steels, V has a much greater contribution to incremental yield stress, especially at its highest content (0.074%). This phenomenon is due to the precipitation of V(C,N) mainly in the ferrite.

C(iii) Grain refinement with high temperature deformation is much better for the highest Ti content (0.074%), compared with the corresponding V level. This is attributed to the volume fraction of TiN / (TiNb)N which refined the austenite.

C(v) Stress relieving at 650°C for 1 hour did not produce a definite trend in properties; on average the effect is not significant.

(D) The nil HIC results both in the as-rolled and stress relieved conditions can be associated with the cleanness of these steels, spherical nature of the non metallic inclusions after rolling, fine polygonal ferrite grains, absence of pearlite banding, pearlite dilution and presence of fine microalloying carbides/nitrides/carbo-nitrides. Apparently, the presence of coarse precipitates did not lower the HIC resistance of these steels.

D(i) Quenching from a high temperature ($>1100^{\circ}C$) produced a single stress induced HIC in the sample with the highest Ti level (0.074). This sample has correspondingly a high proportion of coarse precipitates, but there was no evidence of these in the path of HIC.

(E) Both the composition of the steels and thermomechanical processing resulted in microstructures of essentially polygonal ferrite with low pearlite volume.

7. RECOMMENDATIONS FOR FURTHER WORK

(1) To examine the prior austenite grains in relation to the ferrite grain size to determine the extent of recrystallisation of the austenite during the thermomechanical treatment of a series of Nb-V-Al-Ti steels.

In addition, the proportion of precipitates greater than 0.5 um should be established. Both investigations should elucidate the ferrite grain size - temperature relationship exhibited by these steels.

(2) Quantitative metallographic techniques should be employed to generate the actual values of percentage pearlite. Such work will throw light on pearlite dilution by microalloys. Also, a possible relationship between actual and theoretical values can be found. Eventually, the actual values would serve as inputs into the relevant structure-property and/or formability equations. In addition, pearlite distribution before and after stress relief is worthy of examination.

(3) The need to generate the full Charpy energy-temperature plots for these steels to:-

a) Establish the Impact Transition Temperature (ITT)

b) Compare these actual values with the theoretical values.

c) Seek a relationship (if any) between the actual and calculated values.

(4) The curves of true stress - true strain of these steels should be plotted in order to deduce the relevant formability parameters which can be compared with the theoretical values.

(5) It is necessary to discriminate between AlN and Al in these steels. The outcome of such an investigation may serve as a guide for Al addition to a multiple microalloyed steel.

(6) Comparative study of precipitate analyses by both carbon extraction replica and thin foil technique using ion beam method is suggested to elucidate the presence of iron in the precipitates.

(7) Further work on the model of mixing pioneered by Embury et al is required due to the composite nature of these precipitates.

Table 1 (52)

Properties of Carbides and Nitrides involved in the present study

Metal	carbide	Crystal Type	Structure Spacings Å	Molecules per unit cell	Density (X-ray)	Melting Points °C (approximate)	ΔT	Other properties
Group IV								
Ti	TiC	Cubic,B1	4.3280 at TiC – 4.3127 at TiC 0.61	4	4.94 at TiC – 4.57 at TiC 0.61	3140	+1340	E=32.200 $\beta = 7.8*10^{-6}$ (10-100)
Group V								
V	VC/V_3C_4	B1	4.1655 at VC 0.87 – 4.1310 at VC 0.73	4	5.649 at VC – 5.607 at VC 0.78	2830	+1030	E = 27600
Nb	NbC/Nb_4C_3	B1	4.4707 at NbC 0.99 – 4.4318 at NbC 0.77	4	7.788 at NbC 0.99– 7.716 at NbC 0.785	3480	+1030	E=34500, X=0.03 $\beta = 6*10^{-6}$ (0-500)
Group VIII								
Fe	Fe_3C (Cementite)	orthorhhombic	a = 5.088 b = 6.744 c = 4.574	4	7.2	1650	+100	$\beta = 1*10^{-6}$ (0-500)

Table 1 [52] (Continued)

Properties of Carbides and Nitrides involved in the present study

Metal	carbide	Crystal Type	Structure Spacings Å	Molecules per unit cell	Density (X-ray)	Melting Points ^{0}C ΔT (approximate)	Other properties
	NITRIDE						
Ti	TiN	cubic B1	4.221 at TiN 0.45 -	4	5.43	2950	E = 8000
V	VN	cubic B1	a = 4.006 at VN 0.72 a = 4.139 at VN 1.00	4	6.1	2050	
Nb	NbN 0.9 to NbN 1.0	cubic B1	a = 4.381 - 4.392	4	8.31 - 7.3	2400-2050	
	Group III						
Al	AlN	hexagonal (wurtzite) (ZnS)		2**	3.26*		

Legend
(1) X = thermal conductivity, cal/cm ^{0}C
(2) E = Young's modulus
(3) β = Thermal expansion coefficients, ^{0}C (linear, mean for the temperature stated in brackets, ^{0}C)
(4) ΔT = difference in melting points between the metal and the compound
(5) * = calculated from cell dimensions obtained from Powder file.
(6) ** = obtained from Powder file.

Table 2 [25]

Chemical compositions (weight %) of typical Linepipe steels and their microstructural constituents.

Steel No.	C	Mn	Si	Mo	Al	Nb	V	Ti	B	Other	Microstructural Constituents
Ferrite-Pearlite Steels											
1	0.06	1.69	0.21	-	0.026	0.04	0.03	-	-	0.31 Ni	-
2	0.05	1.74	0.29	-	0.04	0.05	-	-	-	0.18 Cr	-
3	0.07	1.65	0.23	0.27	0.026	0.031	-	-	-	0.16 Cr	-
4	0.065	1.48	0.045	-	-	0.03	-	0.048	-	-	-
Bainite/Acicular ferrite Steels											
5	0.08	2.18	0.10	0.32	0.02	0.069	-	-	-	-	Acicular ferrite, martensite
6	0.07	1.63	0.04	0.25	-	0.05	-	-	-	0.02 Cr 0.09 Ni 0.21 Cr	Acicular ferrite Polygonal ferrite
7	0.05	2.16	0.38	-	0.05	0.05	-	0.02	0.001	0.12 Ni 0.81 Cu	Low-carbon bainite
8	0.02	1.95	0.25	0.31	-	0.04	-	0.02	0.001	0.38 Ni	Ultra-low carbon bainite
Multiphase-Steels											
9	0.07	1.90	0.24	0.08	0.06	-	0.43	-	-	0.05 Cu	Ferrite, martensite bainite
10	0.08	1.60	0.25	-	0.04	0.04	0.06	-	-	0.2 Ni 0.2 Cu	Ferrite, martensite bainite
11	0.06	1.51	0.05	-	-	-	-	-	-	-	Ferrite, upper bainite

Table 3 [31]

Data showing the change in yield stress and inpact transition temperature per weight % of the varying alloying elements is shown below

	Change per 1 weight % of alloying elements		
Element	Yield stress (MN/m^2)	Tensile strenght (MN/m^2)	Impact Transition Temp. ^0C
C	+4600	+6800	-
N_f	+4600	+6800	+700*
P	+670	+670	+400
Sn	+140	-	+150
Si	+85	+85	+44
Cu	+39	+9	-
Mn	+32	+38	0
Mo	+11	+45	-
Ni	0	+9	-
Cr	-30=	-28=	-
Al	0	0	+75"

* = Not linear
" = Al in solid solution only
= = Negative, possibly due to removal of interstitial solutes.

Table 4[31]

The effects of varing microstructural and compositional parameters on the change in Impact Transition Temperature per 15 MN/m^2 increase in yield stress.

Parameter	Change in Impact Transition Temperature per 15 MN/m^2 increase in yield stress	
Pearlite	*	microstructural
Dislocations	+6	
Precipitation	+4	
Grain refinement	-10	
Phosphorus	+53	
Nitrogen	+30	
Tin	+17	
Carbon	+10	Compositional
Silicon	+8	
Manganese	-5	
Aluminium	-27=	

Lengend

* = Does not increase yield stress. 20% Pearlite increases Impact Transition Temperature by 44 ^{0}C

= = Large negative factor due to removal of free nitrogen from interstitial solid solution.

Table 5A:

Steel Analyses

SERIAL No.	C %	Si %	Mn %	S %	Al %	Nb %	Ti %	V %	Ca %	O %	N %
0	0.09	0.24	1.22	0.002	0.03	0.042	0.007	0.009	0.023	0.0051	0.0070
1	0.09	0.20	1.13	0.002	0.042	0.047	0.007	0.073	0.042	0.0040	0.0120
2	0.09	0.21	1.20	0.002	0.034	0.047	0.007	0.043	0.025	0.0040	0.010
3	0.09	0.25	1.21	0.002	0.041	0.043	0.007	0.030	0.017	0.0036	0.012
4	0.09	0.21	1.13	0.003	0.059	0.043	0.074	ND	0.028	0.0043	0.010
5	0.09	0.23	1.23	0.003	0.060	0.048	0.037	-	0.017	0.0032	0.011
6	0.09	0.27	1.31	0.002	0.052	0.049	0.027	-	0.024	0.0033	0.012

N.D - not determined

Table 5B

Other Elements

SERIAL No.	Cu %	Ni %	P %	Sn %	Cr %	Mo %	B %	C.E %	Pcm %
0	0.27	0.03	0.014	0.018	0.02	0.01	0.0009	0.33	0.18
1	0.29	0.04	0.013	0.018	0.02	0.01	0.0010	0.31	0.18
2	0.28	0.02	0.015	0.018	0.02	0.01	0.0011	0.32	0.18
3	0.30	0.01	0.013	0.018	0.01	0.01	0.0006	0.33	0.18
4	0.26	0.02	0.011	0.018	0.01	0.01	0.0008	0.31	0.17
5	0.26	0.03	0.013	0.018	0.01	0.01	0.0008	0.33	0.18
6	0.29	0.01	0.012	0.018	0.01	0.01	0.0008	0.34	0.18

Table 5C

Aluminium Analysis After Hot Rolling

SERIAL No.	Al %
0	0.028

$$C.E = \%C + \frac{Mn}{6} + \frac{Si}{24} + \frac{(Ni + Cu)}{15} + \frac{(Cr + Mo)}{10}$$

$$Pcm = \%C + \frac{Si}{30} + \frac{(Mn + Cu + Cr)}{20} + \frac{Ni}{60} + \frac{Mo}{15} + 5B$$

Table 6

Hot rolling plan for 1250^{0}C, 1100^{0}C, 1000^{0}C, 900^{0}C

Pass number	Thickness (mm)	Change in thickness (mm)	% Reduction/ pass
0	32.00+0.5	0.00	0.00
1	26.9	5.1	16
2	20.8	6.1	23
3	14.7	6.1	29
4	10.8	3.9	27

Table 7A

Mechanical Properties of The As Rolled Steels

STEEL	YS(MPa) ± 2%	UTS(MPa) ± 2%	YS/UTS	Elon % ± 4%	RA (%) ± 4%	Frac.Str ±0.04%	Charpy (J) R D	Charpy (J) T D
BASE STEEL								
A_0	354	480	0.74	36	75	1.40	>300	282
B_0	346	474	0.73	35	73	1.30	>300	295
C_0	368	466	0.79	30	71	1.22	>300	>300
D_0	314	432	0.73	30	74	1.33	>300	>300
Nb-Ti-Al-V STEELS								
A_1	389	500	0.78	35	74	1.35	268	200
A_2	336	420	0.80	39	75	1.42	290	>300
A_3	350	471	0.74	34	76	1.41	>300	>300
B_1	400	531	0.75	33	73	1.26	260	245
B_2	360	483	0.75	36	72	1.27	>300	>300
B_3	335	440	0.76	36	72	1.53	>300	>300
C_1	356	463	0.77	30	70	1.16	261	255
C_2	354	468	0.76	36	78	1.51	>300	>300
C_3	363	464	0.78	38	77	1.47	>300	272
D_1	355	461	0.77	35	76	1.41	>300	236
D_2	338	461	0.73	37	79	1.54	>300	>300
D_3	333	449	0.74	33	81	1.64	>300	>300
Nb-V-Al-Ti STEELS								
A_4	381	478	0.80	39	76	1.43	>300	>300
A_5	387	498	0.78	30	75	1.39	>300	294
A_6	390	497	0.78	36	74	1.34	>300	>300
B_4	308	426	0.72	35	79	1.55	245	>300
B_5	335	458	0.73	35	78	1.51	>300	>300
B_6	337	462	0.71	36	77	1.48	>300	274
C_4	389	473	0.82	36	78	1.50	>300	>300
C_5	358	468	0.76	36	77	1.47	>300	>300
C_6	352	470	0.75	33	77	1.45	>300	295
D_4	314	449	0.70	37	78	1.49	>300	>300
D_5	322	435	0.74	39	78	1.50	>300	>300
D_6	340	458	0.74	35	77	1.48	>300	>300

Legends

(1) A,B,C,D refer to the rolling temperature of 1250°C, 1100°C 1000°C, and 900°C respectively.
(2) Subscripts refer to steel composition shown in Table 5
(3) RD is Rolling Direction.
(4) TD is Transverse Direction.

Table 7B

Mechanical Properties of Samples Stress Relieved at 650°C for 1 Hour.

STEEL	YS(MPa) ± 2%	UTS(MPa) ± 2%	YS/UTS	Elon % ± 4%	RA (%) ± 4%	Frac.Str ±0.04%	Charpy (J) R D	Charpy (J) T D
A_0	358	464	0.77	37	78	1.50	>300	>300
B_0	333	460	0.72	36	78	1.53	>300	>300
C_0	316	432	0.73	33	70	1.15	>300	>300
D_0	335	462	0.73	33	78	1.52	>300	>300
NB-TI-AL-V STEELS								
A_1	423	533	0.79	30	75	1.37	160	148
A_2	432	551	0.77	33	76	1.38	>300	130
A_3	382	507	0.75	30	77	1.49	>300	>300
B_1	394	501	0.79	31	73	1.32	198	124
B_2	351	470	0.75	31	77	1.48	>300	>300
B_3	328	441	0.74	35	76	1.43	>300	278
C_1	367	467	0.80	35	73	1.29	>300	>300
C_2	371	458	0.81	36	75	1.40	>300	276
C_3	388	452	0.86	39	80	1.61	>300	>300
D_1	354	456	0.78	38	77	1.48	>300	294
D_2	355	455	0.78	35	79	1.54	>300	291
D_3	340	447	0.76	34	73	1.32	>300	>300
NB-AL-TI STEELS								
A_4	370	459	0.81	30	78	1.50	>300	>300
A_5	382	474	0.81	32	76	1.42	232	>300
A_6	382	481	0.79	30	76	1.42	>300	282
B_4	308	421	0.73	37	77	1.49	>300	>300
B_5	324	437	0.74	35	76	1.43	>300	245
B_6	332	450	0.74	35	79	1.57	>300	228
C_4	387	467	0.82	35	79	1.58	>300	>300
C_5	349	449	0.78	36	79	1.57	>300	>300
C_6	360	455	0.79	33	72	1.28	>300	>300
D_4	386	438	0.88	36	76	1.44	>300	>300
D_5	336	437	0.77	39	79	1.56	>300	>300
D_6	332	442	0.75	37	77	1.46	>300	>300

Legends
YS = yield stress (MPa); UTS = Ultimate Tensile Strength (MPa)
Elon = % Elongation; R A = % Reduction in Area;
Frac.Str = Fracture strain

Table 8A

Typical non-metallic inclusion parameters.

Sample identity	Specimen orientation	Mean Length (μm)	Area Fraction %	Mean projected* length (cm^{-1})
A_4.	R D	2.14	0.0547	3.22
O = 0.0043 S = 0.003 P = 0.011	T D	2.16	0.0562	3.11
rolled at 1250°C	Z D	2.20	0.0660	3.07
B_4	R D	2.06	0.0578	3.45
same composition	T D	1.94	0.0582	3.55
(rolled at 1100°C)	Z D	2.15	0.0621	3.29
C_4	R D	2.08	0.0545	2.95
same composition	T D	2.29	0.0538	3.23
rolled at 1000°C	Z D	N D	N D	N D
D_4	R D	2.00	0.0522	3.01
same composition	T D	2.29	0.0538	3.23
rolled at 900°C	Z D	2.07	0.0648	3.44

Note

(1) The sample identity has the same meaning as defined previously.
(2) R D, T D and z D refer respectively to rolling, transverse and short transverse directions.
(3) N D, Not determined.

* defined by Baker and Charles[186] as the product of number of inclusions per unit area and mean lenght.

Table 8B

Assessment of Cleanness of these steels

Sample Serial No.	Sum of O, S, P (Wt. %)
0	0.0211
1	0.0190
2	0.0210
3	0.0186
4	0.0183
5	0.0192
6	0.0173

Table 9A

Grain Size Distribution of the As Rolled steels

STEEL	No. of fields exam.(n)	Total No. of grains	Mean No. of grains	Standard deviation	Grain Size (d) mm	μ_m	$d^{-1/2}(mm)^{-1/2}$
BASE STEEL							
A_0	50	566	11.32	1.35	0.0177	18	7.52
B_0	50	528	10.56	1.70	0.0189	19	7.27
C_0	50	742	14.84	1.73	0.0135	14	8.61
D_0	50	746	14.92	1.82	0.0134	13	8.64
Nb-Ti-Al-V STEELS							
A_1	50	600	12.00	1.33	0.0167	17	7.74
A_2	50	558	11.16	1.60	0.0179	18	7.47
A_3	49	600	12.24	2.02	0.0163	16	7.83
B_1	50	560	11.20	1.49	0.0179	18	7.47
B_2	49	608	12.41	1.35	0.0161	16	7.88
B_3	50	819	16.38	2.44	0.0122	12	9.05
C_1	50	789	15.78	2.97	0.0127	13	8.87
C_2	50	806	16.12	2.85	0.0124	12	8.98
C_3	50	809	16.18	2.13	0.0124	12	8.98
D_1	50	760	15.20	2.28	0.0132	13	8.70
D_2	50	694	13.88	1.87	0.0144	14	8.33
D_3	49	732	14.94	1.86	0.0134	13	8.64
Nb-V-Al-Ti STEELS							
A_4	50	810	16.20	1.75	0.0123	12	9.02
A_5	50	786	15.72	1.96	0.0127	13	8.87
A_6	50	729	14.58	1.65	0.0137	14	8.54
B_4	50	724	14.48	1.91	0.0115	12	9.33
B_5	50	738	14.76	2.44	0.0136	14	8.57
B_6	51	891	17.48	2.80	0.0114	11	9.37
C_4	50	617	12.34	1.94	0.0162	16	7.85
C_5	50	929	18.58	2.41	0.0108	11	9.62
C_6	50	812	16.24	2.66	0.0123	12	9.02
D_4	49	591	12.06	2.04	0.0166	17	7.76
D_5	50	727	14.54	2.03	0.0138	14	8.51
D_6	49	601	12.27	1.69	0.0163	16	7.83

Table 9B

Grain Size Distribution of the Stress Relieved Steels

STEEL	No. of fields exam.(n)	Total No. of grains	Mean No. of grains	Standard deviation	Grain Size (d) mm	μ_m	$d^{-1/2}$ (mm)$^{-1/2}$
BASE STEEL							
A_0	50	578	11.56	1.47	0.0173	17	7.60
B_0	50	695	13.90	1.87	0.0148	15	8.22
C_0	50	786	15.72	1.55	0.0127	13	8.87
D_0	50	700	14.00	1.98	0.0143	14	8.36
Nb-Ti-Al-V Steels							
A_1	50	587	11.74	1.47	0.0170	17	7.67
A_2	49	587	11.98	1.48	0.0179	18	7.47
A_3	50	633	12.06	1.73	0.0158	16	7.96
B_1	49	484	9.88	1.51	0.0202	20	7.04
B_2	50	590	11.80	1.39	0.0170	17	7.67
B_3	50	644	12.85	1.51	0.0155	16	8.03
C_1	50	1021	20.42	1.91	0.0098	10	10.10
C_2	50	727	14.54	2.37	0.0138	14	8.53
C_3	50	768	15.36	2.14	0.0130	13	8.77
D_1	50	850	17.00	1.84	0.0118	12	9.21
D_2	49	729	14.88	2.36	0.0134	13	8.64
D_3	50	832	16.64	2.46	0.0120	12	9.13
Nb-V-Al-Ti Steel							
A_4	50	780	15.60	2.03	0.0128	13	8.83
A_5	50	680	13.88	2.06	0.0144	14	8.33
A_6	50	722	14.44	1.83	0.0139	14	8.48
B_4	50	583	11.66	1.65	0.0172	17	7.62
B_5	50	571	11.42	1.61	0.0175	18	7.56
B_6	50	612	12.24	2.06	0.0163	16	7.83
C_4	50	843	16.86	2.65	0.0119	12	9.17
C_5	50	855	17.81	2.09	0.0112	11	9.44
C_6	50	874	17.48	1.85	0.0114	11	9.37
D_4	49	830	16.94	2.24	0.0118	12	9.21
D_5	50	652	13.04	1.98	0.0153	15	8.08
D_6	52	658	12.65	1.84	0.0158	16	7.96

Table 10A

STEM - EDAX Precipitate Analyses(AS ROLLED)

Sample	Precipitate Form	Analyses Wt %	Analyses Atom %	Alloying Element Activities
A_0 Analyses	Fine, spherical	Nb 90.8±6.0	80.7±5.3	f_{Ti} = 0.90
N 0.007%		Ti 6.7±0.8	11.5±1.4	a_{Ti} = 0.006
O 0.0051%		Al 2.5±0.5	7.7±1.6	f_{Al} = 1.07
Nb 0.042%	Less fine	Nb 90.6±1.5	82.6±1.4	a_{Al} = 0.032
Al 0.030%	spherical	Ti 8.8±0.2	15.5±0.4	f_V = 1.11
V 0.009%		Al 0.6±0.1	1.9±0.2	a_V = 0.010
Ti 0.007%				
A_1 Analyses	Fine, spherical	Nb 88.7±4.5	74.3±3.8	f_{Ti} = 0.87
N 0.012%		Ti 3.8±0.6	6.3±0.8	a_{Ti} = 0.006
O 0.004%		Al 3.3±0.4	9.5±1.5	f_{Al} = 1.09
Nb 0.047%		V 6.3±0.6	10.0±1.0	a_{Al} = 0.046
Ti 0.007%				
Al 0.042%		Nb 47.8±2.5	21.9±1.1	
V 0.073%	Angular	Ti 1.5±0.2	1.4±0.2	f_V = 1.09
	(hexagonal)	Al 46.3±1.3	73.1±2.0	a_V = 0.079
		V 4.31±0.4	3.6±0.3	
	Plate (Cuboid)	Nb 53.6±2.3	26.3±1.1	
		Ti 1.4±0.2	1.3±0.2	
		Al 41.4±1.1	55.7±1.4	
		V 3.7±0.3	3.2±0.3	
A_2 Analyses	Fine, spherical	Nb 55.8±9.0	47.2±6.5	f_{Ti} = 0.88
N 0.01%		Ti 7.3±1.6	10.2±2.2	a_{Ti} = 0.006
O 0.0040%		Al 7.3±1.4	18.1±3.4	f_{Al} = 1.09
Nb 0.047%		V 8.51±1.7	11.2±2.2	a_{Al} = 0.037
Ti 0.007%				
Al 0.034%	Long Plate	Nb 42.9±1.6	18.2±0.7	
V 0.043%	(Needle)	Ti 1.7±0.2	1.41±0.1	f_V = 1.09
		Al 54.3±0.9	79.5±1.3	a_V = 0.047
		V 1.2±0.1	0.9±0.1	
	Plate (Cuboid)	Nb 62.4±2.8	34.4±1.5	
		Ti 2.11±0.3	2.3±0.3	
		Al 32.8±1.1	60.7±2.0	
		V 2.8±0.3	2.7±0.3	

Table 10A (CONTINUED)

STEM – EDAX Precipitate Analyses

Sample	Precipitate Form	Analyses Wt %	Analyses Atom %	Alloying Element Activities
A_3 Analyses	Fine, Spherical	Nb 52.8±1.7	32.4±4.7	f_{Ti} = 0.92
N^3 0.0120%		Ti 8.10±1.5	9.7±1.8	a_{Ti} = 0.006
O 0.0036%		Al 16.0±2.2	33.8±4.6	
Nb 0.043%		V 6.3±1.3	7.01±1.5	f_{Al} = 1.10
	Coarse, Spherical			a_{Al} = 0.045
Ti 0.007%		Nb 58.5±7.3	33.3±4.11	
Al 0.041%		Ti 5.41±1.11	6.0±1.20	
V 0.030%		AL 25.91±2.5	50.8±4.9	f_V = 1.12
		V 3.21±0.9	3.5±0.9	a_V = 0.033
	Plate (cubold)	Nb 41.7±4.8	21.0±2.4	
		Ti 4.0±0.7	4.0±1.00	
		Al 42.4±2.2	64.6±2.2	
		V 2.51±0.6	2.3±0.6	
A_4 Analyses	Fine, spherical	Nb 56.7±11.0	38.9±7.5	
N^4 0.01%		Ti 39.8±4.5	53.1±6.0	f_{Ti} = 0.88
O 0.0043%		Al 3.4±1.4	7.9±3.2	a_{Ti} = 0.066
Nb 0.043%				
Ti 0.074%		Nb 47.9±3.9	31.8±7.5	f_{Al} = 1.09
Al 0.059%	Needle	Ti 50.8±2.0	65.3±2.6	a_{Al} = 0.064
		Al 1.3±0.3	2.9±0.8	
	Plate(Cubold)	Nb 50.4±3.0	34.0±2.0	
		Ti 48.6±1.5	63.5±1.9	
		Al 1.1±0.2	2.5±0.5	
A_5 Analyses	Fine, spherical	Nb 55.8±6.4	40.1±4.5	
N^5 0.011%		Ti 29.81±2.3	41.4±3.2	f_{Ti} = 0.92
O 0.0032%		Al 1.1±0.2	2.5±0.5	a_{Ti} = 0.034
Nb 0.048%				f_{Al} = 1.11
Al 0.060%	Plate(Cubold)	Nb 54.8±5.4	39.6±3.8	a_{Al} = 0.067
Ti 0.043%.		Ti 26.21±1.8	36.8±2.5	
		Al 0.9±0.4	2.3±0.9	

Table 10A (Continued)

STEM - EDAX Precipitate Analyses

Sample	Precipitate Form	Analyses Wt %	Analyses Atom %	Alloying Element Activities
A_6 Analyses	Fine, spherical	Nb 65.4±4.9	47.9±3.6	
N 0.012%		Ti 24.4±1.5	34.7±2.1	f^*_{Ti} = 0.92
O 0.0033%		Al 3.9±0.6	9.9±1.6	a_{Ti} = 0.025
Nb 0.049%		Nb 70.9±3.3	55.6±2.6	
Ti 0.027%	Plate (Cuboid)	Ti 25.5±1.0	38.9±1.5	f_{Al} = 1.12
Al 0.025%		Al 0.6±0.2	1.6±0.4	a_{Al} = 0.058

* For a multicomponent system, the following relationships[179] are valid

e.g $f_{Ti} = \Sigma wt\ \% \times e^{x}_{Ti}$

$a_{Ti} = f_{Ti} \times wt\ \%\ Ti$

Table 10B

STEM - EDAX Precipitate Analyses (AS CAST)

Sample	Precipitate Form	Analyses Wt %	Atom %
BASE STEEL (SUBSCRIPT 0)			
AS CAST	Fine, spherical	Nb 84.6±3.8	73.5±3.3
No 0		Ti 15.0±0.8	25.3±1.3
N 0.007%		Al 0.4±0.1	1.2±0.4
O 0.0051%			
Nb 0.042%			
Ti 0.007%	Less fine,	Nb 79.8±5.8	62.9±4.5
Al 0.030%	Spherical	Ti 14.9±1.2	22.7±1.8
V 0.009%		Al 5.3±0.8	14.4±2.1
HIGHEST V CONTAINING STEEL (1)			
AS CAST	Fine, spherical	Nb 84.1±0.7	68.5±8.7
N 0.012%		Ti 6.7±1.5	10.6±2.4
O 0.0040%		Al 5.5±1.4	15.4±3.9
Nb 0.047%		V 3.7±1.1	5.5±1.7
Ti 0.007%			
Al 0.042%	Less fine,	Nb 34.8±6.4	13.8±2.5
V 0.073%	spherical	Ti 2.5±0.8	1.9±0.7
		Al 59.6±4.3	81.9±5.9
		V 3.2±1.0	2.3±0.7
HIGHEST Ti CONTAINING STEEL(4)			
AS CAST	Fine, spherical	Nb 60.7±4.4	43.0±3.2
No 4		Ti 38.2±1.7	52.9±2.4
N 0.010%		Al 1.7±0.4	4.2±0.9
O 0.0042%			
Nb 0.043%			
Ti 0.074%	Less fine,	Nb 58.7±2.2	41.8±1.6
Al 0.059%	spherical	Ti 40.3±0.9	55.7±1.3
		Al 1.07±0.2	2.5±0.4

Table 10C

Actual and Theoretical Precipitate Analyses (wt %).

Sample		Actual (mean value)	Theoretical	Difference (app.)
A_0	Nb	90.7	86	5
	Ti	7.7	14	-6
	Al	1.6	0	1.6
A_1	Nb	63.4	34	29
	Ti	2.2	5	-3
	Al	30.3	8	22
	V	4.8	53	-48
A_2	Nb	53.7	45	9
	Ti	3.7	7	-3
	Al	31.4	7	25
	V	4.1	41	-37
A_3	Nb	51	47.1	4
	Ti	5.8	7.5	-2
	Al	28.1	12.8	15
	V	4	32.6	-29
A_4	Nb	52	37	15
	Ti	46.4	63	-17
	Al	1.8	0	2
A_5	Nb	55.3	56.5	-1
	Ti	28	43.5	-16
	Al	1	0	0
A_6	Nb	68	67.7	0
	Ti	25	36.3	-11
	Al	2.3	0	2.3

Table 11

Analyses of High Temperature Precipitates

A_O + W/Q*	Fine, dense spherical	Nb 42.7±3.0 Ti 56.5±2.0 Al 0.7±0.2	27.7±2.0 70.7±2.1 1.6±0.5
A_O + 20% reduction + W/Q	Fine, dense, spherical	Nb 47.3±3.4 Ti 51.8±1.6 Al 0.6±0.2	31.5±2.3 67.2±2.3 1.4±0.5
	Less dense, fine, spherical	Nb 80.7±3.9 Ti 18.5±0.9 al 0.7±0.2	67.7±3.0 30.1±1.5 2.3±0.5
A_4 + W/Q	Plate (cubold)	Nb 26.4±0.9 Ti 73.1±1.2 Al 0.5±0.1	15.5±0.5 83.5±1.4 1.0±0.1

* W/Q is Water Quenched.

Table 12

Hot Rolling Plan for the Examination of High temperature Precipitation ($1250^{0}C$)

Pass No.	Thickness (mm)	Change in Thickness (mm)	% Reduction per pass
0	18 + 0.5	0.0	0.0
1 W/Q*	15 W/Q	3 W/Q	17 W/Q
2 W/Q	15 + 0.5 W/Q	3.5 W/Q	23 W/Q

W/Q* = Water quenched.

Table 13

NACE Test Conditions for HIC

Solution	5 % Nacl solution
H_2S concentration (ppm)	134000
H_2S flow rate after saturation	17 c.c/min/litre
Initial pH of solution	2.40
Final pH of solution	3.20
pH controlling agent	CH_3COOH (0.5 %)
specific volume (CC/cm^2)	7.0
Loading stress	None
Temperature (^{0}C)	16 - 18
Duration (hours)	96

Table 14A

Actual and Calculated strengths of the As rolled steels

STEEL	Actual YS (MPa)	Cal. YS (MPa)	ΔYS (MPa)	Actual UTS (MPa)	Cal. UTS (MPa)	ΔUTS(MPa)
BASE STEELS						
A_0	354	244	110	480	447	+33
B_0	346	240	106	474	445	+29
C_0	368	263	105	466	455	+11
D_0	314	264	50	432	455	-23
Nb-Ti-Al-V Steels						
A_1	389	242	147	500	434	+66
A_2	336	240	96	420	458	-37
A_3	350	250	100	471	446	+25
B_1	400	237	163	531	432	+99
B_2	360	247	113	483	461	+22
B_3	335	271	64	440	453	-15
C_1	356	262	94	463	443	+20
C_2	354	267	87	468	470	-2
C_3	363	270	93	464	455	+9
D_1	355	259	50	461	447	+19
D_2	338	262	96	461	468	-7
D_3	333	264	76	449	452	-3
Nb-Al-V-Ti Steels						
A_4	381	265	116	478	448	+30
A_5	387	267	120	498	455	+43
A_6	390	267	123	497	460	+37
B_4	308	241	67	426	451	-25
B_5	335	262	73	458	454	+4
B_6	337	282	54	462	466	+4
C_4	389	268	121	473	439	+34
C_5	358	218	78	468	462	+6
C_6	352	276	76	470	463	+7
D_4	314	268	46	446	439	+7
D_5	322	261	61	435	453	-18
D_6	340	255	85	458	454	+4

Note:
Both Alphabets and Subscripts have the same meaning as those in Table 7A

Table 14B

Actual and Calculated strengths for Samples Stress Relieved at 650^{0}C For 1 hour

STEEL	Actual YS (MPa)	Cal. YS (MPa)	ΔYS (MPa)	Actual UTS (MPa)	Cal. UTS (MPa)	ΔUTS(MPa)
BASE STEELS						
A_0	358	246	112	464	447	+17
B_0	333	256	77	460	452	+8
C_0	316	268	48	432	457	-25
D_0	335	239	96	462	453	+9
Nb-Ti-Al-V Steels						
A_1	423	240	183	533	433	+100
A_2	423	245	178	551	423	+128
A_3	382	252	130	507	447	+60
B_1	394	229	165	501	429	+72
B_2	351	244	107	470	458	+11
B_3	328	254	74	441	448	-7
C_1	367	283	84	467	452	+15
C_2	371	259	112	458	466	-8
C_3	388	266	122	452	453	-1
D_1	354	268	86	456	445	+11
D_2	355	260	95	455	467	-12
D_3	340	272	68	447	456	-9
Nb-Al-V-Ti Steels						
A_4	370	262	108	459	447	-12
A_5	382	258	124	474	452	+22
A_6	382	267	115	481	460	+21
B_4	308	241	67	421	437	-16
B_5	324	244	80	437	446	-9
B_6	332	254	78	450	454	-4
C_4	387	268	119	467	449	+18
C_5	349	277	72	449	460	-11
C_6	360	281	79	455	466	-11
D_4	386	268	118	438	450	-12
D_5	336	253	83	437	450	-13
D_6	332	257	75	442	455	-13

Table 15A

The Possible effect of Microalloy Precipitates on Impact Transition Temperature (ITT) for As Rolled Steels.

STEEL	YS (MPa)	I.T.T_{cal} (^{O}C)	$\frac{\Delta YS}{15} \times 4$ (^{O}C)	I.T.T_{eff} (^{O}C)
BASE STEEL				
A_0	110	-71	29	-42
B_0	106	-68	28	-40
C_0	105	-84	28	-56
D_0	50	-84	13	-71
Nb-Ti-Al-V Steels				
A_1	147	-81	39	-42
A_2	96	-75	26	-49
A_3	100	-77	27	-50
B_1	163	-77	43	-34
B_2	113	-80	30	-50
B_3	64	-91	17	-74
C_1	94	-94	25	-69
C_2	87	-93	23	-70
C_3	93	-90	25	-65
D_1	50	-92	26	-66
D_2	96	-90	20	-70
D_3	76	-86	18	-68
Nb-Al-V-Ti Steels				
A_4	116	-93	31	-62
A_5	120	-85	32	-53
A_6	123	-82	33	-49
B_4	67	-97	18	-79
B_5	73	-84	20	-64
B_6	54	-92	14	-78
C_4	121	-78	32	-46
C_5	78	-96	21	-75
C_6	76	-88	20	-68
D_4	46	-79	12	-67
D_5	61	-84	16	-68
D_6	85	-74	23	-51

Table 15B

The Possible effect of Microalloy Precipitates on I.T.T for Samples Stress Relieved at 650°C for 1 hour.

STEEL	YS (MPa)	I.T.T$_{cal}$ (°C)	$\frac{\Delta YS}{15} \times 4$ (°C)	I.T.T$_{eff}$ (°C)
BASE STEELS				
A_0	112	-72	30	-42
B_0	77	-79	21	-58
C_0	48	-87	13	-74
D_0	96	-81	26	-55
Nb-Ti-Al-V Steels				
A_1	183	-80	49	-31
A_2	178	-79	47	-31
A_3	130	-78	35	-43
B_1	165	-73	49	-29
B_2	107	-78	29	-49
B_3	74	-79	20	-59
C_1	84	-108	22	-86
C_2	112	-87	30	-57
C_3	122	-87	33	-54
D_1	86	-98	23	-75
D_2	95	-89	25	-64
D_3	68	-92	18	-74
Nb-Al-V-Ti Steels				
A_4	108	-91	29	-62
A_5	124	-82	33	-49
A_6	115	-82	31	-51
B_4	67	-77	18	-59
B_5	80	-73	21	-52
B_6	78	-74	21	-53
C_4	119	-95	32	-63
C_5	72	-94	19	-75
C_6	79	-92	21	-71
D_4	118	-95	32	-63
D_5	83	-72	22	-50
D_6	75	-73	20	-53

Table 16A

Theoretical Properties of The As Rolled Steels

STEEL	YS(MPa) ±2	UTS(MPa) ±5	I.T$_{0}$T ±3(^{0}C)	Flow Stress ± 16	Work Hard. rate (MPa) ±3	Maximum uniform Strain(E_u) ±0.02	E_T
BASE STEELS							
A_0	244	447	-71	994	551	0.07	1.55
B_0	240	445	-68	990	548	0.07	1.55
C_0	263	455	-84	1010	568	0.07	1.57
D_0	264	455	-84	1011	569	0.07	1.56
Nb-Ti-Al-V Steels							
A_1	242	434	-81	945	547	0.11	1.57
A_2	240	458	-75	978	546	0.10	1.56
A_3	250	446	-77	994	555	0.08	1.58
B_1	237	432	-77	940	542	0.11	1.56
B_2	247	461	-80	984	549	0.10	1.57
B_3	271	454	-91	1012	574	0.08	1.60
C_1	260	443	-94	961	564	0.11	1.59
C_2	354	470	-93	1001	569	0.10	1.58
C_3	270	455	-90	1111	573	0.08	1.60
D_1	259	447	-92	959	562	0.11	1.58
D_2	262	468	-90	997	565	0.10	1.58
D_3	264	452	-86	1006	554	0.08	1.59
Nb-Al-V-Ti Steels							
A_4	265	448	-93	967	565	0.09	1.58
A_5	267	455	-85	1013	550	0.07	1.57
A_6	267	460	-82	1054	570	0.07	1.60
B_4	241	451	-97	972	570	0.09	1.58
B_5	262	454	-84	1012	548	0.07	1.57
B_6	282	466	-92	1062	582	0.07	1.62
C_4	268	439	-78	950	548	0.09	1.58
C_5	280	462	-96	1027	565	0.07	1.58
C_6	276	463	-88	1061	577	0.07	1.62
D_4	268	439	-79	949	546	0.09	1.56
D_5	261	453	-84	1011	548	0.07	1.57
D_6	255	454	-74	1044	559	0.07	1.60

Table 16B

Theoretical Properties of The Stress Relieved Steels

STEEL	YS(MPa) ±2	UTS(MPa) ±5	I.T$_{0}$T ±3(^{0}C)	Flow Stress ± 16	Work Hard. rate (MPa) ±3	Maximum uniform Strain(E_u) ±0.02	E_T
BASE STEELS							
A_0	246	447	-72	995	553	0.07	1.55
B_0	256	452	-79	1005	562	0.07	1.56
C_0	268	457	-87	1014	562	0.07	1.57
D_0	239	453	-81	1006	564	0.07	1.56
Nb-Ti-Al-V Steels							
A_1	240	433	-80	943	546	0.11	1.57
A_2	245	423	-78	982	550	0.10	1.57
A_3	252	447	-78	996	557	0.08	1.58
B_1	229	429	-73	985	536	0.11	1.56
B_2	244	458	-78	981	549	0.10	1.56
B_3	254	448	-79	997	559	0.08	1.58
C_1	284	452	-108	990	583	0.11	1.60
C_2	259	466	-87	994	562	0.10	1.58
C_3	266	453	-87	1008	570	0.08	1.59
D_1	268	445	-98	985	570	0.11	1.59
D_2	260	467	-89	996	564	0.10	1.58
D_3	272	456	-92	1013	575	0.08	1.62
Nb-Al-V-Ti Steels							
A_4	262	447	-91	965	564	0.09	1.57
A_5	258	452	-82	1008	545	0.07	1.56
A_6	267	460	-82	1054	569	0.07	1.61
B_4	241	437	-77	947	544	0.09	1.56
B_5	244	446	-73	997	533	0.07	1.55
B_6	254	454	-74	1044	559	0.07	1.62
C_4	268	449	-95	970	568	0.09	1.58
C_5	277	460	-94	1025	562	0.07	1.58
C_6	281	466	-92	1066	582	0.07	1.62
D_4	268	450	-95	970	568	0.09	1.56
D_5	253	450	-72	1004	541	0.07	1.56
D_6	257	455	-73	1045	561	0.07	1.60

E_T = Fracture Srain

Table 17A

Actual and Calculated Fracture Strain (E_T) for the As Rolled Steels

	Actual E_T	Calculated E_T	Deviation From Calculated
BASE STEELS			
A_0	1.40	1.55	0.15
B_0	1.30	1.55	0.25
C_0	1.22	1.57	0.35
D_0	1.33	1.56	0.23
Nb-Ti-Al-V Steels			
A_1	1.35	1.57	0.22
A_2	1.42	1.56	0.14
A_3	1.41	1.58	0.17
B_1	1.26	1.56	0.30
B_2	1.27	1.57	0.30
B_3	1.53	1.60	0.07
C_1	1.16	1.59	0.43
C_2	1.51	1.58	0.07
C_3	1.47	1.60	0.13
D_1	1.41	1.58	0.17
D_2	1.54	1.58	0.04
D_3	1.64	1.59	-0.05
Nb-Al-V-Ti Steels			
A_4	1.43	1.58	0.15
A_5	1.39	1.57	0.18
A_6	1.34	1.60	0.26
B_4	1.55	1.58	0.03
B_5	1.51	1.57	0.06
B_6	1.48	1.62	0.14
C_4	1.50	1.58	0.08
C_5	1.47	1.58	0.11
C_6	1.45	1.62	0.17
D_4	1.49	1.56	0.07
D_5	1.50	1.57	0.07
D_6	1.48	1.60	0.12

Table 17B

Actual and Calculated Fracture Strain (E_T) for Stress Relieved Samples

	Actual E_T	Calculated E_T	Deviation From Calculated
BASE STEELS			
A_0	1.50	1.55	0.05
B_0	1.53	1.56	0.03
C_0	1.15	1.57	0.42
D_0	1.52	1.56	0.04
Nb-Ti-Al-V Steels			
A_1	1.37	1.57	0.20
A_2	1.38	1.57	0.19
A_3	1.49	1.58	0.09
B_1	1.32	1.56	0.24
B_2	1.48	1.56	0.08
B_3	1.43	1.58	0.15
C_1	1.29	1.60	0.31
C_2	1.40	1.58	0.18
C_3	1.61	1.59	-0.02
D_1	1.48	1.59	0.11
D_2	1.54	1.58	0.04
D_3	1.32	1.60	0.28
Nb-Al-V-Ti Steels			
A_4	1.50	1.57	0.07
A_5	1.42	1.56	0.14
A_6	1.42	1.61	0.19
B_4	1.49	1.56	0.07
B_5	1.43	1.55	0.12
B_6	1.57	1.62	0.05
C_4	1.58	1.58	0.00
C_5	1.57	1.58	0.01
C_6	1.28	1.62	0.34
D_4	1.44	1.56	0.12
D_5	1.56	1.56	0.00
D_6	1.46	1.60	0.14

Table 18[80]

Examples of Fracture - Toughness Requirements.

YEAR	PIPELINE	GRADE	ABSORBED ENERGY (J) (ft-lb)	DWTT SHEAR, AREA %
1967	IRAN, OIL	X60	(≥27), ≥20/ -10*	-
1970	ALASKA, OIL	X65	(≥46), ≥34/ -10	-
1972	NORTH SEA, OIL	X65	(≥82), ≥61/ -10	-
1973	NORTH SEA, OIL	X65	(≥82), ≥61/ -10	≥75 at 0*
1973	AUSTRALIA, GAS	X65	(≥82), ≥61/ 0	≥50 at 0
1975	ALASKA, GAS	X65	(≥92), ≥68/ -24	≥75 at -24
1977	USSR, GAS	X70	(≥85), ≥63/ -20	≥85 at -20
1980	NORTH SEA	X65	(≥147), ≥109/-10	≥65 at -10

* In degrees Centigrade

Table 19

Variation of the Theoretical Austenite To Ferrite Transformation* Temperature with composition.

Steel No.	Calculated Transformation Temperature (^{0}C)
0	717
1	716
2	716
3	717
4	716
5	716
6	717

* $(^{0}C)^{(53)} = 723 - 10.7\,(Mn) - 16.9\,(Ni) + 29.1\,(Si) + 16.9\,(Cr) + 290\,(As) + 6.38\,(W)$

Table 20[182]

ELEMENT	At.No.	Electron Arrangement										Atomic Radii (10-12 m)	Ionic Radii (10-12 m)	Density (g/cm^{-3})	Melting Point (^{0}C)
		K	L		M				N						
	Orbitals	1s	2s	2p	3s	3p	3d	4s	4p	4d	4f	pm	pm		
C	6	2	2	2								71/77	16	2.3	>3527
N	7	2	2	3								71	16	1.17	-209.7
O	8	2	2	4								60	132	1.33	-218.3
Al	13	2	2	6	2	1						142	51	2.7	660.3
Tl	22	2	2	6	2	6	2	2				146	68	4.54	1675
V	23	2	2	6	2	6	3	2				131	74	6.1	1887
Fe	26	2	2	6	2	6	6	2				123	74	7.87	1535
Nb	41	2	2	6	2	6	10	2	6	4	1	143	69	8.57	2468

Table 21A

Summary of Calculations for A_0

Phase	T_{start} (^{0}C)	T_{finish} (^{0}C)	Quantity of Phase	% wt. Fraction	Theoretical wt % of metal in precipitate	
TIN	1352/1578	1217	0.0089	0.7	0.0069Ti =	14.1
Nb(C,N)	1179	999	0.0408	3.1	0.0319Nb =	65.4
						85.9
NbC	946	657	0.0113	0.9	0.0100Nb =	20.5
AlN	-	-	-	-	-	
Fe_3C	716	-	1.269	95.4	-	
			1.330	100	0.0488	100

Table 21B

Data for the construction of TIN Solvus

Ti (wt %)	N (wt %)	% wt Fraction	Temperature (^{0}C) Solid data	Temperature (^{0}C) Liquid data
0.007	0.007	0.0	1578	1352
0.005	0.0064	0.20	1538	1323
0.003	0.0058	0.41	1483	1283
0.001	0.00517	0.61	1383	1210
0.0005	0.0051	0.66	1328	-
0.0001	0.005	0.70	1217	-

Table 21C

Data for the Construction of Nb(C,N)SOLVUS

Nb(wt %)	N (wt %)	C (wt %)	% wt fraction	Temperature (^{O}C)
0.042	0.005	0.09	0.00	1179
0.037	0.0042	0.0894	0.49	1160
0.032	0.0035	0.0887	0.97	1140
0.027	0.0027	0.0881	1.46	1117
0.022	0.0020	0.0874	1.94	1090
0.017	0.0012	0.0868	2.43	1058
0.012	0.0005	0.0861	2.92	1018
0.010	0.0001	0.0859	3.1	999

Table 21D

Data for the Construction of NbC Solvus

Nb (wt %)	C (wt %)	% wt Fraction	Temperature (^{O}C)
0.0101	0.0859	0.00	946
0.005	0.0852	0.46	890
0.003	0.0850	0.64	853
0.001	0.0847	0.82	782
0.0005	0.0847	0.86	741
0.0001	0.0846	0.90	657

Table 22A

Summary of Results for A_1

Phase	T_{start} (^{o}C)	T_{finish} (^{o}C)	Quantity of Phase	% wt. Fraction	Theoretical wt % of metal in precipitate
TIN	1633/1390	1262	0.00891	0.8	0.00690Ti = 5%
AlN	1246	750	0.0176	1.50	0.01160Al = 8%
Nb(C,N)	1200	1078	0.0340	2.90	0.02660Nb = 34%
NbC	1006	657	0.0229	1.90	0.02030Nb
VC	791	526	0.0897	7.60	0.07290V = 53%
Fe_3C	716	-	1.007	85.33	
			1.1801	100.03	0.13828

Table 22B

Data for the Construction of TIN Solvus.

% wt Fraction	cummulative wt. fraction	Temp.(^{o}C) solid data	Temp.(^{o}C) for liquid data
0.00	0.00	1633	1390
0.23	0.23	1594	1362
0.46	0.46	1539	1323
0.70	0.70	1437	1250
0.75	0.75	1380	-
0.80	0.80	1262	-

Table 22C

Data for Construction of AlN Solvus.

% wt fraction	Cummulative % wt, fraction	Temp.(^{o}C)
0.00	0.80	1246
0.50	1.30	1198
0.65	1.45	1183
1.29	5.14	1106
1.50	9.54	750

Table 22D

Data for Construction of Nb(C,N) Solvus.

% wt fraction	Cummulative % wt, fraction	Temp.(^{O}C)
0.00	1.30	1198
1.31	2.76	1154
1.86	3.31	1132
2.40	3.85	1108
2.90	8.04	1078

Table 22E

Data for Construction of NbC Solvus.

% wt fraction	Cummulative % wt, fraction	Temp.(^{O}C)
0.0	8.51	1006
0.22	8.73	995
0.88	9.39	952
1.44	9.95	890
1.86	10.37	740
1.90	10.41	657

Table 22F

Data for Construction of VC Solvus.

% wt fraction	Cummulative % wt, fraction	Temp.(^{O}C)
0.00	10.30	791
1.04	11.34	782
2.09	12.39	771
3.13	13.43	760
4.17	14.47	746
5.21	15.51	727
6.25	16.55	700
7.60	17.90	526

Table 22G

Data for the Co-precipitation curve of AlN and Nb(C,N)

% wt fraction	New Phase	Temperature (^{O}C)
0.00	AlN	1246
1.30	AlN	1198
1.45	AlN	1183
2.76	Nb(C,N)	1154
3.31	Nb(C,N)	1132
3.85	Nb(C,N)	1108
5.14	AlN	1106
8.04	Nb(C,N)	1078
9.54	AlN	750

Table 23A

Summary of Results for A_2

Phase	T_{start} (^{o}C)	T_{finish} (^{o}C)	Quantity of Phase	% wt. Fraction	Theoretical wt % of metal in precipitate
TIN	1614/1377	1247	0.00891	0.70	0.00690Ti = 7
Nb(C,N)	1198	1063	0.0372	3.00	0.0291Nb
AIN	1181	741	0.01063	0.86	0.0070Al = 7
NbC	995	657	0.0202	1.63	0.0179Nb,
VC	764	529	0.0528	4.25	0.0429V = 41
Fe_3C	716	-	-	90.0	
				100	100.0

Table 23B

Data for the Construction of TIN Solvus.

% wt Fraction	cummulative wt. fraction	Temp.(^{o}C) solid data	Temp.(^{o}C) for liquid data
0.0	0.00	1614	1377
0.20	0.20	1575	1349
0.41	0.41	1520	1310
0.61	0.61	1419	1237
0.66	0.66	1363	
0.70	0.70	1247	

Table 23C

Data for Construction of Nb(C,N) Solvus.

% wt fraction	Cummulative % wt, fraction	Temp.(^{o}C)
0.00	0.70	1198
0.50	1.20	1181
1.24	2.66	1154
1.76	4.92	1132
2.37	7.19	1108
3.00	12.34	1063

Table 23D

Data for Construction of AlN Solvus.

% wt fraction	Cummulative % wt, fraction	Temp.(^{O}C)
0.00	1.30	1181
0.12	1.42	1167
0.50	3.16	1138
0.61	7.80	1106
0.74	8.54	1089
0.80	9.34	1080
0.86	13.20	741

Table 23E

Data for Construction of NbC Solvus.

% wt fraction	Cummulative % wt, fraction	Temp.(^{O}C)
0.00	12.70	995
0.46	13.16	967
0.91	13.61	926
1.37	14.07	853
1.54	14.24	781
1.63	14.33	657

Table 23F

Data for Construction of VC Solvus.

% wt fraction	Cummulative % wt, fraction	Temp.(^{O}C)
0.00	14.30	764
0.99	15.29	750
1.98	16.28	731
2.97	17.27	704
3.96	18.26	643
4.25	18.55	529

Table 23G

Data for the Co-precipitation curve of Nb(C,N) and AlN

% wt fraction	New Phase	Temperature (^{O}C)
0.00	Nb(C,N)	1198
1.30	Nb(C,N)	1181
1.42	AlN	1167
2.66	Nb(C,N)	1154
3.16	AlN	1138
4.92	Nb(C,N)	1132
7.19	Nb(C,N)	1108
7.80	AlN	1106
8.54	AlN	1089
9.34	AlN	1080
12.34	Nb(C,N)	1063
13.20	AlN	741

Table 24A

Summary of Results for A_3

Phase	T_{start} (°C)	T_{finish} (°C)	Quantity of Phase	% wt. Fraction	Theoretical wt % of metal in precipitate
TIN	1633/1390	1262	0.00891	0.70	0.00690Ti = 7.5
AIN	1244	748	0.0178	1.39	0.01172Al = 12.8
Nb(C,N)	1188	1062	0.0317	2.48	
					0.0431 Nb = 47.1
NbC	997	657	0.0207	1.62	
VC	747	530	0.0368	2.88	0.0299 V = 32.6
Fe_3C	717	-	1.163	90.94	
			1.279	100.0	100.0

Table 24B

Data for the Construction of TIN Solvus.

% wt Fraction	cummulative wt. fraction	Temp.(°C) solid data	Temp.(°C) for liquid data
0.00	0.00	1633	1390
0.20	0.20	1595	1462
0.41	0.41	1539	1323
0.61	0.61	1437	1250
0.66	0.66	1380	
0.70	0.70	1250	

Table 24C

Data for Construction of AIN Solvus.

% wt fraction	Cummulative % wt, fraction	Temp.(°C)
0.00	0.70	1244
0.54	1.24	1188
0.59	1.29	1181
1.19	3.98	1104
1.30	7.28	1086
1.39	11.15	748

Table 24D

Data for Construction of Nb(C,N) Solvus.

% wt fraction	Cummulative % wt, fraction	Temp.(^{O}C)
0.00	1.24	1188
1.00	2.29	1147
1.50	2.79	1125
2.00	5.98	1099
2.30	9.58	1081
2.48	9.76	1062

Table 24E

Data for Construction of NbC Solvus.

% wt fraction	Cummulative % wt, fraction	Temp.(^{O}C)
0.00	10.10	997
0.44	10.54	969
0.88	10.98	930
1.50	11.60	860
1.59	11.69	713
1.62	11.72	657

Table 24F

Data for Construction of VC Solvus.

% wt fraction	Cumulative % wt, fraction	Temp.(^{O}C)
0.00	11.69	747
0.48	12.17	737
0.96	12.65	727
1.44	13.13	712
1.93	13.62	695
2.41	14.10	665
2.88	14.57	530

Table 24G

Data for the Co-precipitation curve of AlN and Nb(C,N)

% wt fraction	New Phase	Temperature (^{O}C)
0.00	AlN	1244
1.24	AlN	1188
1.29	AlN	1181
2.29	Nb(C,N)	1147
2.79	Nb(C,N)	1125
3.98	AlN	1104
5.98	Nb(C,N)	1099
7.28	AlN	1086
9.58	Nb(C,N)	1081
9.76	Nb(C,N)	1062
11.15	AlN	748

Table 25A

Summary of Results for A_4

Phase	T_{start} (°C)	T_{finish} (°C)	Quantity of Phase	% wt. Fraction	Theoretical wt % of metal in precipitates
TIN	1889/1564	1362	0.0438	3.47	0.0269 Ti = 29
NbC	1082	651	0.0484	3.84	0.0429 Nb = 37
TIC	1075	729	0.0500	3.97	0.0400 Ti = 34
					Ti = 63
Fe_3C	716	-	1.1169	88.70	
				100.00	100.00

Table 25B

Data for the Construction of TIN Solvus.

% wt Fraction	cummulative wt. fraction	Temp.(°C) solid data	Temp.(°C) for liquid data
0.00	0.00	1889	1564
0.70	0.70	1846	1536
1.40	1.40	1798	1530
2.11	2.11	1734	1502
2.81	2.81	1643	1460
3.16	3.16	1566	1397
3.18	3.18	1530	1343
3.47	3.47	1362	1195

Table 25C

Data for Construction of NbC solvus

% wt fraction	Difference in % wt fraction	Cummulative % wt fraction	Temp. (°C)
0.00	0.00	3.47	1082
0.134	0.134	3.604	1075
0.654	0.52	4.616	1060
1.102	0.448	5.565	1044
1.550	0.448	6.505	1025
1.998	0.448	7.453	1003
2.445	0.447	8.392	977
2.896	0.451	9.343	943
3.341	0.445	10.281	892
3.840	0.499	11.28	651

Table 25D

Data for construction of TIC solvus

% wt fraction	Difference in % wt fraction (TIC)	Difference in % wt fraction (NbC)	Cummulative Temp. (^{O}C)	
0.00	0.00	0.00	3.604	1075
0.492	0.501	0.52	4.096	1062
0.993	0.492	0.448	5.117	1050
1.485	0.500	0.448	6.057	1035
1.985	0.492	0.448	7.005	1018
2.477	0.500	0.447	7.945	997
2.977	0.493	0.451	8.892	969
3.470	0.500	0.445	9.836	926
3.970	0	0.499	10.781	729

Table 25E

Data for the Construction of (NbTI)C solvus

Cummulative % wt fraction	Temperature (^{O}C)
3.47	1082
3.60	1075
4.10	1062
4.62	1060
5.12	1050
5.57	1044
6.06	1035
6.51	1025
7.01	1080
7.45	1003
7.95	997
8.39	977
8.89	969
9.34	943
9.84	926
10.28	892
10.78	729
11.28	651

Table 26A

Summary of Results for A_5

Phase	T_{start} (°C)	T_{finish} (°C)	Quantity of Phase	% wt. Fraction	Theoretical wt % of metal in precipitates
TIN	1812/1512	1046	0.0477	3.51	0.03693 Ti = 43.5
NbC	1093	657	0.0541	3.98	0.04792 Nb = 56.5
Fe_3C	716	-	92.5		
			100.00		100.00

Table 26B

Data for the Construction of TIN Solvus.

% wt Fraction	cummulative wt. fraction	Temp.(°C) solid data	Temp.(°C) for liquid data
0.00	0.00	1812	1512
0.19	0.19	1798	1503
0.67	0.67	1762	1478
1.14	1.14	1720	1450
1.62	1.62	1671	1416
2.09	2.09	1612	1375
2.57	2.57	1536	1321
3.04	3.04	1420	1238
3.98	3.98	1046	

Table 26C

Data for Construction of NbC Solvus.

% wt fraction	Cummulative % wt, fraction	Temp.(°C)
0.00	3.50	1093
0.25	3.75	1086
0.66	4.16	1073
1.08	4.58	1059
1.50	5.00	1044
1.91	5.41	1026
2.33	5.83	1005
2.74	6.24	979
3.16	6.66	944
3.57	7.07	890
3.98	7.48	657

Table 27A

Summary of Results for A_6

Phase	T_{start} (°C)	T_{finish} (°C)	Quantity of Phase	% wt. Fraction	Theoretical wt % of metal in precipitates
TIN	1784/1493	1205	0.03475	2.58	0.0269 Ti = 36.3
Nb(C,N)	1199	1083	0.0332	2.48	0.0259 Nb = 67.7
NbC	1011	657	0.0240	1.78	0.0213 Nb
Fe_3C	716	-	1.257	93.18	

Table 27B

Data for the Construction of TIN Solvus.

% wt Fraction	cummulative wt. fraction	Temp.(°C) solid data	Temp.(°C) for liquid data
0.00	0.00	1784	1493
0.19	0.19	1769	1483
0.67	0.67	1727	1455
1.15	1.15	1677	1420
1.63	1.63	1615	1377
2.11	2.11	1525	1314
2.58	2.58	1205	

Table 27C

Data for Construction of Nb(C,N) Solvus.

% wt fraction	Cummulative % wt, fraction	Temp.(^{O}C)
0.00	2.58	1199
0.38	2.96	1186
0.86	3.44	1168
1.34	3.92	1148
1.82	4.40	1127
2.29	4.87	1104
2.48	5.06	1083

Table 27D

Data for Construction of NbC Solvus.

% wt fraction	Cummulative % wt, fraction	Temp.(^{O}C)
0.00	5.06	1011
0.12	5.18	1005
0.54	5.60	979
0.95	6.01	944
1.37	6.43	890
1.78	6.84	657

Table 28

Variation of theoretical excess Al with sample.

Sample	Available Al* (wt %)	Excess (free) Al (wt %)
A_0	0.024	0.024
A_1	0.038	0.018
A_2	0.030	0.023
A_3	0.037	0.025
A_4	0.054	0.054
A_5	0.056	0.056
A_6	0.048	0.048

* = Total amount of Al available for AlN precipitation.

Table 29

Variation of theoretical % Pearlite with sample.

Sample	% Pearlite	Pearlite Dilution
A_0	10.6	0.70
A_1	8.4	2.9
A_2	9.3	2.0
A_3	9.7	1.6
A_4	9.3	2.0
A_5	10.5	0.8
A_6	10.5	0.8

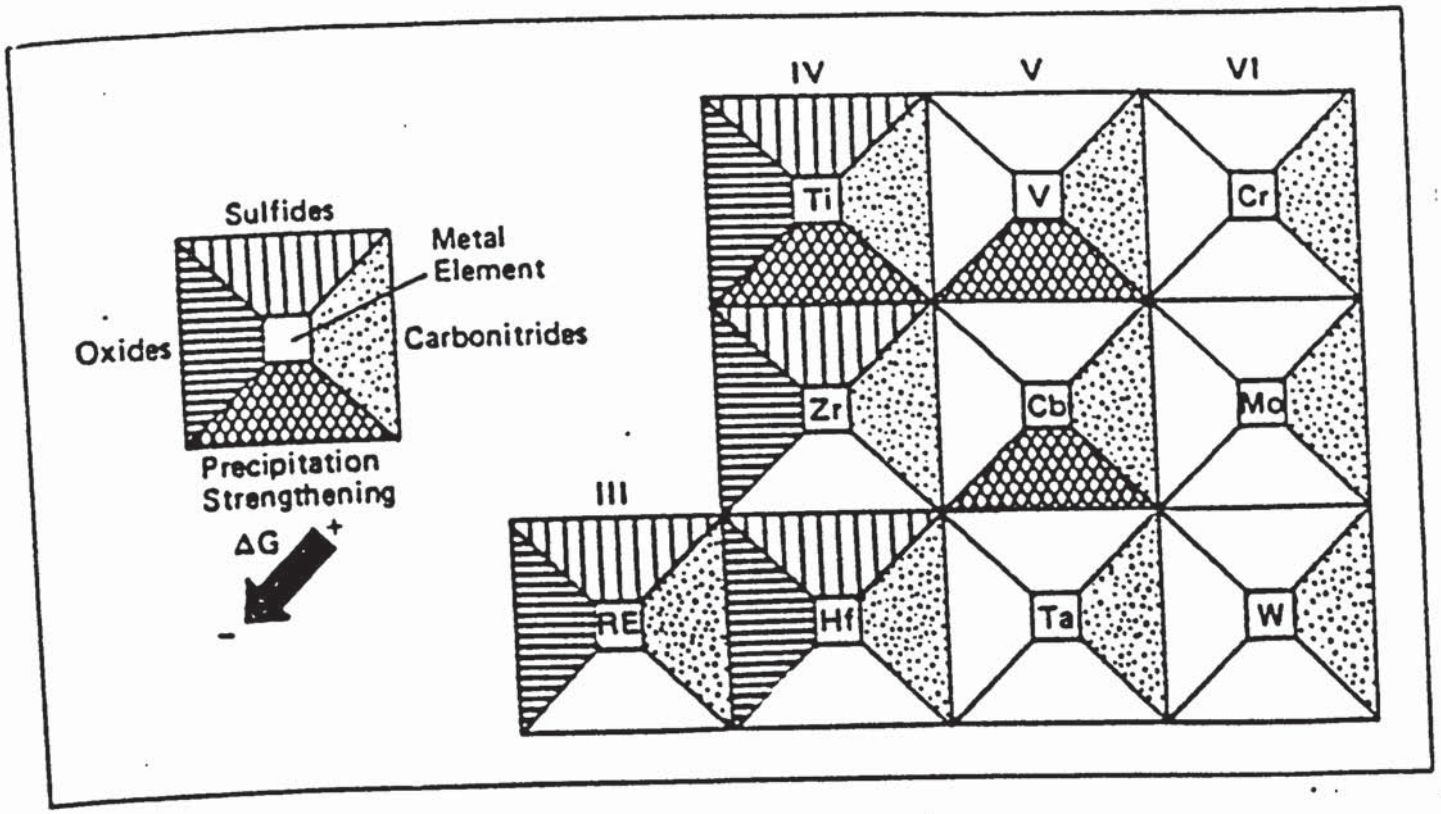

FIGURE-1. The Potential of Certain Metals to Form Oxides, Sulphides, Carbides, and Nitrides and their Precipitation Strengthening Potential (Arranged Similar to the Periodic Table) (37).

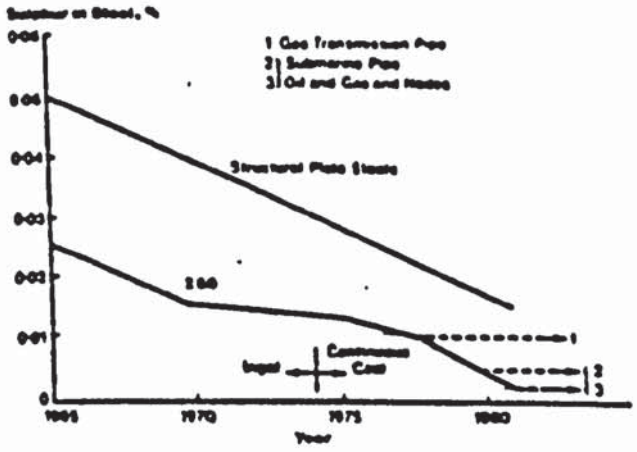

FIGURE-2. Changes in Sulphur Specification for Pipeline Grades of Steel(56).

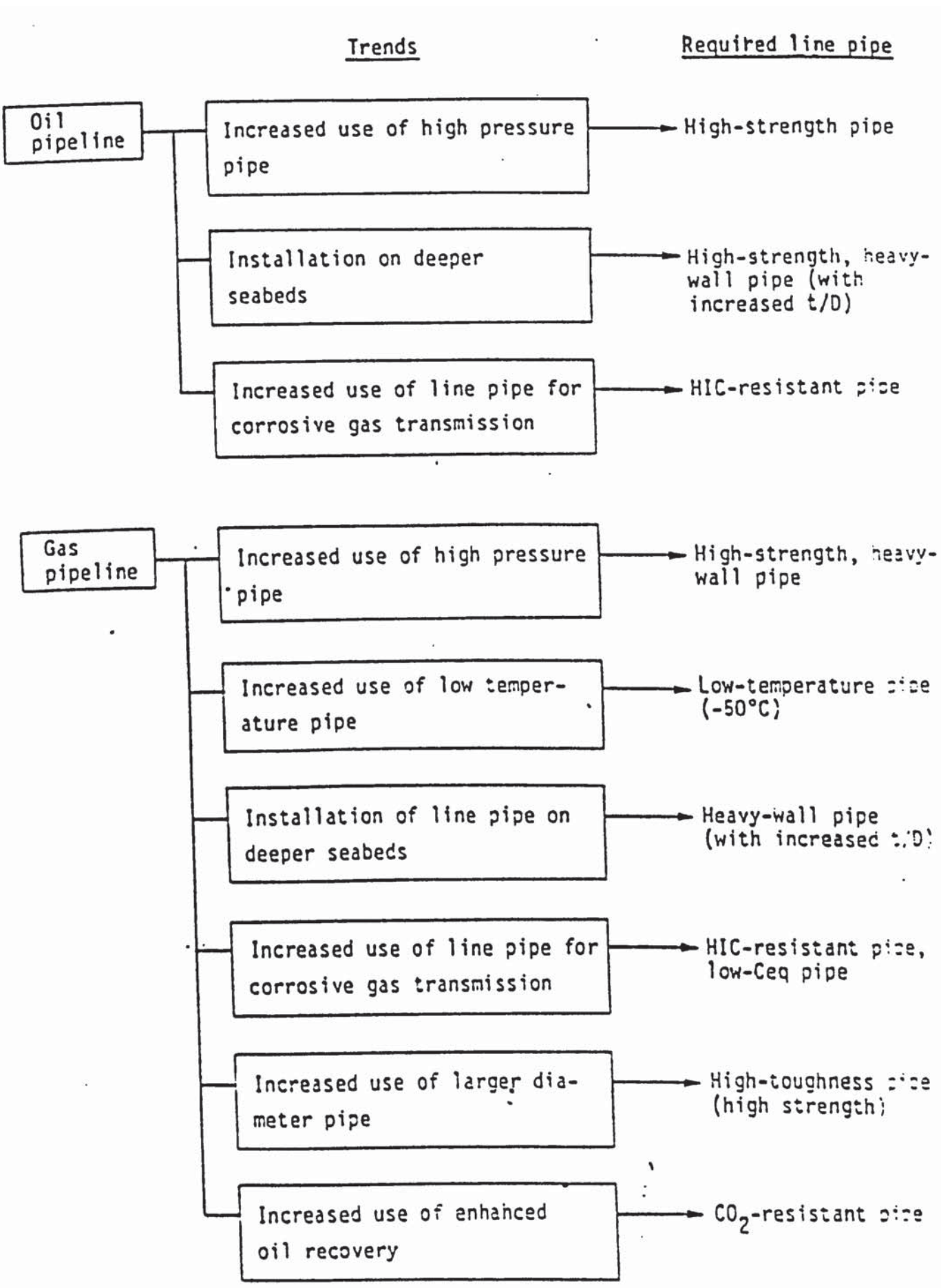

FIGURE-3. Pipeline Trends and Required Line Pipe(171).

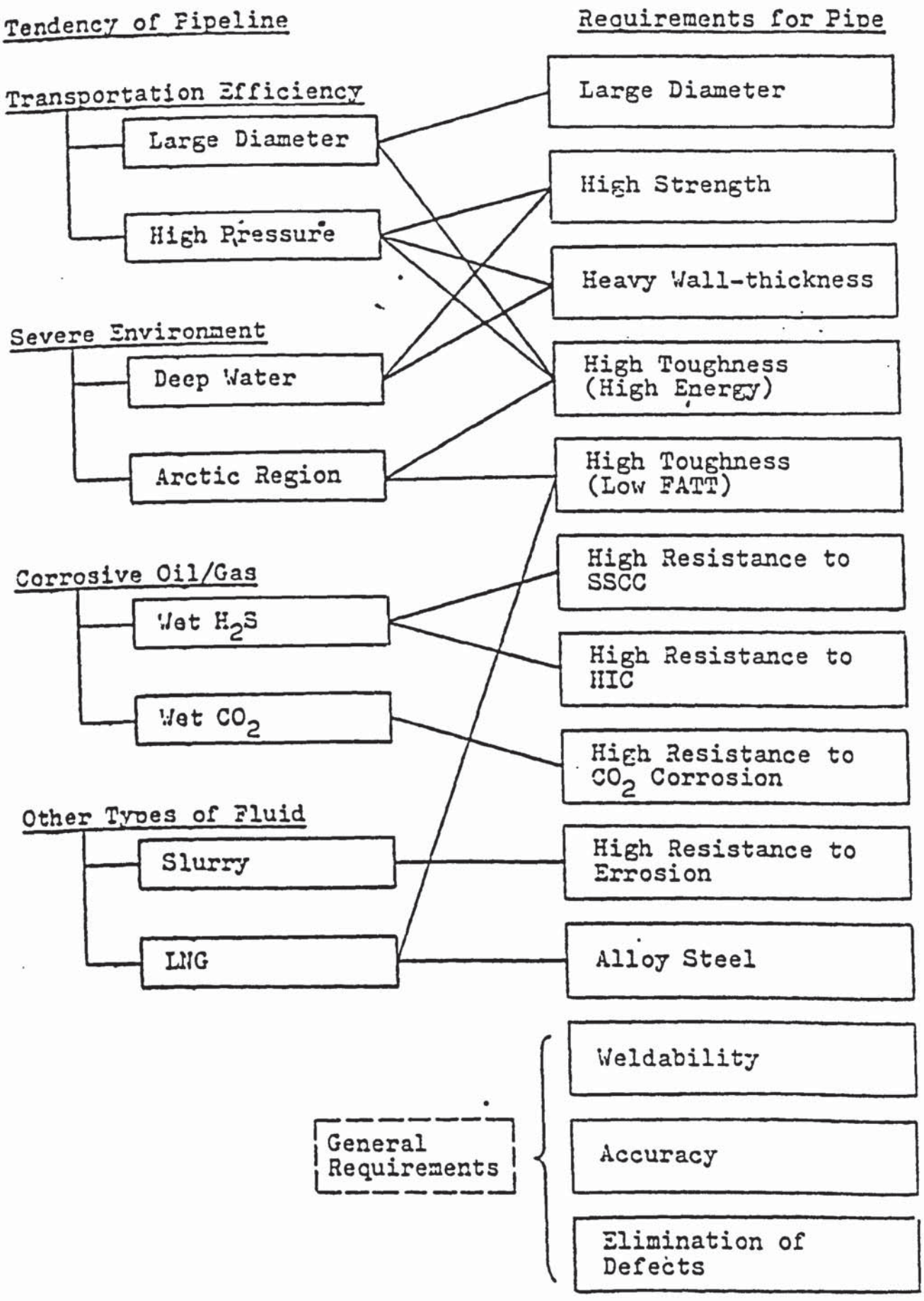

FIGURE-4 Relationship Between Pipeline tendency and Requirements to Line Pipe(55).

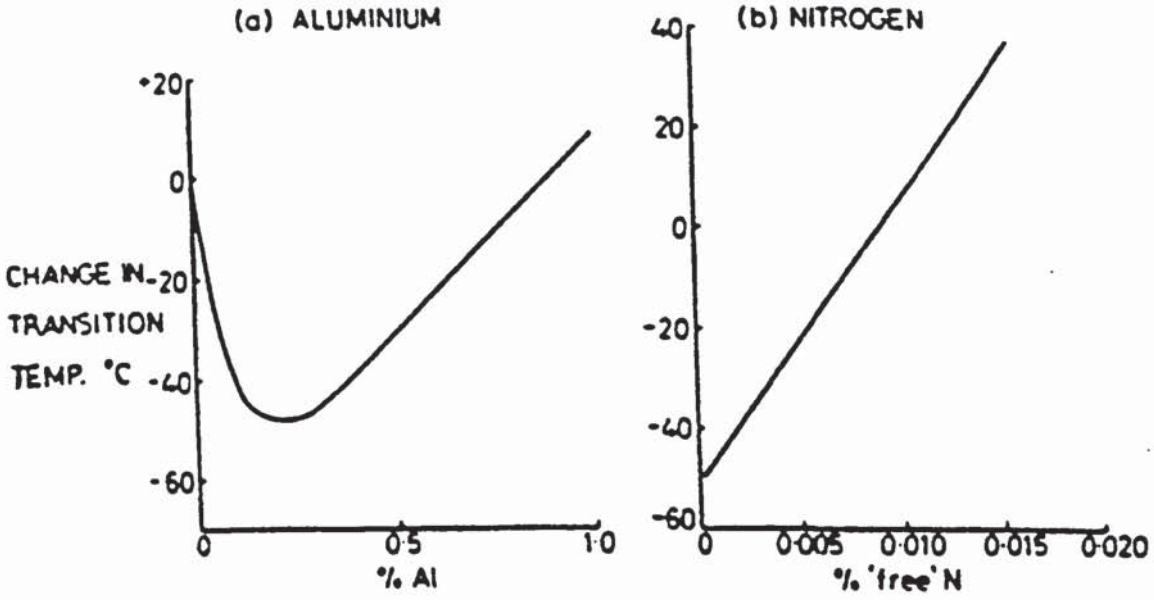

FIGURE-5 The Effects of Aluminium and Nitrogen on The Impact Transition Temperature of Low Alloy High Strength Steels Comprising Ferrite-Pearlite Structures(31)

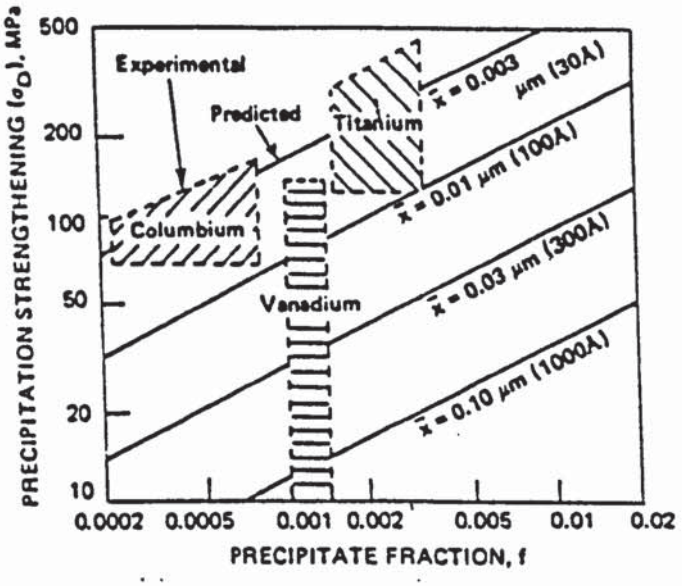

FIGURE-6. The Dependence of Precipitation Strengthening on Precipitate Size ($\bar{X}$) and Volume Fraction According to The Ashby-Orowan Model, Compared with Experimental Observation for Given Microalloying Addition (90).

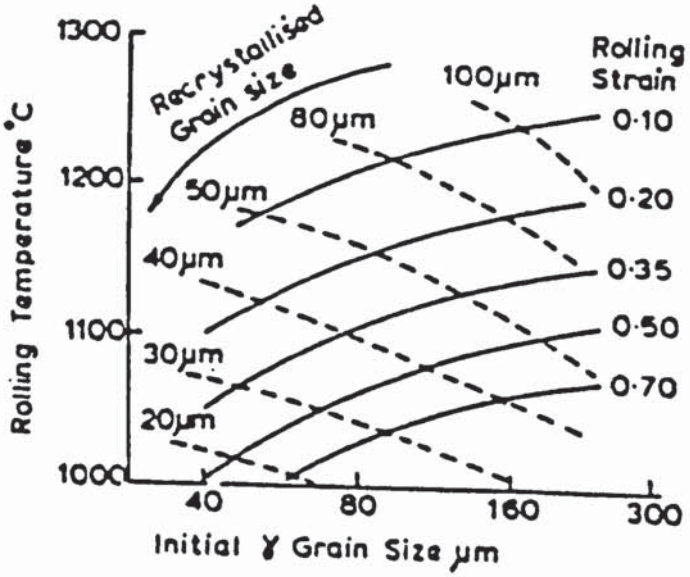

FIGURE-7. Effect of Initial Austenite Grain Size,Rolling Temperature and Rolling Strain on The Recrystallised Austenite Grain Size in Nb Treated HSLA Steel (28).

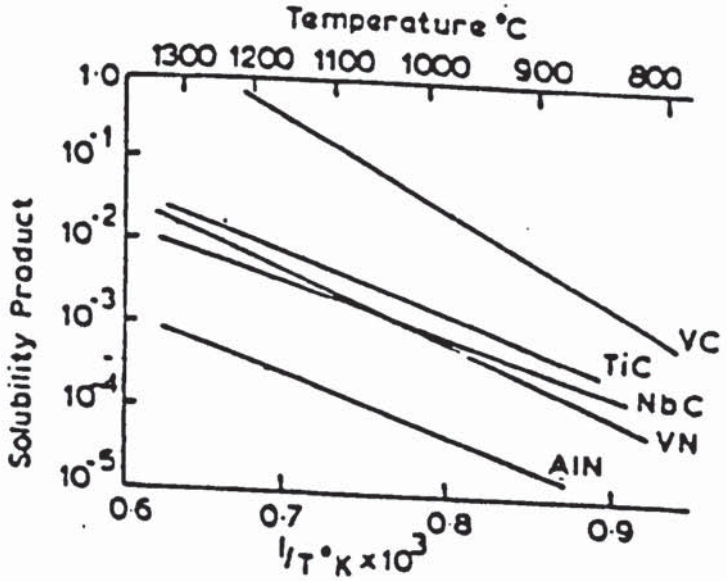

FIGURE-8. Solubility Relationships For microalloy Carbides And Nitrides (66).

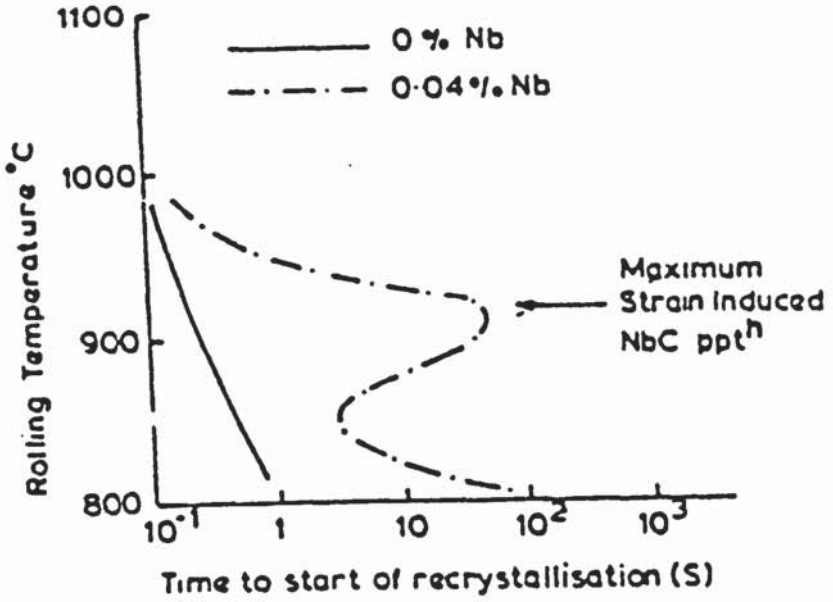

FIGURE-9. Retardation of Austenite Recrystallisation by Strain Induced NbC Precipitation During hot Rolling (28).

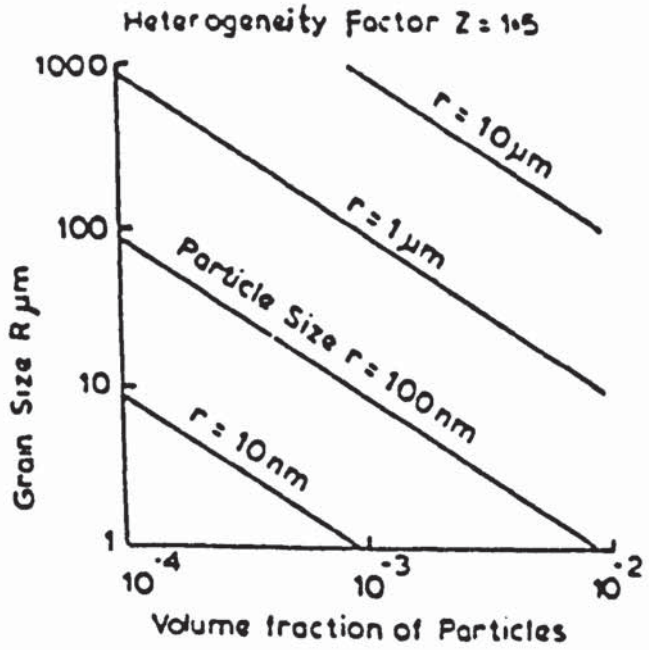

FIGURE-10. Effect of Volume Fraction and Size of Particles on Austenite Grain Size Using The Gladman Model for Grain Boundary Pinning (66).

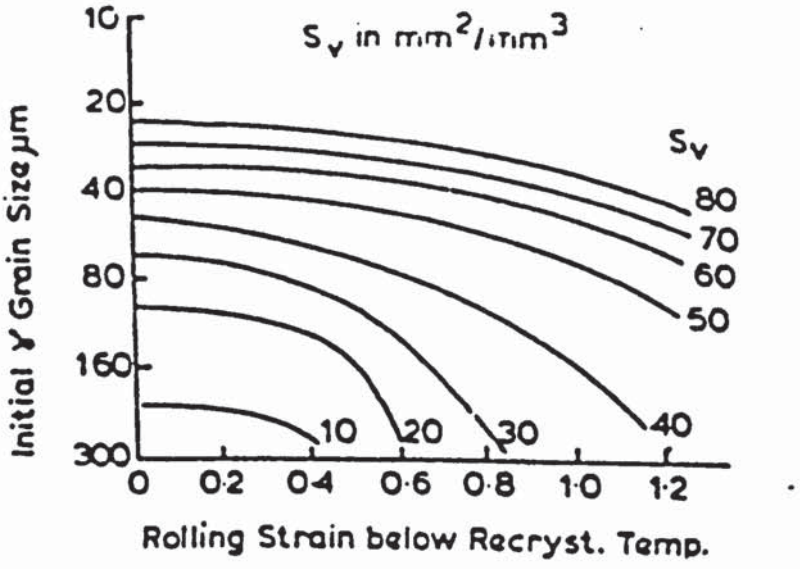

FIGURE-11. Dependence of Austenite Grain Boundary Surface Area Per Unit Volume (Sv) on The Initial Austenite Grain Size and The Strain Below The Recrystallisation Temperature(66).

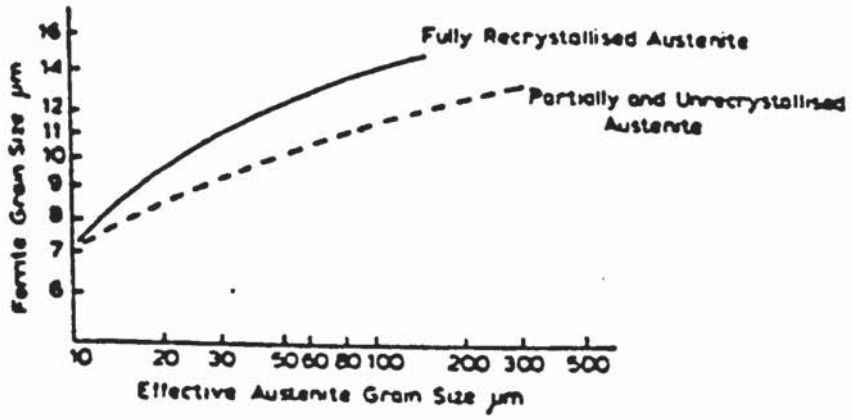

FIGURE-12. Effect of State of Austenite Recrystllisation on The Relationship Between The Austenite Grain Size and The Transformed ferrite Grain Size(28).

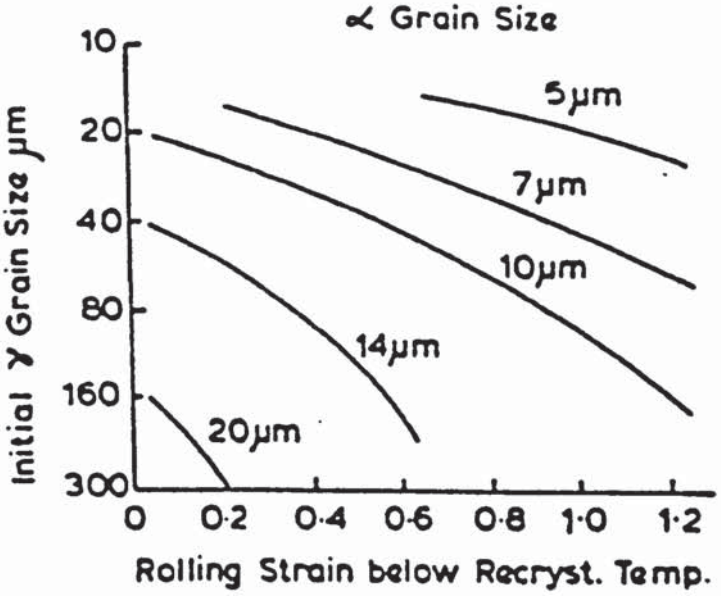

FIGURE-13. Dependence of Transformed Ferrite Grain Size on The Initial Austenite Grain Size and The Rolling Strain Below The Recrystallisation Temperature(66).

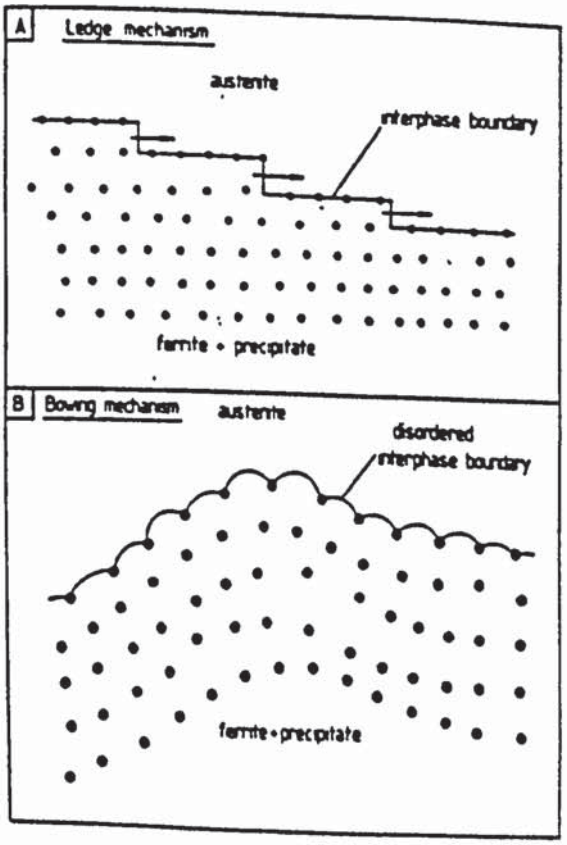

FIGURE-14. Two Types of Precipitate/Interphase Boundary Interaction (a) Step Migration. (b) Bowing of Boundary Around Precipitates(32).

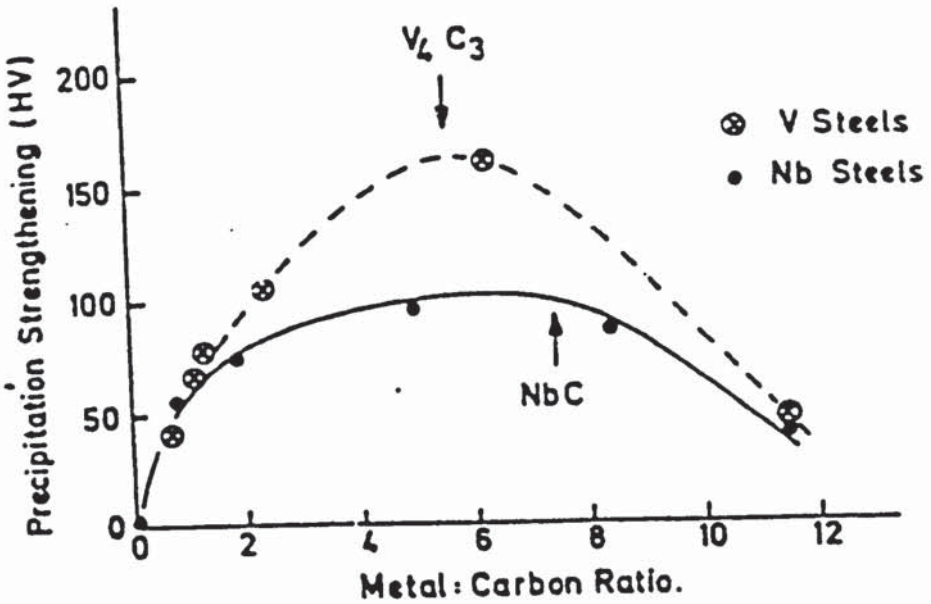

FIGURE-15. Effect of Metal :Carbon Ratio on Precipitation Strengthening in Rolled HSLA Steels Containing V or Nb,Showing Maximum Strengthening at The Stoichiometric Ratio(66)

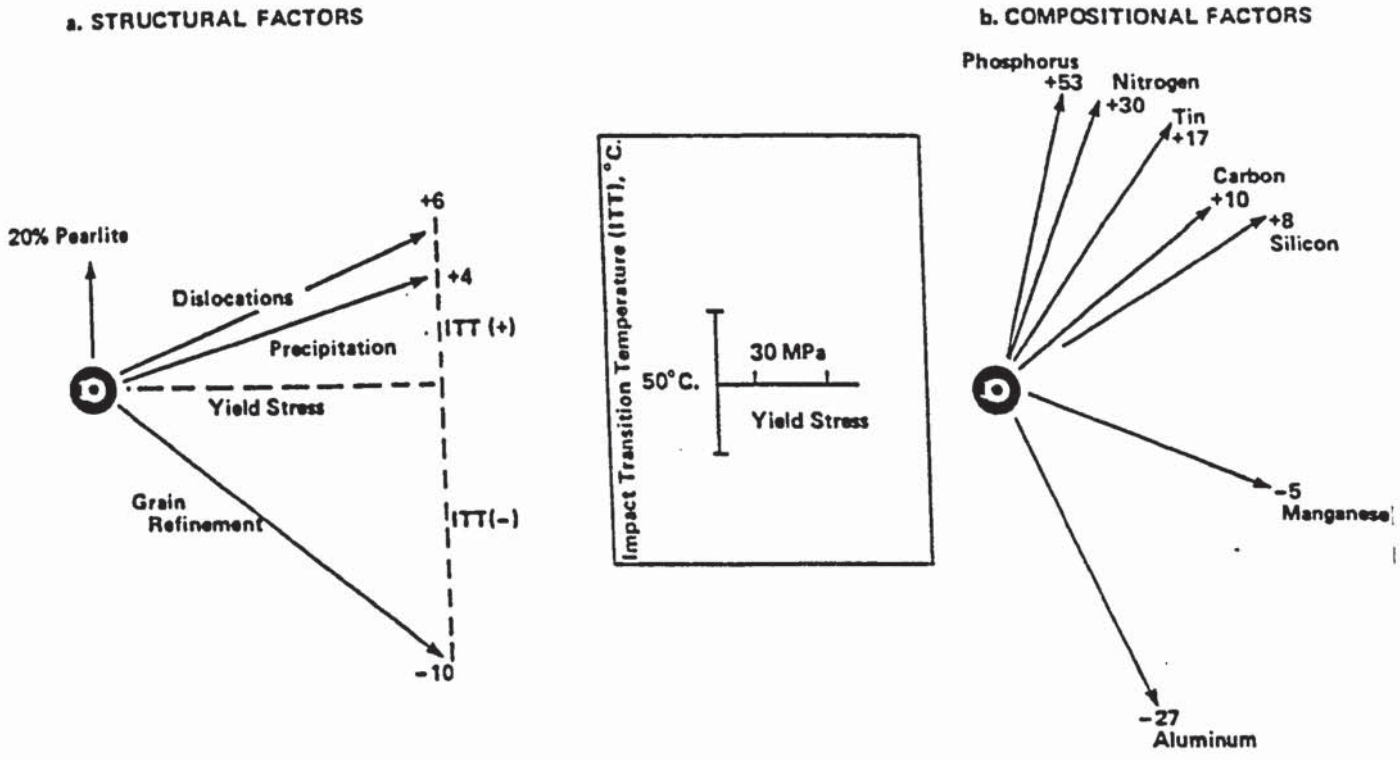

FIGURE-16. Factors Affecting Yield Strength and Impact Transition Temperature. Ratios Indicate The Change in Transition temperature Per 15 MPa Increase in Yield Strength(57).

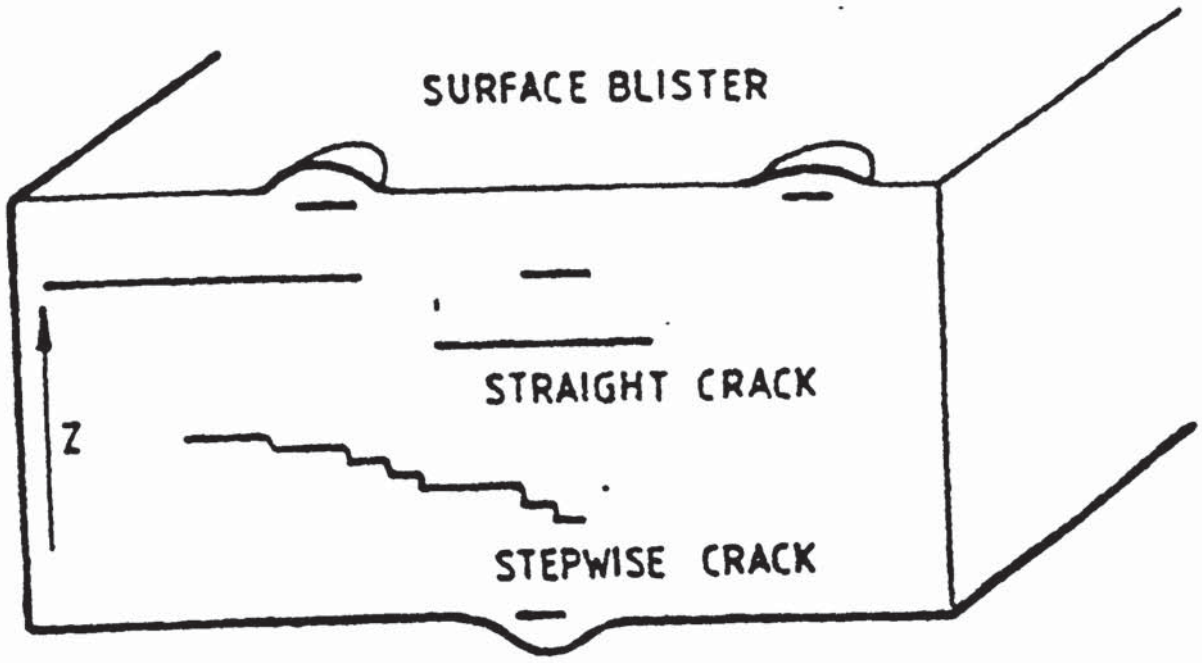

FIGURE-17. Schematic representation of H.I.C(168).

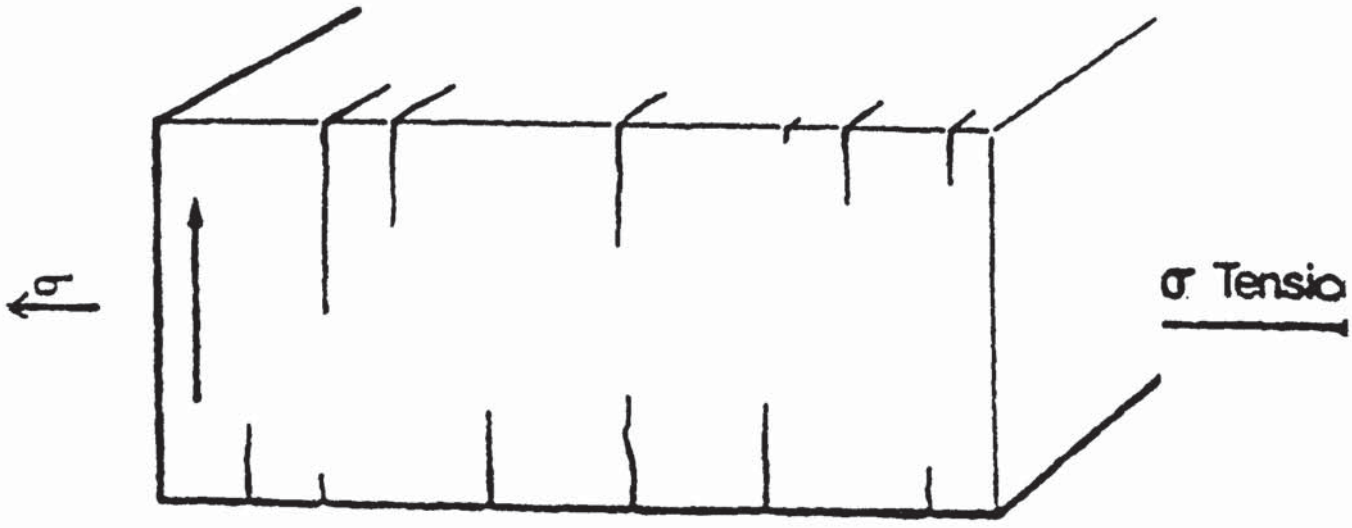

FIGURE-18. Schematic representation Of SSCC(168).

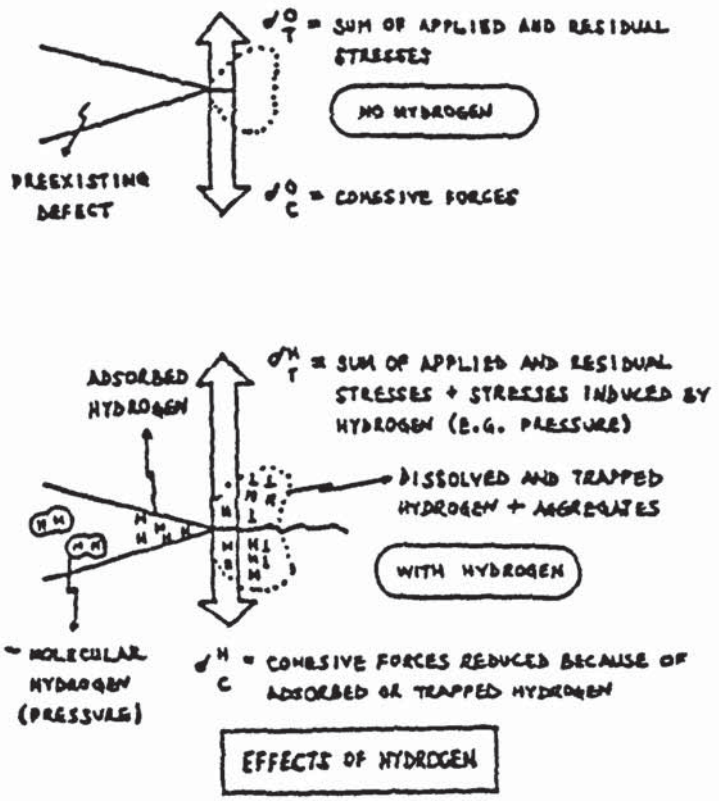

FIGURE-19. Synthesis of Current HE Theories(137).

The following parameters are used to measure HIC by the metallographic method

$$\text{Crack Length Ratio (CLR)} = \frac{\Sigma a}{N \times W} \times 100$$

$$\text{Crack Thickness Ratio (CTR)} = \frac{\Sigma b}{N \times T} \times 100$$

$$\text{Crack Sensitivity Ratio (CSR)} = \frac{\Sigma a \times b}{N \times W \times T} \times 100$$

N = number of sections

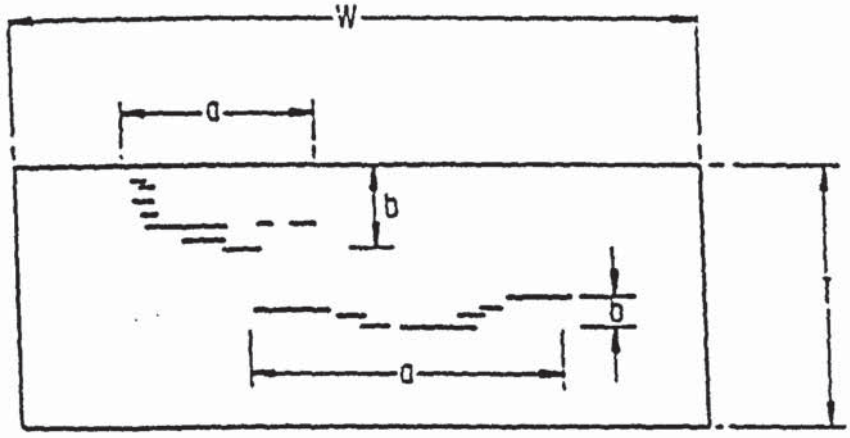

A crack is considered to be a single crack if segments are separated by no more than 0.5 mm

FIGURE-20. Measurement of HIC(48).

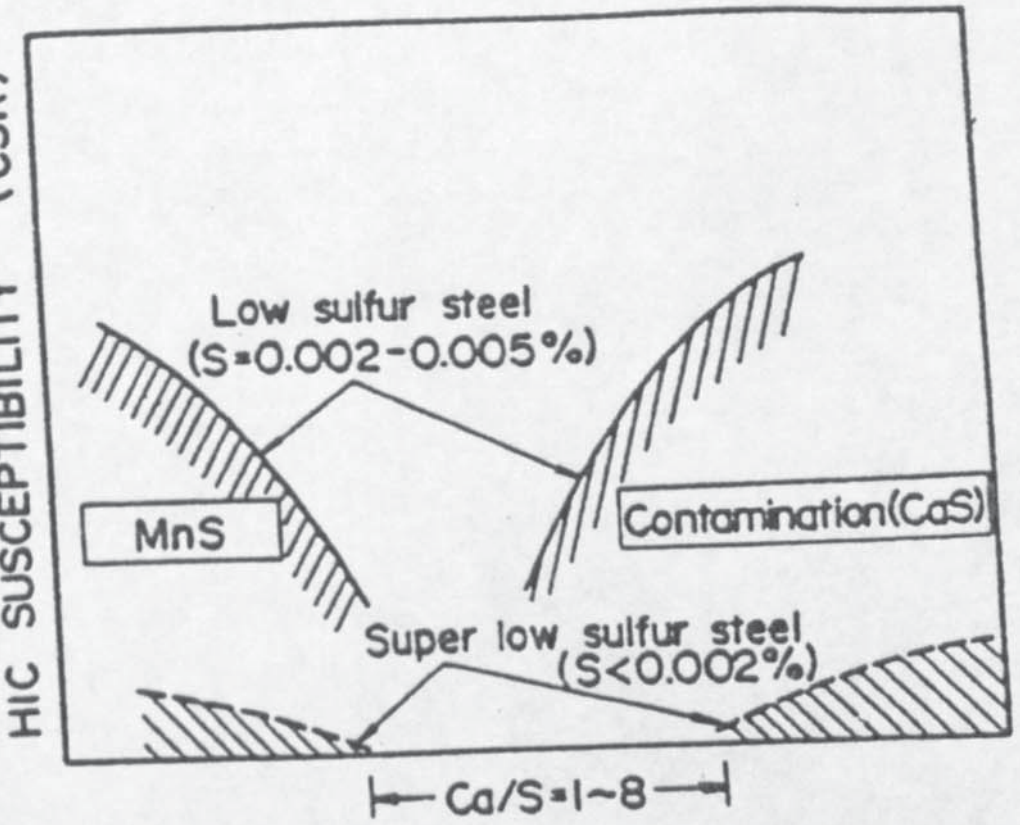

FIGURE-21. Schematic Representation for Effect of Ca:S Ratio on HIC Resistance (161).

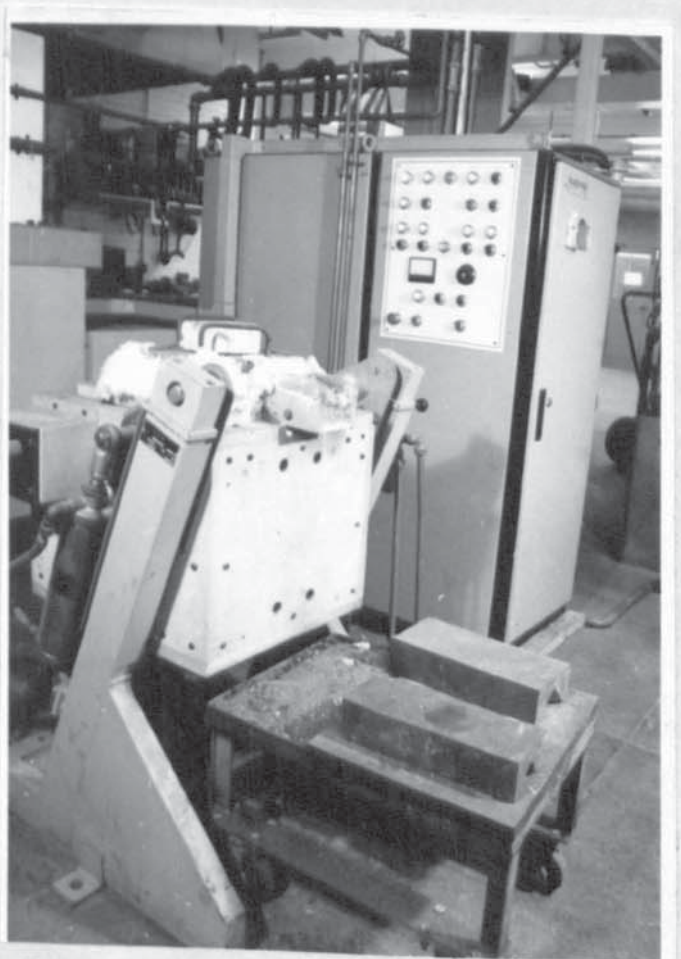

FIGURE-22. The Furnace Assembly.

All Dimensions in mm

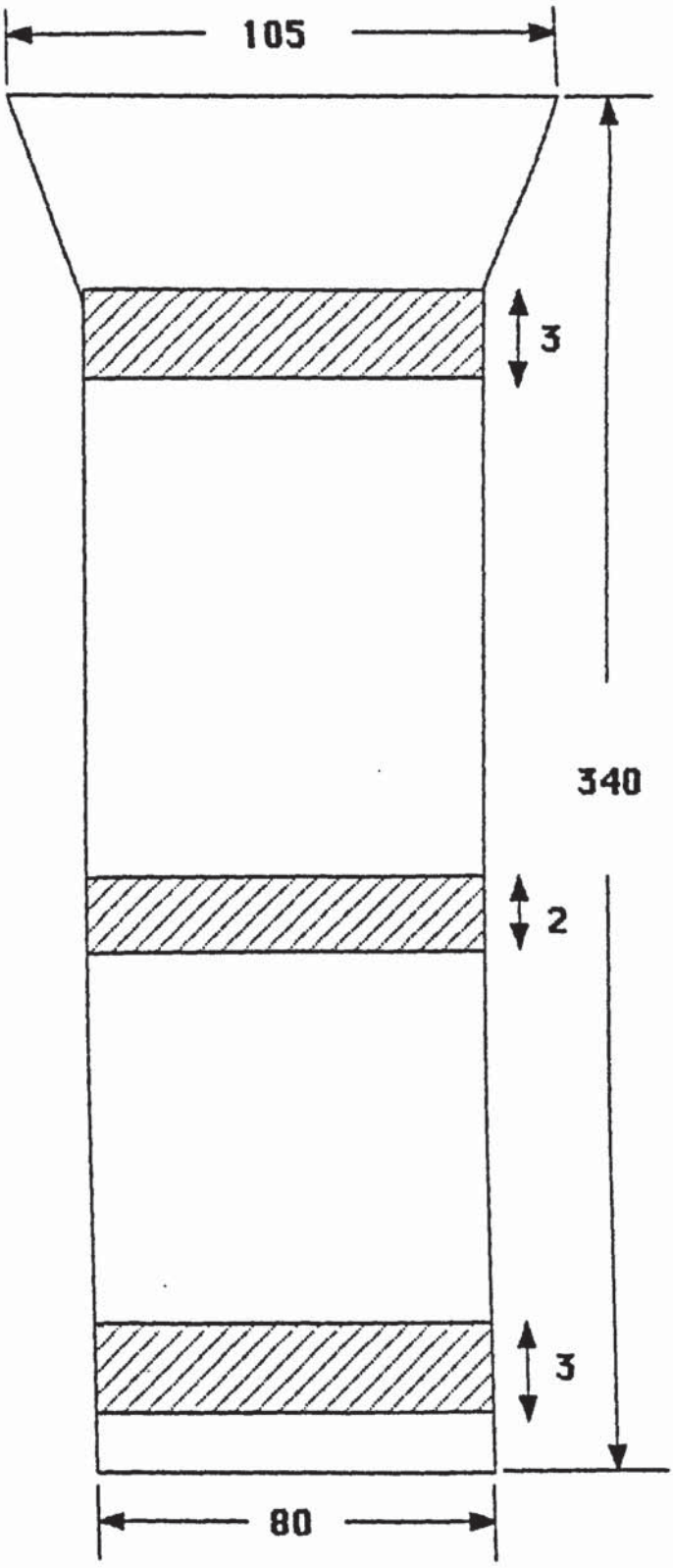

FIGURE-23 Sampling Locations for Chemical Analyses

FIGURE-24. Sulphur Prints Showing Minimum Segregation.

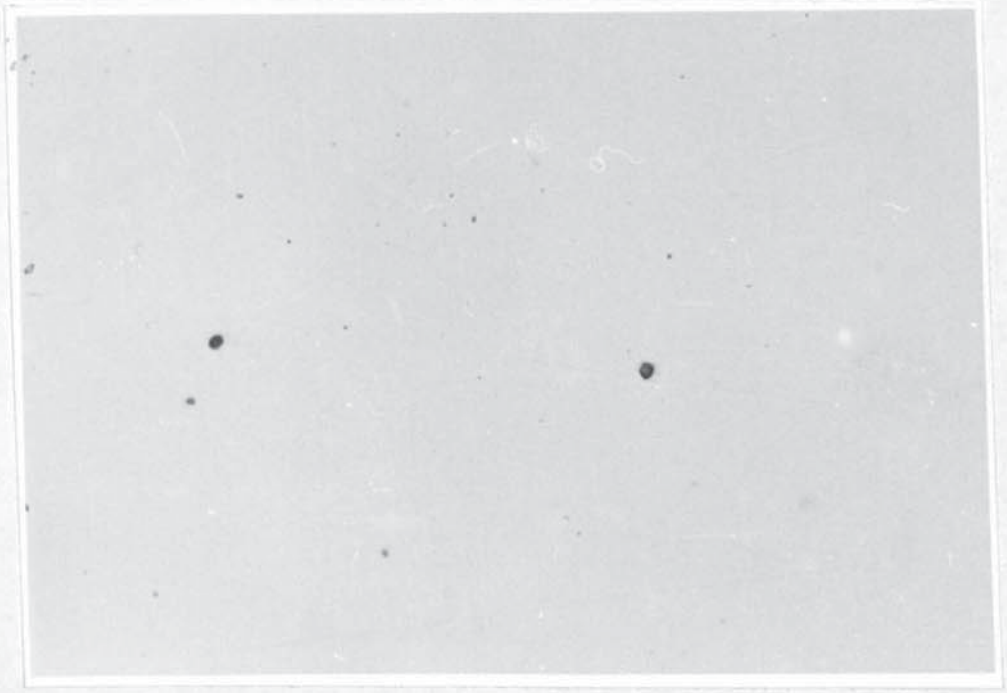

FIGURE-25. Unetched Microstructure Showing Non Metallic Inclusion Morphology and Distribution in Sample A4.(X420)

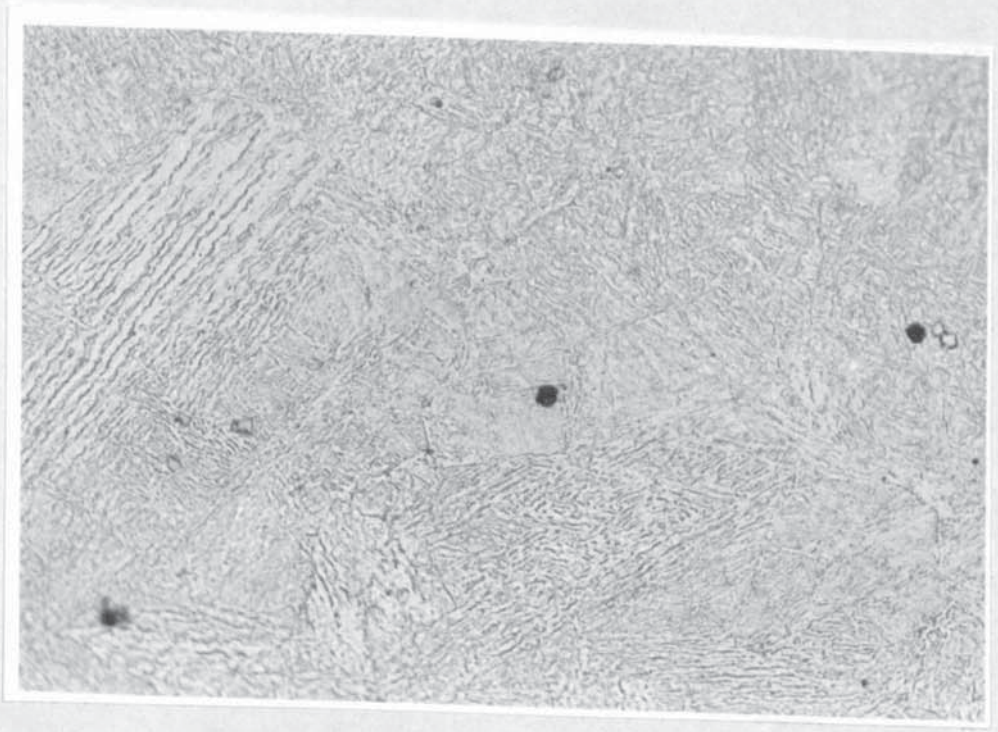

FIGURE-26. Lath Martensite Structure of Sample A4 Quenched from The Rolls Showing some (TiNb)NC Cuboids. (X420).

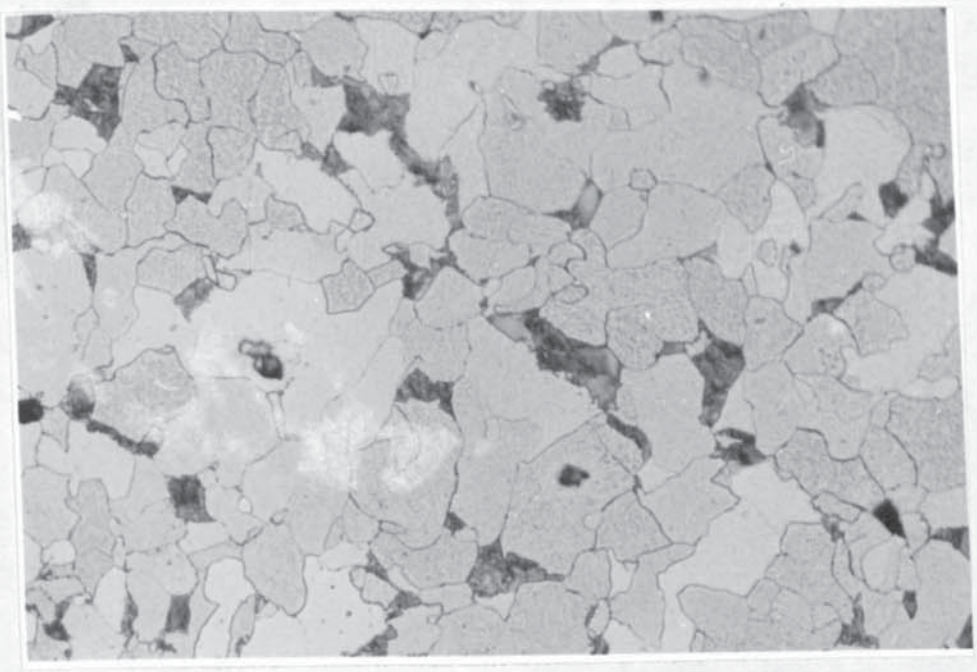

FIGURE-27A. Microstructure of The Base Steel Rolled at 1250°C Showing Ferrite and Pearlite.(X420).

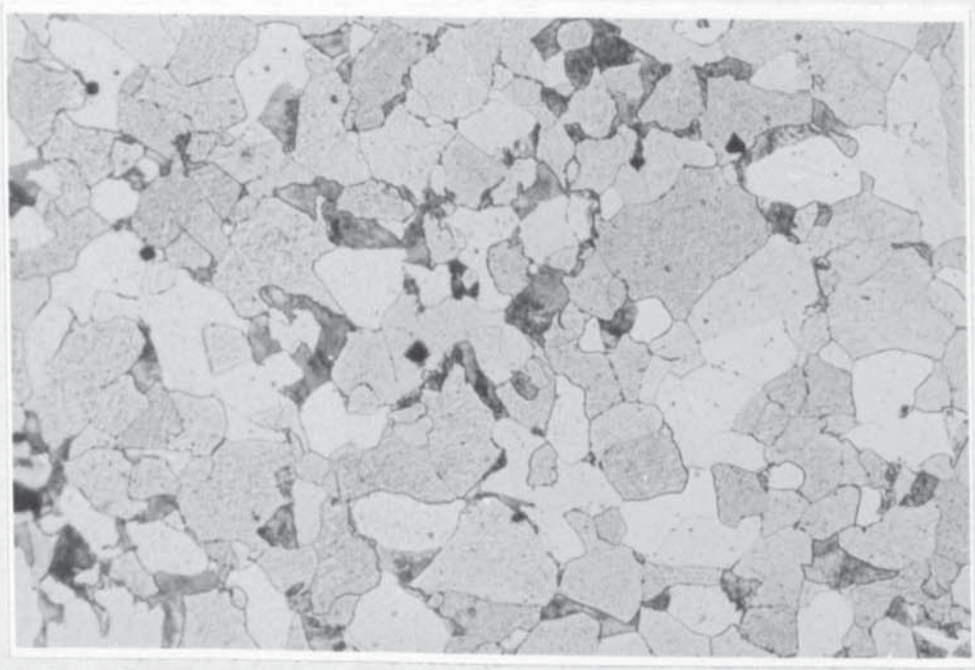

FIGURE-27B. Microstructure of The Base Steel Rolled at 900°C Showing Relatively Finer Ferrite Grains.(X420).

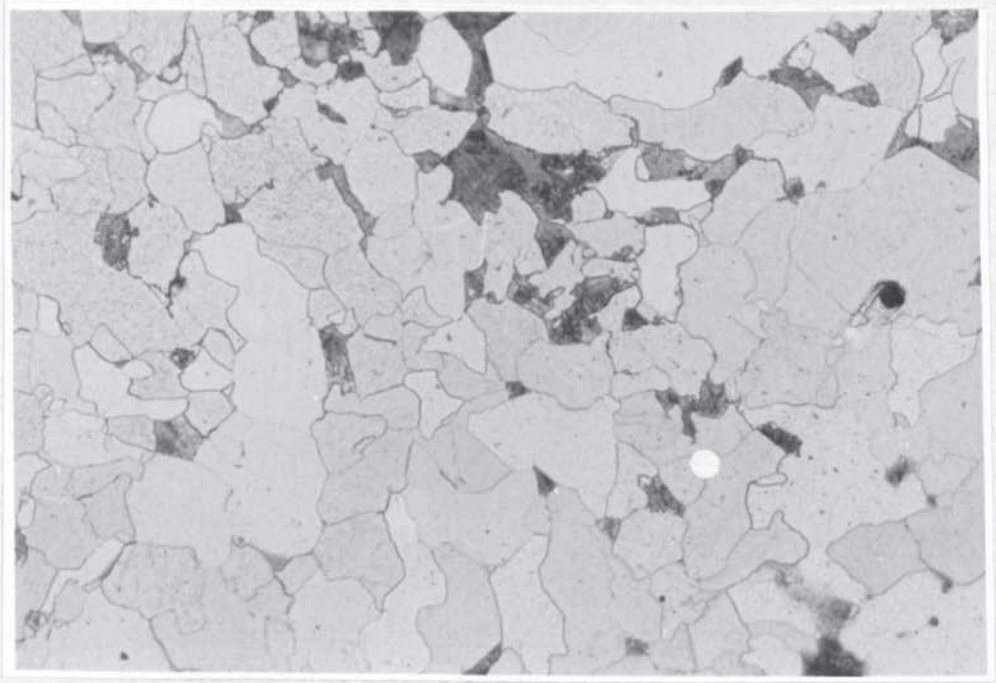

FIGURE-27C. Microstructure of Steel1 Rolled at 1250°C Showing Ferrite and Pearlite.(X420).

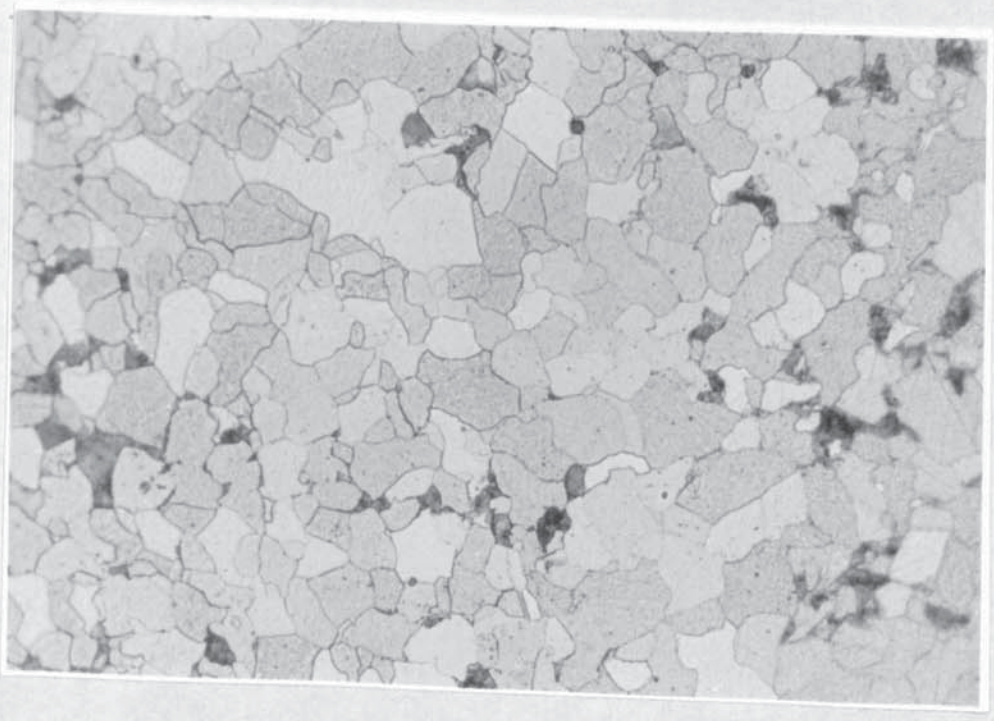

FIGURE-27D. Microstructure of Steel1 Rolled at 900°C Showing Ferrite and Pearlite.(X420).

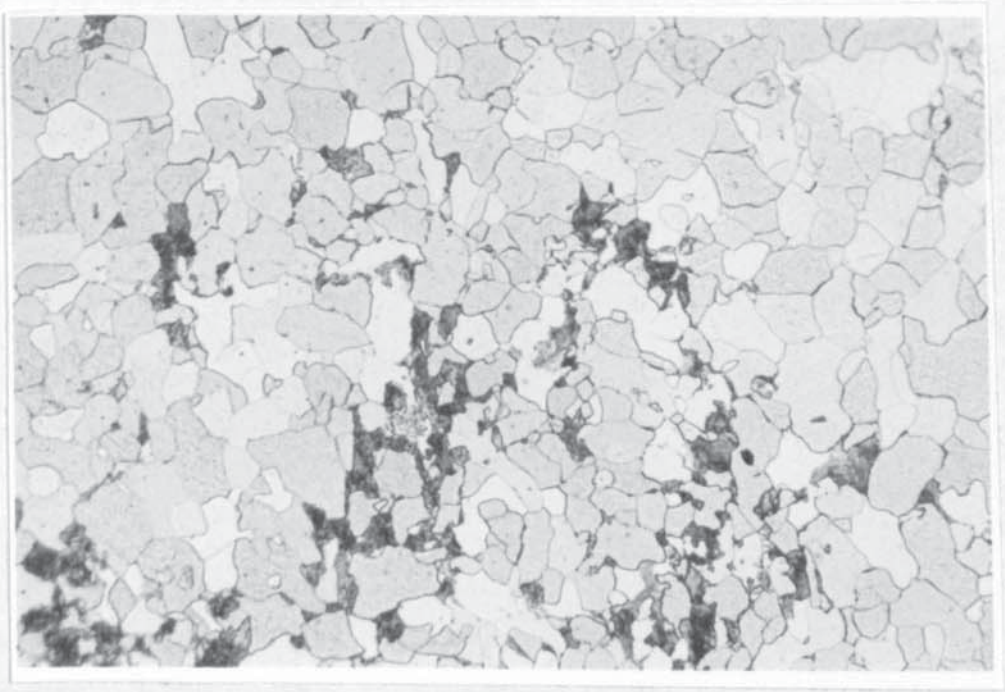

FIGURE-27E. Microstructure of Steel4 Rolled at 1250°C Showing Ferrite and Pearlite,But Finest Ferrite Grains Relative to Others.(X420).

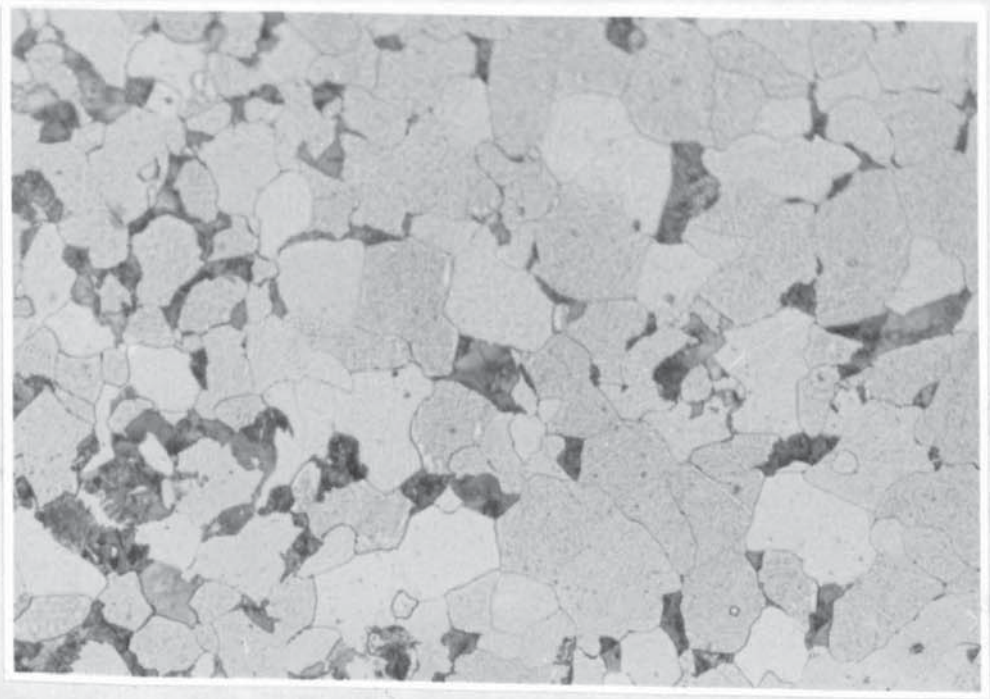

FIGURE-27F. Microstructure of Steel4 Rolled at 900°C Showing The Same Ferrite and Pearlite.(X420).

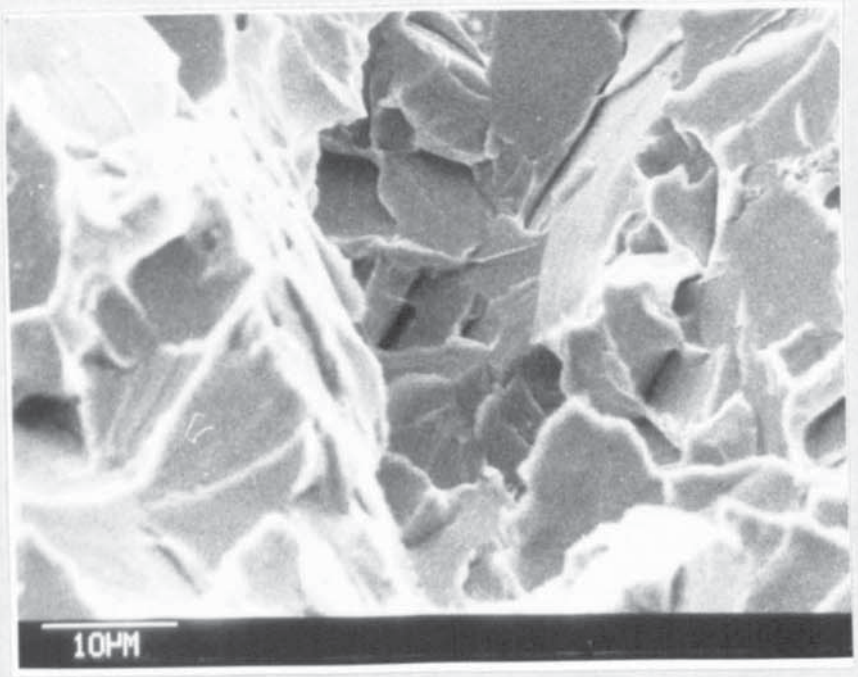

FIGURE-28A. Fracture Surface of Sample B1(stress Relieved) Showing Transcrystalline Brittle Fracture

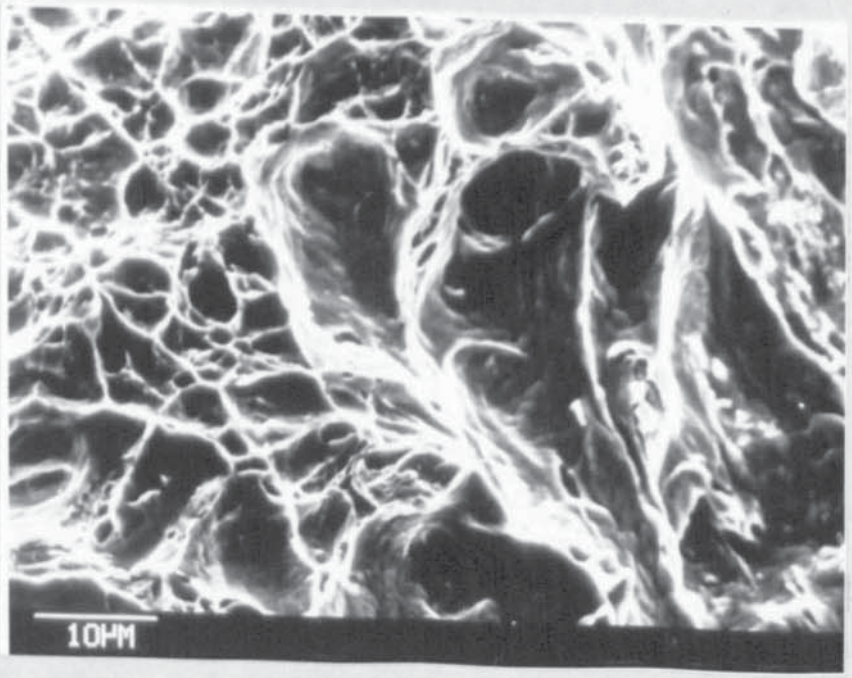

FIGURE-28B. Fracture Surface of Sample C3 (As Rolled) Showing Ductile Fracture.

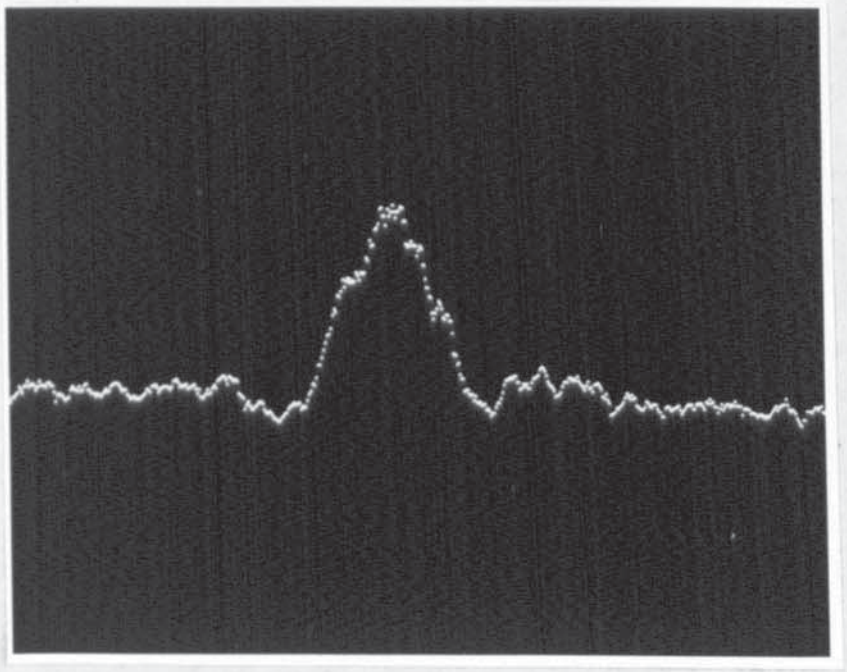

FIGURE-29. SEM Concentration Profile of Al Content in a Non Metallic Inclusion.

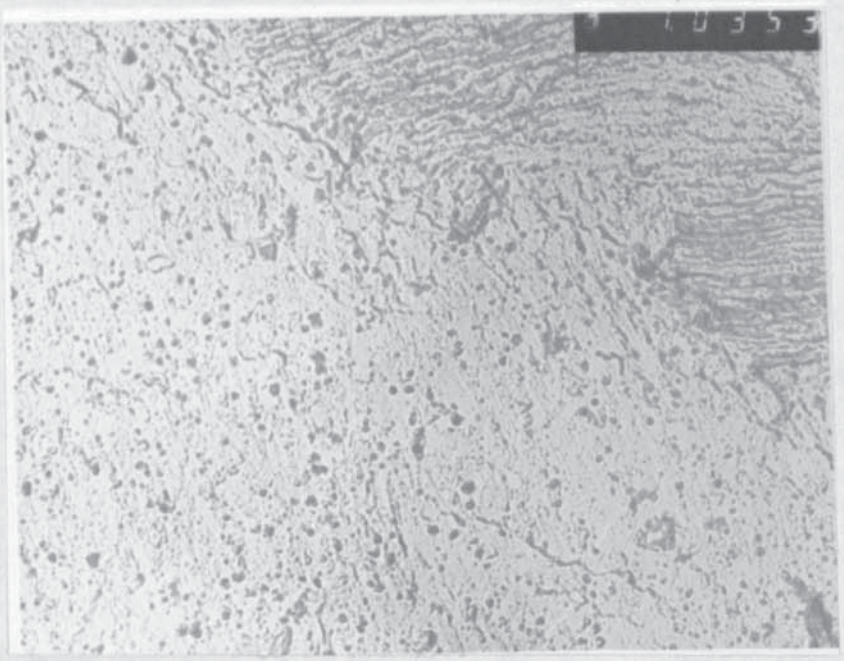

FIGURE-30A. Precipitate Morphology and Distribution in Sample Ao (Carbon Extraction Replica) X25K.

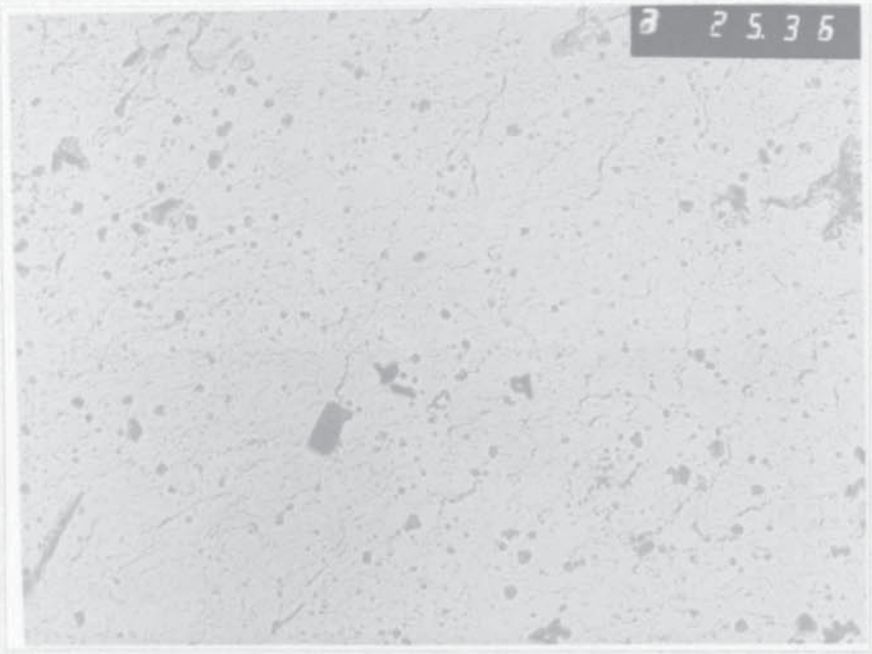

FIGURE-30B. Precipitate Morphologies and Distribution in Sample A1(Carbon extraction Replica) X25K.

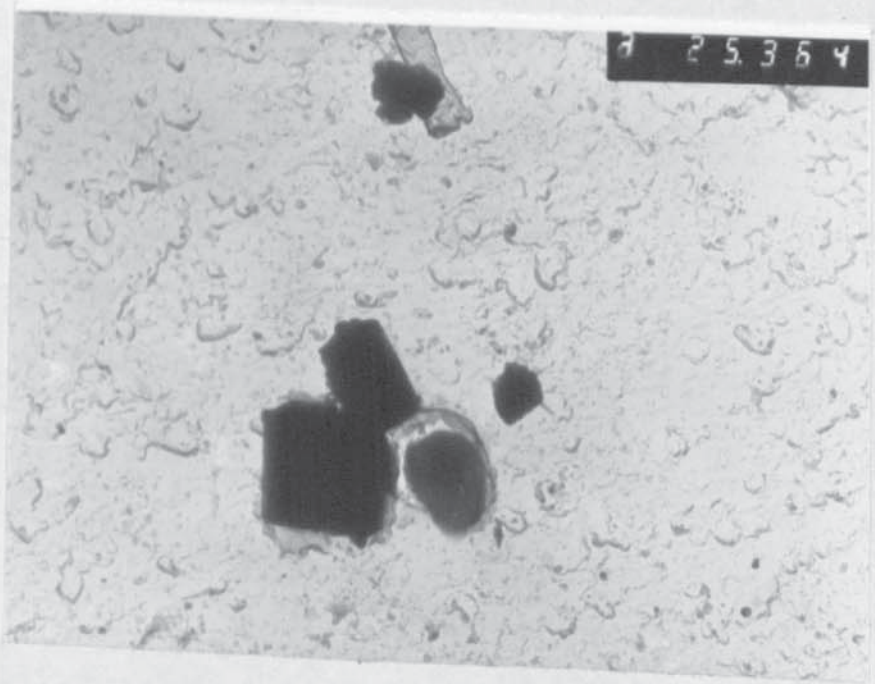

FIGURE-30C. Precipitate Morphologies and Distribution in Sample A4 (Carbon Extraction Replica) X25K

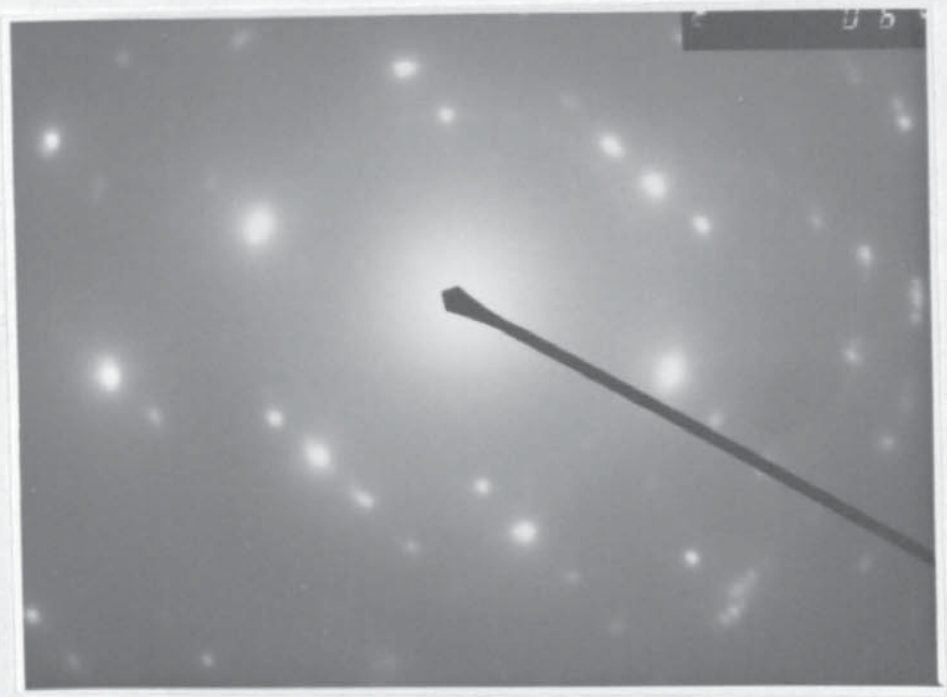

FIGURE-30D. Electron Diffraction Spots of Sample A4(X50K)

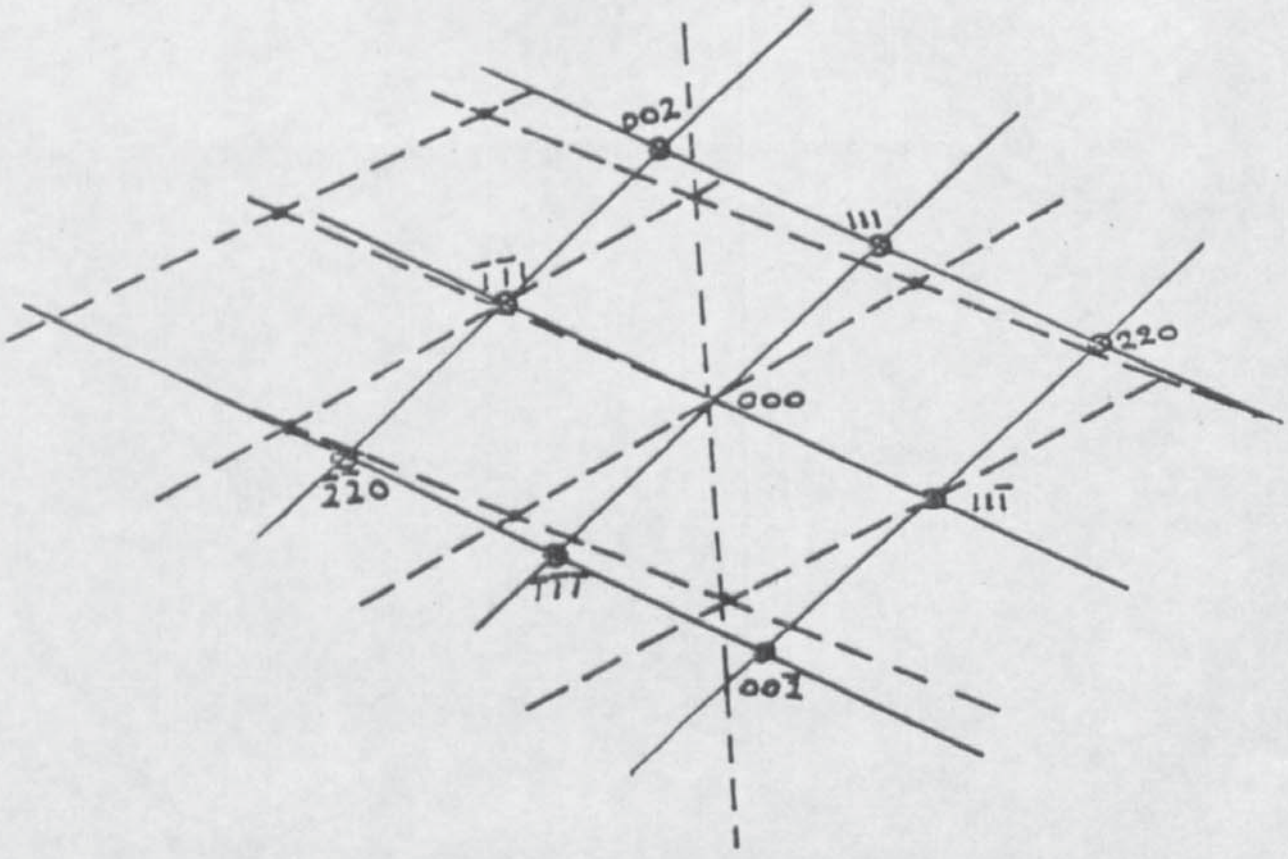

FIGURE-30E. Solution to Electron Diffraction Pattern of Sample A4.

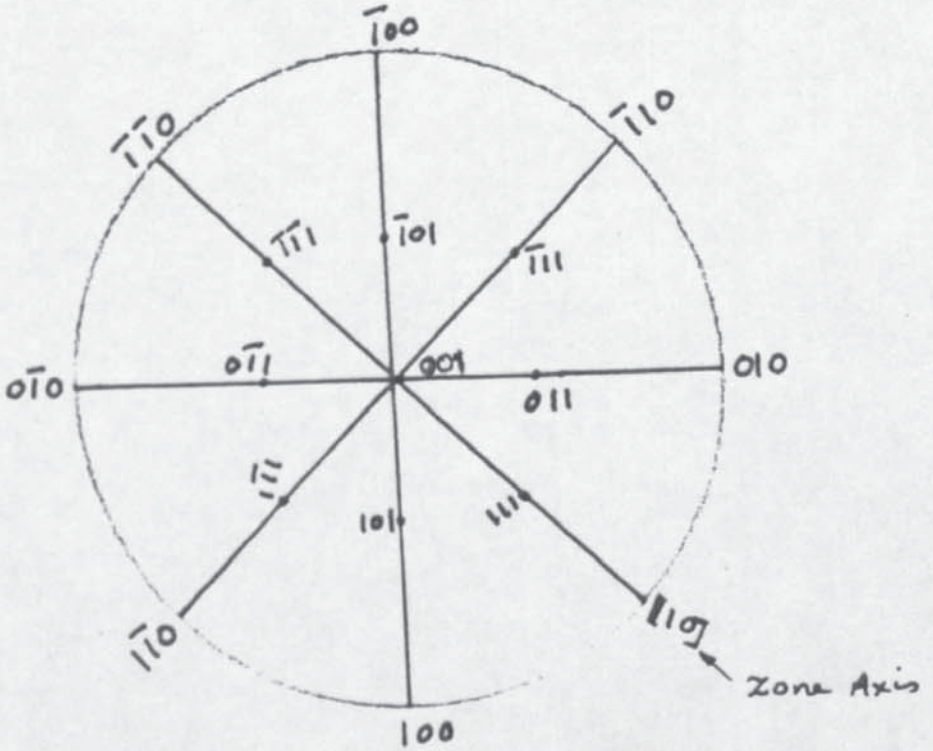

FIGURE-30F. Stereographic Projection Showing the Zone Axis.

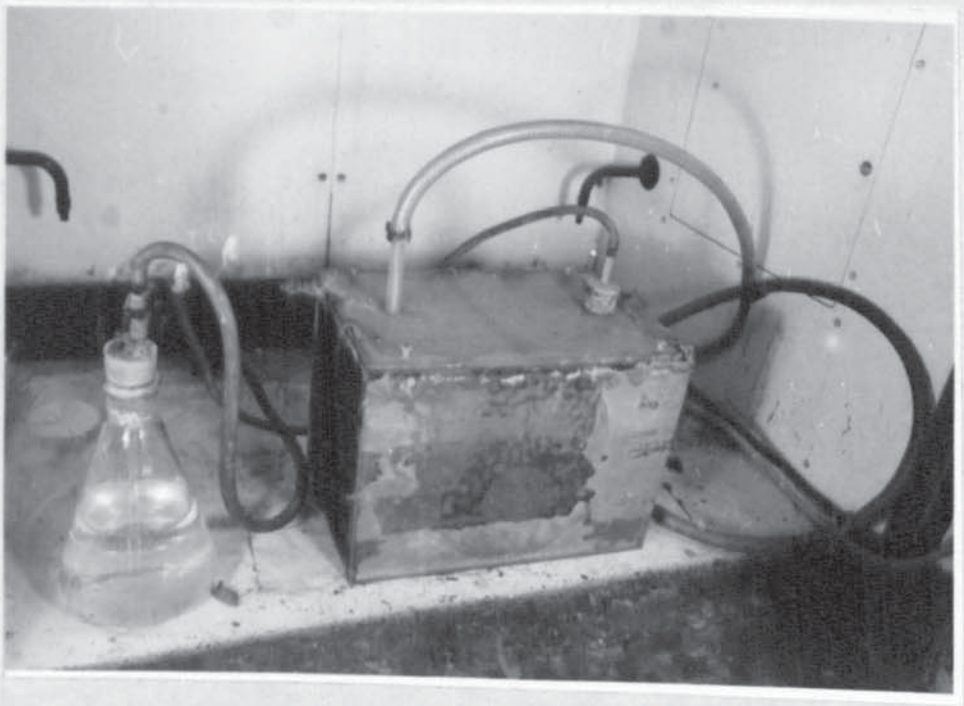

FIGURE-31. The Diagram of HIC Experiment.

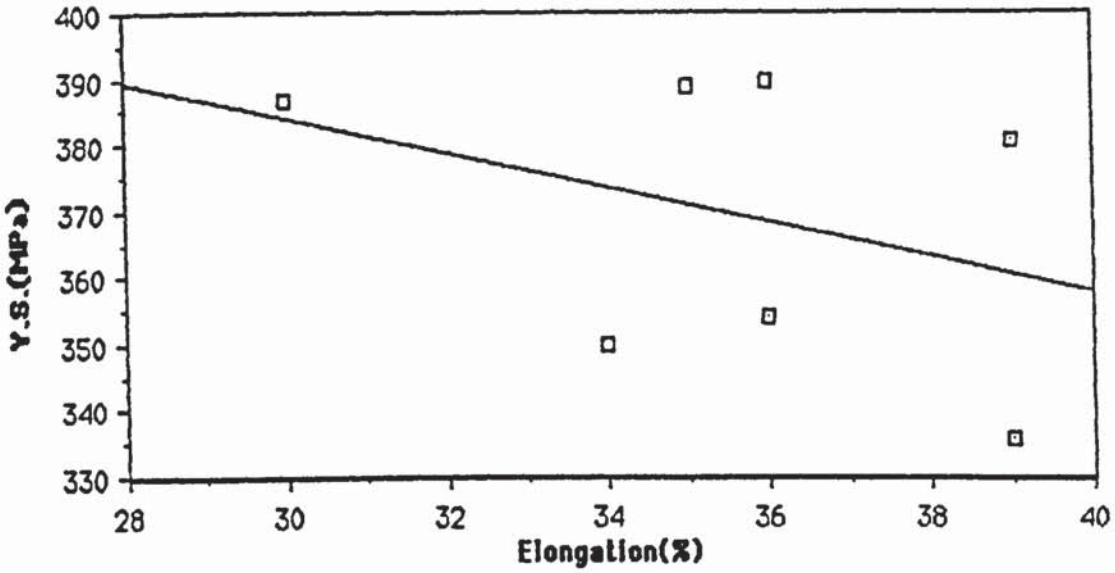

Fig.32(a).Variation of Y.S with % elongation , rolled at 1250°C.

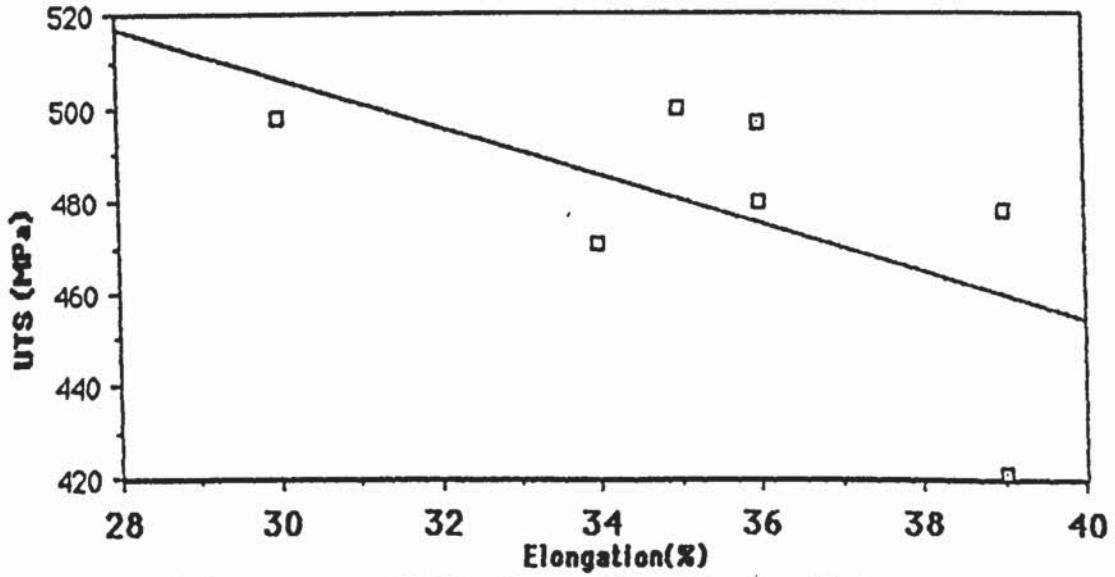

Fig.32(b).Variation of UTS with % Elongation , rolled at 1250°C.

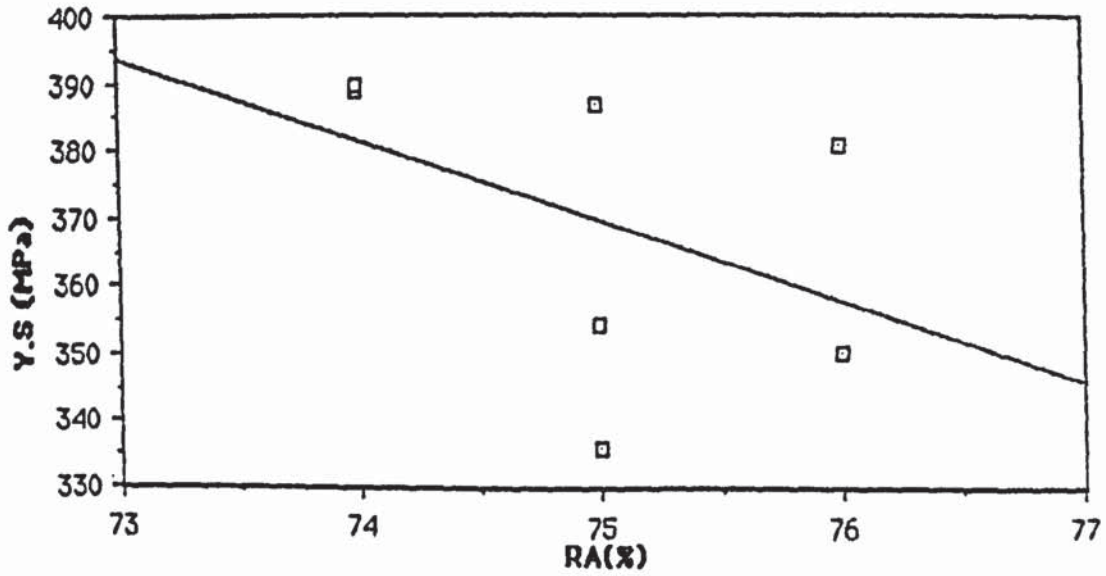

Fig.32(c).Variation of Y.S with %RA , rolled at 1250°C.

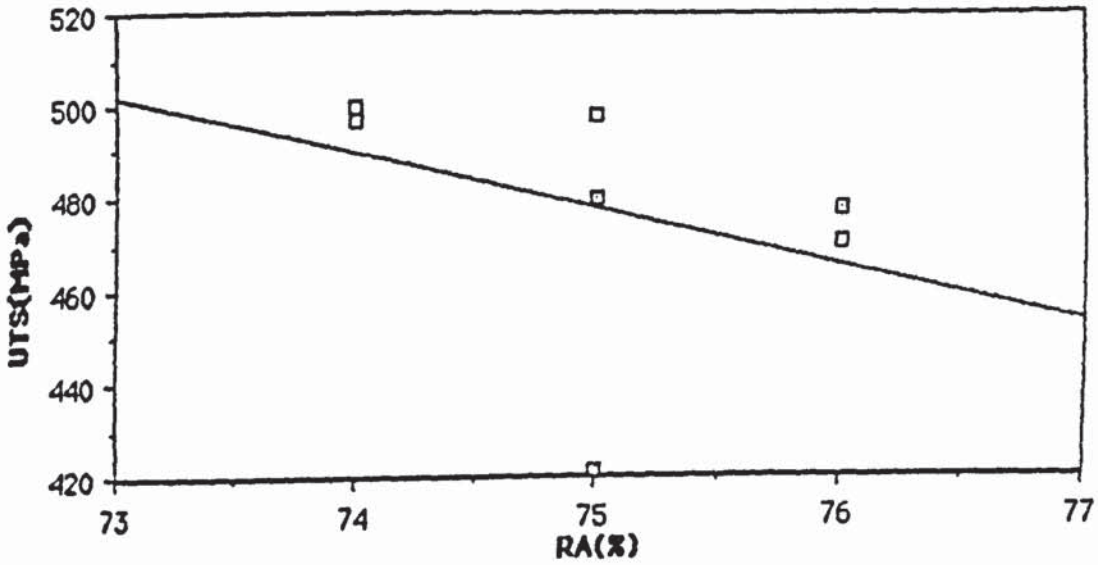

Fig.32(d).Variation of UTS with %RA, rolled at 1250°C.

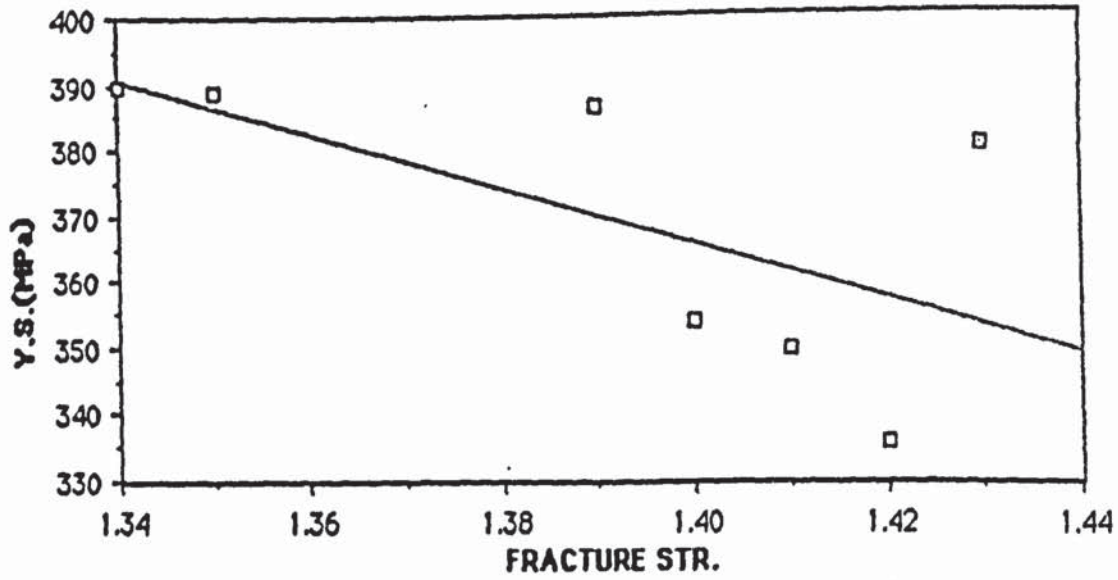

Fig.32(e).Variation of Y.S with Fracture Strain, rolled at 1250°C.

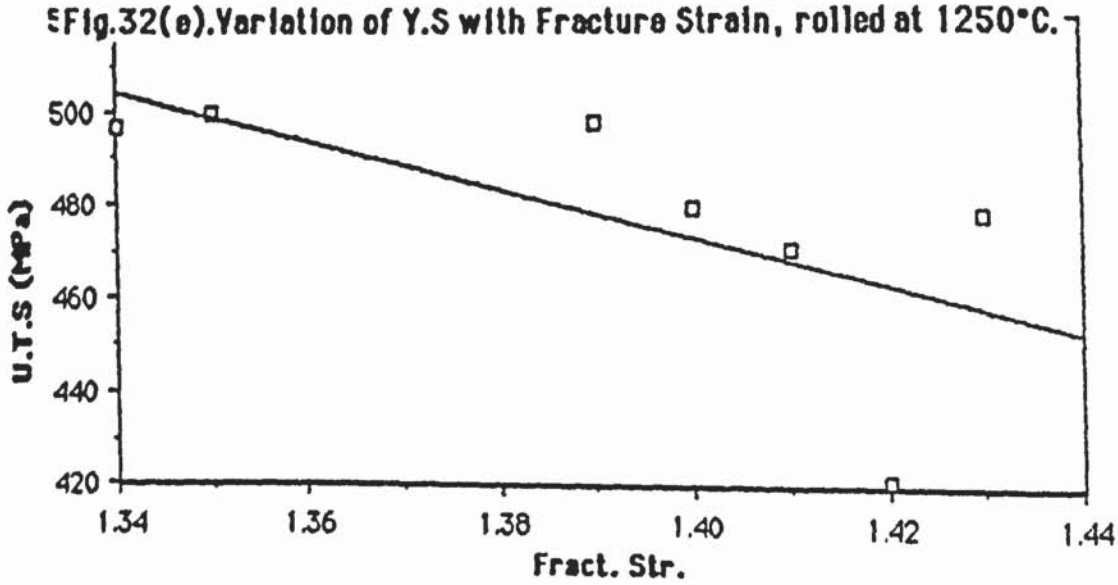

Fig.32(f).Variation of UTS with Fracture Strain, rolled at 1250°C.

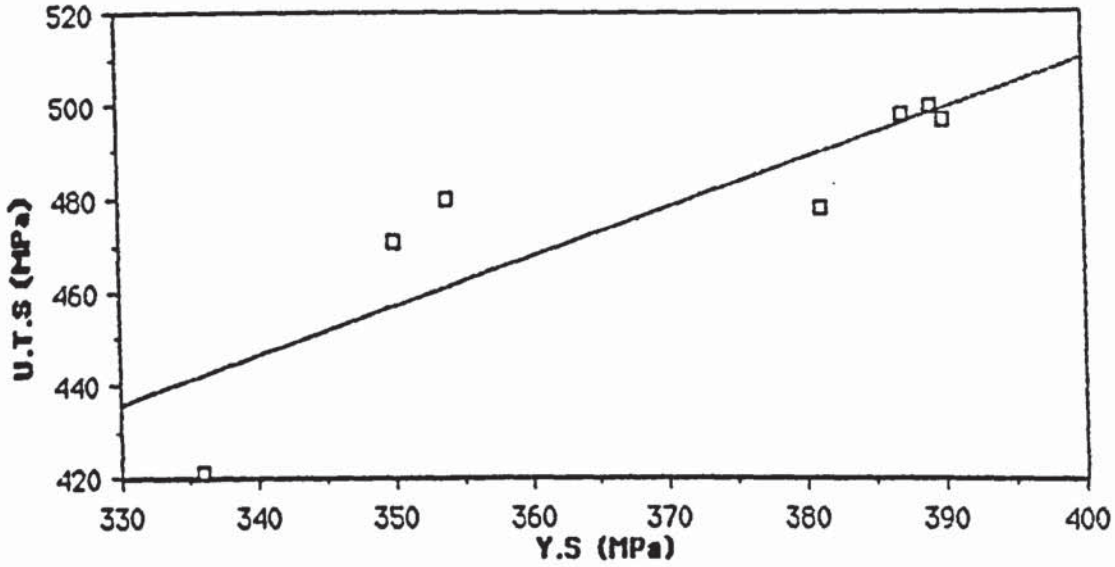

Fig.32(g).Variation of Y.S with UTS , rolled at 1250°C.

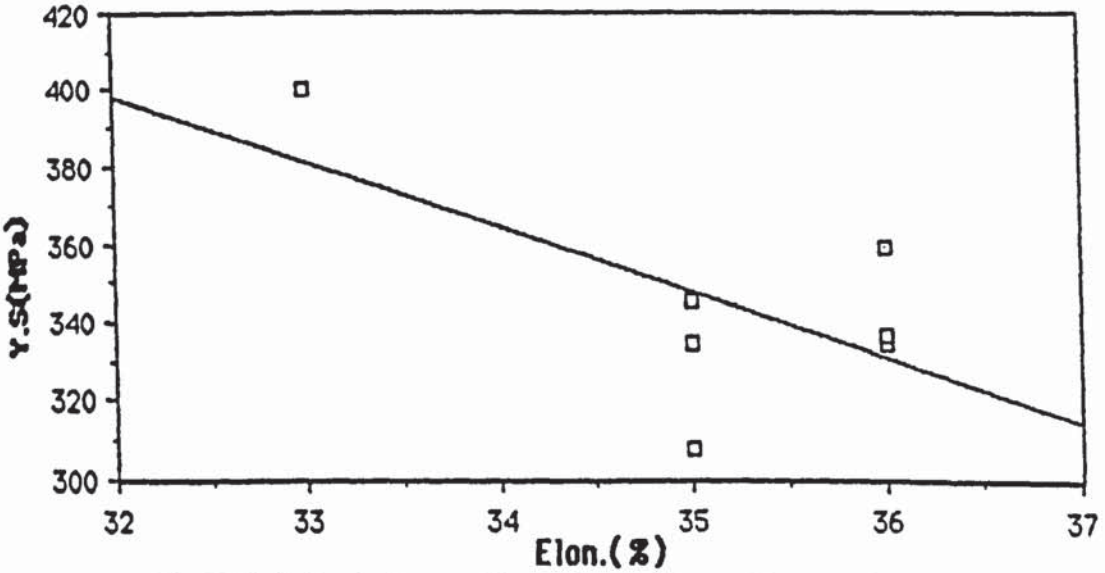

Fig.33(a).Variation of Y.S with %Elongation, rolled at1100°C

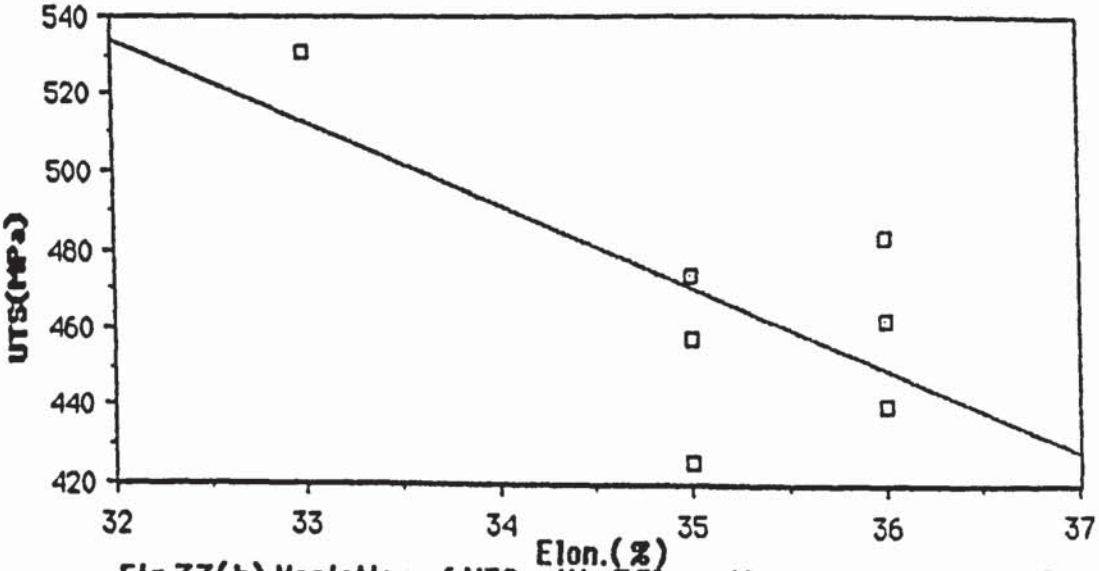

Fig.33(b).Variation of UTS with %Elongation,rolled at 1100°C

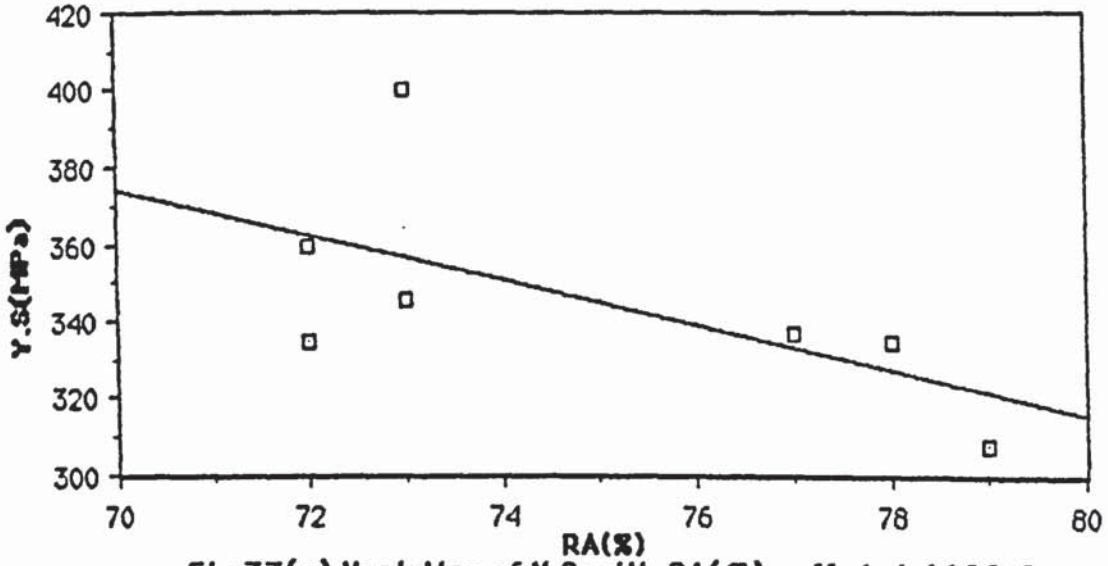

Fig.33(c).Variation of Y.S with RA(%),rolled at 1100°C

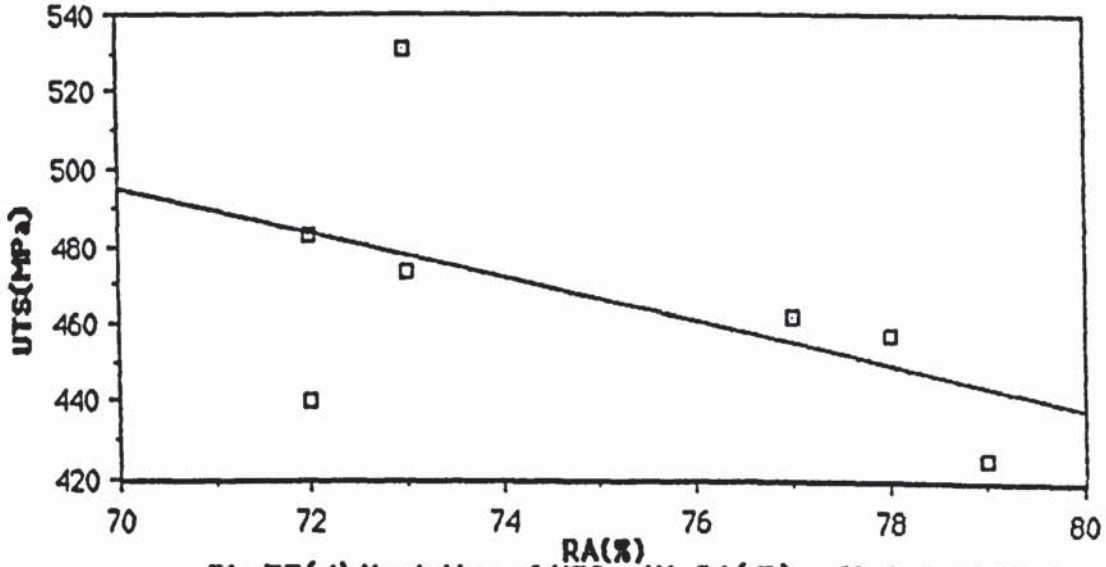

Fig.33(d).Variation of UTS with RA(%),rolled at 1100°C

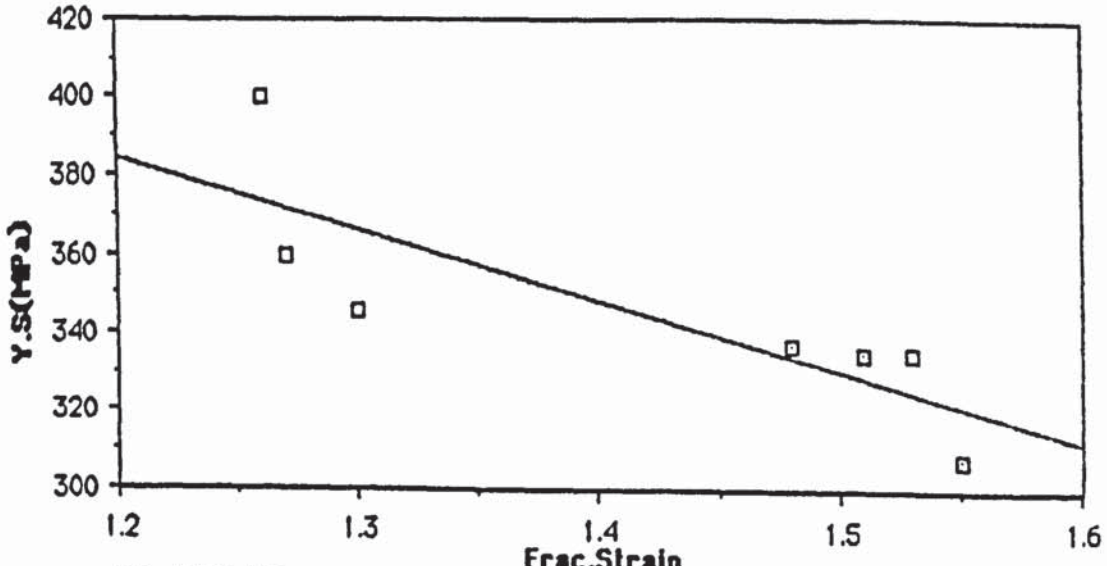

Fig.33(e).Variation of Y.S with Fracture Strain,rolled at 1100°c

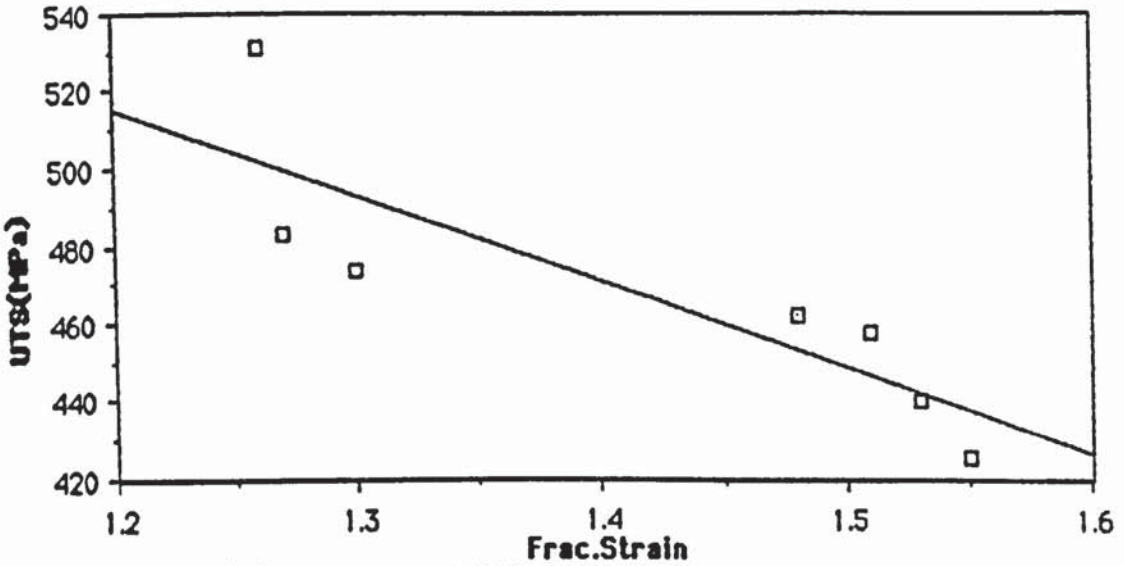

Fig.33(f).Variation of UTS with Fracture Strain,rolled at 1100°c

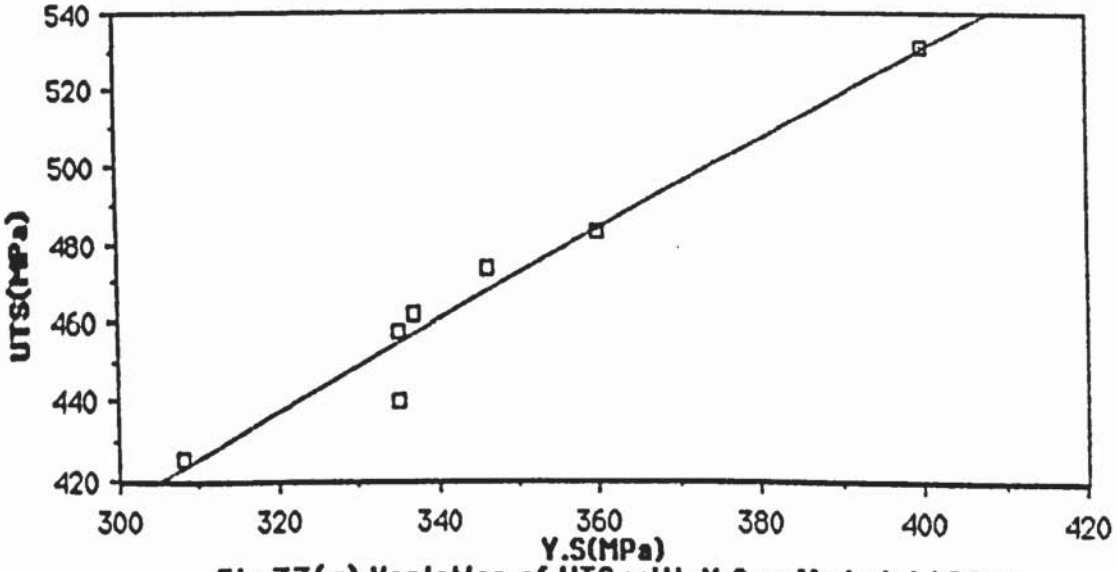

Fig.33(g).Variation of UTS with Y.S,rolled at 1100°C

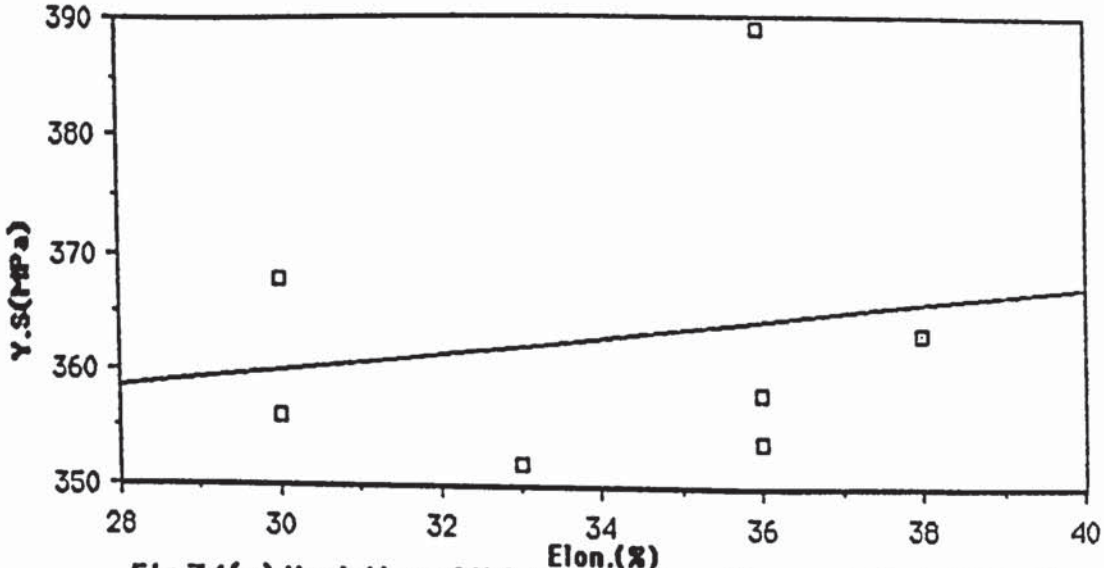

Fig.34(a).Variation of Y.S with %Elongation,rolled at 1000°C

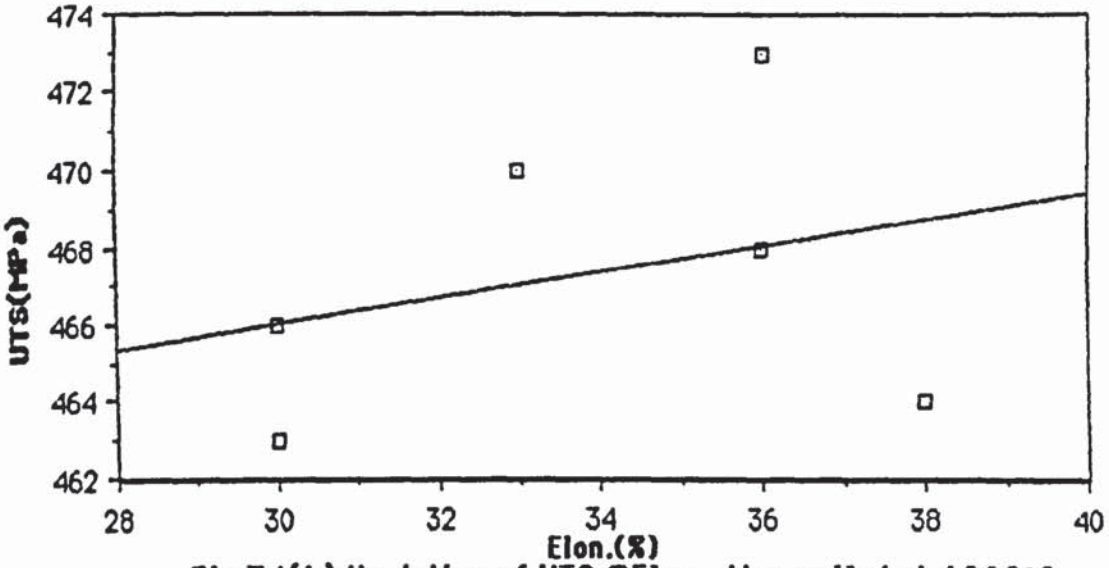

Fig.34(b).Variation of UTS %Elongation,rolled at 1000°C

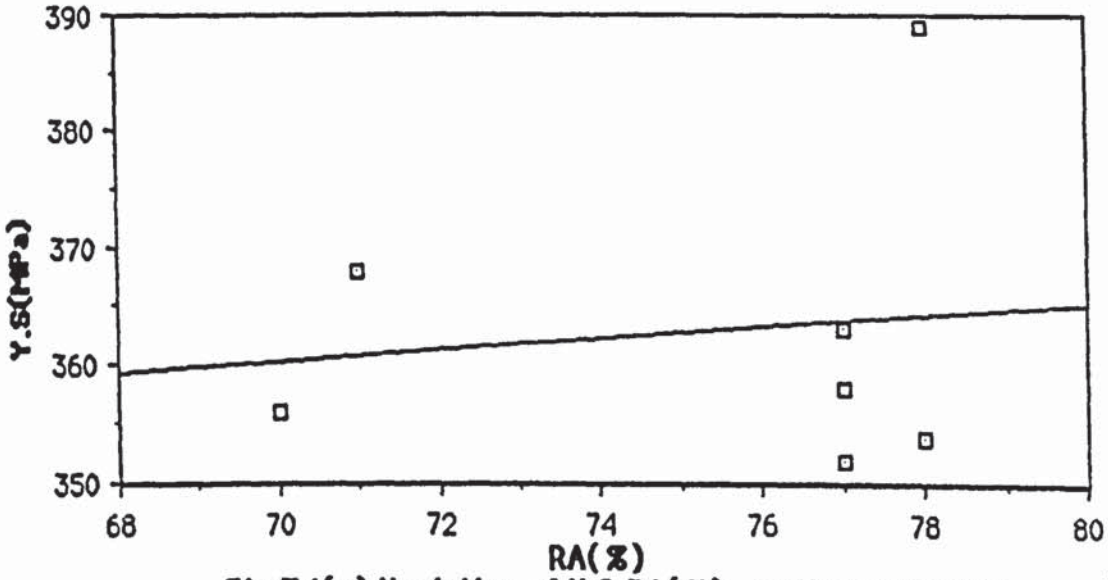

Fig.34(c).Variation of Y.S RA(%) , rolled at1000°C

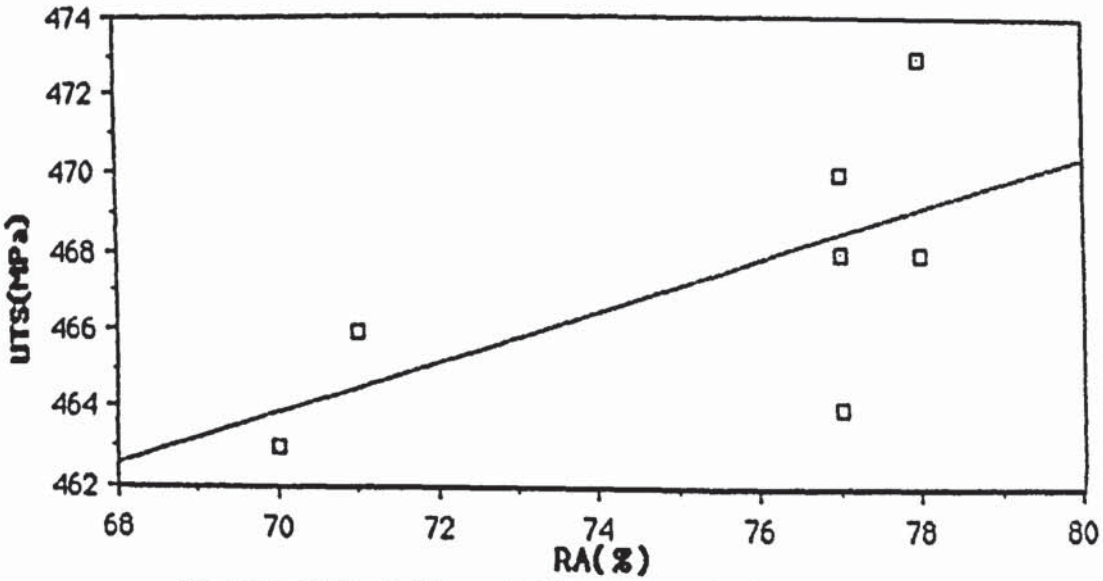

Fig.34(d).Variation of UTS with RA(%) , rolled at1000°C

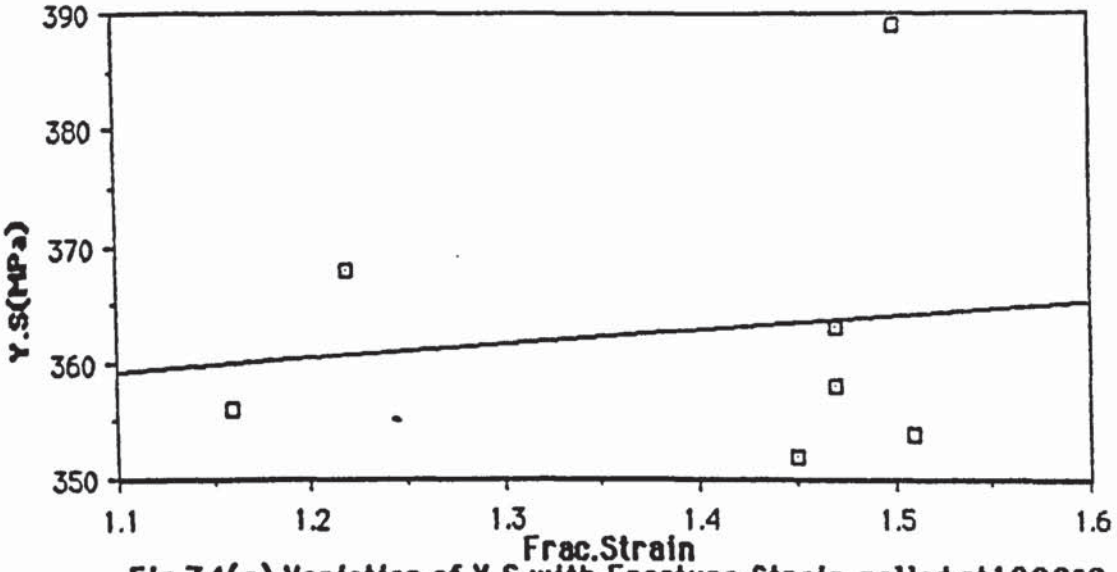

Fig.34(e).Variation of Y.S with Fracture Strain,rolled at1000°C

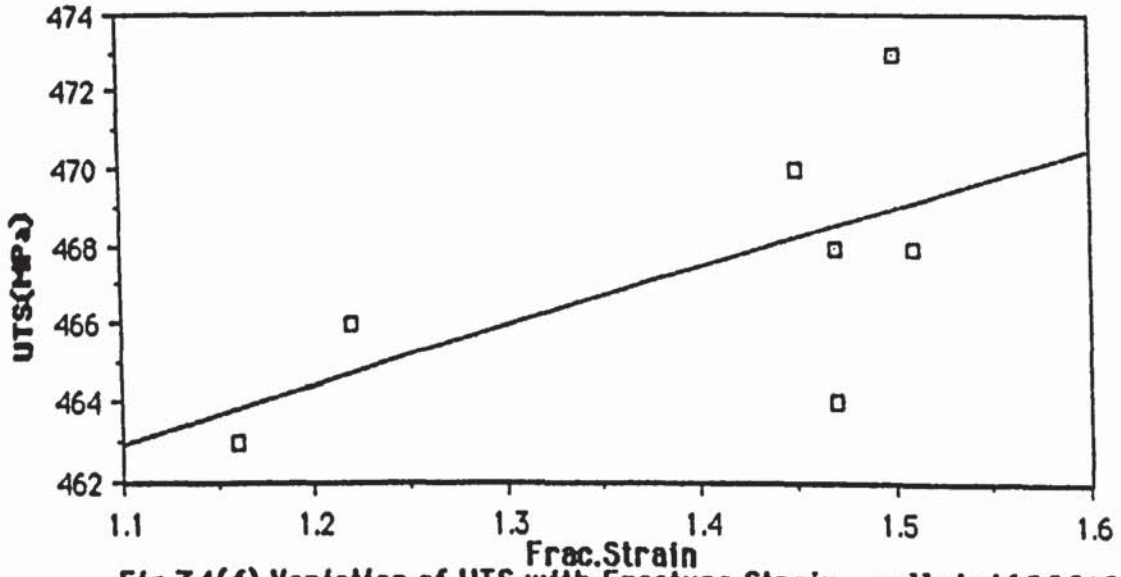

Fig.34(f).Variation of UTS with Fracture Strain , rolled at1000°C

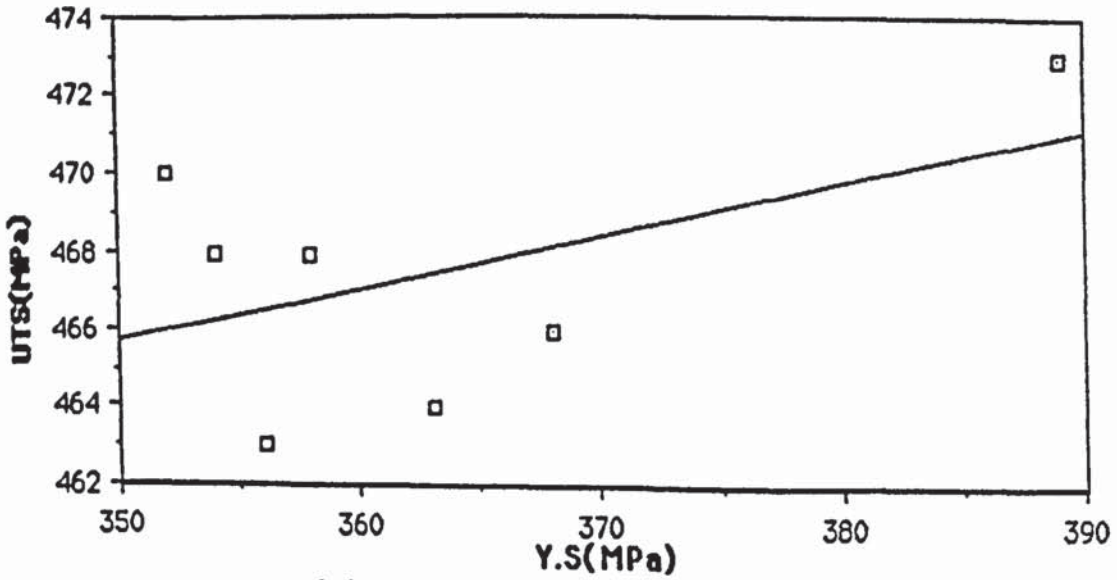

Fig.34(g).Variation of UTS with Y.S, rolled at1000°C

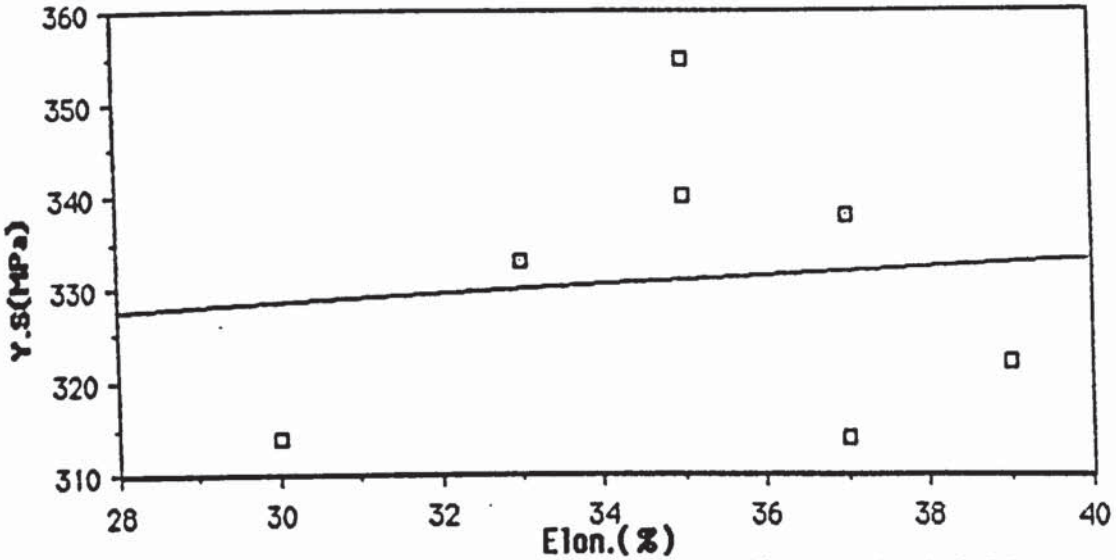

Fig.35(a).Variation of Y.S with %Elongation , rolled at 900°C

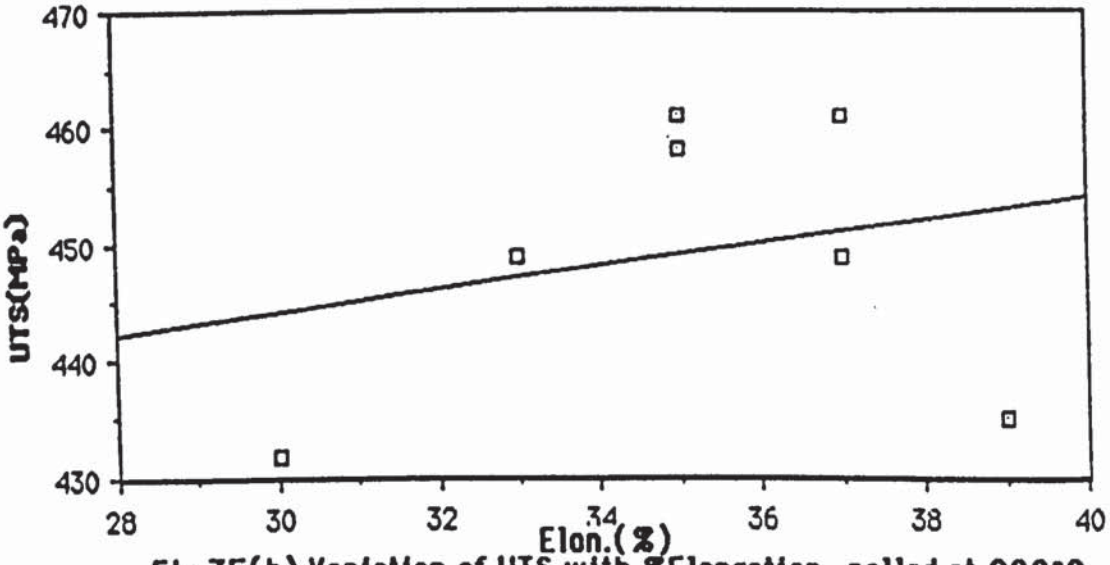

Fig.35(b).Variation of UTS with %Elongation, rolled at 900°C

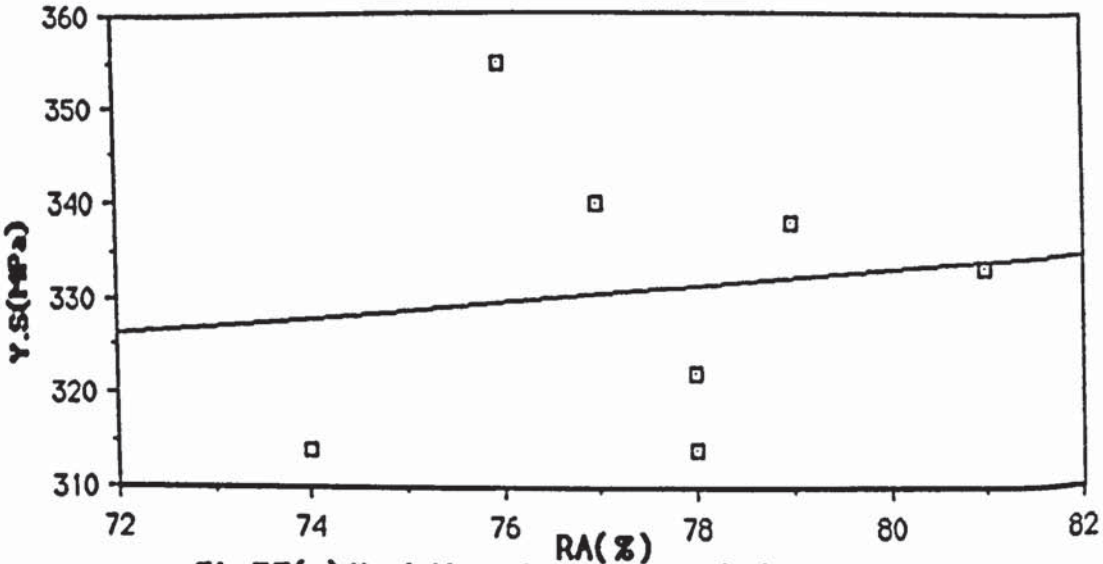

Fig.35(c).Variation of Y.S with RA(%), rolled at900°C

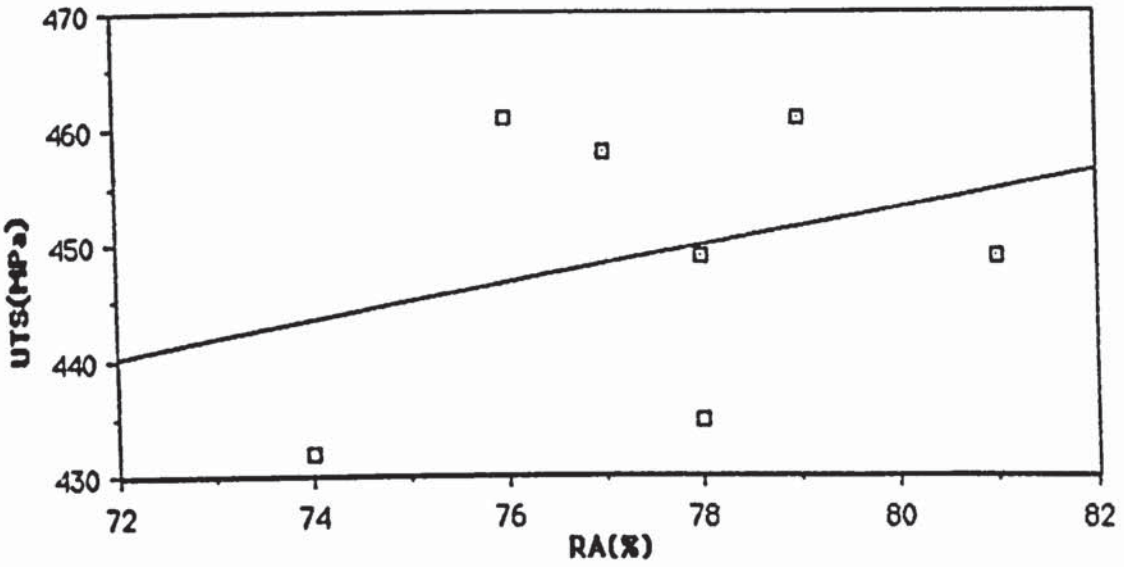

Fig.35(d).Variation of UTS with %RA , rolled at 900°C.

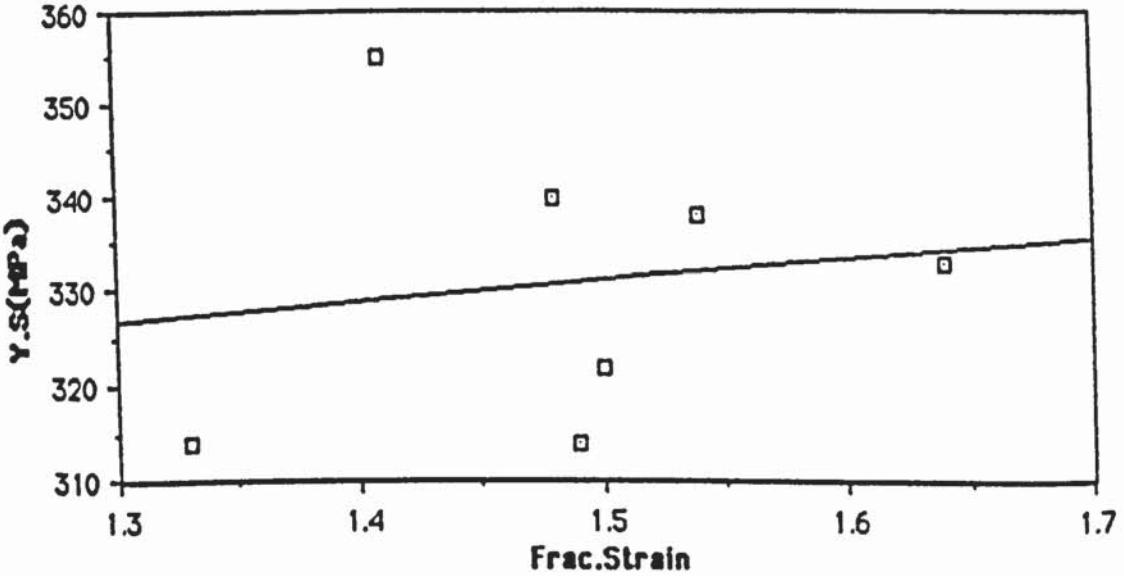

Fig.35(e).Variation of Y.S with fracture strain,rolled at 900°C.

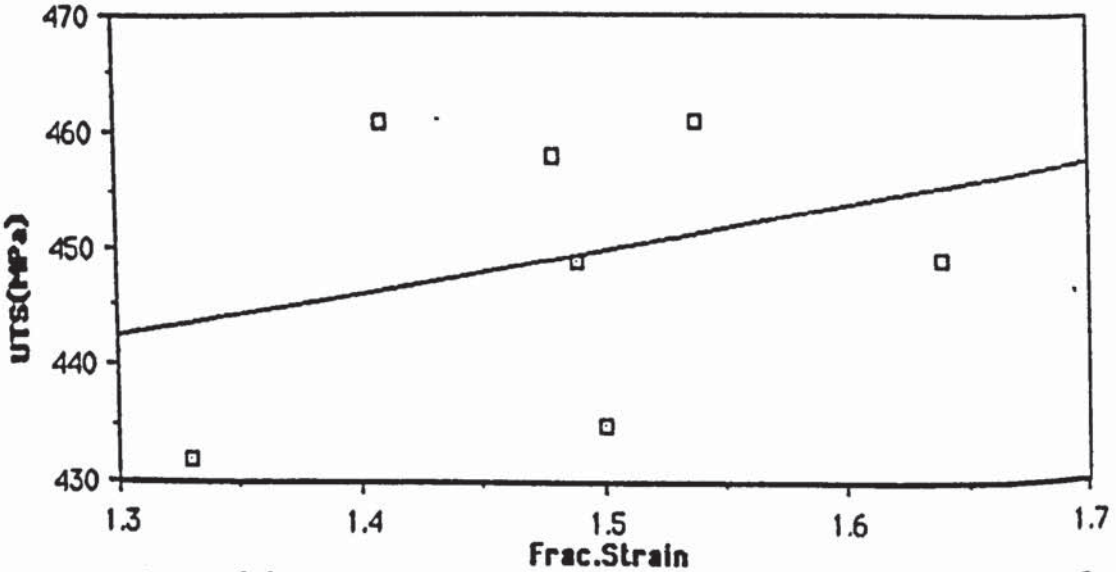

Fig.35(f).Variation of UTS with fracture strain,rolled at 900°C.

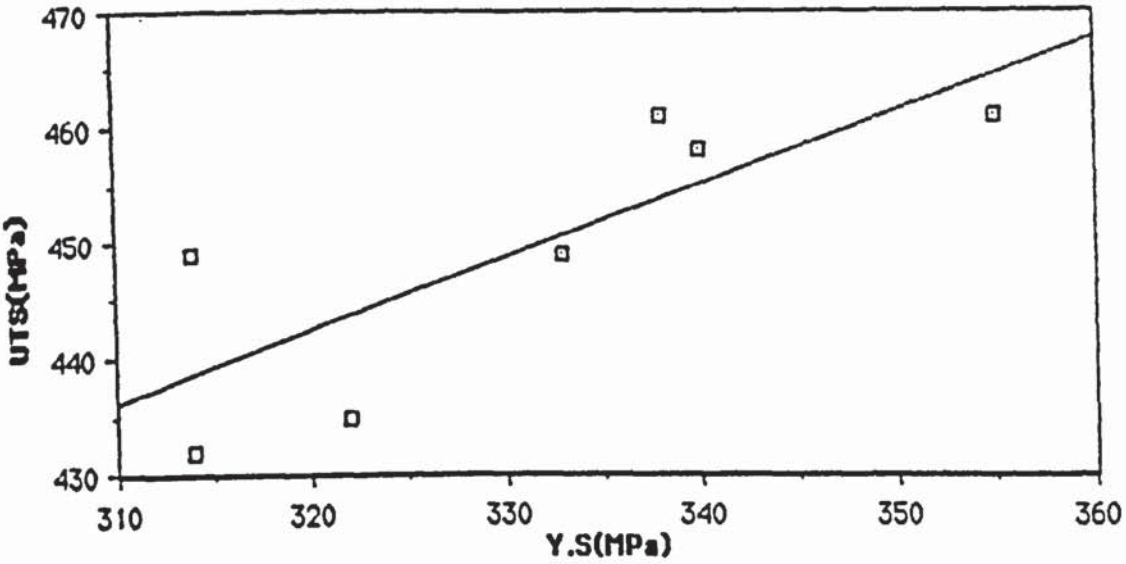

Fig.35(g).Variation of UTS with YS,rolled at 900°C.

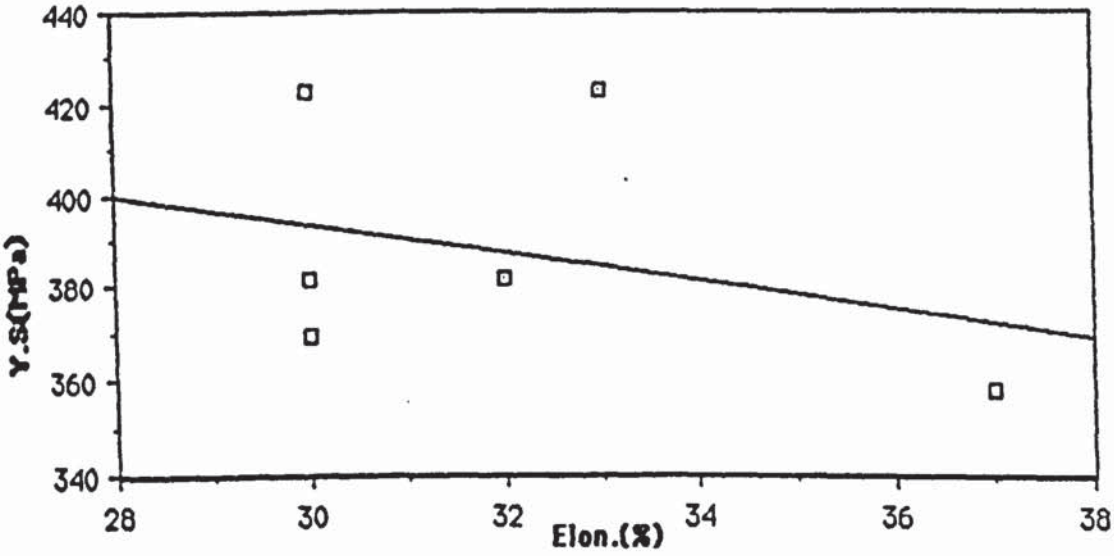

Fig.36(a).Variation of YS with % Elongation, A-Series, stress relieved

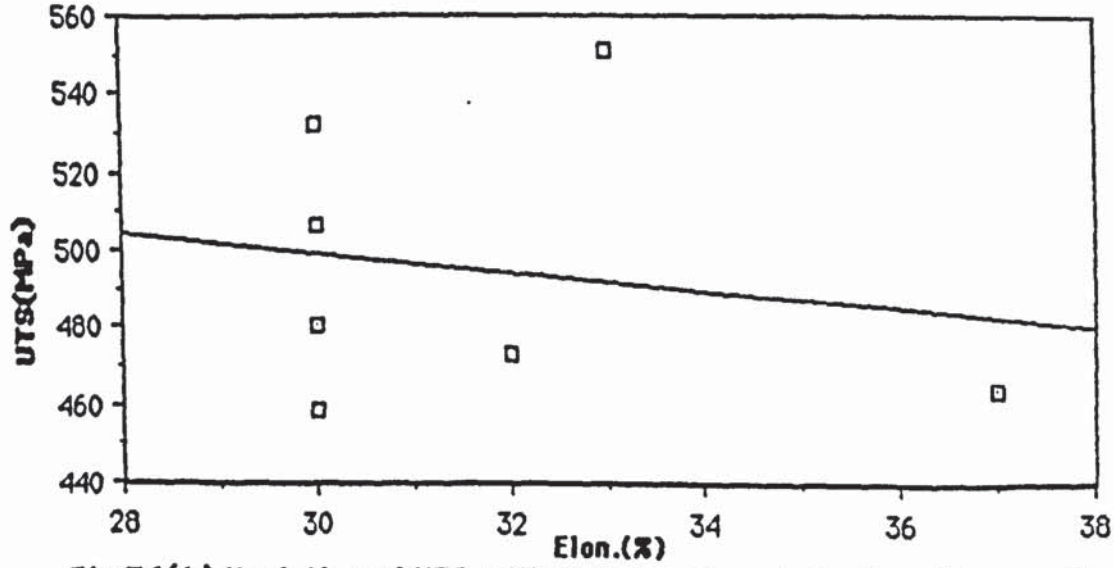

Fig.36(b).Variation of UTS with % Elongation, A-Series, Stress relieved

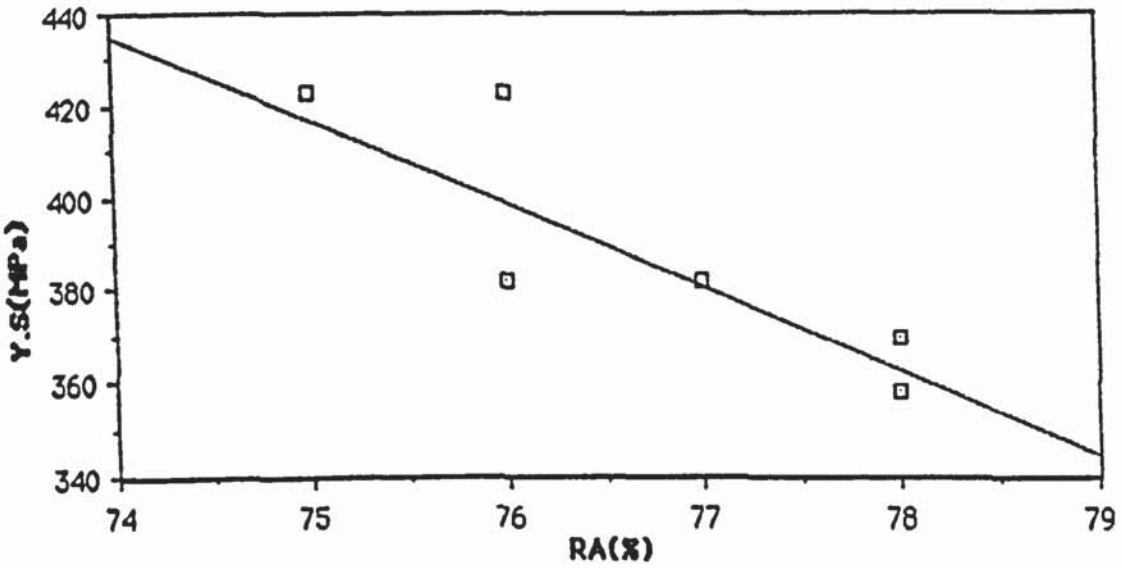

Fig.36(c).Variation of YS with %RA, A-Series, stress relieved

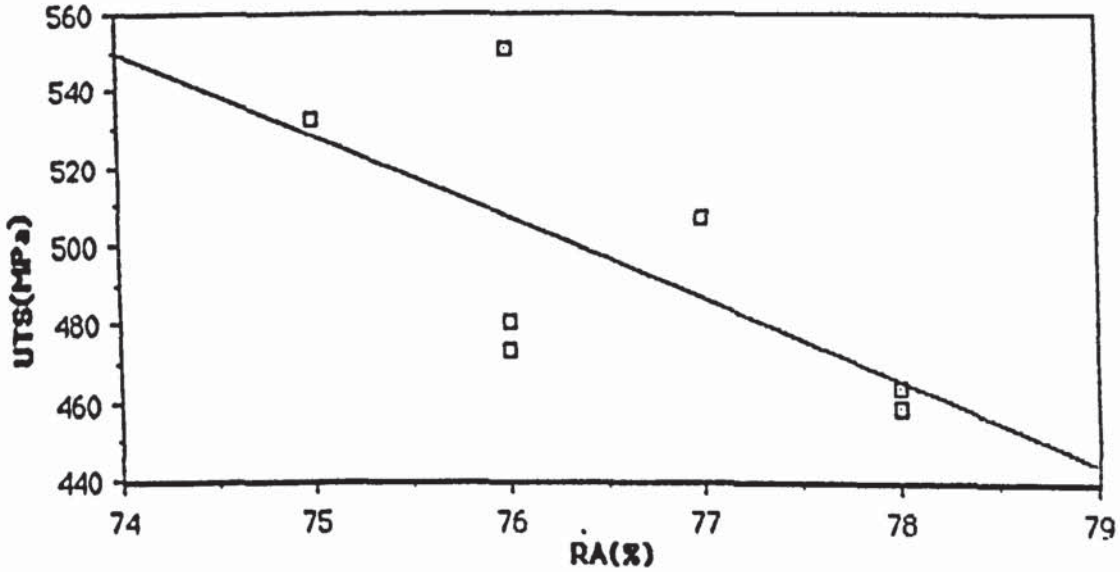

Fig.36(d).Variation of UTS with %RA, A-Series, stress relieved

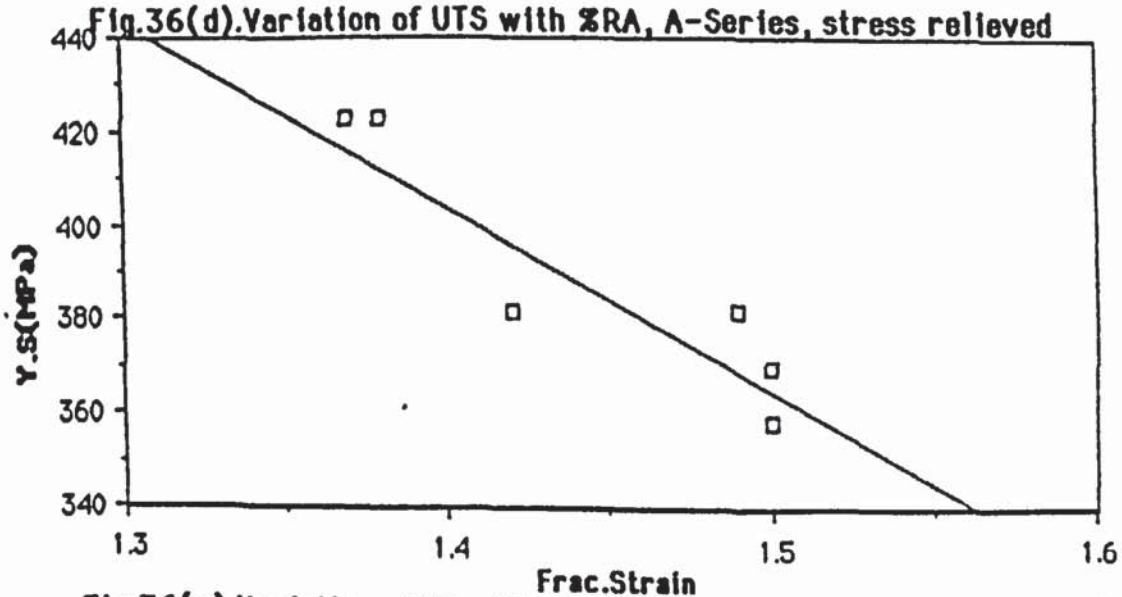

Fig.36(e).Variation of YS with Fracture strain, A-Series, stress relieve

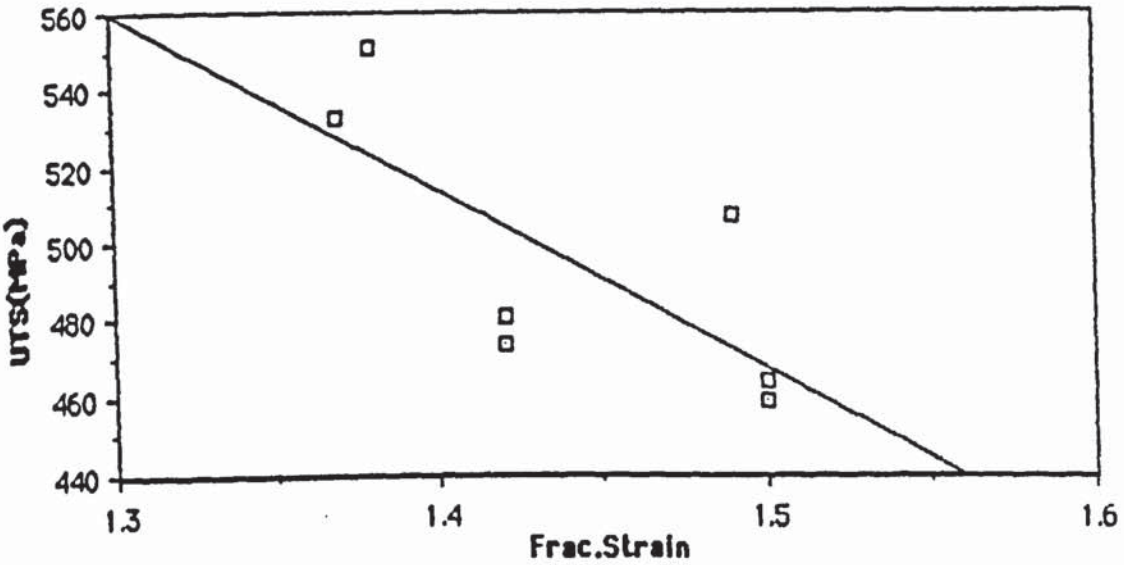

Fig.36(f).Variation of UTS with Fracture strain, A-Series, stress relieved

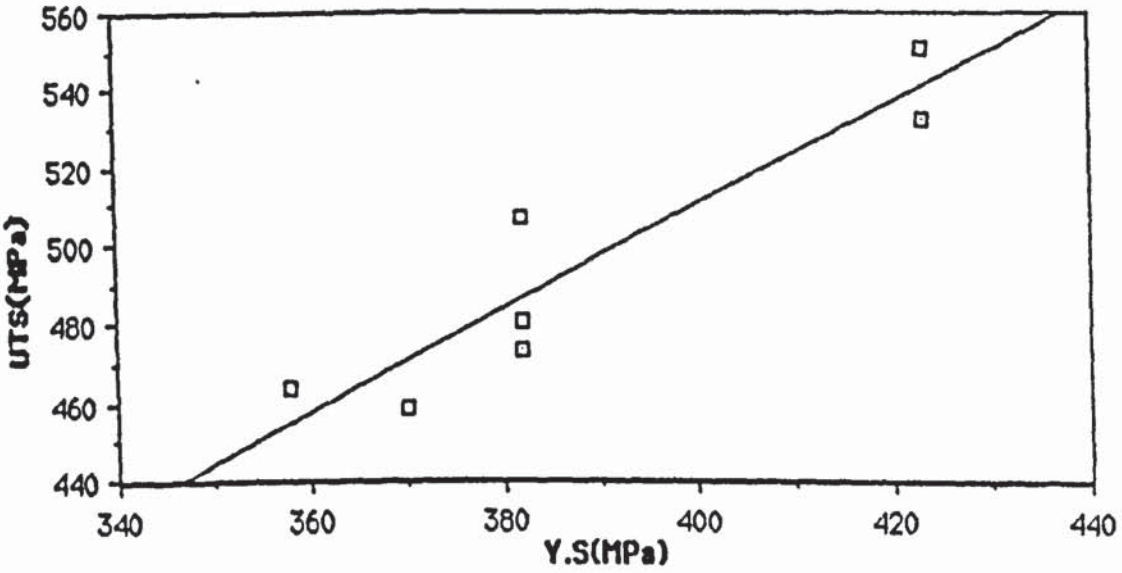

Fig.36(g).Variation of UTS with YS, A-Series, stress relieved

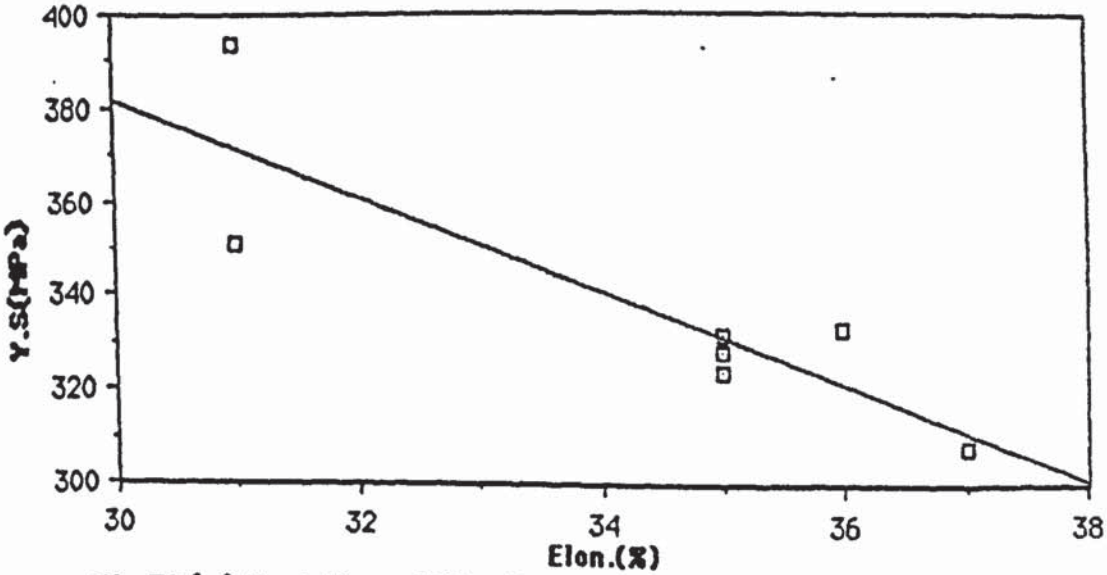

Fig.37(a).Variation of YS withn%Elongation B-Series, stress relieved

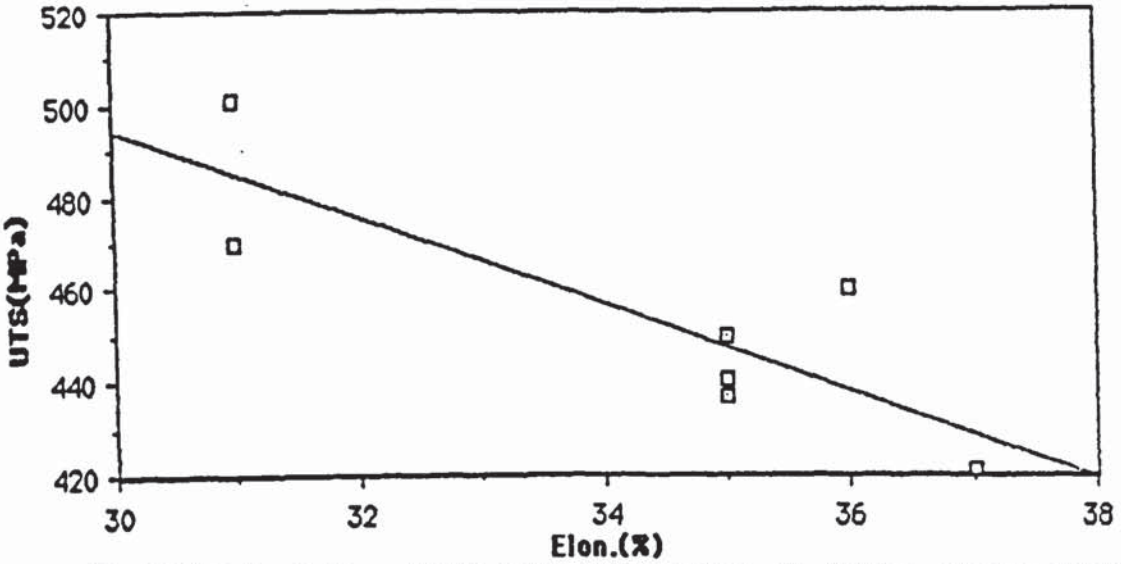

Fig.37(b).Variation of UTS with %Elongation, B-Series, stress relieved

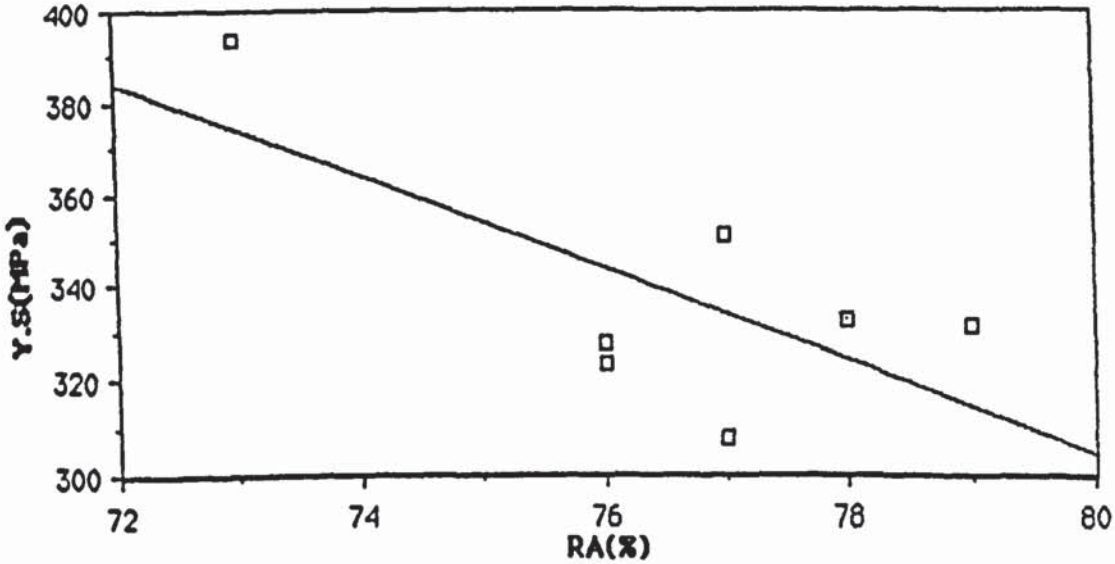

Fig.37(c).Variation of YS with %RA, B-Series, stress relieved

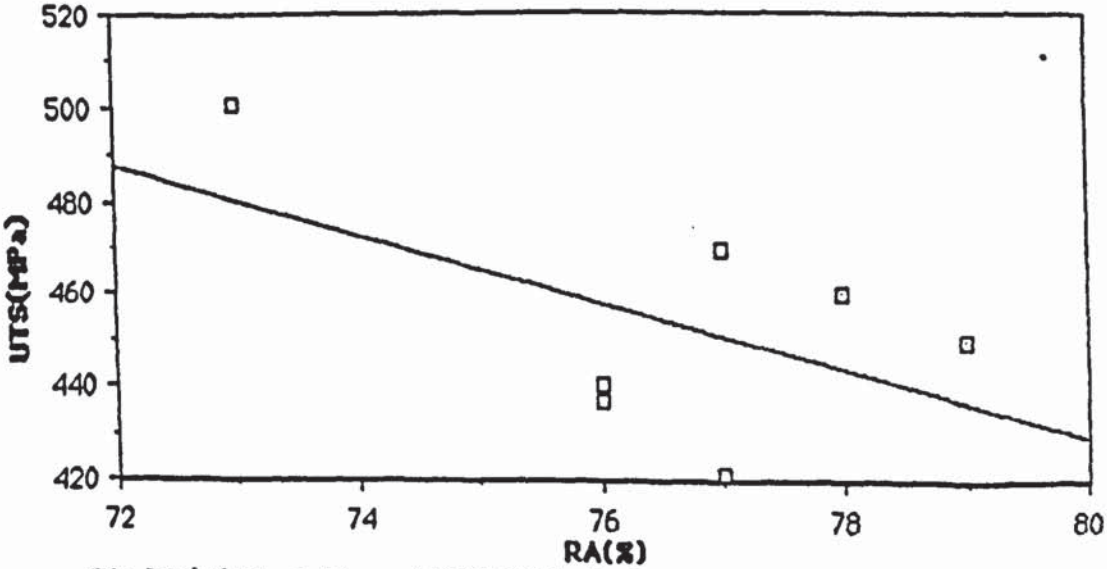

Fig.37(d).Variation of UTS %RA, B-Series, stress relieved

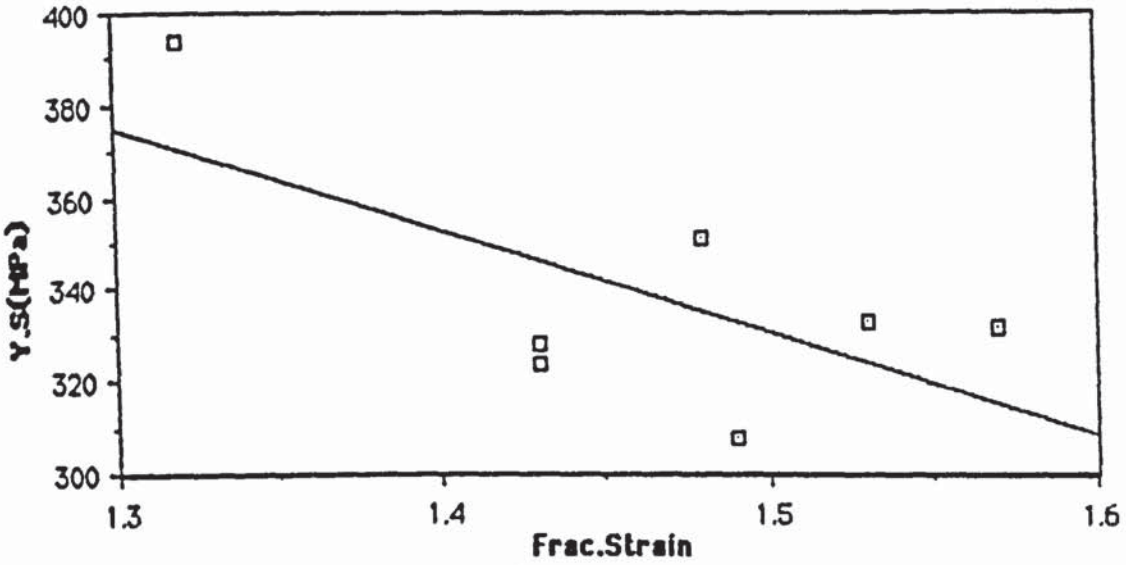

Fig.37(e).Variation of YS with Fracture strain, B-Series, stress relieved

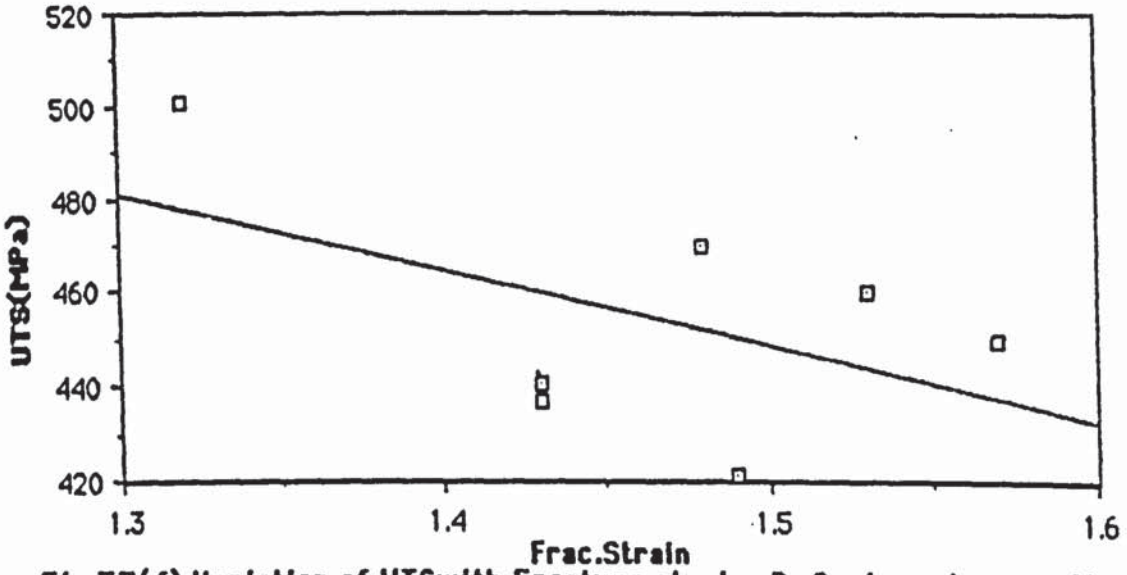

Fig.37(f).Variation of UTSwith Fracture strain, B-Series, stress relieved

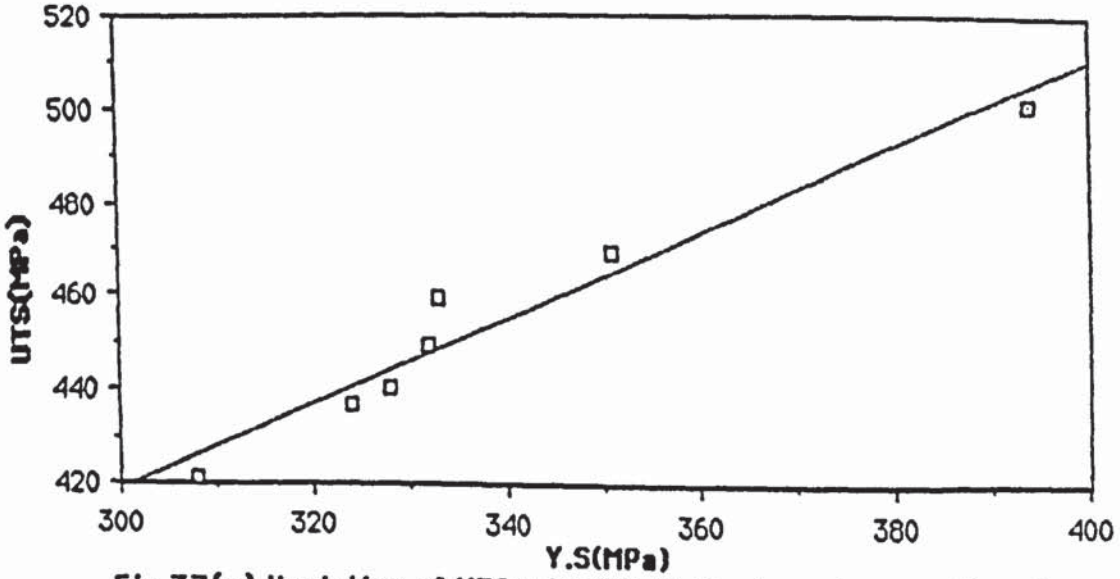

Fig.37(g).Variation of UTS with YS, B-Series, stress relieved

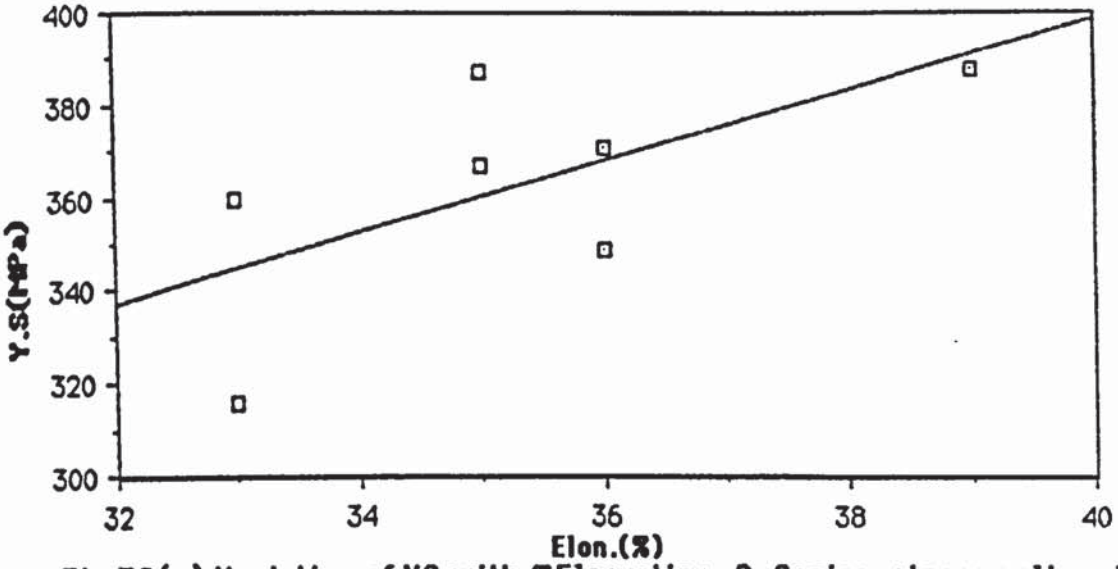

Fig.38(a).Variation of YS with %Elongation, C-Series, stress relieved

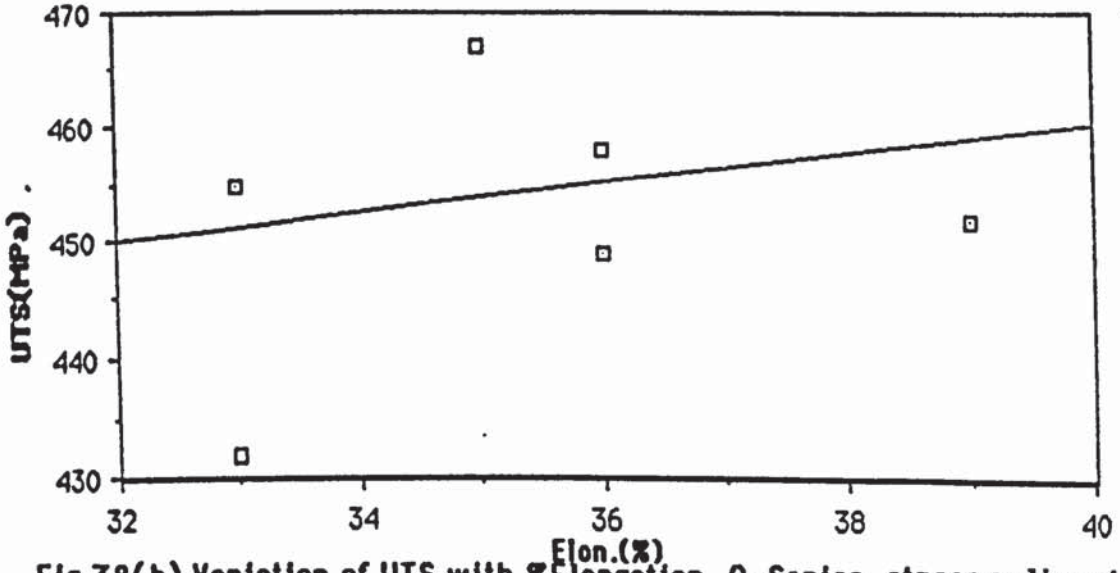

Fig.38(b).Variation of UTS with %Elongation, C-Series, stress relieved

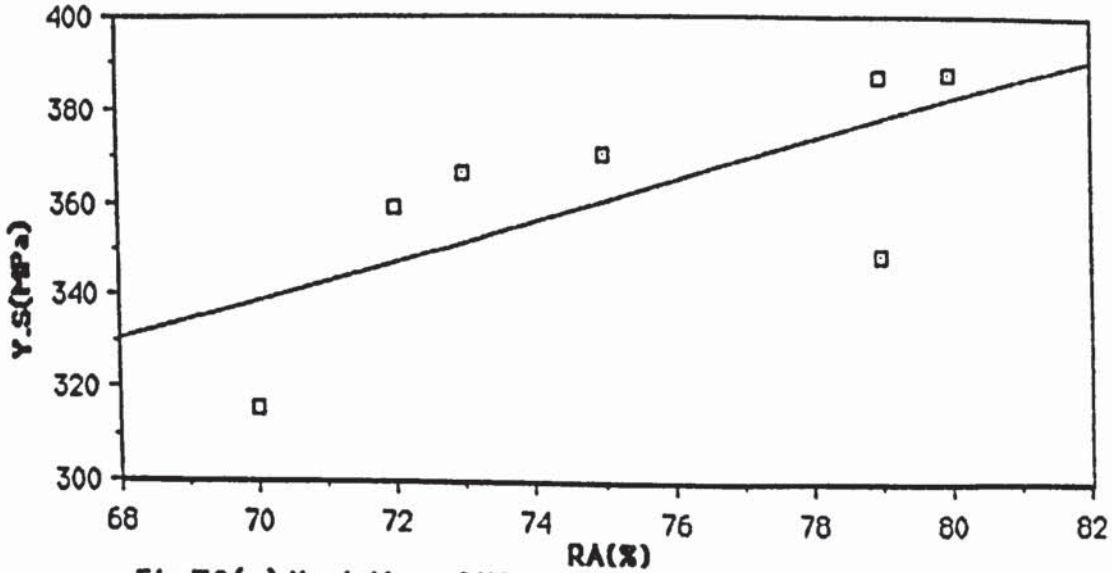

Fig.38(c).Variation of YS with %RA, C-Series, stress relieved

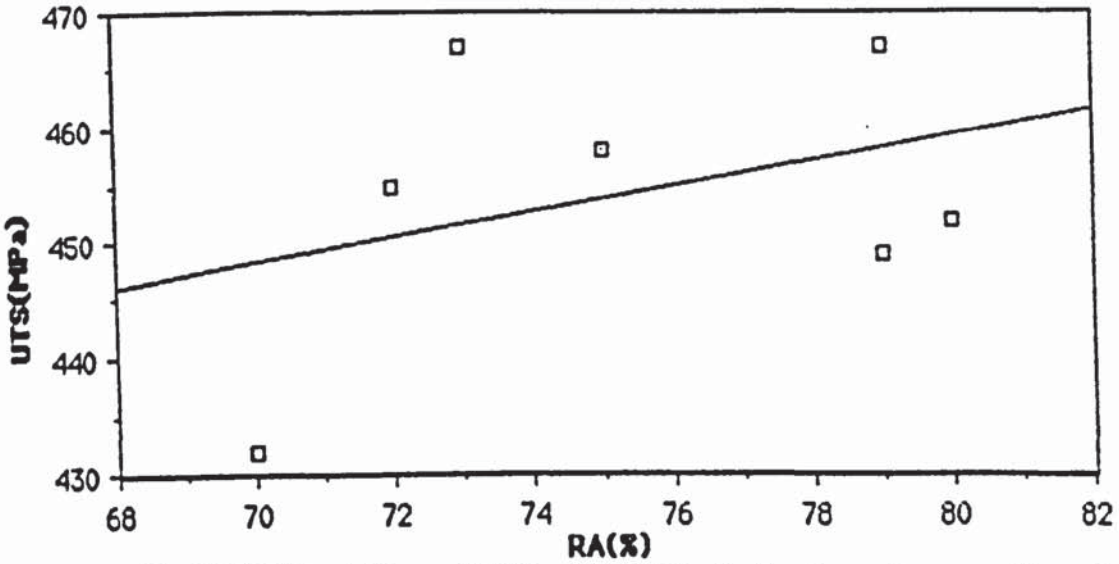

Fig.38(d).Variation of UTS with %RA, C-Series, stress relieved

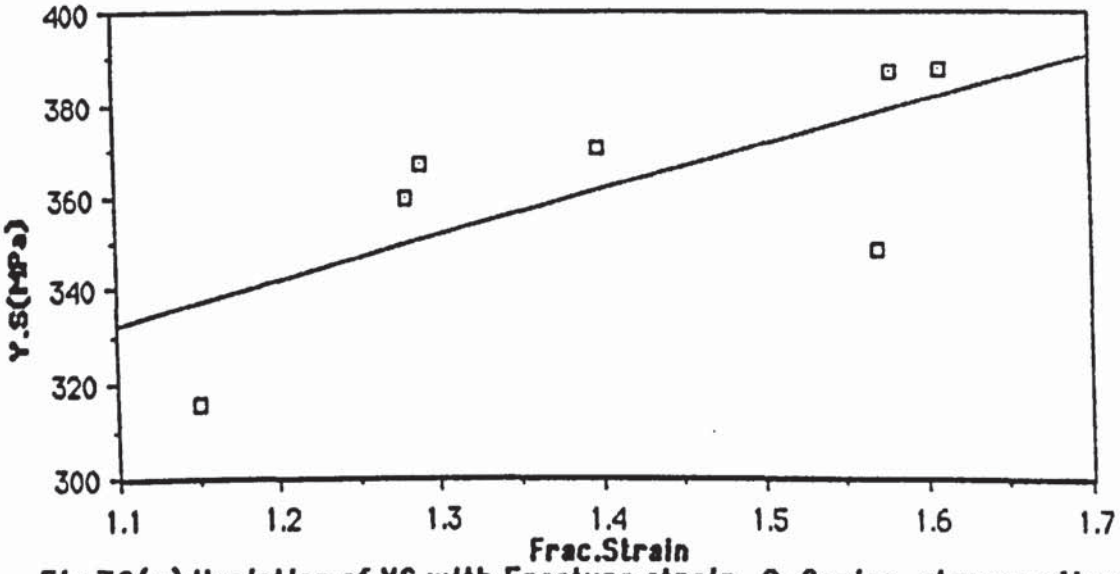

Fig.38(e).Variation of YS with Fracture strain, C-Series, stress relieved

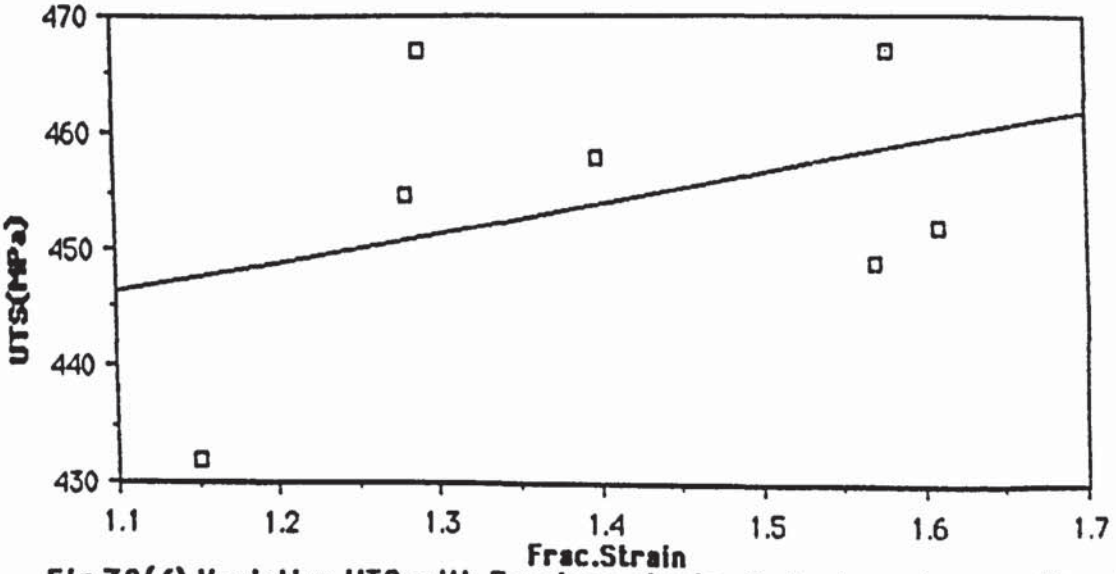

Fig.38(f).Variation UTS with Fracture strain, C-Series, stress relieved

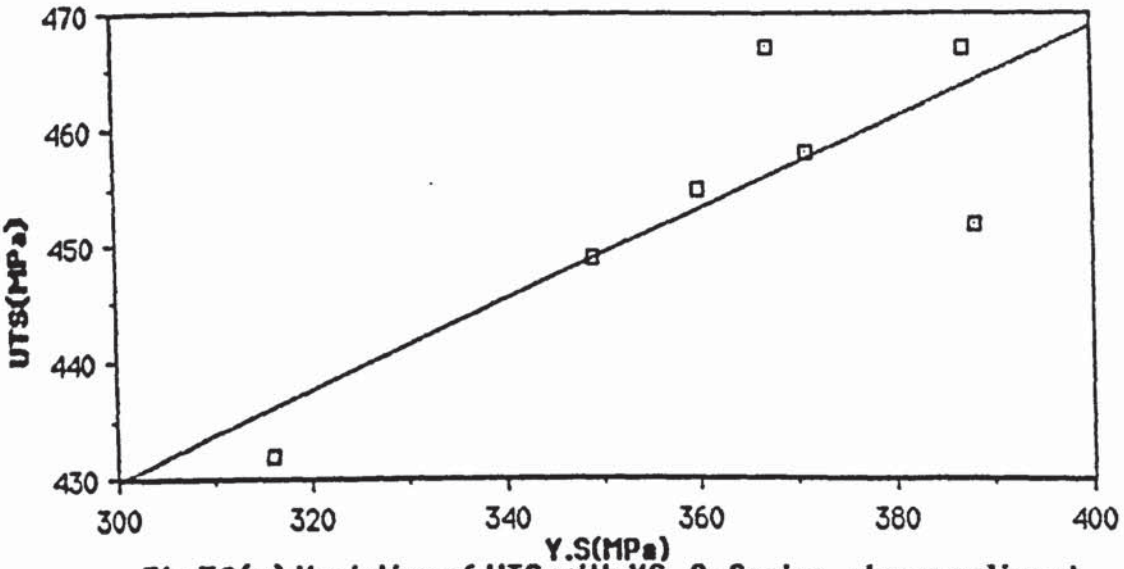

Fig.38(g).Variation of UTS with YS, C-Series, stress relieved

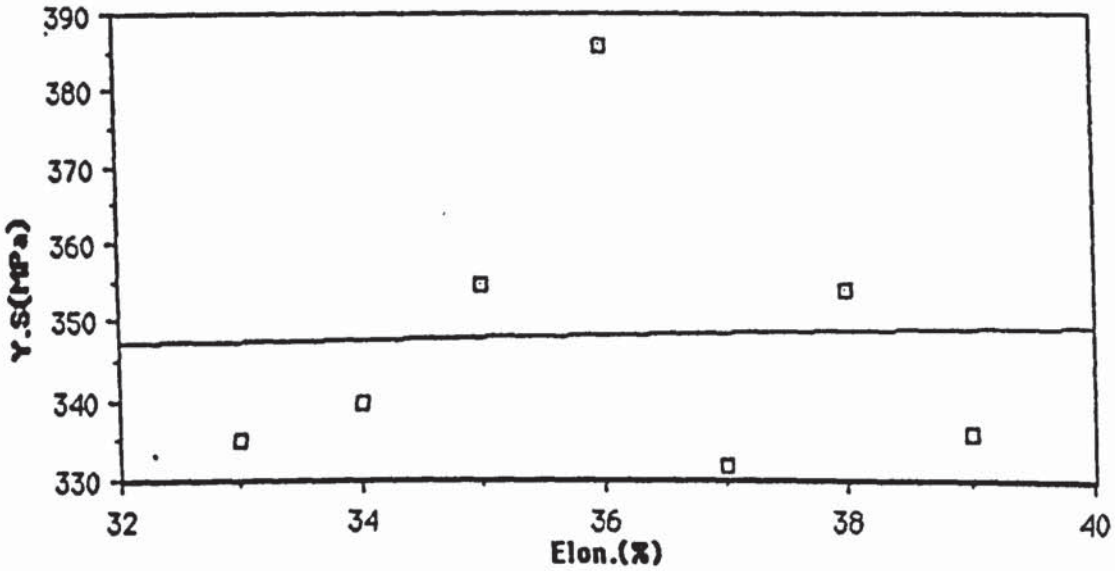

Fig.39(a).Variation of YS with %Elongation, D-Series, stress relieved

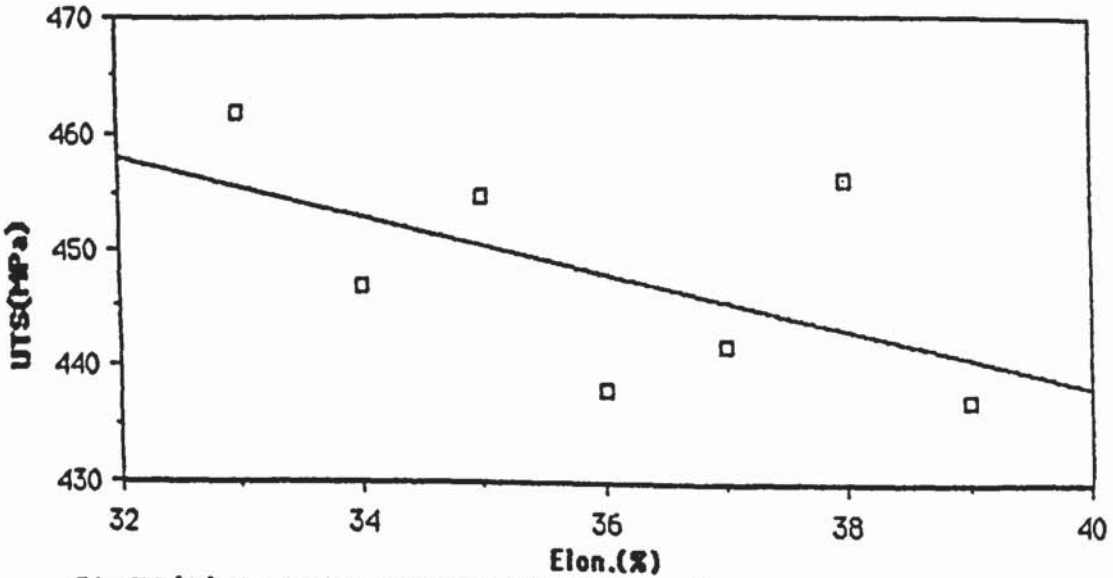

Fig.39(b).Variation of UTS with %Elongation, D-Series, stress relieved

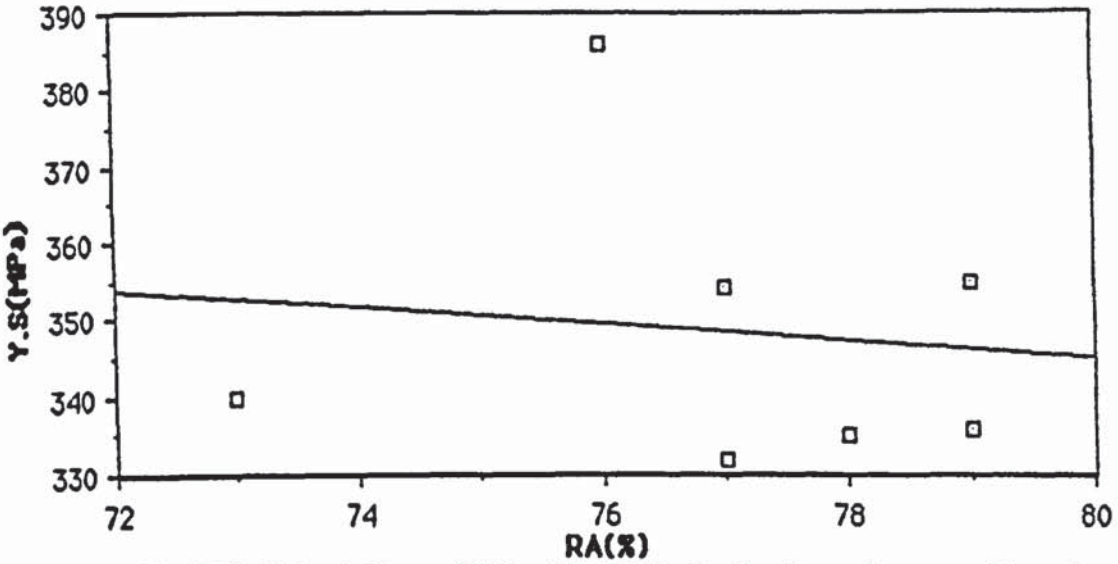

Fig.39(c).Variation of YS with %RA, D-Series, stress relieved

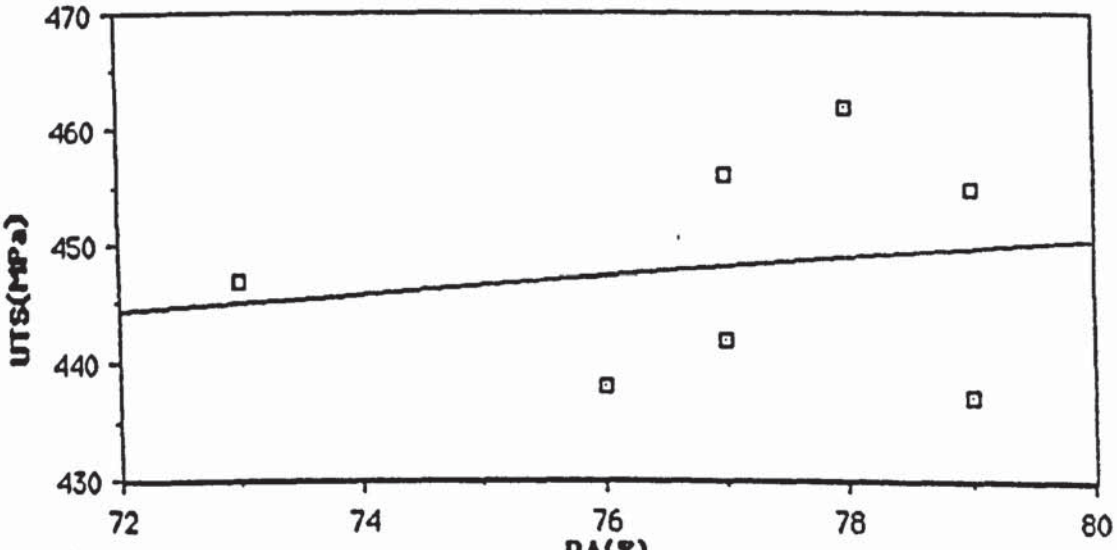

39(d).Variation of UTS with %RA, D-Series, stress relieved

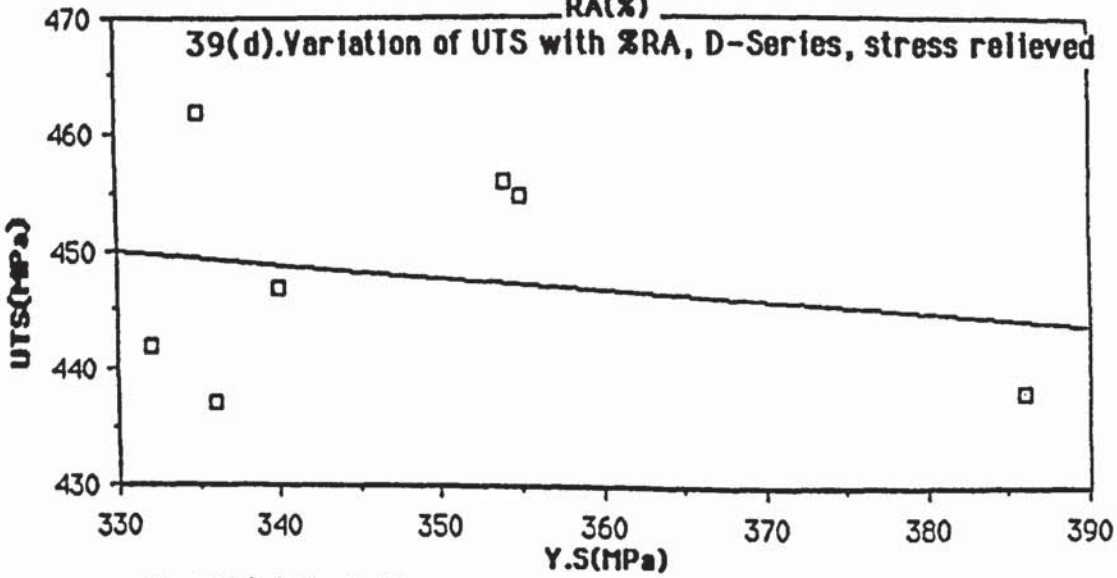

Fig.39(e).Variation of UTS with YS, D-Series, stress relieved

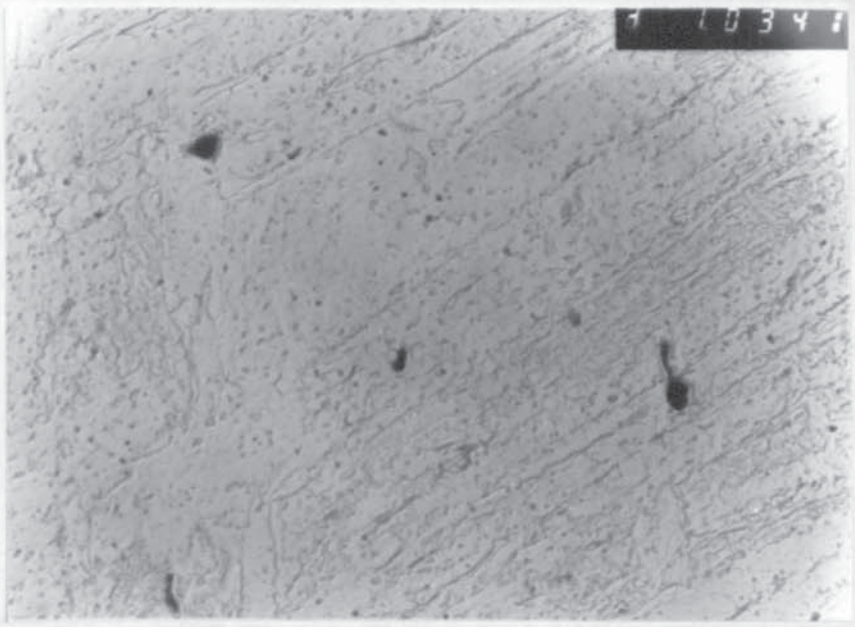

FIGURE-40A(1). Base Steel Soaked at 1250°C and Water Quenched Showing Insoluble Dense Ti Rich Precipitates and Less Dense Soluble Precipitates. X10K

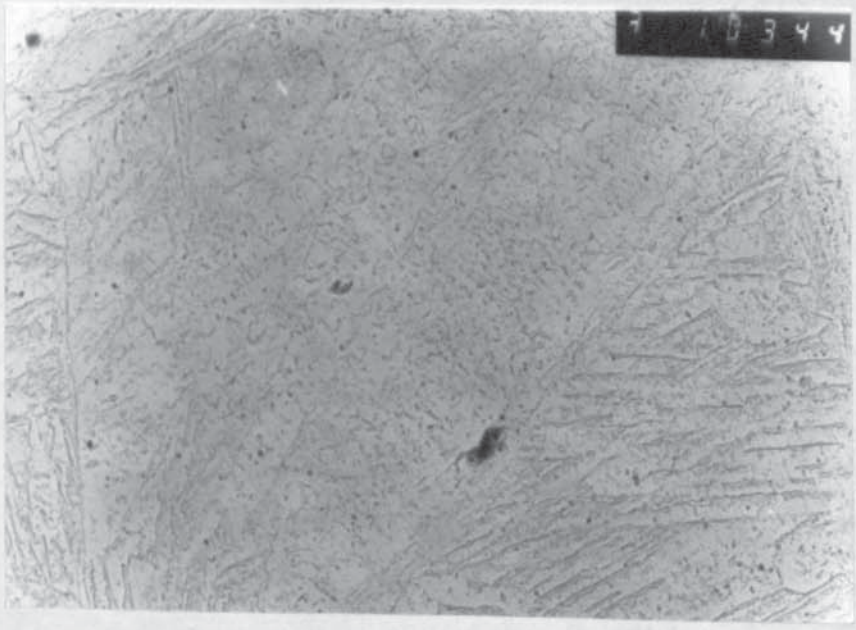

FIGURE-40A(2). Base Steel Soaked at 1250°C , Rolled (20%,1Pass) and Water Quenched Indicating an Increase in Number of Dense Precipitates. X10K

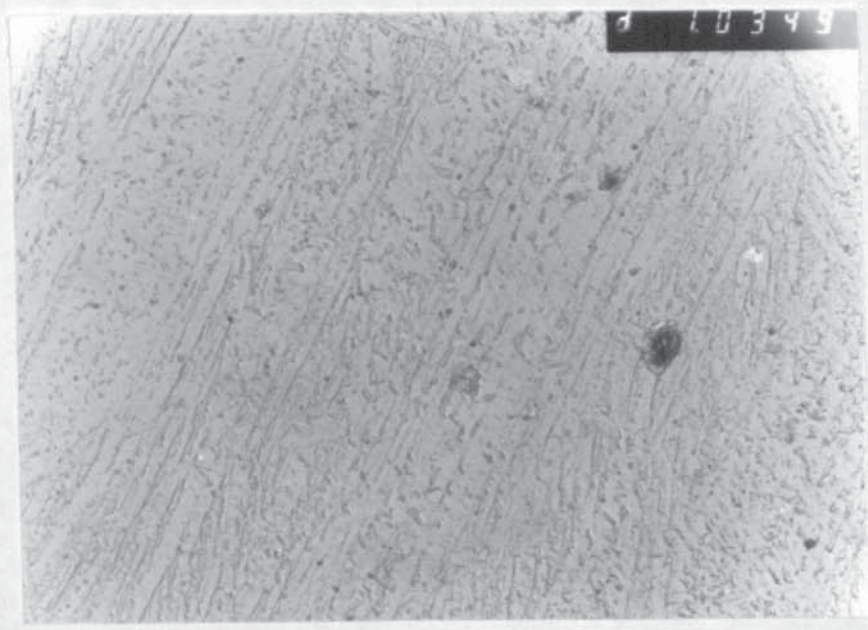

FIGURE-40B(1). Steel 4 Soaked at 1250°C and Water Quenched Showing Denser Insoluble Precipitates Compared with The Base Steel. X10K.

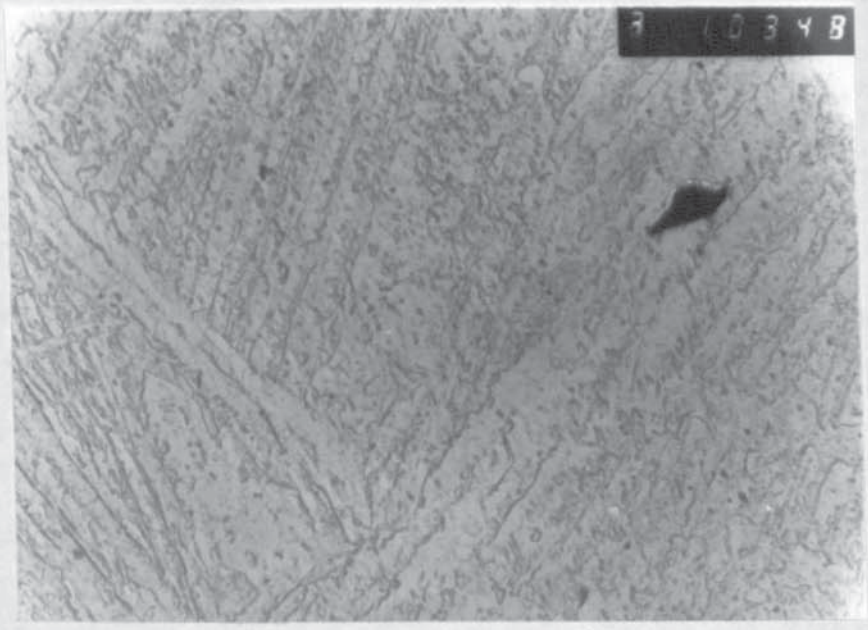

FIGURE-40B(2). Steel 4 Soaked at 1250°C,Rolled (20%,1Pass) and Water Quenched Indicating Apparently No Significant Difference to The Above. X10K.

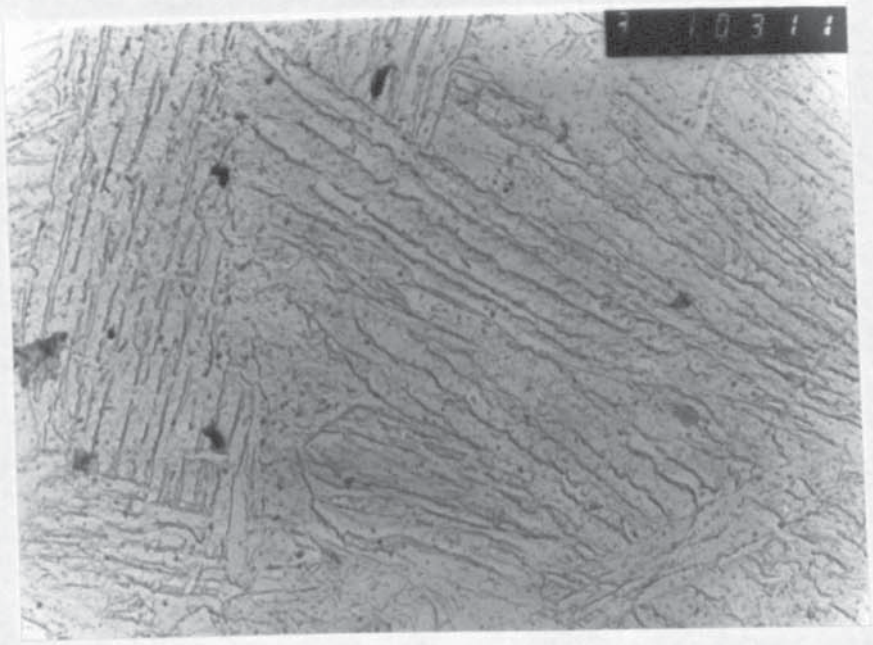

FIGURE-41A(1). Base Steel Soaked at 1250°C, Rolled (20%,1Pass) and Water Quenched , Reheated at 1250°C and Water Quenched. X10K.

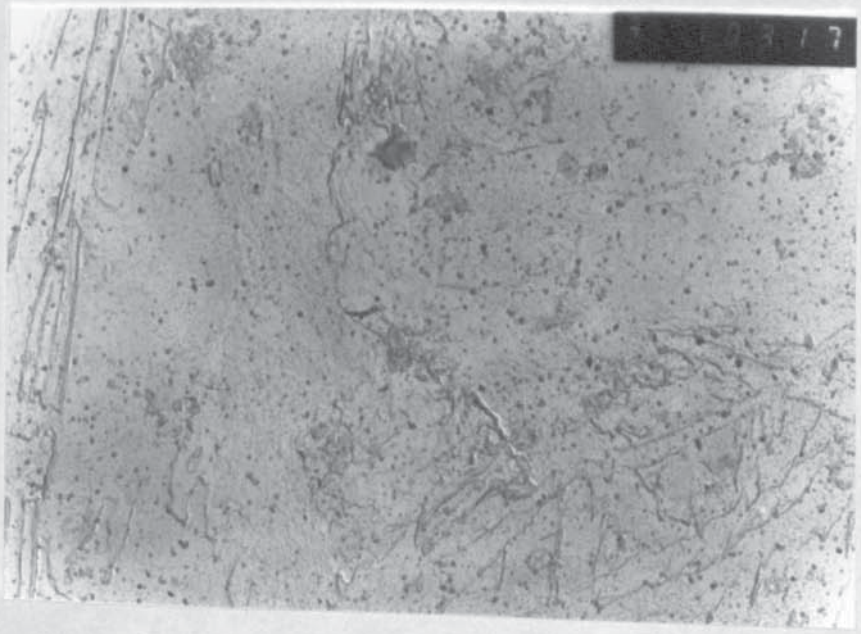

FIGURE-41A(2). Base Steel Soaked at 1250°C, Rolled (20%,1Pass) and Water Quenched, Reheated at 1250°C, Rolled (23%,Pass No.2) and Water Quenched. X10K.

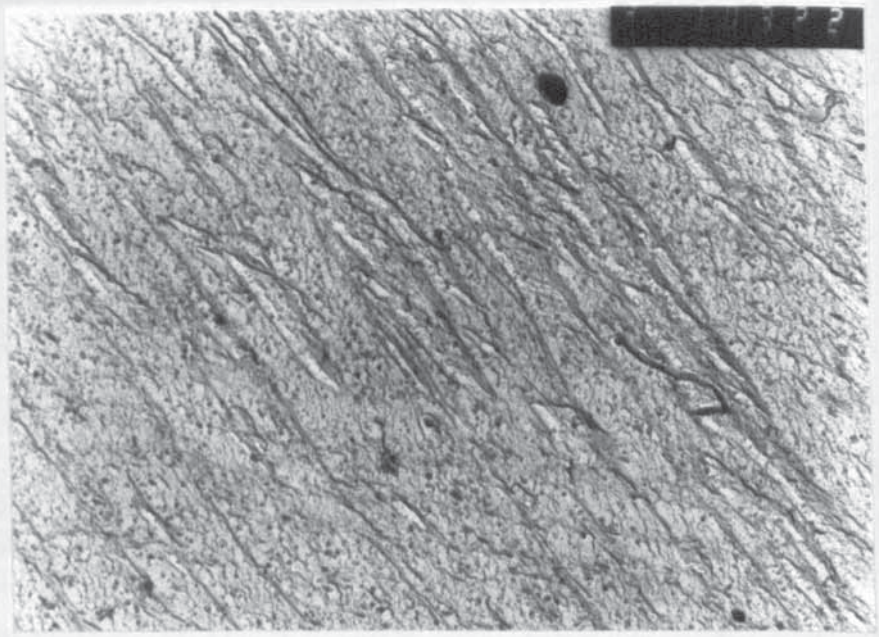

FIGURE-41B(1). Steel 4 Soaked at 1250°C, Rolled (20%,1Pass) and Water Quenched, Reheated at 1250°C and Water Quenched. X10K.

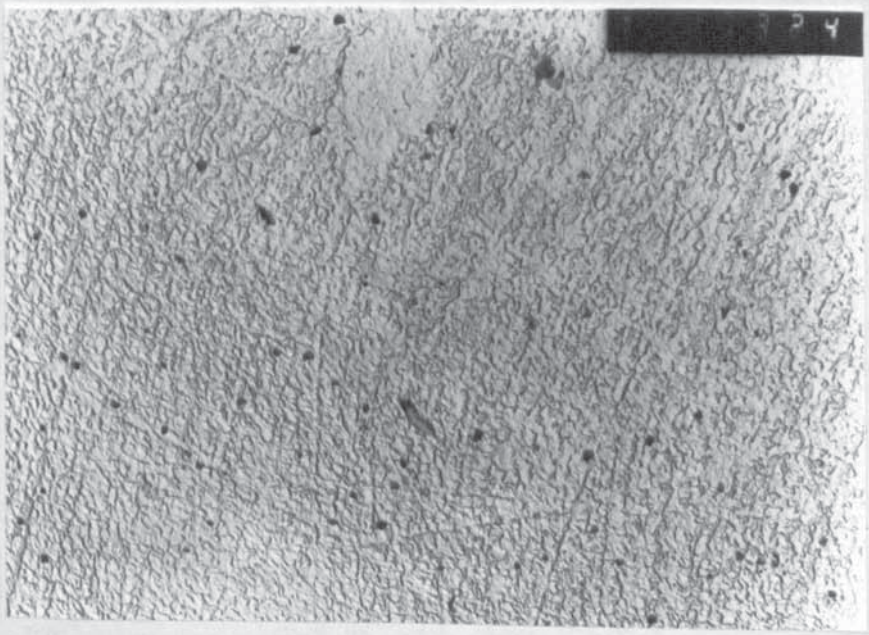

FIGURE-41B(2) Steel 4 Soaked at 1250°C ,Rolled (20%,1Pass) and Water Quenched ,Reheated at 1250°C,Rolled (23%,Pass No.2) and Water Quenched. X10K.

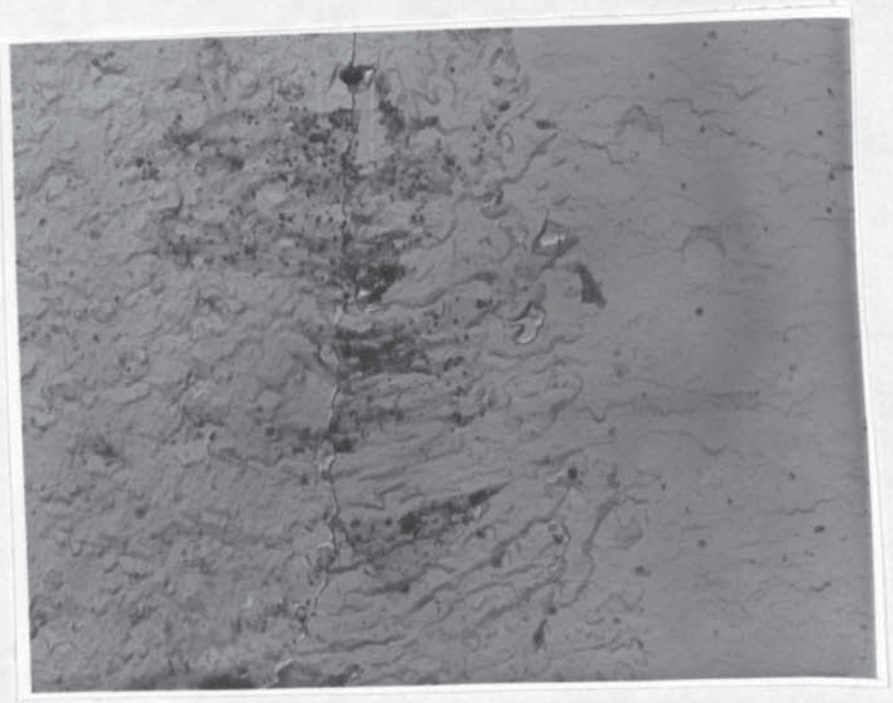

FIGURE-42. Steel 4 Soaked at 1250°C and Rolled at 900°C Showing Copious Precipitates in The Vicinity of Prior Austenite Grain Boundary. X25K.

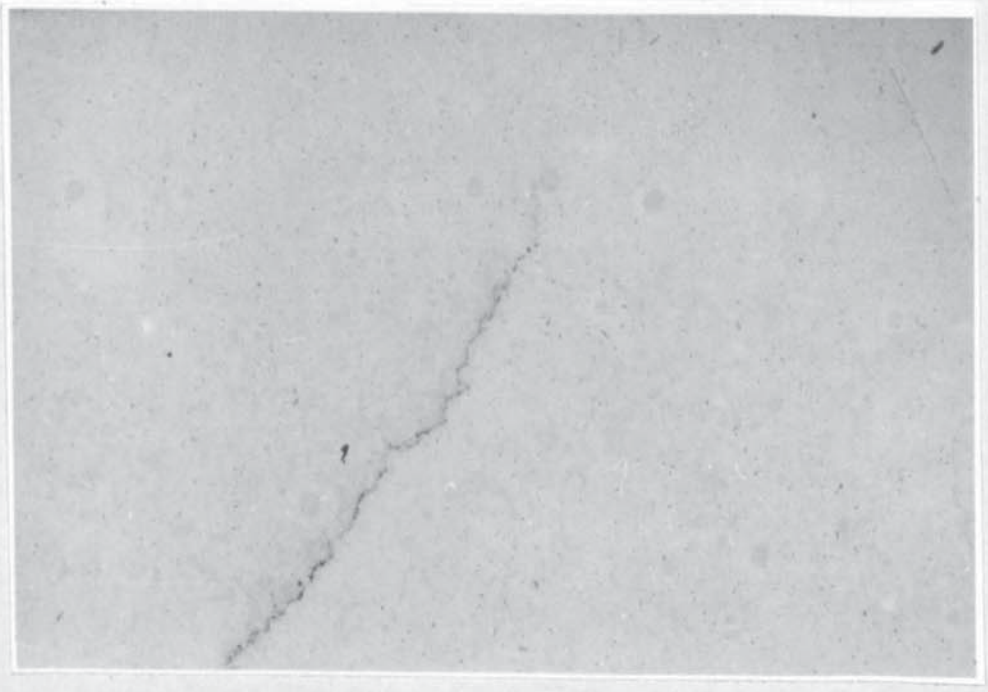

FIGURE-43. A Section of Single HIC in Steel 4,Soaked at 1250°C ,Rolled (20%, 1Pass) and Water Quenched. X27.

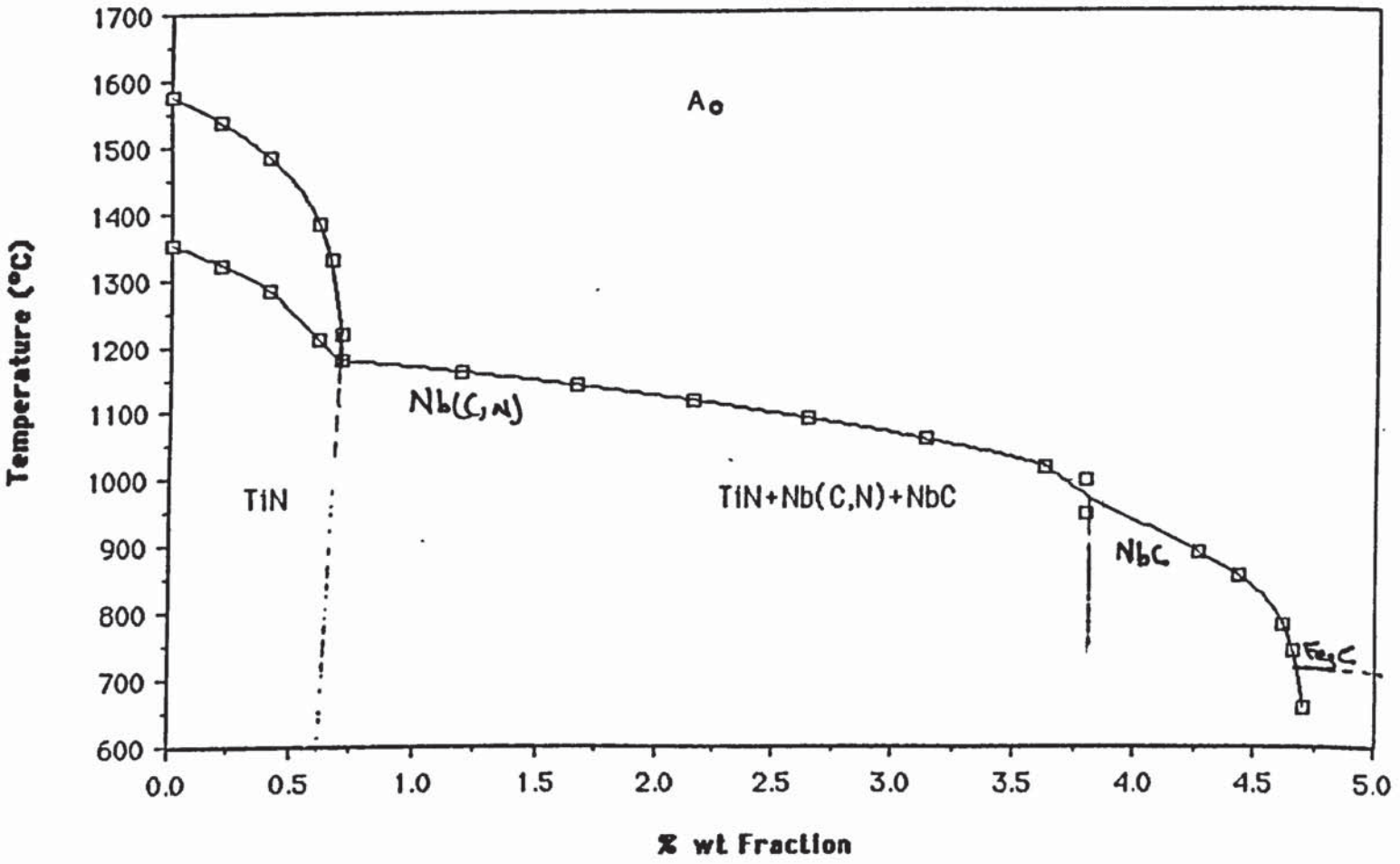

Fig.44. Variation of temperature with %wt fraction of precipitates.

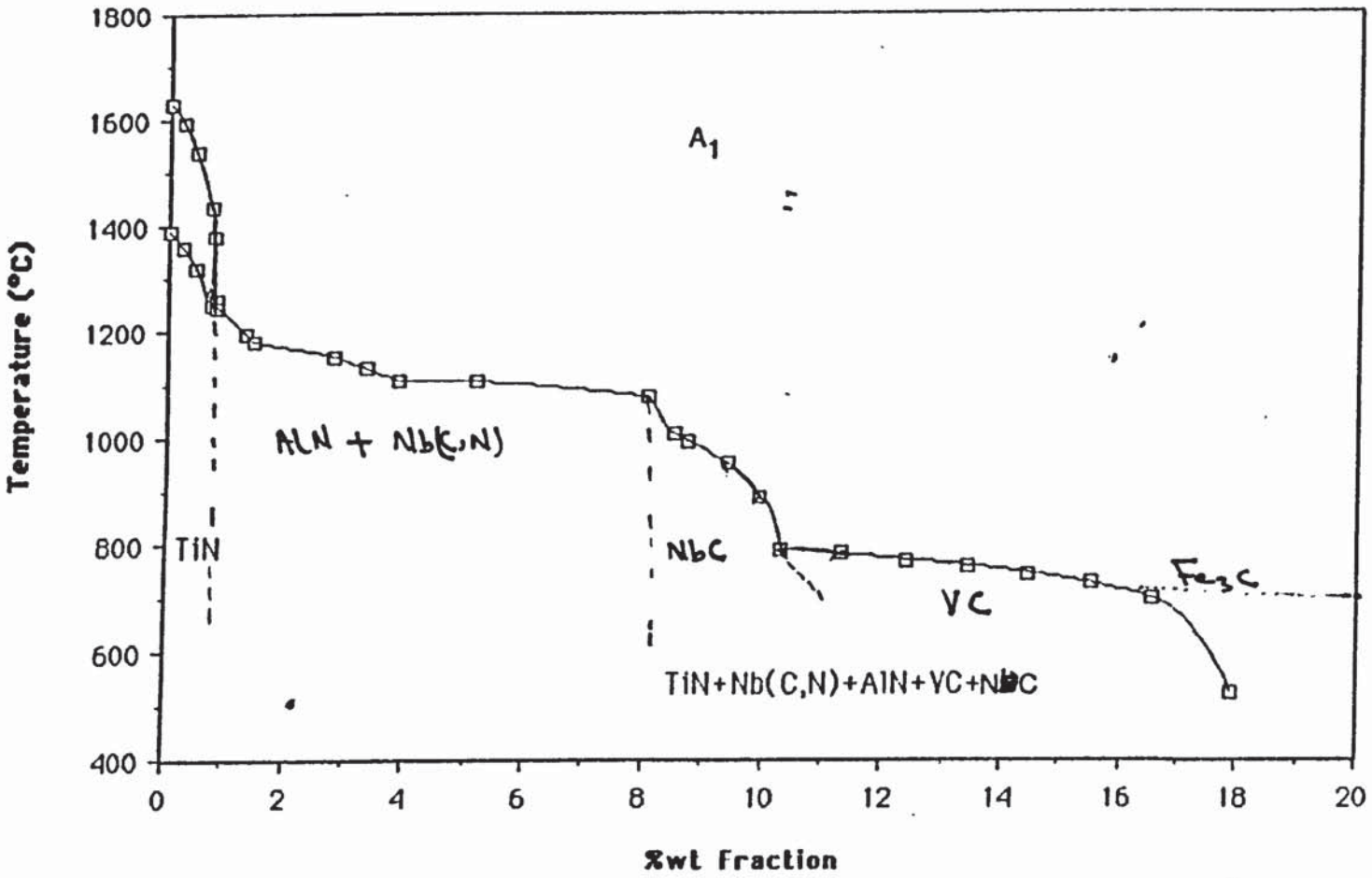

Fig.45. Variation of temperature with %wt fraction of precipitates.

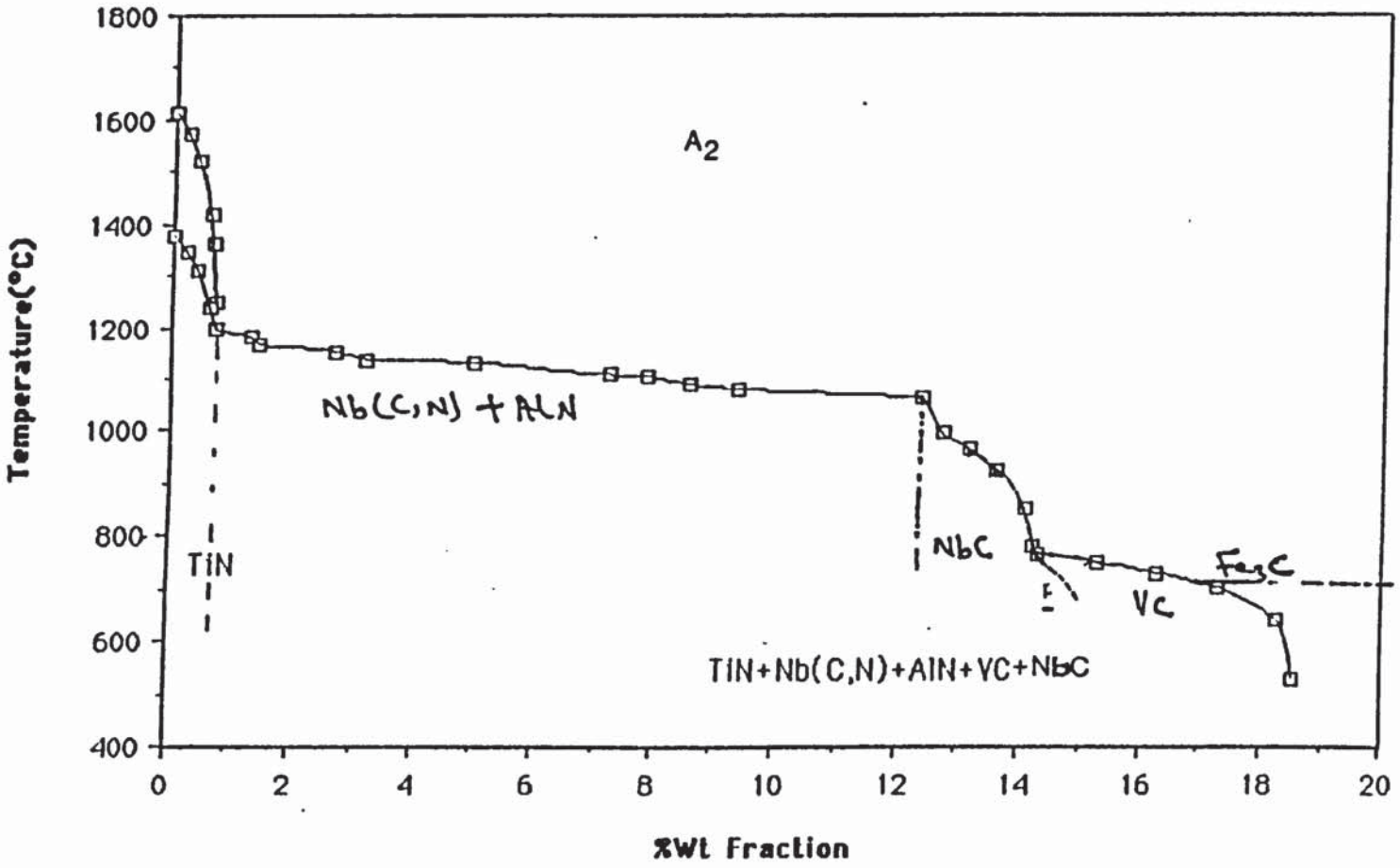

Fig.46. Variation of temperature with %wt fraction of precipitates.

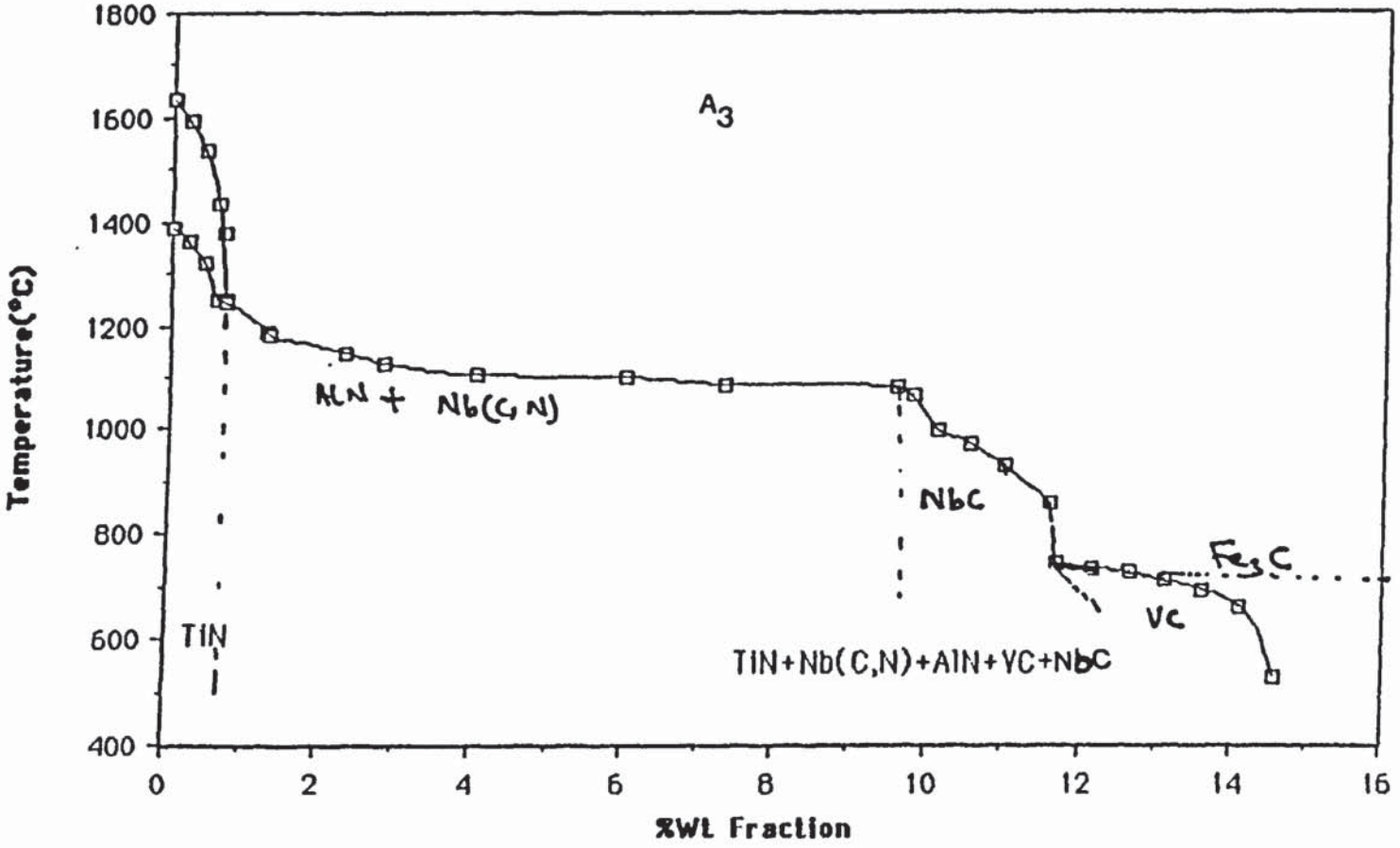

Fig.47. Variation of temperature with %wt fraction of precipitates.

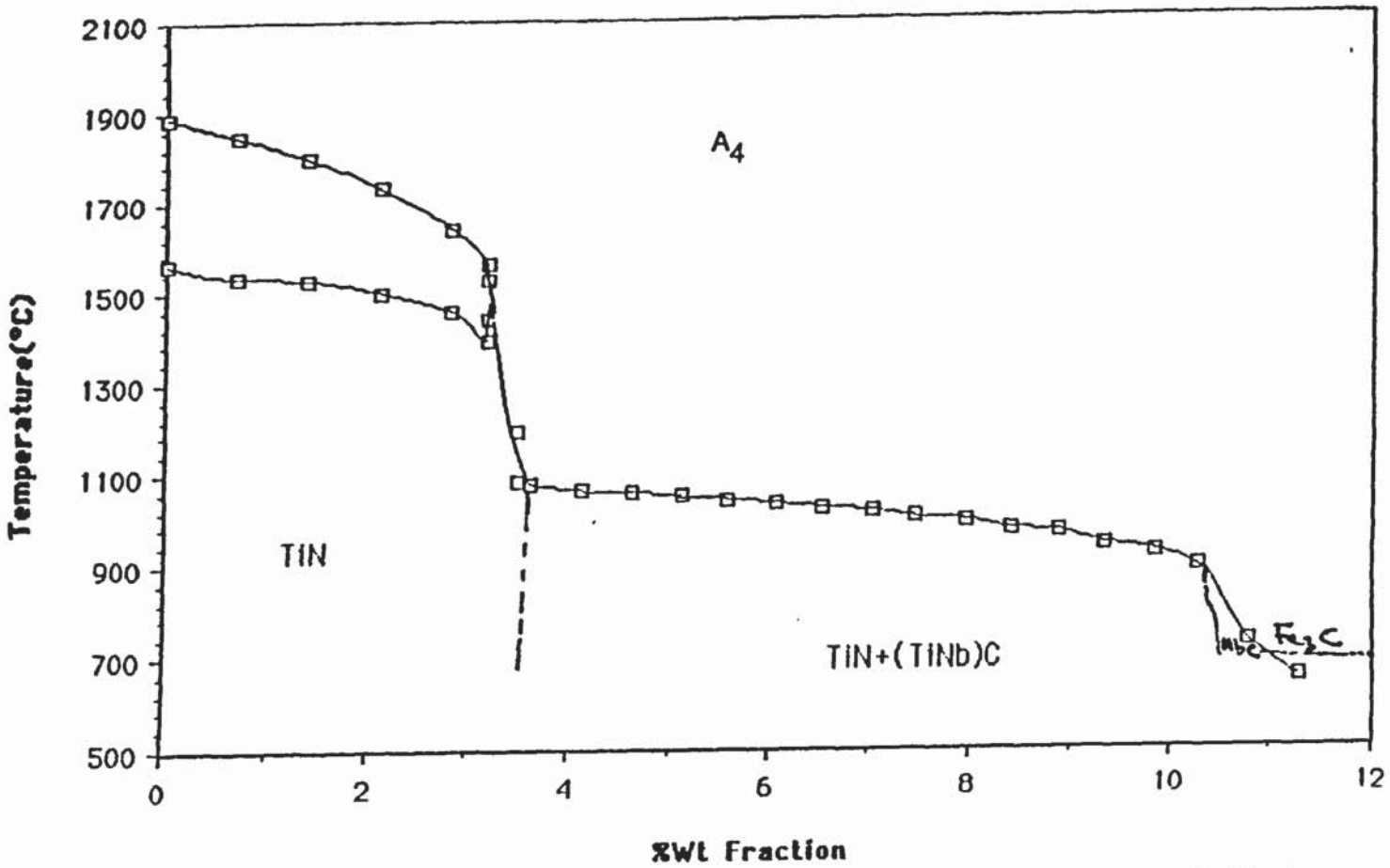

Fig.48. Variation of temperature with %wt fraction of precipitates.

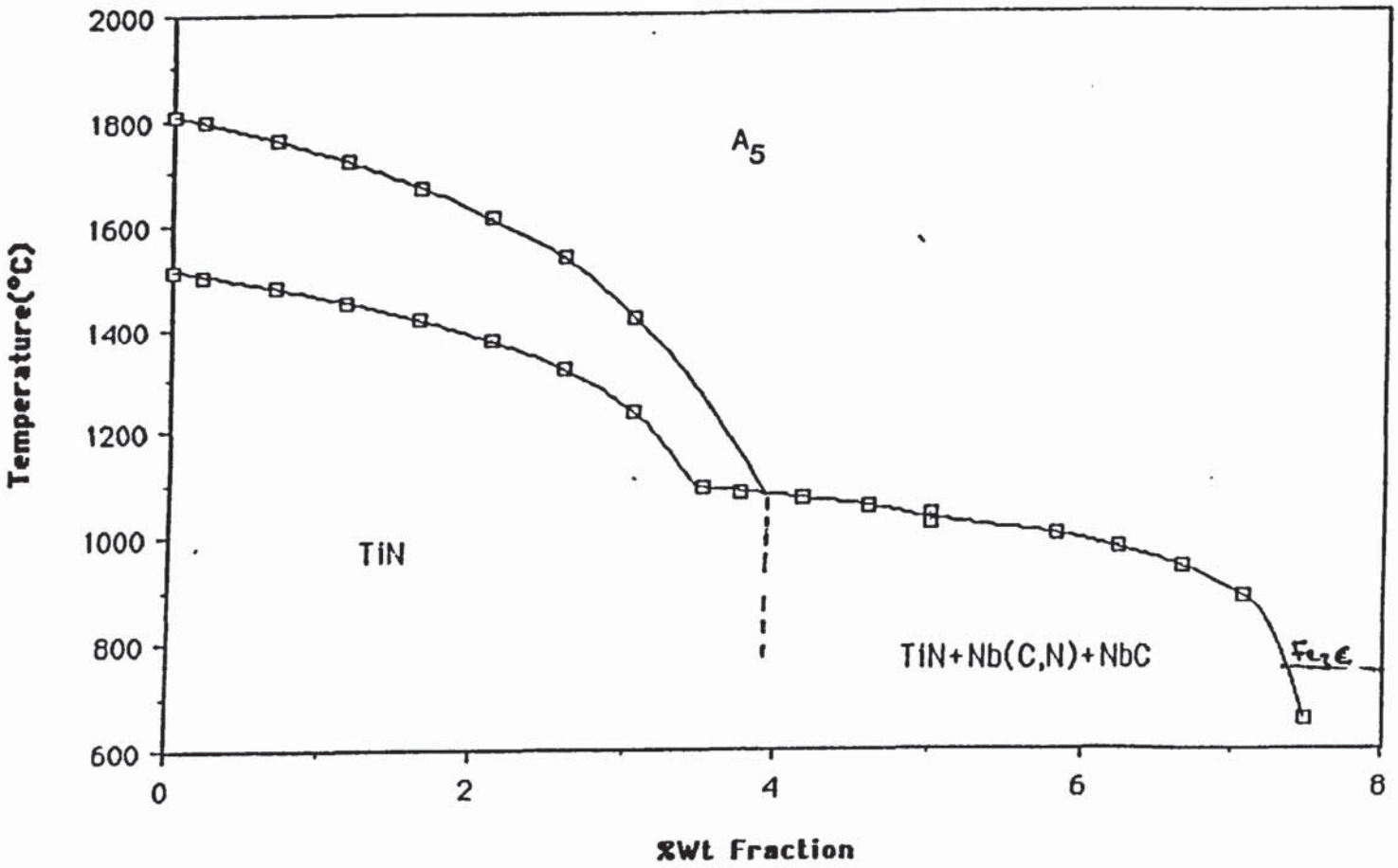

Fig.49. Variation of temperature with %wt fraction of precipitates.

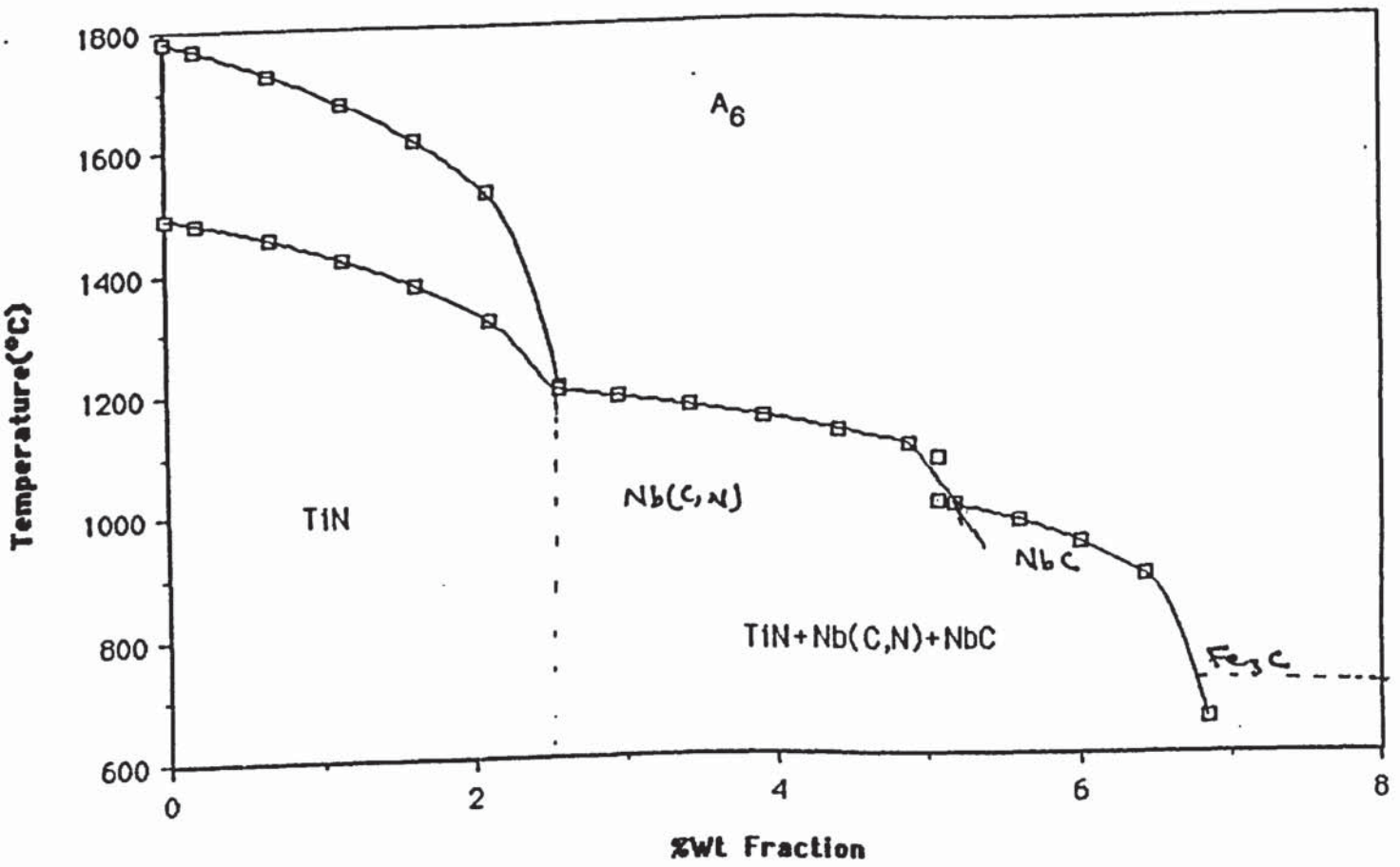

Fig.50. Variation of temperature with %wt fraction of precipitates.

APPENDIX

THE CALCULATION OF EMBURY TYPE DIAGRAM FOR ALLOY A_o USING MODEL 1 (107)

Chemical analysis of steel (wt %)

C 0.09, Nb 0.042, Ti 0.007, V 0.009, Al 0.030, O 0.0051, N = 0.0070

For this alloy, it is assumed that the precipitation sequence is TiN, TiC, AlN, Nb(C,N), NbC, VN, VC, Fe_3C

Precipitation temperatures for these compounds are established from their solubility product data over a wide temperature range.

TiN

For TiN, using Narita's derived solid data(88) giving

$$\log(\text{wt \%Ti X wt \%N}) = -\frac{15200}{T} + 3.9; \quad T \text{ is in K}$$

i.e. $$\log 0.007 \text{ X } 0.007 = -\frac{15200}{T} + 3.9$$

Start precipitation temperature, T = 1586°C

However, using his practical equilibrium liquid data

$$\log 0.007 \text{ X } 0.007 = -\frac{16586}{T} + 5.9$$

$$T = 1352^{\circ}C$$

It can be seen that the solid data gives a temperature in the liquid state, whereas the liquid data gives a temperature

for solid precipitation. This cannot be resolved and therefore, the solvus for TiN is plotted on each diagram for both sets of data.

The intermediate temperatures for TiN are given in Table 21B e.g. for 0.005%Ti and 0.0064%N, the temperature is given by:

$$\log 0.005 \times 0.0064 = -\frac{15200}{T} + 3.9; \quad T = 1538^{\circ}C$$

Or, using the liquid data:

$$\log 0.005 \times 0.0064 = -\frac{16586}{T} + 5.9; \quad T = 1323^{\circ}C$$

The ratio of titanium to nitrogen in this alloy (1.0) is less than the Stoichiometric Ratio (SR=3.43) and therefore, all the titanium is used up to produce titanium nitride.

Let it be assumed that the final titanium content left after TiN is finished precipitating is 0.0001%

$\underline{N}$ left at Ti = 0.0001% is given by

$$\underline{N} \quad 0.007 - \frac{0.0069}{48} \times \frac{14}{1} = 0.0050\%$$

Then TiN finish temperature is given by:

$$\log 0.0001 \times 0.0050 = -\frac{15200}{T} + 3.9; \quad T = 1217^{\circ}C$$

$$\text{The quantity of TiN formed} = \frac{0.0069 \times 62}{48} = 0.00891\%$$

AlN

Before this calculation can be done it is necessary to correct the aluminium for the alumina likely to be present, taking oxygen content as a measure of this alumina present, then the aluminium left for nitride formation is given by:

$$\%Al - \frac{54}{48}\%O \quad \text{viz } (0.03 - 0.0051 \times \frac{54}{48})\% = 0.02426\%$$

The solubility product of AlN is $\log(\%Al \times \%N) = -\frac{6770}{T} + 1.03$ (87)

The start precipitation is given by:

$$\log 0.02426 \times 0.0050 = -\frac{6770}{T} + 1.03$$

$$T = 1096^{o}C \text{ , assuming } \underline{N}_{start} \text{ is } 0.0050\%$$

Nb(C,N)

A similar calculation for the precipitation of Nb(C,N) can be made assuming $\underline{N}_{start} = 0.0050$ and the solubility data is given by

$$\log \left[(\%Nb)\ (\%C + \frac{12}{14}\%N)\right] = -\frac{6770}{T} + 2.26 \quad (87)$$

$$\text{i.e } \log \left[(0.042)\ (0.09 + 0.0050 \times \frac{12}{14})\right] = -\frac{6770}{T} + 2.26$$

$$T = 1179^{o}C$$

Because the start precipitation temperature of Nb(C,N) is $1179^{o}C$ and that for AlN is $1096^{o}C$ it would seem that there is a probability of co-precipitation of these two phases below $1096^{o}C$.

To determine the $\underline{N}$ remaining at $1096^{o}C$ after Nb has precipit-

ated Nb(C,N) it is assumed that the nitrogen removed is n% leaving (0.005 - n)% for co-precipitation.

Then $\log \left[(Nb - \frac{93n}{14})\ (C - \frac{12n}{14} + \frac{12}{14}\ (N-n)\right] = -\frac{6770}{1369} + 2.26$

Taking antilog

$$(Nb - 6.643n)\ (C - 0.857n + 0.857N - 0.857n) = 0.00206$$

If Nb = 0.042, C = 0.09 and N = 0.005,

Then $(0.042 - 6.643n)\ (0.09 - 0.857n + 0.00428 - 0.857n) = 0.00206$

$$(0.042 - 6.643n)\ (0.09428 - 1.714n) = 0.00206$$

$$11.386\,n^2 - 0.69829n + 0.00396 = 0.00206$$

i.e $$11.386\,n^2 - 0.69829n + 0.0019 = 0$$

$$n = \frac{0.69828 \pm (0.48761 - 0.08653)^{\frac{1}{2}}}{23.772}$$

$$= \frac{0.69829 \pm 0.63331}{23.772} = \frac{0.06498}{23.772}$$

n = 0.0029%, since the other root does not satisfy the original equation.

Thus, the Nb left at 1096°C = (0.042-6.643X0.0029) = 0.0227%

N left at 1096 = 0.005 - 0.0029 = 0.0021%

C left at 1096 = $0.09 - \frac{12}{14} \times \frac{0.0029}{1} = 0.0875\%$

The start temperature for AlN precipitation is given by

$$\log 0.0243 \times 0.0021 = -\frac{6770}{T} + 1.03$$

T = 999°C ($\approx$ 1000°C)

If it is assumed that T = 1000°C (1273K) then the Nb(C,N) precipitation calculation becomes:

$$\log\ (0.042-6.643n_1)(C-0.857n_1+0.857N-0.857n_1) = -\frac{6770}{T} + 2.26$$

At T = 1273K(1000°C), N = 0.005, Nb = 0.042, C = 0.09

$$\log\ (0.042-6.643n_1)(0.0942-1.714n_1) = -\frac{6770}{1273} + 2.26$$

Taking antilog and simplifying

$$11.386n_1^2 - 0.69829n_1 + 0.00396 = 0.000875$$

i.e. $$11.386n_1^2 - 0.69829n_1 + 0.003085 = 0$$

$$n_1^2 - 0.06133n_1 + 0.00027 = 0$$

$$n_1 = \frac{0.06133 \pm \left(3.761 \times 10^{-3} - 1.08 \times 10^{-3}\right)^{\frac{1}{2}}}{2}$$

$$= \frac{0.06133 \pm 0.05178}{2}$$

real value of n_1 = 0.0048

Thus, the Nb left at 1000°C = (0.042-6.643X0.0048) = 0.0101 %

the N left at 1000°C = 0.005 - 0.0048 = 0.0002 %

the C left at 1000°C = $0.09 - \frac{12}{14} X \frac{0.0048}{1}$ = 0.0859 %

The quantity of Nb(C,N) formed = $\frac{0.0048X119}{14}$ = 0.0408 %

Since the nitrogen left for AlN formation is 0.0002%, the AlN precipitation temperature is given by:

$$\log 0.0002 \times 0.0243 = -\frac{6770}{T} + 1.03$$

$$T = 794°C$$

Thus, it would seem that AlN would not form. To check, it is assumed that N 0.0001 %

Therefore, Nb(C,N) finish precipitation temperature is given by:

$$\log\ (0.0101)(0.0859 + 0.0001 \times \frac{12}{14}) = -\frac{6770}{T} + 2.26$$

$$T = 999^{o}C$$

Therefore, NO AlN IS FORMED because the nitrogen has all been used up.

NbC

The solubility relationship is given by:

$$\log\ (\%Nb.\ \%C) = -\frac{7900}{T} + 3.42 \quad (88)$$

Upon substitution of Nb = 0.0101 and C = 0.0859%, the start precipitation temperature is:

$$\log\ 0.0101 \times 0.0859 = -\frac{7900}{T} + 3.42$$

$$T = 946^{o}C$$

Since Nb / C $\frac{0.0101}{0.0859}$ = 0.12 is the S.R. (7.75

all the Nb is consumed. (Finish Nb is 0.0001 %)

The amount of NbC formed = $\frac{0.0100}{93} \times 105$ = 0.0113 %

Excess C = $0.0859 - \frac{0.0100}{93} \times \frac{12}{1}$ = 0.0846 %

NbC finishing temperature is given by:

$$\log\ 0.0001 \times 0.0846 = -\frac{7900}{T} + 3.42$$

$$T = 657^{o}C$$

VC

The solubility relationship is given by:

$$\log (\%V.\%C) = -\frac{9500}{T} + 6.72 \quad (88)$$

The start precipitation temperature is given by:

$$\log 0.009 \times 0.0846 = -\frac{9500}{T} + 6.72$$

$$T = 693^{o}C$$

Since this temperature is lower than the calculated austenite to ferrite transformation of $717^{o}C$ (Table 18), it is unlikely that any VC was formed and this was confirmed by the STEM - EDAX analysis where no V was detected. This behaviour of V at such a low (trace) level contrasts sharply with comparable Ti levels.

Since the finish precipitation temperature of NbC is less than the calculated austenite to ferrite transformation temperature of $717^{o}C$, therefore the percentage of carbon used up between $946^{o}C$ and $717^{o}C$ is given by:

$$\log (0.0101 - \frac{93C}{12})(0.0859 - C) = -\frac{7900}{990} + 3.42$$

$$\text{ie } (0.0101 - 7.75C)(0.0859 - C) = 2.7555 \times 10^{-5}$$

$$7.75C^{2} - 0.6758C + 8.6759 \times 10^{-4} = 2.7555 \times 10^{-5}$$

$$7.75C^{2} - 0.6758C + 8.4003 \times 10^{-4} = 0$$

$$C^{2} - 0.0872C + 1.0839 \times 10^{-4} = 0$$

$$C = \frac{0.0872 \pm (7.6038 \times 10^{-3} - 4.3356 \times 10^{-4})^{\frac{1}{2}}}{2}$$

$$= \frac{0.0872 \pm 0.0847}{2}$$

real value of C = 0.0013 %

C remaining at 717°C = 0.0859 - 0.0013 = 0.0846 %

Nb used up = $\frac{0.0013}{12} \times 93$ = 0.0100 %

the whole of Nb is used up before the start of austenite to ferrite transformation.

Cementite (Fe_3C) formed = $\frac{0.0846}{1} \times \frac{180}{12}$ = 1.269 %

For a hypo eutectoid steel, % pearlite = $\frac{0.0846}{0.8} \times \frac{100}{1}$ = 10.6 %

Pearlite without microalloys = $\frac{0.09}{0.8} \times \frac{100}{1}$ = 11.3 %

Deficit due to microalloys = 11.3 - 10.6 = 0.7

% dilution of pearlite = $\frac{0.7}{11.3} \times \frac{100}{1}$ = 6.20

This last calculation shows that the bulk of the carbon exists as cementite (Fe_3C).

The generation of the data for the construction of the different 'C' curves involved the calculation of the intermediate temperatures and percentage weight fraction of precipitates, and the results summarised in Tables 21A - 21D and Embury type diagram is shown in Figure44 . This style was adopted for steels A_1 to A_6 and the solvus type diagrams are shown in Figures45 - 50.

BIBLIOGRAPHY

1) 'Towards Improved Toughness and Ductility', Climax Molybdenum Co. Ltd., Kyoto, (1972)

2) Microstructure and Design of Alloys Publ. No.36, The Institute of Metals/ Iron and Steel Institute, London, (1973)

3) 'Processing and Properties of Low Carbon Steel', Ed. J.M.Gray, AIME, New York, (1973)

4) 'Mechanical Working and Steel Processing', Proceedings of 14th - 19th Conferences, AIME, New York, (1972-1977)

5) 'Controlled Processing of HSLA Steels', Proceedings of York Conference, British Steel Corporation, (1976)

6) 'Microalloying 75', Ed. M.Korchynsky, Union Carbide Corporation, New York, (1977)

7) 'Hot Deformation of Austenite', Ed. J.B.Ballance, AIME, New York, (1977)

8) 'Structural Steels for the Eighties', AIME, Warrendale, (1977)

9) 'Low Carbon Steels for the Eighties', The Institution of Metallurgists, London, (1977)

10) 'Recrystallisation of Metallic Materials', Ed. F.Haessner, Rieder-Verlag GmbH.

11) 'Dual Phase and Cold Processing of Vanadium Steels in the Automobile Industry', Proceedings of Berlin Conference, Vanitec, (1978)

12) 'Welding of HSLA (Microalloyed) Structural Steels', Eds. A.B.Rothwell and J.M.Gray, ASM, Cleveland, (1978)

13) 'Hardenability Concepts with Applications to Steels', Eds. D.V.Doanne and J.S.Kirkaldy, AIME, Warrendale, (1978)

14) 'Pipe Welding', Proceedings of International Conference, the Metals Society, London, (1979)

15) 'Structure and Properties of Dual Phase Steels, Eds. R.A.Kot and J.W.Morris, AIME, Warrendale, (1979)

16) 'Vanadium in High Strength Steels' Publication No.140, Vanitec, London, (1979)

17) 'Vanadium in Rail Steels', Proceedings of Vanitec Chicago Conference, Vanitec, London, (1979)

18) 'Arctic Pipe Line', Proceedings of Golden Gate Conference, San Francisco, ASM, Cleveland, (1979)

19) 'Micon 78', Optimisation of Processing Properties and Service Performance through Microstructural Control, Eds. H.Abrams, G.N.McNair, D.A.Nail, H.D.Solomon, STP 672, ASTM, Philadelphia, (1979)

20) 'Hot Working and Forming Processes', Eds. C.M.Sellars and G.J.Davies, The Metals Society, London, (1980)

21) 'Technology and Applications of Vanadium Steels', Proceedings of Vanitec Conference Krakow, Poland, Published by Vanitec, (1980)

22) 'Thermomechanical Processing of Microalloyed Austenite', (Proc. Conf.), Pittsburg, Pennsylvania, (1981), Eds. A.J.De Ardo, G.A.Ratz and P.J.Wray

23) 'Steels for Line Pipe and Pipeline Fittings', (Proc. Conf.), Metals Society and Welding Institute, London, (1981)

24) 'HSLA Steels. Technology and Application', (Proc. Conf.), (1983), Ed. M.Korchynsky, Philadelphia, USA.

25) Kim, N.J., Journal of Metals, April (1983) 21

26) Coldren,A.P. and Oakwood,T.G. ibid, (1983) 28

27) Stuart,H. and Jones,B.L., ibid

28) Platts,G.K., Vassiliou,A.D. and Pickering,F.B., Metallurgists and Materials Technologist, September 1984

29) Gray,J.M. and Jones,B.L., Perspective in Metallurgical Development, Centenary of Sheffield University Metallurgy Department 1884-1984 (Proc. Conf.) 1984

30) Woodhead,J.H., ibid

31) Physical Metallurgy and the Design of Steels, Ed. F.B.Pickering, Applied Science Publ. London.

32) Honeycombe,R.W.K., Trans. Jap. Inst. of Metal, 24 (1983), No.4

33) Brown,E.L. and DeArdo, A.J., 'Aluminium Nitride Precipitation in C-Mn-Si and Microalloyed Steels', Thermomechanical Processing of Microalloyed Austenite, Eds. A.J.DeArdo, G.A.Ratz, P.J.Wray, P.319

34) Keown,S.R. and Wilson,W.G., 'Prediction of Precipitate Phases in Microalloyed Steels containing Niobium, Carbon, Nitrogen and Aluminium', ibid, 343

35) Michael,J.P. and Jonas,J.J., Acta Met. 29, 513, (1981)

36) Taguchi,S. and Sakakura,A., ibid, 14, 405 (1966)

37) Meyer,L., HeisterKamp,S., Mueschenborn,W. See ref.6,p 130

38) Woberts,W. and Sanberg,A., 'The Composition of V(C,N) as Precipitated in HSLA - Steels Microalloyed with Vanadium', Swedish Institute for Metals Research No. IM - 1489 (1980)

39) HeisterKamp,F. and Hulka,K., Metals Technology, 11 (1984) 535

40) Weiss,I., Fitzsimons,C.L., Mielityinen-Tiitto,K. and DeArdo,A.J., ibid, 33

41) Ianc,P.P. and Dragan,N.I., ibid, 361

42) White,M.J. and Owen,W.S., Met. Trans. 11A 1980

43) Kim,S.G., Ph.D. Thesis, University of Sheffield, 1982

44) Baker,R.G. and Nutting,J., Precipitation Processes in Steels, London, Iron and Steel Institute Special Report (1969), 1262-1266

45) Smith,E., Acta Met. 14 (1966)

46) Tanino,M. and Mishida,T., Trans. Jap. Inst. of Metals 9, (1968)

47) Paxton,H.W., Alloys for the Eighties, Climax Moly. Co. Ltd., London, 1981

48) Jones,C.L., Rodgerson,P. and Brown,A., ref.24, 809

49) Usui,T., Yamada,K., Miyashita,Y., Tanabe,H., Hanmyo,M. and Taguchi,K., SCAN INJECT II, 12:1

50) Courtenay,J.H., Pheasant, S.T. and Smith,J.S., Iron And Steel Inst. (1981)

51) Irvine,K.J., Gladman,T., Orr,J. and Pickering,F.B. J.I.S.I. (1970) 717

52) Goldschmidt,H.J., Interstitial Alloys published by Butterworth, London, (1967)

53) Andrews,K.W., J.I.S.I. 203 (1965) 721

54) Inagaki, H., Tanimura,M., Matsushima,I. and Nishimura,T., Trans. I.S.I.J., 18 (1978)

55) Nara,Y., Kyogoku, Yamura,T. and Takeuchi,I. ref.23

56) Baker,R., Cavaghan,N.J., Herbert,A and Mormanton,A.S., Perspective in Metallurgical Development, Centenary of Sheffield University Metallurgy Department, 1884-1984 (Proc. Conf.), 1984, 77

57) Pickering,F.B. ref.6 p.3

58) Wadsworth,J., Woodhead,J.H. and Keown,S.R., Met. Science, 10 (1976), 342

59) Belliot,J. and Gantois,M., Trans. ISIJ, 8 (1978) 546

60) Gaspard,C., Messien,P. and Greday,T., Met. Science, 16 (1982) 105

61) Spitzig,W.A., Met. Trans. 14A (1983) 271

62) Spitzig,W.A., ibid 14A (1983) 471

63) Miglin,M.T., Hirt,J.P. and Rosenfield,A.R., ibid, 14A (1983) 2055

64) Spitzig,W.A. Met. Trans. 15A (1984) 1259

65) Tanaka,T., JISI 17, 70th Annual Meetings and Conf., Vienna, Austria, 2nd - 5th Oct. (1983) 68

66) Pickering,F.B., ref.24, 1

67) Smith,Y.E., Coldren,A.P. and Cryderman,R.L., Towards Improved Ductility and Toughness, Climax Moly. Co. Ltd., Ann Arbor, (1967) 109

68) Coldren,A.P., Cryderman,R.L. and Smith Y.E., Processing and Properties of Low Carbon Steels, Ed. J.M.Gray, AIME, New York (1973), 163

69) Pickering,F.B., 'Transformation and Hardenability in Steel', Climax Moly. Co. Ltd., Ann Arbor (1967) 109

70) Whiteman,J.A., 'Low Carbon Steels for the Eighties', The Institution of Metallurgists, London, (1977) I.1

71) Coldren,A.P., Bliss,V and Oakwood,T.G. ref.22 591

72) Tanaka,T., Int. Met. Rev. No.4 (1981) 185

73) Baker,T.N., Scientific Progress, 65, 493, Blackwell Scientific Publications, Oxford, (1978)

74) Gladman,T. and Pickering,F.B., 'Flow and Fracture in Polycrystalline Metals', Ed. Baker,T.N., Appl. Sc. Pub. London

75) Ohtani,H., Terasaki,F. and Kunitake,T., Trans. ISIJ 12 (1972) 118

76) Woodhead,J.H. and Whiteman,J.A., 'Processing and Properties of Low Carbon Steels', Ed. Gray,J.M., AIME, New York, (1973), 145

77) Roberts,M.J., Met. Trans. 1, (1970) 3287

78) Browrigg,A., Scripta Met., 7, (1973), 1139

79) Shigq,C., Amano,K., Hotomura,T., Saito,Y., Hirose,K. and Choji,T., ref.23, paper No.12

80) Nara,Y., Kyoguku,T., Yamura,T. and Takenchi,I., Metals Technology, 10(8) (1983) 322

81) Anderson,K., Martin,I.W., Chapman,J.A. and Smith,G.C., ibid, 315

82) Jones,B.L. ref.24, 710

83) Pickering,F.B. 'Towards Improved Tuoghness and Ductility' Climax Moly., Co. Ltd., Kyoto (1972) 9

84) Robert,W., Scan. Jo. of Met. 9 (1980) 13

85) Heedman,P.J. and Sjostrom,A., ibid 9 (1980) 21

86) Sage,A.M., Metals Technology, 10(6) (1983) 224

87 Irvine,K.J., Pickering,FB. and Gladman,T., JISI, 205 (1967) 161

88) Narita,K., Trans. ISIJ, 15 (1975) 147

89) Strid,J. and Easterling,K.E., Acta Met., 21, (1985) 11

90) Gladman,T., Dulieu,D. and McIvor,I.A., ref.6, 25

91) LeBon,A.B. and de Saint-Martin,L.N., ref.6, 72

92) Tanaka,T., Tabata,N., Hatomura,T. and Shiga,C., ref.6, 88

93) Kozasu,I., Ouchi,C., Sampei-Tand Okita,T., ref.6 100

94) Amin,R.K. and Pickering,F.B., ref.22, 1

95) Sakai,T., Akben,M.G. and Jonas,J.J., ibid, 237

96) Bacroix,B., Akben,M.G. and Jonas,J.J., ibid, 293

97) Jonas,J.J. and Akben,M.G., Metals Forum, 4 (1981) 92

98) Cuddy,L., ref.22, 129

99) Yamamoto,S., Ouchi,C., and Osuka,T., ibid, 613

100) Akben,M.G., Weiss,I. and Jonas,J.J. Acta Met., 29 (1981) 111

101) Ueda,S., Ishikawu,M., Kamada,A. and Ohashi,N., Trans. ISIJ 205 (1967) 161

102) Chandra,T., Akben,M.G. and Jonas,J.J., Strength of Metals and Alloys, Proc. 6th Int. Conf., Melbourne, 1 (1982) 499

103) Melloy,G.F. and Dennison,J.D., The Microstructure and Design of Alloys, The Metals Society, London, 1, (1973) 60

104) Amin,R.K., Korchynsky,M. and Pickering,F.B., Metals Technology, 8(7) (1981) 250

105) Ballinger,N.K. and Honeycombe,R.W.K., Met. Trans. 11A (1980) 421

106) Ballinger,N.K. and Honeycombe,R.W.K., Met. Science, 14 (1980) 421

107) Houghton,D.C., Weatherly,G.C. and Embury,J.D., ref.22, 267

108) Barker,T.N., 'Hot Working and Forming Processes', Eds. Sellars,C.M. and Davies,G.J., The Metals Society, London, (1983) 32

109) Parker,B.A. and Hirch,Y.C., 'Advances in Physical Metallurgy and Applications of Steels', The Metals Society, London, (1983) 26

110) Gladman,T., Proc. Roy. Soc., 266A (1966) 298

111) Nilsson,T., Scan. J. of Met. 9 (1980) 69

112) Roberts,W., ref.24, 33

113) Roberts,W., Sanberg,A., Siwecki,T. and Werlefors, T., ref.24, 67

114) Zheng,Y. and DeArdo,A.J., ref.24, 85

115) Siwecki,T., Sanberg,A. and Roberts,W., ref.24, 19

116) Bufalini,P., De Vito,A., Pontremoli,M. and Amprile,A., ref.24, 743

117) Coldren,A.P., Oakwood,T.G. and Tither,G., ref.24, 755

118) Almond,E.A., Mitchell,P.S. and Irani,R.S., Metals Technology (1979) 205

119) Sellars,C.M. and Whiteman,J.A., 'Controlled Processing of HSLA Steels', Proceedings of York Conference, British Steel Corporation, paper 5 (1976)

120) Sellars,C.M. and Whiteman,J.A., Met. Science 13, (1979) 187

121) Siwecki,T., Sanberg,A., Roberts Wand Lagneborg,R., ref.22, 163

122) Licka,S., Woznik,J., Kosar,M. and Prnka, ibid, 521

123) Amin,R.K. and Pickering,F.B., ibid, 377

124) Roberts,W., Lidefelt,H. and Sanberg,A., 'Hot Working and Forming Processes', Eds. Sellars,C.M. and Davies,G.J. The Metals Society, London (1980) 38

125) Roberts,W., ibid, 45

126) Chandra,T., Weiss,I. and Jonas,J.J., Met. Science, 16, (1982) 97

127) Wey,M.Y., Sakuma,T. and Nishizawa,T., Trans. Jap. Inst. of Metal, 22(10), (1981) 733

128) Gladman,T. and Pickering,F.B., JISI, 205 (1967) 633

129) Picks,R.A., Howell,P.R. and Honeycombe,R.W.K., Met. Trans., 10A (1979) 1049

130) Picks,R.A., Howell,P.R. and Honeycombe,R.W.K., Met. Science, 14A (1980) 562

131) Moore,E.M. and Warga,J.A., Material Performance, June (1976) 17

132) Biefer,G.J., ibid, June (1982) 19

133) Haycook,E.H., Corrosion, 40(7) (1984) 337

134) Berstein,I.M. and Thompson,A.W., Int. Met. Rev. No.212 (1976) 269

135) Taira,T. and Kobayashi,Y., ref.23, 170

136) Pressouyre,G.M., Blondeau,R. and Cadiou,L., ref.24, 827

137) Pressouyre,G.M., Blondeau,R., Primon,G. and Cadiou,L., 'Current Solutions to Hydrogen in Steels', Proc. of the 1st Int. Conf., ASM (1982), Eds. Interrante,C.G. and Pressouyre,G.M., 212

138) Pressouyre,G.M., ibid, 18

139) Hill,R.T. and Iino,M., ibid, 196

140) Hay,M.G. and Dautovich,D.P., ibid, 191

141) D.Le T. and Wilde,B.E., ibid, 413

142) Lea,C., Corrosion 40(7) (1984) 337

143) Herbsleb,G., Poepperling,R.K. and Schwenk,W., Corrosion, 36(5) (1981) 247

144) Wilde,B.E., Kim,C.D. and Phelps,E.H., ibid, 36(11) (1980) 625

145) Brown,A. and Jones,C.L., ibid, 40(7), (1984) 330

146) Yamada,K., Satoh,Y., Tanaka,N., Muruyama,H., Chano,Z. and Itoh,K., ref.24, 835

147) Sponseller,D.L., Garber,R. and Cox,T.B., ref.137, 200

148) Interrante,C.G., ibid, 3

149) Berstein,I.M., Thompson,A.W., Gutierrex-Solana,F. and Christodoulou, ibid, 259

150) Taira,T., Kobayashi,Y., Matsumoto,K., Matsumoto,S., Terunuma,T. and Arikata,K., ibid, 173

151) Kargol,J.A. and Interrante,C.G., ibid, 438

152) Troiano,A.R. and Hehemann,R.F., ibid, 299

153) Viswanathan,R. and Jaffee,R.I., ibid, 275

154) Iino,M., Normura,N., Takexawa,H. and Takeda,T., ibid, 159

155) Yoshino,Y., Corrosion, 39(11), (1983) 435

156) Taira,T., Tsukada,K., Kobayashi,Y., Inagaki,H. and Watanabe, ibid, 37(1) (1981) 5

157) Ikeshima,T., Trans. ISIJ, 19, (1979) 583

158) Nakai,Y., Kuramashi,H., Emi,T. and Haida,O., ibid, 403

159) Hills,D., Private communication, 1986

160) Chan,S.L.I., Martinez-Madrid,M. and Charles,J.A., Int. Congress on Metallic Corrosion, (Proc.Conf.), Vol.2, Toronto, Canada, (1984) 237

161) Taira,T., Kobayashi,Y., Matsumoto,K and TsuKada,K., Corrosion, 40(9), (1984) 478

162) Venkatasubramanian,T.V. and Baker,T.J., Met. Science, 16, (1982) 543

163) Venkatasubramanian,T.V. and Baker T.J., ibid, 18, (1984) 241

164) Current Solutions to Hydrogen Problems in Steels, Proc. of the 1st Int. Conference, Eds. Interrante,C.G. and Pressouyre,G.M.

165) Pumphrey,P.H., Met. Science, 16 (1982) 41

166) Turn,J.C., J.R., Wilde,B.E. and Troignos,C.A., Corrosion, 39(9), (1983) 364

167) Latanision,R.M., Atomistics of Fracture (Proc. Conf.) Nato Conference Series, Material Science Vol.5, Eds., Latanision and Pickens (1981) Corsica, France

168) Rodgerson,P. and Jones,C.L., ref.23, Paper No.32

169) Taira,T. and Kobayashi,Y., ibid, Paper No.18

170) Shimogori,K., Torii,Y. and Kitahata,K., R & D Kobe Steel Engineering Reports / Vo.34, No.2, 21

171) Obinata,T., ref.23, Paper No.19

172) Loberg,B., Nordgren,A., Strid,J. and Easterling,K.E., Met. Trans. 15A (1984) 33

173) Lagneborg,R., Scand. J. Metallurgy 14 (1985) 289-298

174) Pickering,F.B., Private communication, 1986

175) Honeycombe,R.W.K., Structure and Strength of Alloy Steels, Climax Moly. Co. Ltd., London, P.7

176) Pickering,F.B., 'Inclusions', Institute of Metallurgists Monograph No.3 (1979) 117

177) Gawne,P.T. and Lewis,G.M.H., Mats. Science and Technol. 1 (1985) 183

178) Pontremoli,M., Bufalini,P., Aprile,A. and Jannone,C., Metals Technol. 11, (1984) 504

179) Bodsworth,C. and Bell,H.B., Physical Chemistry of Iron and Steel Manufacture, 2nd Edn., Logman, P.61

180) Uko,D., Sowerby,R. and Embury,J.D., Metals Technol. (1980) 368

181) Andrews,K.W., Dyson,D.J. and Keown,S.R., Interpretation of Electron Diffraction Patterns, 2nd Edn. (1971), publ. Adam Hilger Ltd., London

182) Tennet,R.M., Science Data book, publ. Longman

183) Asante,J.C.B., Ph.D. Thesis (1980) Aston University, Birmingham.

184) Cuddy,L.J. and Raley,J.C., Met. Trans., 14A (1983) 1989

185) Chen,Z., Lorreto,M.H. and Cockrane,R., Inst. of Phys. Conf. Serial No.78, Chapter 8

186) Baker,T.J. and Charles,J.A., JISI 209 (1972) 702